Defining the regulatory network that governs effector gene expression during plant infection by the blast fungus *Magnaporthe oryzae*

Camilla Molinari

Thesis submitted to the University of East Anglia for the Degree of Doctor of Philosophy

The Sainsbury Laboratory
Norwich, UK

March 2025

Abstract

Rice blast disease, caused by the filamentous fungus *Magnaporthe oryzae*, threatens global rice production. To invade the host plant, the fungus secretes a battery of effector proteins with distinct functions and subcellular targets. In *M. oryzae*, effector-encoding genes are subject to strict spatiotemporal regulation that aligns with disease progression. However, our understanding of infection-related transcriptional control remains limited in plant pathogenic fungi. This thesis explores effector gene regulation in *M. oryzae* through two complementary approaches: a forward genetic screen to identify novel regulatory components and a reverse genetic strategy to enhance our understanding of established regulatory pathways. The forward screen is based on the hypothesis that most effector genes are only expressed in the host plant and require transcriptional regulation for this expression profile. By mutagenesis of *MEP3-GFP* strains, I isolated three putative constitutive effector regulator (*CER*) mutants showing constitutive *MEP3-GFP* expression. Analysis of the *CER* mutants identified the G-protein regulator *RGS1*, previously reported to repress late expression effectors in *M. oryzae* prior to plant infection. This finding, consistent with earlier research, provides new insight into the regulatory role of *RGS1* and its broader function in infection-related transcriptional networks. This prompted the second approach, in which we demonstrate that the transcription factor Bip1 (B-ZIP Involved in Pathogenesis-1) is a component of the conserved Pmk1 MAPK /Mst12 signalling pathway—essential for appressorium formation, penetration, and invasive growth. Global transcriptome analysis revealed Bip1 and Mst12 co-regulate a common subset of genes, including effectors, during pathogenesis. Furthermore, Bip1 is phosphorylated during plant infection in a Pmk1-dependent manner, *BIP1* expression is Mst12-dependent, and it physically interacts with Mst12, suggesting heterodimer formation. These findings support a model in which Bip1 and Mst12 are components of a hierarchy of co-ordinately controlled transcription factors that regulate *M. oryzae* pathogenesis, offering new mechanistic insights into fungal virulence.

Table of Contents

List of Figures

List of Tables

List of Abbreviations

ArpA	Alkaline protease
ATP	adenosine triphosphate
Avr	Avirulence
BAK1	BRI1-associated kinase 1
BAS	Biotrophy associate
BASTA	*Bar* gene to confer bialophos resistance
BIC	Biotrophic Interfacial Complex
Bip1	B-ZIP Involved in Pathogenesis-1
Bp	base pair
BRI1	Brassinosteroid insensitive 1
bZIP	Basic Leucine Zipper
CEBiP	Chitin elicitor binding protein
cAMP	cyclic AMP
CER	Constitutive Effector Regulator
CERK	Chitin elicitor receptor kinase
ChIP-Seq	Chromatin immunoprecipitation sequencing
CME	Clathrin-mediated endocytosis
COX	Cytochrome c oxidase
DAMP	Damage-associated molecular pattern
DEG	Differentially expressed gene
DIC	Differential Interference Contrast
Ecp6	Extracellular protein 6
EFR	ELONGATION FACTOR TU RECEPTOR
EHMI	Extrainvasive hyphal membrane
ER	Endoplasmic reticulum
ET	Ethylene
ETI	Effector triggered immunity
FIMO	Find individual motif occurrences
FLS2	FLAGELLIN SENSING 2
GATK	Genomic Analysis Toolkit

GDP	Guanosine diphosphate
GFP	Green fluorescence protein
Git1	G-protein-coupled receptor kinase interactor-1
GO	Gene ontology
GTP	Guanosine triphosphate
HMA	Heavy metal-associated
Hph	Gene coding for hygromycin B phosphotransferase
Hpi	Hour post inoculation
HR	Hypersensitive response
Hrp	Hypersensitive response and pathogenicity
HTR1/2	Host Transcription Reprogramming ½
IH	Invasive hyphae
JA	Jasmonic acid
JAZ	Jasmonate ZIM-domain
LB	Lysogeny broth
LysM	Lysine motif
MAPK	Mitogen-activated protein kinase
MAPKK	MAP kinase kinase
MAPKKK	MAP kinase kinase kinase
MAX	Magnaporthe AVRs and ToxB-like
MDS	Multidimensional scaling
MEP	Magnaporthe effector protein
Mg	*Medicago truncatula*
Mo	*Magnaporthe oryzae*
MYB	Myeloblastosis
NAD	Nicotinamide adenine dinucleotide
NLR	Nucleotide-binding leucine-rich repeat
NLS	Nuclear localisation signal
NRC	NLR required for cell death
ORF	Open-reading frame
Pac2	Proteasome assembly chaperone
PAMPs	Pathogen-associated molecular patterns

PBS1	AvrPphB susceptible 1
Pc	*Phytophthora capsici*
PCR	Polymerase Chain Reaction
Pep1	Protein essential during penetration 1
Pi	*Phytophthora infestans*
Pmk1	Pathogenicity MAP kinase 1
Pph	*Pseudomonas syringae* pv *phaseolicola*
PRRs	Pattern recognition receptors
Ps	*Phytophthora sojae*
PTI	PAMP triggered immunity
Pto	*Pseudomonas syringae* pv *tomato*
qRT-PCR	Quantitative real-time polymerase chain reaction
R gene	Resistance gene
RGS	Regulator of G protein
RIN4	RPM1-interacting protein 4
RLCK	Receptor-like cytoplasmic kinase
RNA-Seq	RNA sequencing
ROS	Reactive oxygen species
Ros1	Regulator of sporogenesis 1
RPM1	Resistance to *Pseudomonas syringae* pv. *macuolicola 1*
SA	Salicylic acid
Slp1	Secreted LysM Protein 1
SNP	Single Nucleotide Polymorphism
SP	Signal peptide
SS15	SPRYSEC15
SUGR-1	SUbventral Gland Regulator 1
T3SS	Type III Secretion System
T4SS	Type IV Secretion System
T6SS	Type VI Secretion System
TAL	Transcription activator-like
TF	Transcription factor
VCF	Variant Call Format

Vd	*Verticillium dahlia*
WGS	Whole Genome Sequencing
Wor1	White–opaque regulator 1
WT	Wild type
Xcc	*Xanthomonas campestris*
Xo	*Xanthomonas oryzae* pv. *oryzae*
Y2H	Yeast-two-hybrid
ZIM	Zinc-finger inflorescence meristem

Acknowledgements

Firstly, I would like to thank my supervisor, Prof. Nick Talbot, for the opportunity to work in the laboratory as a predoc and subsequently as a PhD student. Your encouragement, trust, and mentorship have significantly contributed to my scientific and personal growth over the past few years. Your enthusiasm for research is always inspiring, and I am truly grateful for everything I have learnt from you and this research experience.

I would like to express my gratitude to the Norwich Research Park Doctoral Training Partnership (NRPDTP), funded by the Biotechnology and Biological Sciences Research Council (BBSRC), for their generous financial support throughout my doctoral research.

Thank you to every member of my supervisory committee for your time and guidance throughout my PhD: Dr Matthew Moscou for mentoring me at the beginning of my project; Prof. Wenbo Ma for taking the role of my secondary supervisor halfway through and for all the insightful suggestions in our meetings; and Dr Lauren Ryder for her guidance in the lab, support, and friendship.

I am very grateful to all the past and present members of the Talbot Lab for all the help, for some productive scientific discussions and for the fun times shared over the years: Matt, Nef, Lauren, Bozeng, Andy, Neha, Xia, Jave, Angus, Iris, Mary, Diana, Weibin, Berlaine, Fabio, Luyao, Gulnara and Vinni. Special shoutouts to Xia and Neha; your support was crucial during my research project, providing me with feedback and assisting with bioinformatic analyses. Diana, thank you for your encouragement and friendship from day one. Mary, thanks for your support and taking care of me. Matt, thank you for joining the lab and for always being there. Being bench buddies and sharing our love for Beyonce and *Magnaporthe* has been so much fun.

I want to express my gratitude to everyone at TSL for creating a fantastic work environment that promotes collaboration, discussion, and growth. I appreciate all the TSL support teams for their exceptional and ongoing assistance. I am very thankful for the wonderful TSL student community (TSLytherins), who are always there to inspire, help, and enjoy fun breaks in the sun. Thank you to the TMMRC members, particularly Alex, Daniel, Nef, and Marquitos, who encouraged me to start running. I now love running, and it has helped me immensely as I conclude my PhD. Thank you to Everton, Andy, Sara, Kelly, Mau, AmirAli, and all the friends I have made over the years at TSL for your advice, for making work enjoyable, and for all the parties and constant motivation. TSL and its people have profoundly influenced this journey and empowered me as a researcher.

Special thanks to all the friends I have made in Norwich over the years: Carlos, it was wonderful living together; Isa (cara Pizza), thank you for being my first friend in this fine city, for always laughing at my jokes and for being there; Sr Alfano, thank you for your friendship and for making me feel closer to Argentina with all your delicious cooking; Scarlett, thank you and your beautiful family for being a source of joy; Vasiliki, thank you for being a wonderful housemate, for all the fun times and taking care of Tortellini and me with so much love; Natalia, thanks for all the shared dances over the years; and Joanna, thank you for your unwavering support, belief in me, and sense of humour, which have been invaluable throughout this journey.

I would also like to express my gratitude to my friends who do not live in Norwich but are always there. Gadea, thank you for being my rock, for giving me the best advice and for your loving friendship. Jani and Bruno, thanks for your endless jokes, our solid friendship and your visits to Norwich over the years. I want to thank my Biotechnology Degree friends from Salamanca (Los Reales) for inspiring me to pursue this scientific career and for being so silly and fun. A heartfelt thank you to Olga for celebrating and supporting me at every step of this journey; I am incredibly grateful for your unconditional loving friendship.

Finally, I would like to acknowledge my family around the world. Big thank you to all my beautiful family in Argentina, gracias por tanto amor que hace que las distancias desaparezcan. Thank you Lindsey and Willow, for becoming my family and being two of my greatest sources of support over the past two years. Nan, I could not have done this without your loving encouragement. Jackie, thank you for being the best godmother anyone could ask for and for your continuous support. Phoenix, I am deeply grateful for your love, patience, belief in me, reassurance, and for being my forever and always running partner. You have truly kept me motivated and determined to push forward. Lastly, I want to thank Sarah, Agustin, Luca and Francesca. Gracias por siempre estar y motivarme en este camino de ser una científica loca, por ser la mejor familia y por el amor y apoyo incondicional. Todo esto es gracias a ustedes, les quiero.

Chapter 1: General Introduction

1.1 Introduction to effectors and plant immunity

Plants are constantly exposed to pathogens, including viruses, bacteria, oomycetes, fungi, nematodes, as well as parasitic plants and insect herbivores. These organisms have developed sophisticated mechanisms to adapt to the colonising environment and to suppress plant immunity (Abramovitch *et al.*, 2006, Kamoun, 2006, Hogenhout *et al.*, 2009, Toruño *et al.*, 2016, Oliveira-Garcia *et al.*, 2024). One important strategy is the secretion of small, specialised proteins known as effectors. Effectors in plant pathogens were initially discovered following formulation of the gene-for-gene interaction model between a pathogen avirulence (*Avr*) gene, now regarded as an effector-encoding gene, and the product of a plant disease resistance (*R*) gene (Flor, 1971). Originally, *Avr* gene products were always thought to be recognised directly by *R* gene products, leading to immune activation and an incompatible interaction that stops disease progression (Dangl & Jones, 2001). However, with the discovery of more pathogen-secreted proteins with various functions, the broader term 'effector' was adopted to include all secreted proteins, whether recognised by the host or not (Hogenhout *et al.*, 2009, Win *et al.*, 2012).

Plant innate immunity was initially proposed to follow a two-layered model of defence (Jones & Dangl, 2006). In the first layer, pattern recognition receptors (PRRs) recognise cross-species pathogen-associated molecular patterns (PAMPs) along with self-derived molecules, such as damage-associated molecular patterns (DAMPs), to initiate PAMP-triggered immunity (PTI) (Couto & Zipfel, 2016). The recognition of PAMPs, such as flagellin, chitin and glucan, triggers the production of reactive oxygen species (ROS), hydrolytic enzymes (proteinases, chitinases, and glucanases) and antimicrobial compounds while also activating mitogen-activated protein kinase (MAPK) cascades, modulating transcription, cell-wall callose deposition and ion fluctuations (Liu *et al.*, 2013, DeFalco & Zipfel, 2021). This basal immunity often inhibits host colonisation. However, pathogens have evolved to

counteract PTI by targeting PAMP production, PAMP release, and PAMP perception and signalling (Hogenhout *et al.*, 2009, Win *et al.*, 2012, Buscaill & van der Hoorn, 2021). For instance, many plant-pathogenic bacteria can escape flagellin-derived peptide flg22 recognition through the generation of various undetectable peptide epitopes (Cheng *et al.*, 2021, Sanguankiattichai *et al.*, 2022). Additionally, the *Pseudomonas syringae* effector AprA (alkaline protease), a zinc metalloprotease, is able to degrade free flagellin evading perception (Pel *et al.*, 2014). Filamentous pathogen effectors suppress PTI through similar mechanisms. For example, the fungal pathogen *Cladosporium fulvum* secretes a cysteine protease inhibitor suppressing PAMP perception (Rooney *et al.*, 2005), and the oomycete *Phytophthora spp.* secretes both cysteine protease inhibitors (Tian *et al.*, 2004, Tian *et al.*, 2005) and glucanase inhibitors (Rose *et al.*, 2002).

In response to pathogens deploying effectors to suppress PTI, plants activate a secondary layer of defence known as effector-triggered immunity (ETI), formally known as the *Avr-R* interaction (Jones & Dangl, 2006). This secondary layer encompasses the perception of effectors by intracellular immune responses, most of which belong to the nucleotide-binding leucine-rich repeat (NLR) receptor family (Kourelis & van der Hoorn, 2018). ETI is mainly recognised for instigating a localised programmed cell death response known as the hypersensitive response (HR), which inhibits the growth of the pathogen (Dodds & Rathjen, 2010). However, effector-NLR recognition also activates other immune signalling responses, including the ROS burst, MAPK cascades, phytohormone signalling, transcriptional reprogramming, and calcium fluxes (Cui *et al.*, 2015). Therefore, although at first PTI and ETI were thought to act independently, with many similarities between their immunity triggers recent studies have suggested crosstalk between these pathways, leading to an integrated immune response that enhances one another (Thomma *et al.*, 2011, Ngou *et al.*, 2021, Yuan *et al.*, 2021). Equally, effectors have been demonstrated to suppress PTI, ETI, or both, by acting on commonly activated signalling pathways or differentiated components. For instance, the *P. syringae* HopA1 effector has been found to have a dual function, reducing the flagellin-induced PTI response and suppressing ETI-induced HR (Guo *et al.*, 2009), which suggests a dynamic

interaction between plant immunity and pathogen-effector-mediated suppression. This continuous plant-pathogen interaction instigates a rapid co-adaptation of species to survive each other, driving the so-called evolutionary arms race. Pathogens evolve extensive effector repertoires to counter PTI responses which are perceived by immune receptors and then evolve by mutation or loss, to enable virulence once again (Dodds & Rathjen, 2010). This dynamic also underpins the boom-bust cycle in modern agriculture, where the deployment of *R* genes into monocultures triggers an initial 'boom' in productivity; however, under intense selective pressure, pathogens evolve new effectors to evade detection, ultimately resulting in a 'bust' as crop resistance breaks down (Rouxel & Balesdent, 2017, Fouché *et al.*, 2018).

1.2 Effector secretion systems

Effectors can be categorised based on where they function; cytoplasmic effectors are delivered into host plant cells whereas apoplastic effectors act extracellularly in the apoplast (Abramovitch *et al.*, 2006, Birch *et al.*, 2006, Kamoun, 2006, Misas-Villamil & van der Hoorn, 2008). While both cytoplasmic and apoplastic effectors are secreted, their delivery mechanisms vary depending on the pathogen and sometimes the effector function.

The first studied effector delivery system was the Type III Secretion System (T3SS) in Gram-negative bacteria, such as *P. syringae*, *Xanthomonas spp.*, *Salmonella sp.*, *Erwinia amylovora*, and *Ralstonia solanacearum* (Lindgren *et al.*, 1986, Petnicki-Ocwieja *et al.*, 2002, Galán & Wolf-Watz, 2006). The T3SS resembles a syringe-like structure that allows direct effector delivery into the host cells. It does this by connecting the bacterial and host membranes via a filament called a pilus (Roine *et al.*, 1997). Proteins secreted through this machinery typically contain a 50-100 amino acid N-terminal sequence required for translocation, a feature that has served as the foundation for computational predictions of T3SS-delivered effectors in plant and human pathogens (Guttman *et al.*, 2002, Lovelace *et al.*, 2023).

However, Gram-negative bacteria have since been found to possess other effector delivery systems (Costa *et al.*, 2015), including type IV and type VI protein secretion systems, which also cross both pathogen and host membranes (Christie *et al.*, 2005, Filloux *et al.*, 2008).

Gram-positive bacteria and certain phloem and xylem colonisers, such as *Candidatus* Liberibacter, and *Xylella sp.*, do not exhibit a T3SS. However, they possess general secretion (sec) and twin-arginine translocation (tat) pathways (Natale *et al.*, 2008). In contrast to Gram-negative bacteria, their effector delivery relies on the existence of a signal peptide (SP), a short N-terminal amino acid sequence that regulates secretion and translocation, analogous to those found in eukaryotic pathogens (Petre & Kamoun, 2014, Lovelace *et al.*, 2023). Therefore, eukaryotic effectors can also be predicted by the presence of a SP (Sperschneider *et al.*, 2016, Teufel *et al.*, 2022). However, not all secreted proteins function as effectors making it challenging for prediction methods to differentiate between them based solely on SP identification (Lovelace *et al.*, 2023). Identifying additional motifs, such as the N-terminal RXLR translocation-related motif present in effectors of *Phytophthora spp.*, can therefore assist in addressing this issue (Jiang *et al.*, 2008).

Parasitic plants and certain filamentous pathogens, including oomycetes and fungi, uptake host nutrients and deliver effectors through a specialised biotrophic cell called a haustorium (Hahn & Mendgen, 2001, Panstruga, 2003, Kokla & Melnyk, 2018). This peg-like structure separates the pathogen from the host cytoplasm through *de novo* plant-derived membrane called the extrahaustorial membrane (EHM) (Bozkurt & Kamoun, 2020). In filamentous pathogens that grow inside the host without haustoria, such as *Magnaporthe oryzae*, the pathogens can move from cell to cell through intracellular invasive hyphae (IH), which are also enclosed by a newly formed plant-derived membrane compartment, referred to as the extra-invasive hyphal membrane (EIHM) (Kankanala *et al.*, 2007). These membrane-rich structures enable apoplastic effector translocation through a conventional Golgi-dependent pathway from the hyphal tip, and cytoplasmic effectors translocation

through a non-conventional exocyst-dependent pathway (Giraldo *et al.*, 2013, Oliveira-Garcia & Valent, 2021). Before plant internalisation, cytoplasmic effectors localise to a structure called the Biotrophic Interfacial Complex (BIC) (Mentlak *et al.*, 2011, Quime *et al.*, 2025). This is also composed of plant-derived membrane and situated outside of the fungal cell wall. It has been reported in both a fungal and oomycete pathogen that cytoplasmic effectors enter the host cytoplasm through manipulation of host clathrin-mediated endocytosis (Oliveira-Garcia *et al.*, 2023, Wang *et al.*, 2023a).

In plant-parasitic nematodes, effectors are synthesised in the pharyngeal gland cells, which consist of subventral glands and a dorsal gland (Bird, 1983, Hussey & Mims, 1990), thus identifying promoter motifs associated with gland-specific expression has facilitated the prediction of nematode effectors (Eves-van den Akker & Birch, 2016, Espada *et al.*, 2018). Once synthesised, effectors are subsequently delivered into the host through a specialised feeding organ called a stylet, which resembles the T3SS of plant pathogenic bacteria (Davis *et al.*, 2008). Aphids and whiteflies are examples of other plant herbivores that secrete effectors through a feeding stylet (Hogenhout & Bos, 2011). Though different to that of nematodes, these plant-feeding insects produce their effectors within salivary glands (Musser *et al.*, 2002, Harmel *et al.*, 2008, Naalden *et al.*, 2021).

1.3 The plant pathogen effector repertoire

Effectors are known to have a variety of host targets and functions that enable host adaptation and immune suppression (Hogenhout *et al.*, 2009, Win *et al.*, 2012, Toruño *et al.*, 2016). Investigating effector molecular functions has become a widely used approach to understanding the complexity of host-microbe interactions (Hogenhout *et al.*, 2009). Since cloning the first effector-encoding gene, *P. syringae avrA* (Staskawicz *et al.*, 1984) over 40 years ago, abundant research has advanced our knowledge of how effectors operate at the molecular level. In human pathogenic bacteria, effectors have been extensively studied and found to have roles in

manipulating host cell signalling, morphogenesis, vesicle transport, metabolism, and immune systems (Staskawicz *et al.*, 2001, Galán, 2009). However, this introduction will focus exclusively on effectors from plant pathogens.

1.3.1 Enzymatic activity and enzyme inhibition

Numerous plant pathogen effectors possess enzymatic activities such as proteases, ubiquitin ligases (E3 ligase activity), hydrolases, kinases, phosphatases, NADases, and acetyltransferases to modulate host biology (Abramovitch *et al.*, 2006, Kamoun, 2006, Hogenhout *et al.*, 2009, Toruño *et al.*, 2016, Hulin *et al.*, 2023, Oliveira-Garcia *et al.*, 2024). Examples of enzymatic effectors in the apoplast include degrading enzymes that break down plant-derived cellulose and pectin (β-1,4-endoglucanases and pectinases) (Annis & Goodwin, 1997), and pathogenesis-derived proteins (PRs), such as flagellin proteases, glucanases, and chitinases, to prevent recognition (Pel *et al.*, 2014, Martínez-Cruz *et al.*, 2021, Liu *et al.*, 2023). Enzymatic effectors that function within the host cytoplasm include the *P. syringae* T3SS effector proteases AvrPphB and AvrRpt2, which target host PBS1 kinase and immune regulator protein RIN4, respectively, for their cleavage (Chisholm *et al.*, 2005). AvrRpt2 requires a host-derived co-factor cyclophilin for its proper folding and functionality, a discovery which introduced the novel concept of host effector helpers (Coaker *et al.*, 2005, Coaker *et al.*, 2006).

Effectors can also target plant enzymes to inhibit their function. Examples of enzyme-inhibiting apoplastic effectors include Avr2, which is secreted by *C. fulvum* to inhibit defence-related cysteine proteases (Rooney *et al.*, 2005, Shabab *et al.*, 2008), and Pep1, which is secreted by *Ustilago maydis* to suppress host peroxidase activity leading to ROS production inhibition (Hemetsberger *et al.*, 2012). While acting in the host cytoplasm, the T3SS effector AvrPto shows inhibition of immune-related kinase activity (Xiang *et al.*, 2008), and the T3SS effector HopZ1a is an acetyltransferase targeting the plant cytoskeleton, which is thought to disrupt the plant cell wall and secretory pathway (Lee *et al.*, 2012).

1.3.2 Masking PAMPs

Effectors have also been shown to target PAMPs in many ways to prevent plant perception and proteolytic attack (Buscaill & van der Hoorn, 2021). Among the reported strategies, effectors can target PAMP production either at the protein level (Cheng *et al.*, 2021) or through transcriptional downregulation (Sanguankiattichai *et al.*, 2022). Additionally, many effectors are known to degrade or sequester PAMPs to prevent detection. For example, chitin-binding sequestering effectors are conserved among pathogenic fungi and possess a lysine motif (LysM). These include effectors Avr4 and Ecp6 from *C. fulvum* (Van Esse *et al.*, 2007, de Jonge *et al.*, 2010), effectors Mg1LysM and Mg3LysM from *Zymoseptoria tritici* (Tian *et al.*, 2021), and Slp1 from *M. oryzae* (Mentlak *et al.*, 2012), all of which have been reported to inhibit chitin perception to prevent activation of the host chitin elicitor receptor kinase (CERK), suppressing PTI.

1.3.3 Vesicle trafficking modulation

Plants can defend themselves from pathogens through modulating membrane dynamics (Gu *et al.*, 2017). Therefore, different components of the vesicle trafficking machinery are among conserved effector targets. Manipulation of host vesicle trafficking and autophagy are thought to suppress immunity and redirect nutrients to the pathogen (Grosshans *et al.*, 2006, Petre *et al.*, 2021, Oliveira-Garcia *et al.*, 2024). Well-documented examples exist of oomycete effectors disrupting Rab8-mediated vesicle trafficking pathways. For instance, the *P. infestans* effector PexRD52 can selectively activate plant starvation-induced autophagy at the pathogen interface (Pandey *et al.*, 2021). By contrast, the effector PiE354, from the same pathogen, can subvert host immunity-related secretion (Yuen *et al.*, 2024), demonstrating two instances of effectors manipulating host membrane dynamics with different aims. Other reported effectors that disrupt host vesicle trafficking include *P. infestans* effectors Avrblb2 and Avr2 (Bozkurt *et al.*, 2011, Saunders *et al.*, 2012), *Phytophthora capsici* effector Pc12 (Kim *et al.*, 2024), *M. oryzae* effector Avr-Pii (De la Concepcion *et al.*, 2022), *P. syringae* effector HopM1 (Nomura *et al.*, 2006,

Nomura *et al.*, 2023), and *Ralstonia solanacearum* effector RipD (Wang *et al.*, 2023b).

1.3.4 Hormone biosynthesis

Effectors can also target plant hormones, such as salicylic acid (SA), jasmonic acid (JA), auxin, and ethylene (ET), which play critical roles in plant immunity (Shigenaga & Argueso, 2016). For example, the root-knot nematode (*Meloidogyne spp*.) effector Mi-CM-3 can suppress production of SA through transcriptional inhibition (Wang *et al.*, 2018). Similarly, the *M. oryzae* effector lug4 acts as a transcriptional repressor of ET by modulating ET biosynthesis-related transcription factors (Liu *et al.*, 2022b). *P. sojae* and *Verticillium dahliae* effectors Pslsc1 and Vdlsc1 can directly disrupt the plant SA biosynthesis pathway (Liu *et al.*, 2014). While *P. syringae* effectors HopX1 and HopZ1 degrade the JA transcriptional repressor JAZ to induce JA production leading to stomatal opening (Jiang *et al.*, 2013, Gimenez-Ibanez *et al.*, 2014). Additionally, some pathogens can hijack hormone signalling by increasing antagonistic hormones. Effectors like *Xanthomonas campestri* AvrXccC manipulate ET/JA signalling to suppress SA pathways, demonstrating that pathogens evolve to precisely disrupt hormone biosynthesis, tipping the balance toward susceptibility (Kazan & Lyons, 2014).

1.3.5 Transcriptional regulation

The transcription activator-like (TAL) effectors from *Xanthomonas spp*. were the first effectors discovered to modulate plant gene transcription (Chakrabarty *et al.*, 1997, Boch *et al.*, 2009). TAL effectors induce host gene expression by directly binding to the promoters of their targets. For instance, the *Xanthomonas oryzae* pv. *oryzae* effectors PthXo1, AvrXa7, and PthXo target the promoters of the *SWEET* sugar transporter genes to promote bacterial growth (Chen *et al.*, 2010, Streubel *et al.*, 2013). Similarly, *M. oryzae* effectors MoHTR1 and MoHTR2 can translocate to the host nucleus and affect the expression of immunity-related genes (Kim *et al.*, 2020). However, direct binding of host gene promoters is not the only way effectors can

manipulate gene expression (Win *et al.*, 2012, Giraldo & Valent, 2013, Toruño *et al.*, 2016). For instance, the *Phytophthora sojae* effectors PsR1 and PsR2 can suppress host RNA silencing (Qiao *et al.*, 2013), and the conserved cyst nematode (*Heterodera and Globodera spp.*) effector 30D08 can interact with the host spliceosome protein to enhance targeted gene expression (Verma *et al.*, 2018).

1.3.6 Host immunity signalling

Well-documented examples exist for effectors targeting immune suppression and evasion, with bacterial T3SS effectors notably recognised for their immune-inhibiting responses (Abramovitch *et al.*, 2006). For example, the *P. syringae* pv *tomato* AvrPtoB is an E3 ubiquitin ligase that targets PRRs for their degradation, such as FLS2 (FLAGELLIN SENSING 2), EFR (ELONGATION FACTOR TU RECEPTOR) and CERK1 (CHITIN ELICITOR RECEPTOR KINASE 1) (Göhre *et al.*, 2008, Shan *et al.*, 2008, Gimenez-Ibanez *et al.*, 2009). This same effector can also act as a kinase inhibitor (Xing *et al.*, 2007), blocking the receptor kinase BAK1, the signalling partner of both FLS2 and EFR (Zipfel *et al.*, 2006, Chinchilla *et al.*, 2007). Other *P. syringae* effectors reported to inhibit BAK1 include HopF2 and AvrPto (Zhou *et al.*, 2014). However, PRR signalling can be suppressed by effectors through many other mechanisms, such as the inhibition of PRR translation (Nicaise *et al.*, 2013) and PRR downstream components, including plant receptor-like cytoplasmic kinases (RLCKs) and mitogen-activated protein kinases (MAPKs) (Shao *et al.*, 2003, Zhang *et al.*, 2007).

To date, the majority of studied effectors have been shown to suppress PTI; however, some effectors have evolved to interfere with ETI through direct or indirect NLR inhibition or downstream NCR (NLR-Required for Cell death) network components (Wu & Derevnina, 2023). Acting indirectly, the *P. syringae* effector HopBF1 inhibits the chaperone HSP90 necessary for correct folding of immune receptors and protein kinases (Lopez *et al.*, 2019). Acting directly, the *P. syringae* effector HopZ3 is an acetyltransferase which is shown to specifically inactivate the host target NLR, RPM1 (Jeleńska *et al.*, 2021). Additionally, targeting the NRC

network, the effector SPRYSEC15 (SS15) from the cyst nematode *Globodera rostochiensis* can bind to NRC2 and NRC3 to disturb their function in triggering cell death (Derevnina *et al.*, 2021).

Another common immunity-related target for effectors is the heavy metal-associated (HMA)-like proteins. Although the precise role of HMA-like proteins in plant defence remains unclear, effectors from various pathogens have been shown to target them (Imran *et al.*, 2016, Radakovic *et al.*, 2018, Maidment *et al.*, 2021). In *M. oryzae,* for example, effectors targeting HMA-like proteins share structural conservation and temporal co-regulation, suggesting a critical role of these effectors in fungal disease progression (de Guillen *et al.*, 2015, Maidment *et al.*, 2021, Yan *et al.*, 2023, Oikawa *et al.*, 2024). As an evolutionary strategy to stop disease, some host NLRs also possess integrated HMA domains to subvert pathogen effectors that trigger ETI, leading to an incompatible interaction (Cesari *et al.*, 2013, De la Concepcion *et al.*, 2018, Guo *et al.*, 2018).

As pathogens are under selective pressure to evade host immunity, functional redundancy is prevalent among effectors (Win *et al.*, 2012). Examples include *P. syringae* effectors AvrRmp1, AvrB, and AvrRpt2, which can all target the same host protein, RIN4 (Chisholm *et al.*, 2005, Coaker *et al.*, 2005, Grant *et al.*, 2006); the *M. oryzae* effector AvrPiz-t which can interact with both a bZIP-type transcription factor and E3 ligases to suppress plant cell death (Park *et al.*, 2012b, Wang *et al.*, 2016); and *P. infestans* Avr3a which targets GTPase dynamic-related proteins to suppress PTI and E3 ligases, inhibiting HR (Bos *et al.*, 2010, Chaparro-Garcia *et al.*, 2015). Furthermore, it has also been reported that bacteria, which normally possess a suite of 12-40 effectors (Dillon *et al.*, 2019), can cooperatively potentiate the virulence of a population through the activity of individual effectors (Ruiz-Bedoya *et al.*, 2023). However, it is also true that when microorganisms compete for a host, effectors can be secreted to disrupt each other in the race for host colonisation (Snelders *et al.*, 2018). For instance, fungal pathogen *V. dahliae* secretes antimicrobial effectors VdAve1 and VdAMP2 that can manipulate the soil microbiome to promote fungal pathogenesis (Snelders *et al.*, 2020). Consequently, the range of effector functions

and targets expands and becomes more complex when all these factors are considered.

1.4 Effector gene regulation

Successful host colonisation by pathogens relies on the precise spatiotemporal regulation of effector gene expression. Large-scale transcriptomic studies have shown that this regulatory orchestration aligns closely with disease progression, suggesting a meticulous regulation of effector genes (Kleemann *et al.*, 2012, Toruño *et al.*, 2016, Nobori *et al.*, 2020, Siddique *et al.*, 2022, Yan *et al.*, 2023).

1.4.1 Effector gene regulation in bacteria

In Gram-negative bacteria, most T3SS effector genes can be found within a highly conserved genetic locus composed of hypersensitive response and pathogenicity (*hrp*) genes (Alfano *et al.*, 2000, Chang *et al.*, 2005). This *hrp* cluster encodes both the T3SS structural components and T3SS effector genes, allowing for their simultaneous regulation (Xiao *et al.*, 1992, Leach & White, 1996). The *hrp* master regulator is an extracytoplasmic function (ECF) alternative sigma factor (HrpL) that can directly bind the '*hrp-box*' motif within target promoters (Alfano *et al.*, 2000, Lam *et al.*, 2014). Extensive research on *hrpL* transcription has elucidated the different regulatory networks that enable fine-tuning of T3SS deployment (Xiao & Hutcheson, 1994, Hutcheson *et al.*, 2001) and the cues contributing to effector secretion, including plant-derived compounds, quorum sensing, and host-plant environment (Francis *et al.*, 2002, Tsuge *et al.*, 2014, O'Malley & Anderson, 2021). Other gene clusters which harbour secretion structure-encoding genes and effector-encoding genes can be found in Gram-negative bacteria, including the T4SS (Wallden *et al.*, 2010) and the T6SS (Habich *et al.*, 2025) clusters.

Gram-positive bacteria also contain pathogenicity-associated genomic regions; however, effectors do not appear to be organised in compact genomic clusters as

seen for Gram-negative bacteria (Gal-Mor & Finlay, 2006). Consequently, our understanding of how these genes are regulated remains limited. Nevertheless, two-component systems (TCSs) that mediate cellular responses to a range of internal and external stimuli (Stock *et al.*, 2000) have been shown to play a role in effector gene regulation for both Gram-positive and Gram-negative bacteria (Gao & Stock, 2009). Furthermore, a conserved transcription regulator, PrfA, can regulate virulence and effector gene deployment in *Listeria monocytogenes* (Scortti *et al.*, 2007), with post-transcriptional regulation, sRNAs, and the colonising environment regulating PrfA itself (Johansson & Freitag Nancy, 2019).

1.4.2 Effector gene regulation in plant-parasitic nematodes

In plant-parasitic nematodes, targeted transcriptomics led to the identification of a subventral gland transcription factor named SUGR-1 involved in regulating effectors (Pellegrin *et al.*, 2025). Upon perception of plant extract cues, termed effectorstimulins, this positive transcriptional regulator binds the promoter of target genes, including predicted effector genes (Molloy *et al.*, 2024). SUGR-1 was also found to regulate other transcription factors. Therefore, these results suggest that SUGR-1 is part of a hierarchical regulatory network necessary for plant-parasitic nematode infection controlled and potentiated by host stimuli (Pellegrin *et al.*, 2025).

1.4.3 Effector gene regulation in filamentous pathogens

In filamentous fungi, many transcriptional regulators play roles in controlling effector gene expression as well as driving disease progression (Tan & Oliver, 2017, John *et al.*, 2021, Wang *et al.*, 2024). In Ascomycetes and Basidiomycetes, there is significant transcription factor diversification, a trait that is often correlated with more complex regulatory networks (Raffaele & Kamoun, 2012). Among the 80 transcription factor families identified in fungi, the most expanded are the homeodomain-like, Zn_2Cys_6 (C6 zinc cluster), and C_2H_2-like zinc finger proteins (Shelest, 2017). A well-conserved homeodomain transcription factor, for example,

is the fungal-specific Ste12. Initially found to control mating and morphological transitions in *Saccharomyces cerevisiae* downstream of the Fus3/Kiss1-MAPK signalling pathway (Song *et al.*, 1991, Cook *et al.*, 1996, Tedford *et al.*, 1997), which is the functional equivalent of the Pmk1 MAPK pathway in filamentous fungi (Xu & Hamer, 1996). Ste12 orthologues play critical roles in pathogenicity, effector regulation, infection-related and sexual development, sporulation, and nutritional response in pathogenic fungi (Rispail & Di Pietro, 2010, Wong Sak Hoi & Dumas, 2010). An example of a Zn_2Cys_6 transcription factor is the *Alternaria alternata* AbPf2, which is crucial for virulence and acts as a transcriptional activator of a subset of effector-encoding genes (Cho *et al.*, 2013). Pf2 orthologues in necrotrophic fungi *Parastagonospora nodorum* and *Pyrenosphora tritici-repentis* were also reported to regulate important effectors, including ToxA and Tox3 (Rybak *et al.*, 2017, Jones *et al.*, 2019). While Pf2 orthologues in hemibiotrophic fungi, such as *M. oryzae, Zymoseptoria tritici,* and *Fusarium graminearum*, were found to be important in virulence, infection-related morphogenesis, sporulation, stress tolerance, and carbohydrate metabolism (Chung *et al.*, 2013, Oh *et al.*, 2016, Habig *et al.*, 2020). C_2H_2-like zinc finger proteins are well-conserved regulators that are mostly connected to control stress tolerance, development, and metabolic activities (Fedotova *et al.*, 2017, John *et al.*, 2021). However, in *M. oryzae,* a C_2H_2 transcription factor, Con7, was found to be important for hyphal growth and plant invasion, possibly through the control of cell wall-modulating enzymes (Odenbach *et al.*, 2007). Homologues of Con7 were also found to regulate the expression of the necrotrophic effector Tox3 in *P. nodorum* (Lin *et al.*, 2018).

Furthermore, the transcription factor Wor1 of *Candida albicans* is another highly conserved regulator across various fungal species (Huang *et al.*, 2006). This transcription factor belongs to the Git1/Pac2 family known to be regulators of morphological transition, hyphal growth, sexual development, secondary metabolism biosynthesis, and effector-encoding genes (Cain *et al.*, 2012, John *et al.*, 2021). The orthologue of Wor1 regulates virulence and effector gene expression in many plant pathogenic fungi (Michielse *et al.*, 2009, Brown *et al.*, 2014, Chen *et al.*, 2014). In *U. maydis,* the Wor1 orthologue Ros1, was shown to orchestrate

infection-related reprogramming, controlling 80 transcription factors and 198 effectors (Tollot *et al.*, 2016), suggesting its role as a master regulator.

Further transcription factor families in filamentous fungi include the GATA family, the basic leucine-zipper and basic helix-loop-helix families, and the Velvet family (Deppmann *et al.*, 2006, Chen *et al.*, 2012, Ahmed *et al.*, 2013). Although fewer examples have been reported for these regulators, they have all been reported to control various molecular functions, including sporulation, secondary metabolism biosynthesis, hyphal growth, stress tolerance, sexual reproduction, infection-related morphogenesis, and effector-encoding genes (Tan & Oliver, 2017, John *et al.*, 2021).

While transcriptional control is crucial for effector gene expression, both signal transduction pathways and epigenetic modifications can also contribute to this regulation (Soyer *et al.*, 2014, Sakulkoo *et al.*, 2018, Zhang *et al.*, 2021, Tang *et al.*, 2023). For instance, the Pmk1 MAPK has been reported to positively regulate effector-encoding genes during invasive growth (Sakulkoo *et al.*, 2018) and the G-protein regulator Rgs1 has been shown to repress effector gene expression prior to host colonisation in *M. oryzae* (Tang *et al.*, 2023). In *Leptosphaeria maculans*, a switch in chromatin remodelling associated with histone modifications has been reported to drive pathogenesis, suggesting epigenetic control of virulence-associated gene functions (Soyer *et al.*, 2014). Consistent with this idea, an increase in methylation near virulence-associated genes has been shown to be important for their expression in *M. oryzae*, *U. virens,* and *Fusarium spp.* (Dallery *et al.*, 2019, Meng *et al.*, 2021, Tang *et al.*, 2021).

When considering the extensive transcription factor repertoire, signalling cascades, and epigenetic modifications involved in fungal pathogenesis, it becomes clear that effector genes are likely to be subject to complex regulation in pathogens (Tan & Oliver, 2017, John *et al.*, 2021). This is further supported by coordinated effector deployment in 'waves' during disease progression, synchronising fungal development and effector secretion to drive host colonisation (Kleemann *et al.*, 2012, Yan *et al.*, 2023).

In oomycete pathogens, effector genes have similarly been shown to undergo tight temporal regulation that is specific to different developmental stages (Qutob *et al.*, 2002, Schornack *et al.*, 2009). Despite the limited exploration of transcriptional regulators associated with pathogenesis in oomycetes, a MYB-related transcription factor, PsMyb37 from *P. sojae*, was recently identified as contributing to virulence and binding the promoter of 20 effector genes (Qian *et al.*, 2024). Additionally, increased methylation around the effector genes has been demonstrated to drive host adaptation in the same pathogen (Wang *et al.*, 2019). Therefore, despite being under-researched, fungi and oomycetes may regulate effectors through comparable transcriptional regulators and signal transduction pathways.

1.5 *M. oryzae* as a model organism to investigate effector gene regulation in filamentous pathogens

Fungi represent a large and diverse kingdom of eukaryotic life, which are exemplified by their osmotrophic feeding habit, in which depolymerising enzymes are secreted into the external environment to digest complex polymers, such as cellulose, polysaccharides, proteins, and lipids and the resulting simple sugars, amino acids and fatty acids are transported into fungal cells (Walker & White, 2017). Fungi are thought to have emerged ~500 million years ago (Taylor & Berbee, 2006) and can be divided into two major groups: early diverging monokarya (including the Cryptomycota, Chytridiomycota, and Zygomycota) and dikarya which undergo sexual reproduction forming specialised fruiting bodies (basidia) made by Basidiomycota and spore-bearing structures (asci) made by Ascomycota (Choi & Kim, 2017). The latter two groups emerged from a common ancestor comprising most known fungal diversity (Hibbett *et al.*, 2018). Fungi are further classified by their morphological growth and trophic strategies. Yeast-forming fungi, for example, such as *Saccharomyces cerevisiae* and *Candida albicans*, typically grow as unicellular yeasts or are dimorphic, while filamentous fungi (such as the Pezizomycotina) grow as multicellular hyphae, which form a mycelium (Wendland, 2001). Most plant pathogenic fungi are filamentous and exhibit a range of ecological roles, including

biotrophs, necrotrophs, hemibiotrophs, saprotrophs, symbionts, commensals, and endophytes (Crous *et al.*, 2015, Doehlemann *et al.*, 2017). For example, biotrophs, such as *Ustilago maydis*, *Claviceps purpurea* and *Puccinia graminis*, colonise and feed from living tissue (Fei & Liu, 2023), while necrothrophs, like *Botrytis cinerea* and *Sclerotinia sclerotiorum,* kill host cells and survive from necrotic material (Derbyshire & Raffaele, 2023). Hemibiotrophic fungi, including *Fusarium oxysporum* and *Colletotrichum* species, are situated along a spectrum between biotrophy and necrotrophy (Münch *et al.*, 2008, Swett *et al.*, 2016). They establish a biotrophic relationship with the host and then switch to a necrotrophic mode of infection (Koeck *et al.*, 2011, Liao *et al.*, 2022). Saprotrophs, meanwhile, such as *Neurospora crassa* and *Aspergillus* species (Kuo *et al.*, 2014, Fang & Latgé, 2018), decompose organic matter, while symbionts such as *Rhizophagus irregularis* form beneficial mycorrhizal associations with plants (Mathieu *et al.*, 2018).

Magnaporthe oryzae, also known by its synonym *Pyricularia oryzae Sacc.*, is a haploid ascomycete filamentous fungus primarily recognised as the causal agent of rice blast disease (Valent *et al.*, 1991, Talbot, 2003, Zhang *et al.*, 2016). The blast fungus is a prominent example of a hemibiotrophic fungus that can infect over 50 different grass species from tropical and temperate climates; however, *M. oryzae* threatens global food security by causing significant diseases in rice (*Oryza sativa*), barley (*Hordeum vulgare*), wheat (*Triticum aestivum*), and finger millet (*Eleusine coracana*) (Wilson & Talbot, 2009, Langner *et al.*, 2018). By affecting some of the most widely consumed crops, blast disease threatens over 85 countries and destroys between 10% and 30% of the global annual rice harvest (Skamnioti & Gurr, 2009, Wilson & Talbot, 2009). Its rapid host evolutionary adaptability (Huang *et al.*, 2014) and a changing climate favouring humidity-driven pathogens (Bebber & Gurr, 2015) mean that *M. oryzae* continues to be a major global threat. As a result, the global agricultural and economic damage attributed to *M. oryzae* has prompted extensive research on the fungus and its hosts, which have now become established models for investigating fungal pathogenesis and plant immunity. The availability of comprehensive genome sequences for numerous isolates of *M. oryzae* and its host organisms, such as rice and wheat (Dean *et al.*, 2005, Brenchley *et al.*, 2012, Yano

et al., 2016), combined with its amenability for genetic manipulation, presents a compelling justification for its utilisation as a model organism (Molinari & Talbot, 2022). Consequently, the blast fungus has been extensively studied over the past few decades, leading to a deeper understanding of the molecular basis of blast disease (Valent & Chumley, 1991, Talbot, 2003, Wilson & Talbot, 2009, Eseola *et al.*, 2021, Oliveira-Garcia *et al.*, 2024).

1.5.1 Overview of blast disease caused by *M. oryzae*

To cause rice blast disease *M. oryzae* produces asexual spores, known as conidia, released by conidiophores that emerge from disease lesions on the host. These three-celled airborne conidia are transported by water and/or wind to land on new host plants. Attachment to the hydrophobic waxy surface of the leaf is facilitated by the secretion of spore tip mucilage released by the apical cell (Hamer *et al.*, 1988, Bourett & Howard, 1990). Hydrophobin proteins, such as Mpg1 and Mhp1, are implicated in adhesion, surface perception, and the action of cutinases in attaching to the plant surface (Talbot *et al.*, 1993, Talbot *et al.*, 1996, Whiteford & Spanu, 2002, Kim *et al.*, 2005). Upon surface contact and hydration, the conidium rapidly germinates, forming a polarised, narrow germ tube that emerges from the same apical cell (Bourett & Howard, 1990). The tip of the germ tube then starts to swell and differentiate into a specialised single cell known as an appressorium (Ryder *et al.*, 2022). For this to occur, *M. oryzae* switches from polarised to isotropic growth, a critical transition to achieve infection called hooking (Bourett and Howard, 1990). Appressoria are specialised dome-shaped structures required for plant infection by allowing physical rupture of the host cuticle (Wilson & Talbot, 2009). Generating a fully functional appressorium is the most important prerequisite for establishing rice blast disease. The first essential cue in this process is the sensing of a hard-hydrophobic surface. For this to occur *M. oryzae* utilises two key signalling pathways: the Cyclic adenosine monophosphate (cAMP) response pathway, and the highly conserved Pathogenicity MAP Kinase 1 (Pmk1) signalling pathway regulated by G-protein signalling in the developing germ tube (Xu & Hamer, 1996, Talbot, 2003). Additionally, forming a functional appressorium requires the apical conidial

cell to undergo a single round of mitosis, and a daughter nucleus migrates through the germ tube to the insipient appressorium. Consequently, development is tightly controlled by the cell cycle (Saunders *et al.*, 2010, Oses-Ruiz *et al.*, 2016).

To successfully breach the host cuticle, the appressorium must create enormous turgor pressure, up to 8.0 MPa, by generating and accumulating a layer of melanin between the cell plasma membrane and the cell wall (Ryder *et al.*, 2019, Ryder *et al.*, 2023). This allows the appressorium to take up water through osmosis by rapidly accumulating glycerol and polyols (de Jong *et al.*, 1997, Talbot, 2003). These molecules are known to be synthesised *de novo* and recycled through autophagy, which simultaneously happens at the original three-celled (de Jong *et al.*, 1997, Veneault-Fourrey *et al.*, 2006, Kershaw & Talbot, 2009, Wengler & Talbot, 2025). Once the required turgor threshold is reached in the appressorium, this is sensed by a turgor-sensing histidine-aspartate kinase Sln1; pressure is then translated into mechanical force, enabling host penetration (Ryder *et al.*, 2019). Prior to host penetration, the cytoskeleton of the appressorium reorientates at the base of the infecting cell in a melanin-depleted region (Dagdas *et al.*, 2012). A filamentous-actin (F-actin) network is organised around the cell pore, providing cortical rigidity prior to penetration peg emergence (Bourett & Howard, 1992, Dagdas *et al.*, 2012). This actin remodelling requires septin guanosine triphosphatases (GTPases), key cytoskeleton components that can form dynamic hetero-oligomeric complexes (Sirajuddin *et al.*, 2007, Dagdas *et al.*, 2012, Gupta *et al.*, 2015). During rice infection, a septin ring forms at the base of the appressorium, where it co-localises with F-actin, organising polarity components and protein secretion at the appressorium pore (Eisermann *et al.*, 2023). Rupture of the leaf cuticle allows the penetration peg to enter the plant and differentiate into specialised invasive hyphae, representing a second switch from isotropic to polarised growth (Bourett & Howard, 1990).

Once inside the host, *M. oryzae* rapidly adapts to the new environment, and the plant responds to the infection through its two-layered immune system (Jones and Dangl, 2006). In return, *M. oryzae* responds through effector deployment;

apoplastic effectors are secreted through a Golgi-dependent pathway, while cytoplasmic effectors accumulate in a structure known as the Biotrophic Interfacial Complex (BIC), formed within each newly invaded cell (Mentlak *et al.*, 2011, Giraldo *et al.*, 2013). The internalisation of cytoplasmic effectors occurs through a focused region that manipulates host clathrin-mediated endocytosis (Oliveira-Garcia *et al.*, 2023). *M. oryzae* effectors enable adaptation to the colonising environment and suppress plant immunity by manipulating numerous host targets (Oliveira-Garcia *et al.*, 2024). After penetration, primary invasive hyphae rapidly fill epidermal cells, growing biotrophically (Kankanala *et al.*, 2007). Adjacent cells are accessed by the fungus through pit fields where plasmodesmata accumulate (Eseola *et al.*, 2021, Quime *et al.*, 2025). The morphological changes that hyphae undergo to cross to neighbouring cells are similar to appressorium-driven plant penetration, and are also regulated by the Pmk1 MAPK signalling pathway. These include hyphal constriction, forming an actomyosin ring at cell junctions, and establishing a structure called the transpressorium (Sakulkoo *et al.*, 2018, Cruz-Mireles *et al.*, 2021). After 4 to 5 days of initial infection necrotrophy occurs, and this is visually perceived on the leaf surface as small necrotic disease lesions. Under high humidity, new aerial conidiophores develop at this stage, and conidia are released, completing the *M. oryzae* infection cycle (Talbot, 2003), illustrated in Figure 1.1.

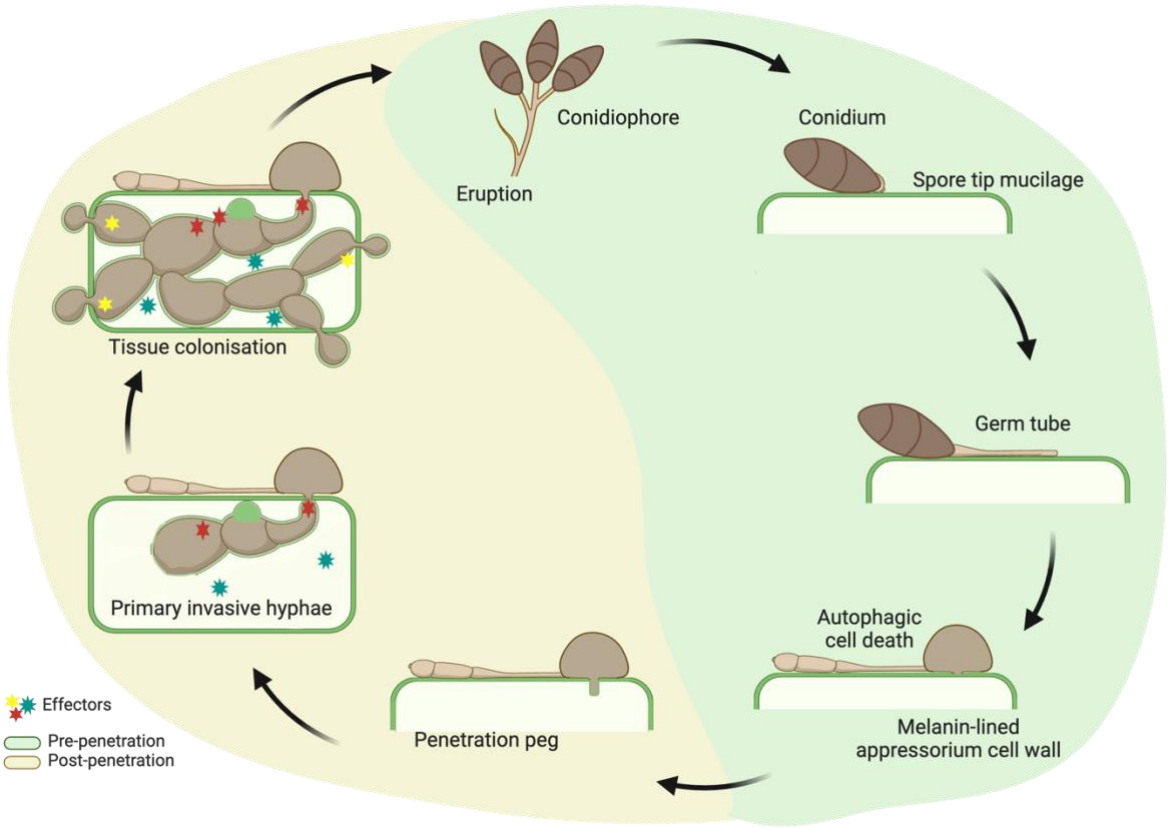

Figure 1.1 *M. oryzae* life cycle. The infection cycle of the rice blast fungus begins when a three-celled conidium, released by the eruption of the conidiophore, lands on the surface of a rice leaf. The spore attaches to the hydrophobic surface via spore tip mucilage and germinates, forming a polarised, narrow germ tube. The germ tube tip differentiates into a specialised cell known as the appressorium. For leaf penetration to occur, the three-celled conidium undergoes degradation through autophagy, and the appressorium matures by becoming melanised and accumulating high turgor pressure. This results in physical force that breaches the leaf cuticle, allowing a penetration peg to enter the rice epidermal cells. Once inside the host, the pathogen invades epidermal cells by filling them with colonising hyphae. After 4-5 days, conidiophores emerge from diseased lesions on the leaf surface, completing the entire cycle (Wilson and Talbot, 2009). (Image created using BioRender.com)

1.5.2 Appressorium development is controlled by the Pmk1 MAPK signal transduction pathway

MAPKs are critical regulators of fungal development and infection-related morphogenesis and have been widely studied in fungal pathogenesis (Zhao & Xu, 2007, Jiang *et al.*, 2018). In *M. oryzae*, the first characterised MAPK cascade was the Pmk1 signalling pathway, an orthologue of the yeast Fus3/Kss1, which is conserved in diverse fungal pathogens and is essential for virulence, regardless of whether the pathogen infects plants using an appressorium or not (Xu & Hamer, 1996, Turrà *et al.*, 2014, Jiang *et al.*, 2018, Frawley & Bayram, 2020). Nearly three decades since its discovery, the Pmk1 pathway has been shown to orchestrate multiple cellular processes, although it is best known for driving morphogenetic transitions during pathogenesis (Xu & Hamer, 1996, Sakulkoo *et al.*, 2018, Osés-Ruiz *et al.*, 2021).

Appressorium development is initiated when fungal cells detect surface hydrophobicity and plant-derived compounds via sensors, such as Msb2 and Sho1, which activate the Pmk1 signalling pathway (Liu *et al.*, 2011). This activation occurs through Ras-mediated signalling that triggers the MAPK cascade, where the MAPKKK Mst11 activates the MAPKK Mst7, subsequently activating the MAPK Pmk1 (Zhao *et al.*, 2005, Jiang *et al.*, 2018). The activation complex, comprising Mst7, Mst11, and the scaffold protein Mst50, modulates Pmk1 MAPK activity (Park *et al.*, 2006). Moreover, this Mst11-Mst7-Mst50 complex can also connect the Pmk1 pathway with the cyclic AMP (cAMP)-dependent protein kinase A pathway (Ryder & Talbot, 2015), integrating signalling through the G-protein coupled receptor Pth11 (DeZwaan *et al.*, 1999) and the G-protein subunit Mgb (Nishimura *et al.*, 2003), both of which regulate cAMP levels critical for appressorium initiation and maturation (Li *et al.*, 2012, Ryder *et al.*, 2022).

Pmk1 controls appressorium development and the subsequent penetration of host tissues by regulating downstream targets (Osés-Ruiz *et al.*, 2021, Cruz-Mireles *et al.*, 2024). Pic5, Hox7, and Znf1 transcription factors, for example, are necessary for appressorium formation (Kim *et al.*, 2009, Zhang *et al.*, 2011b, Cao *et al.*, 2016),

while Slf1 is required for invasive growth, and Mst12 is required for penetration and effector regulation (Park *et al.*, 2002, Kim *et al.*, 2009, Osés-Ruiz *et al.*, 2021). Additionally, Hox7 and Mst12 Pmk1-dependent phosphorylation is crucial to their function (Osés-Ruiz *et al.*, 2021), emphasising the critical role of this conserved MAPK pathway.

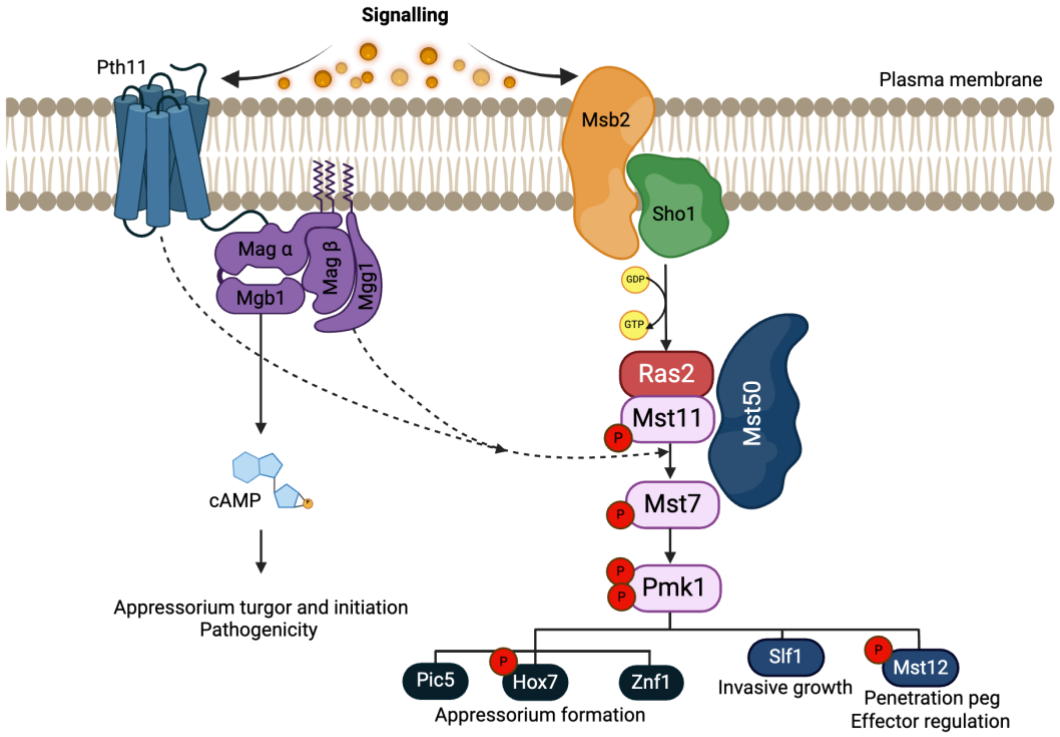

Figure 1.2 The *M. oryzae* Pmk1 MAPK signalling pathway. Schematic representation of the Pmk1 MAPK signalling pathway and its crosstalk with the cAMP-response pathway. Signalling sensors Msb2 and Sho1 activate the MAPK cascade through Ras proteins which initiate the Mst11-Mst7-Pmk1 phosphorelay to the final regulation of transcription factors Pic5, Hox7, Znf1, Slf1 and Mst12, all required for infection. G-protein coupled receptor Pth11 and G-proteins modulate cAMP levels upon external stimuli and crosstalk with the Pmk1 MAPKs pathway through the Mst11-Mst7-Mst50 protein complex (Adapted from Ryder et al., 2022). (Image created using Biorender.com)

1.5.3 Effector function in *M. oryzae*

M. oryzae is predicted to secrete 546 effectors during blast infection to facilitate disease progression and suppress plant immunity (Yan *et al.*, 2023). However, virulence functions—typically studied through expression, localisation, and targets *in planta*—have only been determined for a limited number of these secreted proteins (Valent & Khang, 2010, Oliveira-Garcia *et al.*, 2024).

The *M. oryzae* effector repertoire includes effectors that evade PAMP recognition, such as Slp1 (Secreted LysM Protein 1), a well-characterised secreted protein containing two lysine motifs (LysM) (Mentlak *et al.*, 2012). This effector accumulates at the invasive hyphae outer space, where it binds to chitin oligosaccharides and prevents the activation of the chitin elicitor binding protein (CEBiP). Consequently, the CEBiP receptor cannot activate immune responses such as the generation of ROS and defence-related gene expression (Mentlak *et al.*, 2012). *M. oryzae* can also target immune signalling in the cytoplasm; for example, Avr-Piz-t manipulates both the plant proteasome system and the host potassium uptake, leading to PTI suppression (Park *et al.*, 2012b, Shi *et al.*, 2018). Targeting host transcriptional regulation, MoHTR1 and MoHTR2 are secreted through the BIC and translocated to the host nucleus. They can associate with effector binding elements found in rice DNA, demonstrating host transcriptional reprogramming (Kim *et al.*, 2020). Targeting other host organelles, Avr-Pita encodes a zinc-dependent metalloprotease that localises to mitochondria. It was also the first Avr protein found to evidence fungal delivery into plant cytoplasm (Jia *et al.*, 2000, Orbach *et al.*, 2000). Avr-Pita specifically targets the cytochrome c oxidase (COX) assembly protein OsCOX11 part of the mitochondria electron transport chain, and this interaction is thought to manipulate ROS production (Smirnoff & Arnaud, 2019, Han *et al.*, 2021a). Cytoplasmic effector MoPtep1 (peroxisomes-targeted effector protein 1) targets host peroxisomes (Ning *et al.*, 2022), while Avr-Pik and Pwl2 target host HMA-proteins, evidencing a host defence function associated with HMA-containing proteins that has yet to be further investigated (Maidment *et al.*, 2021, Oikawa *et al.*, 2024, Were *et al.*, 2024). Biotrophy associate effectors include BAS3, which is

shown to localise at cell wall crossing points and is thought to have a potential role in intracellular host movement (Mosquera *et al.*, 2009). Targeting hormone biosynthesis, *M. oryzae* effector Molug4 transcriptionally represses ethylene biosynthesis, while lug6 and lug9 target both salicylic acid and ethylene pathways (Dong *et al.*, 2015, Liu *et al.*, 2022b). Additionally, the hydrolyse inositol pyrophosphate effector MoNUDIX can manipulate the plant phosphate sensing pathway to induce plant growth and exacerbate disease, modulating the host phosphate homeostasis (McCombe *et al.*, 2025).

While these examples illustrate our current knowledge of *M. oryzae* effectors, an overwhelming number of these secreted proteins still lack associated molecular functions. Consequently, high-throughput approaches are essential if we aim to understand the entire blast disease effector repertoire and the relative fitness contribution of each secreted protein (Valent & Khang, 2010, Oliveira-Garcia *et al.*, 2024). Moreover, the analysis of effectors is further complicated by the observation that effector-encoding genes typically demonstrate a significant degree of genetic diversity, which is driven by the evolutionary arms race between a pathogen and its host (Dodds & Rathjen, 2010, Kanzaki *et al.*, 2012). Although sequence-unrelated, structure prediction tools have identified some conservation among effector protein structures (Seong & Krasileva, 2021, Seong & Krasileva, 2023). *Magnaporthe* AVRs and ToxB-like (MAX) effectors illustrate an example of a family of fungal effectors that are sequence-unrelated but structurally similar (de Guillen *et al.*, 2015, Lahfa *et al.*, 2024, Le Naour--Vernet *et al.*, 2025). MAX effectors have been demonstrated to target HMAs, and transcriptomic analysis has revealed temporal co-regulation during rice blast disease (Yan *et al.*, 2023), suggesting an important timed function critical for host colonisation for this family of effectors (Oliveira-Garcia *et al.*, 2024).

1.5.4 Effector regulation in *M. oryzae*

Most *M. oryzae* effector genes are not expressed prior to plant penetration, with their expression peaking between 24 and 48 hours post-host colonisation (Mosquera *et al.*, 2009). Transcriptomic analyses have confirmed this expression

pattern, classifying *M. oryzae* genes into temporal clusters, as shown in Figure 1.3. Effector-encoding genes were predominantly found in modules 4 and 5, showing peak expression during this 24 to 48 hours period following infection (Yan *et al.*, 2023). Such coordinated regulation of effector genes is a common feature among plant pathogens, reflecting the need for precise control over production of these secreted proteins (Kleemann *et al.*, 2012, Toruño *et al.*, 2016, Nobori *et al.*, 2020, Siddique *et al.*, 2022, Yan *et al.*, 2023).

In *M. oryzae*, several transcription factors, signalling cascades, and epigenetic modifications have been implicated in effector gene expression. Notably, Mst12, acting downstream of Pmk1 MAPK signalling, is a transcriptional regulator controlling effector gene expression (Park *et al.*, 2002, Sakulkoo *et al.*, 2018, Osés-Ruiz *et al.*, 2021). Similarly, the Mps1 MAPK pathway regulates effector genes via transcription factors Mig1 and Git1 (Xu *et al.*, 1998, Mehrabi *et al.*, 2008, Li *et al.*, 2016). Additionally, effector regulation has been linked to the Zn_2Cys_6 transcription factor Eitf1 and the bZIP transcription factors Eitf2 and Bip1, although their placement within known signalling pathways remains unclear (Cao *et al.*, 2022, Lambou *et al.*, 2024).

G-protein signalling also plays a role in this regulatory network, either through cAMP level modulation (Zhang *et al.*, 2011a) or via transcriptional repression by the G-protein regulator Rgs1 (Tang *et al.*, 2023). Beyond transcriptional control, epigenetic mechanisms—such as histone modifications and DNA methylation—have also been reported to regulate effector gene expression in *M. oryzae* (Wu *et al.*, 2021, Zhang *et al.*, 2021).

Despite these advances, significant gaps remain in our understanding of how *M. oryzae* orchestrates effector expression. Uncovering additional components, molecular mechanisms, and signalling crosstalk will be crucial to fully reveal this complex regulatory landscape.

1.6 Introduction to the current study

In this study, I set out to investigate the mechanisms governing effector gene regulation in the rice blast fungus, *M. oryzae*, by employing two complementary strategies: a forward genetic screen to identify novel regulatory components, and a reverse genetic approach to deepen our understanding of known regulatory pathways. The rationale for this investigation stems from a significant gap in our knowledge of how filamentous fungal pathogens control disease progression and the expression of effector genes. As effector functions remain largely elusive, dissecting their regulatory networks could offer a systematic framework to understand their roles during infection. Furthermore, a deeper understanding of infection-related transcriptional control may lead to the development of innovative strategies to combat blast disease.

In Chapter 3, I present a forward genetic screen designed to identify regulators of effector gene expression in *M. oryzae*. This approach is based on the hypothesis that the majority of effectors are induced exclusively within the host plant (Mosquera *et al.*, 2009, Yan *et al.*, 2023). I performed UV mutagenesis on *MEP3-GFP* expressing strains to isolate constitutive effector regulator (*CER*) mutants, selected based on the expression of an effector reporter gene during vegetative growth. This screen led to the identification of three mutants—*CER1000, CER1001,* and *CER1002*—showing constitutive *MEP3-GFP* expression. Additionally, I tested an alternative screening method aimed at simplifying the selection of mutants by linking effector promoters to the Hygromycin B resistance gene, enabling the selection of *CER* mutants on antibiotic-containing media. Despite some limitations, I discuss the underlying challenges of such an approach and propose a new strategy to improve future screening efforts.

In Chapter 4, I focus on characterising *M. oryzae MEP3-GFP* constitutively expressing mutants—*CER1000*, *CER1001,* and *CER1002*—obtained from the genetic screen. For *CER1001* and *CER1002,* I identified *RGS1* as the causal gene responsible for constitutive *MEP3* expression, which mirrored previous research

implicating this G-protein regulator in repressing late-stage effector gene expression in *M. oryzae* (Tang *et al.*, 2023). This finding also provides new insight into the genomic regions of *RGS1* necessary for its function. By contrast, I could not verify the regulatory component responsible for *MEP3* constitutive expression in the *CER1000* mutant, though I generated a shortlist of candidate genes for future investigation. Additionally, transcriptomic analysis did not detect *MEP3* transcripts in any of the *CER* mutants, further complicating their study. I propose that newly acquired SNPs may have triggered compensatory mechanisms, suppressing the initial constitutive expression of *MEP3* and highlighting regulatory plasticity in *M. oryzae*.

In Chapter 5, building on the concept that pathogenicity regulators also influence effector gene expression, I investigated the role of a recently reported virulence regulator, Bip1 (Lambou *et al.*, 2024). Through a series of molecular biology assays supported by transcriptomic analysis, I demonstrate that Bip1 is a component of the Pmk1 MAPK signalling pathway, acting downstream of transcription factor Mst12 to coordinate virulence and effector gene expression. Furthermore, I demonstrate that Bip1 has a phosphorylation motif and that it can physically interact with Mst12, consistent with heterodimer formation supporting its role as a transcriptional regulator. I report the set of effector genes regulated by Bip1 and place this in the context of its wider role as a global regulator of infection-related development. I present a model for the regulatory roles of Mst12 and Bip1 during *M. oryzae* infection. These findings provide new evidence that *M. oryzae* utilises a hierarchical transcription factor network under control of the Pmk1 MAPK signalling pathway to regulate effector expression and disease progression during the establishment of rice blast disease.

Overall, this thesis integrates various approaches to provide new insights into how *M. oryzae* regulates effector-encoding genes. It reinforces the link between transcriptional regulators controlling morphogenesis and effector gene expression while uncovering a previously unrecognised connection between a conserved signalling pathway and a novel transcription factor involved in pathogenesis.

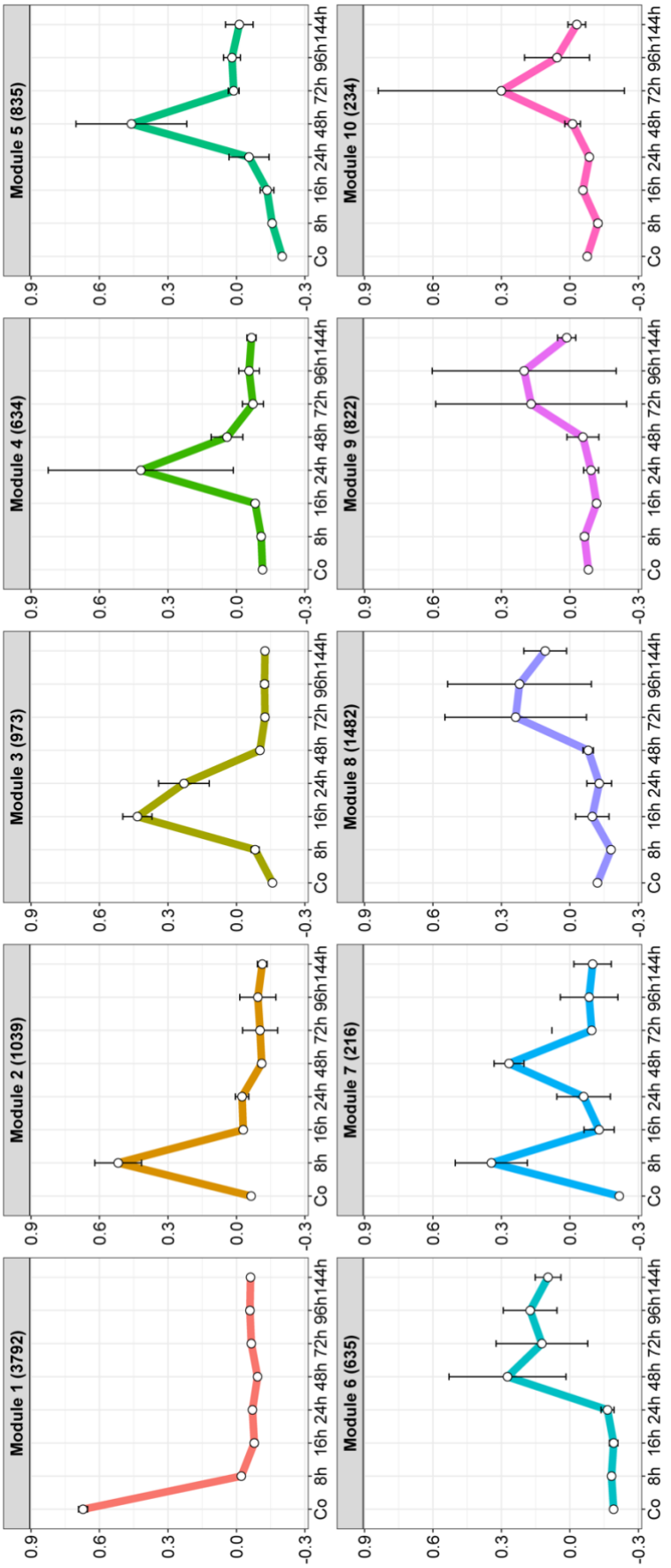

Figure 1.3 Cluster analysis of the temporal expression pattern of *M. oryzae* genes. Expression values were obtained from RNA-Seq analysis of *M. oryzae* strain Guy11 infection on rice cultivar CO39 for eight different time points of rice blast disease (0h, 8h, 16h, 24h, 48h, 72h, 96h and 144h). The number of genes within a module is annotated in brackets on top of each module. The X-axis shows the timepoint, and the Y-axis shows the expression curve obtained for each module. Each module represents a different temporal expression cluster, representing different temporal stages of the plant infection: Modules 1 and 2 "Plant Surface" expression, Modules 3-4-5 "Early Invasive Growth", Modules 5-6-7 "Cell to Cell Movement" and Modules 8-9-10 "Late Colonization" (Yan *et al.*, 2023).

Chapter 2: Materials and Methods

2.1 Molecular biology

2.1.1 PCR (Polymerase Chain Reaction)

Amplification of DNA fragments by PCR was carried out using Q5® High-fidelity DNA polymerase (New England Biolabs) following the manufacturer's protocol. Colony PCR was performed using SapphireAmp® Fast PCR Master Mix (Takara Bio, USA), which was mixed with single colony isolates using a sterile micropipette tip. Annealing temperatures were calculated using the Tm calculator tool from ThermoFisher Scientific, and elongation time was set to 30 s/kb for high-fidelity amplification and 10 s/kb for colony PCR.

2.1.2 DNA restriction enzyme digestion

All restriction endonucleases used in this study were obtained from Promega UK, Ltd and used following the manufacturer's protocol. A 50 μL DNA digestion reaction mix was composed of 1-5 μg of DNA, 1 μL of enzyme (equivalent to 5 to 10 units), 5 μL of compatible buffer and sterile ddH_2O up to the desired final volume. The reaction was gently mixed and incubated at 37°C overnight. Agarose gel electrophoresis and gel purification were used to fractionate and purify digested DNA fragments.

2.1.3 DNA gel electrophoresis and gel purification

DNA size fractionation was performed by gel electrophoresis. DNA products were fractionated in a 1% (w/v) agarose gel prepared with 1x Tris-borate EDTA (TBE) buffer (0.09 M Tris-borate and 2 mM EDTA) and 0.5 μg/mL of ethidium bromide for DNA visualisation using UV-light. To determine the size of samples, 1 kb Plus ladder marker (Invitrogen) was also loaded into the gel. A gel documentation system

(Fujifilm Thermal Imaging) was used to visualise and image separated fragments of DNA in the gel. UV transilluminator (image Master VDS) and a sterile razor blade were used to excise desired DNA fragments of the gel for purification. Wizard ® SV Gel and PCR Clean-Up System kit (Promega) was used following the manufacturer's protocol.

2.1.4 Molecular cloning by In-Fusion™

Constructs used in this work were all assembled using In-Fusion Cloning Kit (Takara Bio, USA), which uses homologous recombination-based technology to join single or multiple DNA fragments into a linearised plasmid vector (Park *et al.*, 2015). Genes of interest were cloned into pscBar-GFP or pscSur-GFP vectors for fungal transformation and/or into pGADT7 or pGBKT7 vectors for yeast-two-hybrid (Y2H) experiments.

To clone by homologous recombination, all primers are designed with a 15-20 bp overhang sequence complementary to the adjacent site of the DNA fragment. In-Fusion reactions were performed using 50-100 ng of purified DNA fragment, an equal amount of linearised plasmid, 1 μL of 5x In-Fusion® HD enzyme premix and sterile water for a total reaction volume of 10 μL. The reaction was incubated on ice for 2 min and then transferred to 50°C for 15 min. Later, 3 μL of the reaction mix was used to transform *Escherichia coli* Stellar ™ (Takara Bio, USA) competent cells.

2.1.5 *Escherichia coli* transformation

Bacterial transformation was achieved through the heat shock method (Froger & Hall, 2007). For this, 50 μL of *Escherichia coli* Stellar ™ (Takara Bio, USA) competent cells were mixed with 3 μL of the In-Fusion reaction and incubated on ice for 30min. Then, cells were transferred to 42°C for 45 sec and immediately after placed on ice for 2 min. Cells were mixed with 500 μL of pre-warmed SOC medium (2 % tryptone, 0.5 % yeast extract, 10 mM NaCl, 2.5 mM KCl, 10 mM $MgCl_2$, 10 mM $MgSO_4$, and 20

mM glucose) to recover at 37°C and 190 rpm for 1 hour. Finally, 100 µL of the cells was plated on solid LB media with the appropriate antibiotic for selection (50 µg/mL kanamycin, 100 µg/mL carbenicillin) and incubated at 37°C overnight. Positive colonies were screened through colony PCR using SapphireAmp® Fast PCR Master Mix (Takara Bio, USA) PCR master mix.

2.1.6 DNA plasmid purification

PureYield™ Plasmid Midi-Prep System (Promega, UK) was used to purify high yields of plasmid DNA. A positive colony was grown in 100 mL of liquid LB media overnight at 37°C and 190 rpm. The liquid was pelleted by centrifugation 14,000 x *g* for 15 min and then resuspended with 3 mL of Cell Resuspension Solution (50 mM Tris (pH 7.5), 10 mM EDTA, and 100 µg mL-1 of RNAse). Once resuspended, 3 mL of Cell Lysis Solution (0.2 M NaOH, 1% SDS) was added and mixed by inversion. After 5 min of incubation, 5 mL of Neutralization solution (4.09 M guanidine hydrochloride, 0.759 M potassium acetate, and 2.12 M glacial acetic acid (pH 4.2)) was added and again mixed by inversion before centrifugation at 14,000 x *g* for 15 min. The supernatant was then poured into an assembled column stack using a blue PureYield™ column on top of a white PureYield™ column. Using a vacuum manifold, the vacuum was applied until the solution passed through both columns. DNA bound to the white column was then treated with 5 mL of Endotoxin Removal solution and washed with 20 mL of the Column Wash Solution (60mM potassium acetate, 8.3 mM Tris-HCl (pH 7.5), 0.04 mM EDTA, 60% ethanol). The column was then dried before the DNA was eluted with 600 mL of nuclease-free water. For storage, the purified DNA was placed at -20°C and 500 µL of the bacterial culture was mixed with 300 µL of glycerol, snap-frozen with liquid nitrogen and placed at -80°C. All plasmids were analysed by Sanger sequencing.

2.2 Yeast-two-hybrid (Y2H) analysis

2.2.1 Preparation of yeast-competent cells

Saccharomyces cerevisiae chemically competent Y2H Gold cells (Takara Bio, USA) were prepared following the Frozen-EZ Yeast Transformation II™ (Zymo Research, UK) kit and procedures. For this, a single colony grown on YPDA (10 g/L yeast extract, 20 g/L Bacto peptone, 20 g/L Glucose monohydrate, 40 g/L Adenine hemisulfate) agar for 48 hours at 28°C was isolated and incubated in 10mL of liquid YPDA media overnight at 28°C and 190rpm. Saturated cultures were then pelleted by centrifugation at 700 x *g* and diluted into fresh YPDA medium for another 4–5-h growth period until the desired OD_{600} of 0.0-1.0 was reached. Later, cells were pelleted again at 700 x *g*, washed with 10 mL of Frozen-EZ Yeast Solution 1 (Tris and EDTA) and resuspended in 1 mL of Frozen-EZ Yeast Solution 2 (DMSO < 10 %). At this point, competent cells were aliquoted into 1.5 mL Eppendorf tubes and used immediately or frozen at -80°C for future use.

2.2.2 Co-transformation of yeast cells for Y2H analysis

Co-transformation of Y2H Gold competent cells was achieved by mixing 100-200 ng of each vector (bait and prey) in less than 5 µL volume, 25 µL of yeast competent cells and 500 µL of Frozen-EZ Yeast Solution 3 (PEG < 45%). This mix was incubated for 90 min at 30°C and 100 rpm. After transformation, cells were plated in SD solid medium not supplemented with leucine or tryptophan (SD-LW) for selection. Colonies were grown for 2-4 days at 28°C. Positively co-transformed colonies were inoculated into 5 mL of SD-LW liquid media and grown overnight at 28°C and 190 rpm. Saturated cultures were adjusted to an OD_{600} of 1.0 to then generate three tenfold serial dilutions (10^{-1}, 10^{-2} and 10^{-3}). 5 µL aliquots of the initial yeast suspension and dilutions were spotted on solid SD-LW, SD-LWH (SD medium not supplemented with leucine, tryptophan or histidine), and SD-LWHA (SD medium not supplemented with leucine, tryptophan, histidine or adenine) containing XαGal. Yeast was grown for 4 days at 28°C before visualisation and documentation.

2.3 *M. oryzae* growth and maintenance

Fungal strains were routinely grown on complete medium (CM) at 24°C with a 12-hour photoperiod. CM contains 10 g/L glucose, 2 g/L peptone, 1 g /L yeast extract (BD Biosciences), 1 g/L casamino acids, 0.1 % (v/v) trace elements (22 mg/L zinc sulphate heptahydrate, 11 mg/L boric acid, 5 mg/L manganese (II) chloride tetrahydrate, 5 mg/L iron (II) sulphate heptahydrate, 1.7 mg/L cobalt (II) chloride hexahydrate, 1.6 mg/L copper (II) sulphate pentahydrate, 1.5 mg/L sodium molybdate dehydrate, 50 mg/L ethylenediaminetra-acetic acid, 0.1 % (v/v) vitamin supplement (0.001 g/L biotin, 0.001 g/L pyridoxine, 0.001 g/L thiamine, 0.001 g/L riboflavin, 0.001 g/L, 0.001 g/L nicotinic acid), 6 g/L $NaNO_3$, 0.5 g/L KCl, 0.5 g/L $MgSO_4$, 1.5 g/L KH2PO_4, [adjust pH to 6.5 with NaOH]), and 15 g/L agar for solid medium (Talbot *et al.*, 1993). All chemicals were from Sigma-Aldrich except those indicated differently above.

For maintenance and long-term storage, *M. oryzae* isolates were grown over sterile Whatman 3mm filter paper pieces, desiccated and stored at -20°C at The Sainsbury Laboratory, Norwich.

2.4 *M. oryzae* protoplast-mediated transformation

To generate viable protoplasts, a piece of *M. oryzae* mycelium (~ 5 cm^2), previously grown on solid CM for 8 to 10 days, was cut and blended in 150 mL of liquid CM before a 48 hour incubation at 25°C and shaking at 125 rpm. The culture was then harvested and washed by filtration using sterile Miracloth and sterile deionised water (SDW). The mycelium was then transferred into a 50 mL falcon tube with 40 mL of OM buffer (1.2 M magnesium sulfate, 10 mM sodium phosphate (pH5.8), Glucanex 5% (Novo Industries, Copenhagen)), slightly shaken and incubated at 30°C and 75 rpm for 3 hours for digestion. The digested culture was then filtered through Miracloth into 50 mL Falcon tubes and centrifuged for 10 min at 5,000 x *g* and 4°C. Protoplasts were then gently resuspended in 1 mL of chilled

STC buffer (sucrose, 1.2 M, Tris-HCl, 10 mM (pH 7.5)) and then topped up to 20 mL of STC for washing. After the wash, they were pelleted through centrifugation for 10 min at 3,000 x *g* and 4°C. The last resuspension was carried out in ~500 µL of chilled STC (this depends on the size of the pellet), and protoplasts were checked microscopically for integrity.

To transform protoplasts, 150 µL of the last protoplast-STC resuspension was mixed with 6-10 µg of DNA in a 1.5 mL Eppendorf tube and incubated for 30 min on ice. Later, 1 mL of PTC buffer (PRG 4000, 60%, Tris-HCl, 10 mM (pH 7.5), calcium chloride) was added to the reaction, gently mixed and incubated for 20min at room temperature. After the protoplast transformation, the reaction was mixed with 20 mL of BDCM liquid media (yeast nitrogen base without amino acids and ammonium sulphate, 1.7 g/L (Difco), ammonium nitrate, 2 g/L asparagine, 1 g/L glucose, 10 g/L sucrose, 0.8 (pH 6)) for an overnight incubation at 25°C at 75 rpm in the dark. Following incubation, 20 mL of protoplast culture was mixed with 15 mL of BDCM with 1% agar and poured into 5 petri dishes. Once solidified, an overlay of BDCM with 1 % agar containing 300 µg/mL of bialaphos (Basta) or sulfonylurea (Sur), for selection of resistant transformants, was poured over the solidified media. Positive transformants were collected for screening from the upper BDCM layer after 10 days of growth at 25°C in the dark.

2.5 Pathogenicity and infection-related development assays

2.5.1 *M. oryzae* induction of appressorium development on glass coverslips

Conidia were harvested from 10-day-old *M. oyrzae* cultures grown on CM using an L-shaped plastic spreader and 3 mL of sterile water. Then, the conidial suspension was filtered through sterile Miracloth and spores were washed with a 15 min centrifugation at 8000 x *g*. The pellet was resuspended in water, and using a haemocytometer (Improved Neubauer, UK), the concentration was adjusted to 7.5

x 10^4 conidia/mL in the presence of 50 ng/µL of 1,16-Hexadecanediol (Sigma-Aldrich). For microscopic visualisation, 30 µL droplets of conidial suspension were placed onto hydrophobic borosilicate glass coverslips (Menzel-Gläser, Fisher Scientific UK), placed on water-soaked paper towels and incubated at 25°C. For large-scale appressorium germination assays, the conidial suspension was poured onto square Petri dishes (120 mm) with ~8 hydrophobic borosilicate glass coverslips glued to them. Petri dishes with 50 mL of conidial suspension were prepared per time-point, and incubated at 25°C with no lid. Sample harvesting was done by scraping the surface of coverslips with a sterile razor blade and immediately freezing in liquid nitrogen, ready to be used or stored at -80°C. Samples were monitored under a light-inverted microscope.

2.5.2 *M. oryzae* fungal infection of rice leaves for microscopy visualisation

To visualise fungal invasive growth inside rice epidermal cells, leaf sheath inoculation assays were performed. 5 cm leaf sheaths were cut from 3-4 week old rice cultivar CO-39 seedlings. *M. oryzae* conidia suspension was prepared following protocol 2.5.1 and adjusted to a concentration of 5 x 10^4 conidia/mL. Then, the conidial suspension was inoculated on the hollow space of the leaf, resulting from removing its outer layer. Inoculated leaf sheaths were incubated at 25°C for 24h. For visualisation with the microscope, leaf sheaths were trimmed with a razor blade, removing the sides and exposing the epidermis above the mid-vein. Sections were cut into 1-2 mm thick and mounted onto a glass slide, aiming to observe three to four cell layers under the microscope (Sakamoto, 1949).

2.5.3 *M. oryzae* leaf-drop pathogenicity assay

M. oryzae conidia were harvested from mycelium as indicated in protocol 2.5.1and the final concentration adjusted to 5 x 10^4 conidia/mL with 0.2% (w/v) gelatin. Leaf drop infections in this work were all performed using 7-day-old seedlings of barley cultivar Golden Promise. Leaves were detached and placed on

water-soaked Whatman 3mm paper placed inside square Petri dishes (120 mm). Each leaf was inoculated with 3 to 4 drops of 10 µL of conidial suspension. Infections were observed and scored 5 days post inoculation (dpi) at 25°C with a 12h photoperiod.

2.6 UV mutagenesis of *M. oryzae*

M. oryzae conidia were harvested from mycelium as described in protocol 2.5.1and the final concentration adjusted to 100 conidia/mL with 0.2% (w/v) gelatin. 3 mL of conidial suspension was poured into a 9 mm petri dish without a lid, and conidia exposed to different UV light dosages using a UV crosslinker (Stratagene). Serial dilutions of the initial conidial suspension treated with UV were then plated onto CM medium. Initially, plates were grown at 25°C for 48 h in complete darkness (wrapped in aluminium foil), to prevent DNA photo-induced repair. After this, plates were transferred to the fungal growth chamber for 4-5 days at 25°C with a 12h photoperiod. UV mutants were then screened to perform forward genetic screens.

2.7 Fungal DNA extraction

To extract DNA from fungal mycelium, *M. oryzae* was grown for 10 days at 25°C with a 12-hour photoperiod on a sterile cellophane disc (Lakeland) placed on a CM agar plate. The cellophane mycelium culture was ground to powder in liquid nitrogen using a pestle and mortar. The powder was then transferred to a 2 mL Eppendorf tube, mixed with 500 µL of warm CTAB buffer (2% (w/v) Hexadecyltrimethylammonium Bromide (CTAB), 100 mM Tris base, 10 mM EDTA, and 0.7 M NaCl) and incubated for 30 min at 65°C with a gentle mixing every 10 min. Samples were centrifuged for 10 min at 14,000 x *g,* and subsequently, the aqueous phase was collected and transferred to a new 1.5 mL Eppendorf tube. An equal amount of chloroform iso-amyl alcohol (CIA) was added, mixed and incubated for 30 min at room temperature and 90 rpm. This was then followed with another 10 min centrifugation at 14,000 x *g*. After repeating this last step twice, the supernatant was

collected, mixed with an equal amount of chilled isopropanol and incubated overnight at -20°C. Samples were then centrifuged for 10 min at 14,000 x *g* to recover the DNA, and the supernatant was discarded. The pellet was left to dry, Eppendorf inverted over a paper towel and then dissolved in 500 µL of sterile distilled water (SDW). 50 µL of sodium acetate (NaOAc) (0.1 vol) and 1000 µL of 100% ethanol were added to re-precipitate nucleic acids. The mixture was incubated at -20°C overnight to pellet the DNA by centrifugation for 20 min at 14,000 x *g*. DNA was washed with 400 µL of 70% ethanol and centrifuged again for 5 min at 14,000 x *g* before resuspension in 100 µL of nuclease-free water.

2.8 Fungal RNA extraction

To extract RNA from fungal mycelium, *M. oryzae* was grown for 10 days at 25°C with a 12-h photoperiod on a sterile cellophane disc (Lakeland) placed on a CM agar plate. Material from other developmental processes was collected according to protocol 2.5.1. The biological material was ground into powder using a pestle and mortar in liquid nitrogen. Total RNA extraction was done using a commercial kit (QIAGEN RNeasy Plant Mini Kit) following the manufacturer's instructions. Briefly, 100 µg of grounded material was vigorously mixed with 450 µL of RTL buffer previously mixed with 10 µL β-mercaptoethanol for every 1 mL of the RLT buffer. The lysate was then transferred to a QIA shredder spin column placed in a 2 mL collection tube and was centrifuged for 2 min at 8,000 x *g*. The elute was then transferred to a new 1.5 mL Eppendorf tube and mixed with 0.5 volume of 100% ethanol. The mix was transferred to an RNAeasy Mini spin column and centrifuged for 15 seconds at 8,000 x *g*. The flow through was then discarded, 350 µL of RW1 buffer was added to the column and centrifuged for 15 sec at 8,000 x *g* before treating the membrane with 80 µL of DNase (RNeasy Free DNase Set QIAGEN). DNAse was prepared by mixing 70 µL of RDD buffer and 10 µL of DNase stock solution. Treatment was incubated for 15 min at room temperature before adding another 350 µL of RW1 buffer and centrifugation for 15 sec at 8,000 x *g*. Lastly, the column was washed twice with 500 µL of RPE buffer by centrifugation for 15 seconds

at 8,000 x *g*. RNA was eluted with 50 µL of RNA-free water into a new 1.5 mL Eppendorf tube through centrifugation for 1 min at 8,000 x *g* and stored at -80°C.

2.9 RNA manipulations

2.9.1 Reverse transcriptase system

To convert mRNA to cDNA, the Reverse Transcription System (Promega) commercial kit was used following the manufacturer's protocol. RNA concentrations were measured using a Nanodrop spectrophotometer (ThermoFisher Scientific) and adjusted to use 500 ng for the reaction. Initially, 1 µL of random primer solution and RNA were mixed in a final volume of 5 µL and incubated for 5 min at 70°C for annealing of the primers. Then, the reaction mix (4 µL of 5 x reaction buffer, 0.5 µL of $MgCl_2$, 1 µL of PCR nucleotide mix, 1 µL of recombinant RNasin ribonuclease inhibitor, 1 µL of reverse transcriptase, and 8 µL of nuclease-free water) were added to the initial 5 µL and incubated for 5 min at 25°C and then for 60 min at 42°C for DNA extension. Lastly, reverse transcriptase was inactivated by incubating the mix for 15 min at 70°C.

2.9.2 Real-time quantitative PCR (q-RT-PCR)

Real-time quantitative PCR was performed using the Bio-Rad CFX Opus QPCR machine. For the reactions, 4 µL of cDNA, at a concentration of 100 ng/µL, was mixed with 0.5 µL of forward primer, 0.5 µL of reverse primer and 5 µL of reaction buffer 1 x SYBR® Premix ExTaq™ (Takara Bio, USA). All q-RT-PCR primer designs were done using the web source Primer3 (Kõressaar *et al.*, 2018). The PCR was set to perform one cycle at 95°C for DNA denaturation, followed by 40 cycles of 5 sec at 95°C (denaturation) and 20 seconds at 60°C (primer annealing, extension and fluorescence reading) and finally one cycle of 1 min at 95°C, 30 sec at 58°C, and 30 sec at 95°C for the dissociation curve. To calculate the fold change of every measurement, an efficiency-corrected calculation model was used by applying the

formula: E target ΔCt target (control – sample) / (housekeeping) ΔCt housekeeping (control – sample).

2.10 Light and epifluorescence microscopy

2.10.1 Fluorescence stereo microscopy

Fluorescence stereo microscope (Leica M205 FC) was used to visualise *M. oryzae* mycelium. 1-week-old *M. oryzae* strains grown on CM agar plates were directly placed under the microscope. GFP was detected using a 505-545 nm laser (Leica, Germany). Constitutive expression of GFP was observed from the growing edge of the colonies.

2.10.2 Epifluorescence microscopy

Differential interface contrast (DIC) microscopy and epifluorescence were performed on an IX81 motorized inverted microscope (Olympus/Visitron, Germany). *M. oryzae* conidia, mycelium and appressoria were visualised using x100/1.4 or x60/1.35 oil objectives. Image capture was carried out using a Photometrics CoolSNAP HQ camera system (Roper Scientific, Germany) controlled by the MetaMorph software package (MDS Analytical Technologies, UK). GFP was excited at 488 nm and RFP at 561 nm.

2.10.3 Laser scanning confocal microscopy

Confocal laser microscopy was performed using a Leica TCS SP8 microscope with a 63x/1.4 oil immersion objective lens. HyD detectors were used to visualise fluorescence, exciting at 488 nm with emissions collected at 500 - 550 nm for GFP detection and exciting at 560 nm with emissions collected at 570 – 620 nm for RFP detection. Images were captured using Leica LAS AF software (Leica Microsystems, USA).

2.10.4 Image processing

All microscopy images were processed using Fiji/ImageJ2 version 2.14.0 software (Schindelin *et al.*, 2012, Rueden *et al.*, 2017).

2.11 Computational analyses

2.11.1 Phylogenetic inference and analyses

Presence/absence annotation of Mep2 and Mep3 effector proteins was carried out using 163 *Magnaporthe* genome sequences that were publicly available or generated and assembled at TSL (Win & Latorre, In prep). Protein sequences were analysed for conservation through BLAST using the TBLASTN function from NCBI (Camacho *et al.*, 2009), and later aligned with miniport (Li, 2023). Data frames were merged, and the phylogenetic tree of 163 *Magnaporthe* isolates reconstructed based on the nucleotide BUSCO sequences (Manni *et al.*, 2021). The tree was visualised and edited using iTOL (Letunic & Bork, 2006).

For ortholog identification of Mst12 and Bip1 sequences in related fungi, a set of species were selected based on a previous study (Cruz-Mireles *et al.*, 2024). Proteomes for these 41 fungal species were sourced from NCBI and JGI Mycocosm, and orthology relationships inferred using OrthoFinder (Emms & Kelly, 2019). The rooted species tree and gene copy number matrix generated from OrthoFinder outputs were used to query the presence/absence of Mst12 and Bip1 proteins. The phylogenetic tree was visualised using ggtree and phytools R packages (Yu *et al.*, 2017, Revell, 2024).

2.11.2 Whole genome sequencing

High-quality DNA samples measured using a Nanodrop spectrophotometer (Fisher Scientific) and Qubit 2.0 (ThermoFisher Scientific) were sent for sequencing

to Novogene (Cambridge, UK). DNA libraries were generated with 350 base pair inserts and sequenced using a pair-end sequencing strategy with a high-throughput sequencer, Illumina HiSeq 2500 (Illumina, Inc).

2.11.3 Data quality control and trimming

Quality control of raw sequencing reads was performed using the FastQC tool for high-throughput sequence data (Babraham Bioinformatics). Then using the program Trimmomatic (Bolger *et al.*, 2014), poor-quality reads, reads below 25 base pairs, and Illumina adapters were trimmed. Routinely after trimming, quality control of the newly generated files was examined again.

2.11.4 Alignment to the reference genome

A *M. oryzae* Guy11 reference genome compiled at The Sainsbury Laboratory by Dr Matthew Moscou and *M. oryzae* reference genome MG8 70-15 were both used in this work. BWA-MEM software from the Burrows-Wheeler Alignment tool (bwa 0.7.7) was used to map the raw reads to the reference genome. Output SAM files were sorted and converted to BAM files using Samtools 1.9 (Li *et al.*, 2009).

2.11.5 IGV visualisation

BAM files were visualised using the Integrative Genomics Viewer (IGV) software (Robinson *et al.*, 2011). The reference genome, GFF3 annotations, and BAM files were all uploaded to the IGV and single genes were searched by location or *MGG* identifier number.

2.11.6 Single Nucleotide Polymorphism (SNP) calling

The Genomic Analysis Toolkit (GATK) HaplotypeCaller was used for variant calling of the genomic data. This toolkit detected SNPs, small deletions, or insertions (indels), and outputted into a Variant Call Format (VCF). VCF files were filtered by

coverage > 20% and then run through SNPEff (Cingolani *et al.*, 2012) for the annotation of genes within the positions where SNPs or indels are identified. Finally, to identify individual SNPs and indels for each VCF file, all generated VCF files were cross-compared, filtering any identical mutations.

2.11.7 RNA sequencing analysis

RNA samples were sent for sequencing to Novogene (Cambridge, UK). RNA libraries were generated with 150 base pair inserts and sequenced using a pair-end sequencing strategy with a high-throughput sequencer, Illumina HiSeq 2500 (Illumina, Inc). Quality control of the raw reads was done following protocol 2.11.3.

2.11.8 Analysis for Differentially Expressed Genes (DEGs)

Kallisto was used to map and quantify the reads (Bray *et al.*, 2016). The edgeR program was used for differential gene expression analysis of the transcript quantifications obtained through Kallisto (Robinson *et al.*, 2009, Pimentel *et al.*, 2017). Differentially expressed genes were determined using a threshold of $\log_2$ fold-change (>=1) and adjusted p-value (p<=0.05).

2.11.9 RNA-Seq analyses: MDS plot, Euler plots, heatmaps, Pearson correlation matrix and GO-term enrichment

Multidimensional scaling (MDS) plot of distances between gene expression profiles was generated using the function plotMDS from the R package limma (Ritchie *et al.*, 2015). Heatmaps and Euler plots for the DEGs were generated with R packages ggplot2 (Wilkinson, 2011), and eulerr (Wilkinson, 2012), respectively. A Pearson correlation matrix was made using the R package corrplot (Hahsler *et al.*, 2008). The TopGO package was used for GO term enrichment analysis of differentially expressed genes (Alexa & Rahnenfuhrer, 2010).

2.11.10 FIMO analysis

The FIMO, "Find individual motif occurrences" web service from the MEME suite 5.5.7, was used to identify DNA motifs in the predicted promoter sequences of *M. oryzae* genes (Grant *et al.*, 2011). An inbuilt upstream *Magnaporthe oryzae* MG8 dataset was used to perform searches.

2.11.11 Protein structure predictions

AlphaFold3 was used to predict *in silico* structures for single proteins, protein complexes, and DNA-protein complexes (Abramson *et al.*, 2024). Distorted regions were removed for visualisation purposes. The best-ranked model with the highest average pLDDT score was used for further analyses. ChimeraX was used to visualise the protein structure (Pettersen *et al.*, 2021).

Chapter 3: Forward genetic screen to identify novel effector gene regulators in *M. oryzae*

3.1 Introduction

Similar to many cereal pathogenic fungi, *M. oryzae* infects its host through a specialised cell called an appressorium (Wilson & Talbot, 2009). Once inside the host during invasive growth, *M. oryzae* deploys a battery of secreted effector proteins. Effector proteins enable adaptation to the new host environment and protect the fungus from the plant immune system (De Wit *et al.*, 2009, Valent & Khang, 2010). Effectors have been typically characterised based on their expression and localisation *in planta,* but to date, biological functions have only been determined for a small number of them (Hogenhout *et al.*, 2009, Valent & Khang, 2010, Wang *et al.*, 2017, Oliveira-Garcia *et al.*, 2024). Most rice pathogen effectors are small-secreted proteins with cytoplasmic localisation, little sequence identity and some structural conservation (Seong & Krasileva, 2021). *M. oryzae* employs two differentiated secretion systems to deliver effectors. Apoplastic effectors are secreted through the endoplasmic reticulum (ER)-Golgi-dependent secretory pathway. Cytoplasmic effectors distinctively accumulate at the Biotrophic Interfacial Complex (BIC) observed in invasive hyphae before they are translocated to the cytoplasm (Mentlak *et al.*, 2011, Giraldo *et al.*, 2013). Delivery of cytoplasmic effectors has been reported to occur through the internalisation of membrane-bound cargos, utilising clathrin-mediated endocytosis (CME) (Oliveira-Garcia *et al.*, 2023).

Characterised effector-encoding genes are highly expressed *in planta* but remain transcriptionally repressed when the pathogen is not growing inside its host (Mosquera *et al.*, 2009). The molecular mechanism of this transcriptional regulation is unknown and is a central question in plant-microbe interactions. High-resolution transcriptomic analysis of the blast fungus during rice infection has confirmed the

temporal regulation of fungal genes involved in pathogenicity (Yan *et al.*, 2023). Most effector-encoding genes are co-expressed between 24h and 48h following plant infection, revealing co-regulation of structurally similar effectors, including the *M*aganaporthe Avrs and ToxB-like (MAX) effectors, characterised by a common β-sandwich fold, which are over-represented among expressed genes (de Guillen *et al.*, 2015, Yan *et al.*, 2023). This strict temporal regulation suggests that effectors must be transcriptionally regulated by unknown factors activated during invasive growth and/or repressed prior to host colonisation. This hypothesis has been further tested through a forward genetic screen that identified mutants showing constitutive effector gene expression. Through this genetic screen, *RGS1,* a regulator of G-protein signalling, was identified and found to regulate the expression of a subset of effector-encoding genes (Tang *et al.*, 2023). The Rgs1 protein has previously been reported to play an important role in appressorium development regulating intracellular levels of cAMP (Liu *et al.*, 2007). Still, this forward genetic screen allowed the identification of a novel function for *M. oryzae* Rgs1 as a repressor of the expression of effector genes prior to plant infection (Tang *et al.*, 2023). The precise mechanisms by which Rgs1 regulates both G-protein signalling and effector gene expression require further investigation because it remains unclear, for example, whether Rgs1, which plays a cytoplasmic role in G-protein signalling, can translocate to the nucleus to direct gene regulation or if this happens indirectly, by targeting a downstream transcriptional regulator.

Regulation of a small sub-set of *M. oryzae* effector genes has also been shown to occur through the Pmk1 MAPK signalling pathway, which regulates appressorium morphogenesis and invasive fungal growth (Sakulkoo *et al.*, 2018). This regulation is thought to happen directly and/or through the phosphorylation of downstream targets, such as the Mst12 transcription factor (Osés-Ruiz *et al.*, 2021), but the precise details remain unclear. In closely related phytopathogens, effector gene regulation has also been shown to occur through distinct signalling pathways. Homologues of *M. oryzae* transcription factors Stu1, which acts downstream of the cAMP pathway, and Git1, which acts downstream of the cell-wall integrity pathway, have been reported to play a role in effector gene expression in *Fusarium oxysporum,*

Cytospora chrysosperma and *Leptosphaeria maculans* (Michielse *et al.*, 2009, Soyer *et al.*, 2015, Han *et al.*, 2021b). Furthermore, the transcription factor Bip1, which has been reported to act independently of Pmk1, also appears to regulate a subset of effector genes in *M. oryzae* (Lambou *et al.*, 2024). In addition, there is compelling evidence of effector regulation through epigenetic mechanisms (Soyer *et al.*, 2014, Wu *et al.*, 2021, Zhang *et al.*, 2021). This demonstrates that the blast fungus orchestrates the regulation of effector-encoding genes via multiple signalling pathways to facilitate such precise temporal control. To date, the overwhelming majority of effector genes and details of corresponding effector gene regulation remain uncharacterised (Oliveira-Garcia *et al.*, 2024). In this context, large-scale genetic screening methods offer a promising strategy to gain new insight into the mechanisms of gene regulation in the blast fungus.

This chapter introduces the use of forward genetic screens to identify novel regulators of effector gene expression in *M. oryzae*. The basis of these screens relies on the tight co-regulation of effector genes, which are expressed *in planta* when the pathogen is growing inside its host but not expressed *ex planta*, in conidia or mycelium. This hypothesis has already been tested by designing *M. oryzae* effector fusions to GFP, applying UV mutagenesis and screening for Constitutive Effector Regulator (*CER*) mutants that show constitutive expression of the selected effector and, therefore, GFP (Tang *et al.*, 2023). In this chapter, I performed new forward genetic screens and identified three *CER* mutants which exhibited constitutive *MEP3-GFP* expression. These mutants were subsequently used to identify putative regulators of *MEP3* gene expression. Additionally, because this method includes extensive GFP screening of *M. oryzae* conidia, I designed and tested an optimised version of the forward genetic screen utilising an alternative selectable marker. The chapter reports new insights into using forward genetic screens, aimed at increasing our understanding of the basis of plant infection.

3.2 Results

3.2.1 Forward genetic screen pipeline to identify effector gene regulators in *M. oryzae*

Most *M. oryzae* effector-encoding genes are not expressed prior to plant penetration in conidia and mycelium but are highly expressed during invasive growth when the pathogen grows inside its host (Mosquera *et al.*, 2009, Yan *et al.*, 2023). This temporal regulation suggests that effector-encoding genes must be transcriptionally regulated so that they are activated during invasive growth or repressed during the early time points of the *M. oryzae* life cycle. To test this hypothesis, a forward genetic screen was designed to identify *M. oryzae* mutants showing constitutive effector gene expression (Tang *et al.*, 2023). To perform the screen, effector-GFP fusions were transformed into *M. oryzae*. Then, following UV mutagenesis, Constitutive Effector Regulator (*CER*) mutants were identified by selection of fluorescent conidia. These mutant conidia constitutively express the effector-GFP fusion, suggesting a mutation in a regulator of effector gene expression. After verifying the mutants using q-RT-PCR analysis, they were sent for whole genome sequencing. Sequencing results were then used to perform SNP calling analysis to identify putative effector regulator candidates. The design of this screen, which combines molecular biology, quantitative imaging, and bioinformatics is shown in Figure 3.1.

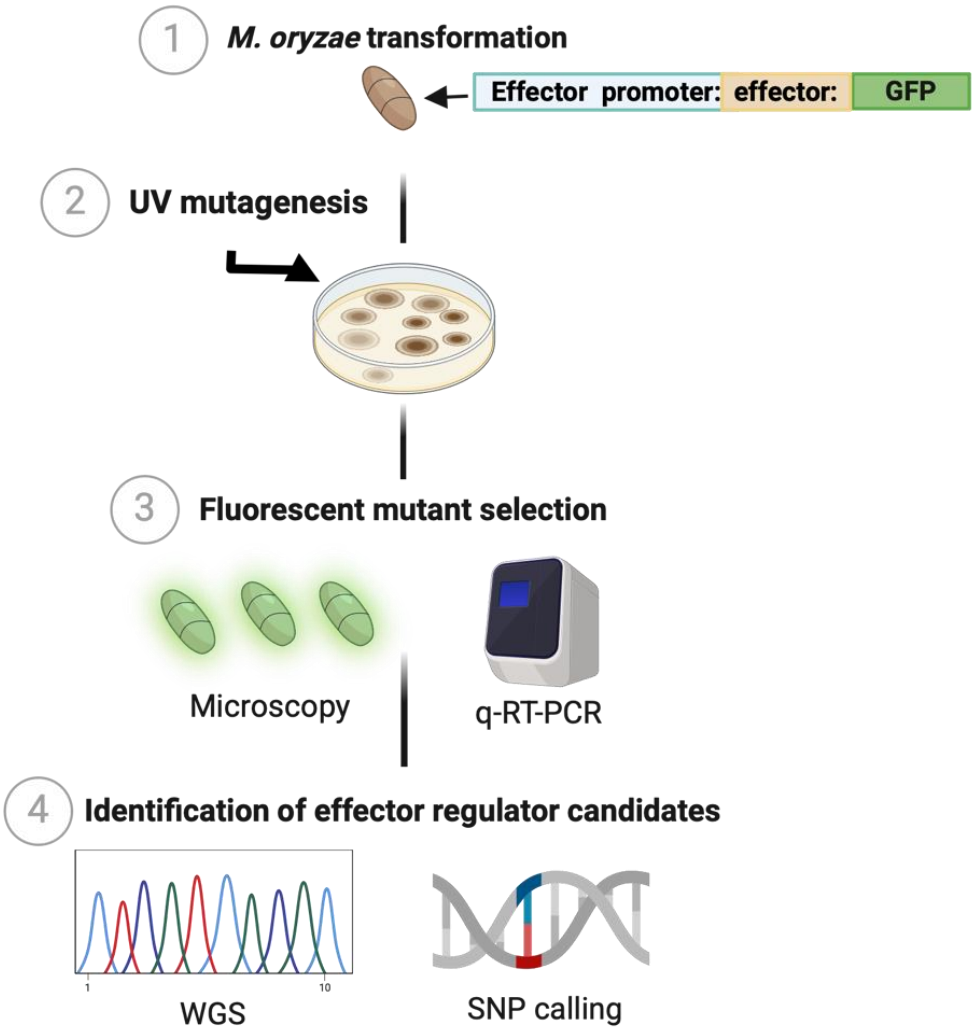

Figure 3.1 Forward genetic screen pipeline to identify putative regulators of effector-gene expression in *M. oryzae*. Schematic representation of the forward genetic screen: (1) Effector-GFP fusion constructs are transformed into *M. oryzae*. (2) Transformants are then subjected to UV mutagenesis. (3) Mutants with constitutive expression of effector-GFP fusions are screened through microscopy and verified by q-RT-PCR analysis. (4) Constitutive Effector Regulator (*CER*) mutants are sent for whole genome sequencing to perform SNP calling analysis, thereby identifying putative effector regulators. (Image created with BioRender.com)

3.2.2 *M. oryzae* UV exposure kill curve

UV irradiation is extensively used for mutagenesis (Miller, 1985). Different dosages of UV light are correlated with a specific death rate. To establish the UV dosage needed to achieve mutants for a forward genetic screen, I generated a UV mutagenesis kill curve for *M. oryzae,* as shown in Figure 3.2. For this, I exposed conidia from *M. oryzae* strain Guy11 to 6 different dosages of UV light (0.1 J/m^2, 0.2 J/m^2, 0.3 J/m^2, 0.4 J/m^2, 0.5 J/m^2 and 0.6 J/m^2). The percentage of surviving fungal colonies was calculated with data from 5 individual replicates.

Previous forward genetic screens performed in the laboratory used a 90% kill rate of conidia to obtain *CER* mutants (Tang *et al.*, 2023). Using the generated UV mutagenesis kill curve for *M. oryzae*, I determined that 0.4 J/m^2 of UV is needed to achieve a 90% conidial kill rate.

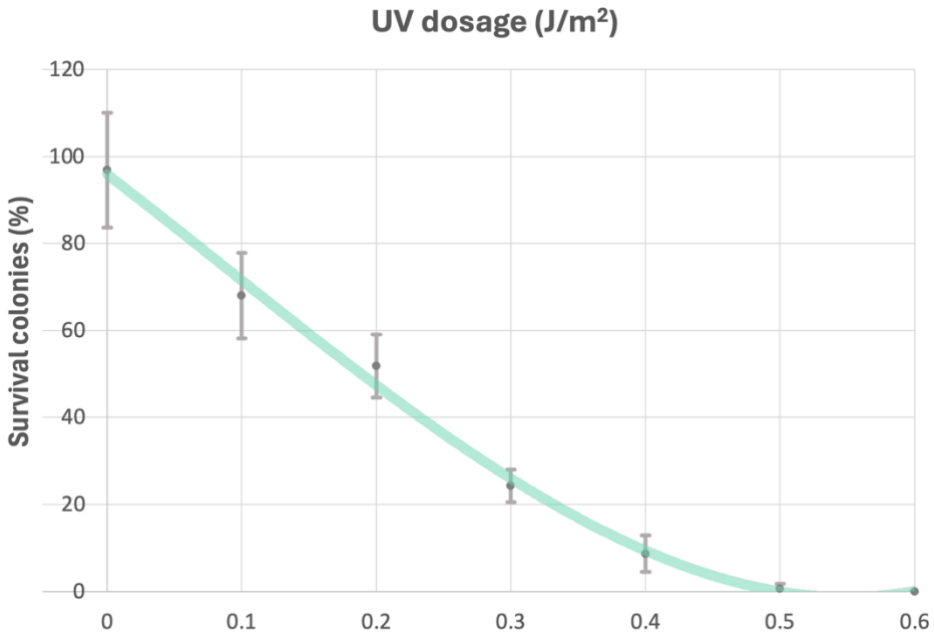

Figure 3.2 *M. oryzae* UV exposure kill curve. Survival of *M. oryzae* conidia was shown for six different UV light dosage exposures (0.1 J/m^2, 0.2 J/m^2, 0.3 J/m^2, 0.4 J/m^2, 0.5 J/m^2 and 0.6 J/m^2). The percentage of survival fungal colonies was calculated using the data of 5 individual replicates; the trend line is green, and the error bars show the standard deviation for each data point.

3.2.3 Gene expression, sequence conservation and structure prediction make *M. oryzae MEP3* effector gene a perfect candidate for performing forward genetic screenings

To perform new forward genetic screens for the identification of novel effector regulator candidates in *M. oryzae,* the cytoplasmic ***M****agnaporthe* **e**ffector **p**rotein **3** (Mep3) was selected. This predicted effector exhibited all the desired features to perform the screen. Firstly, *MEP3* is not expressed prior to plant penetration and is highly expressed during invasive growth (Yan *et al.*, 2023). Using the publicly assembled *M. oryzae* high-throughput transcriptomic data, I extracted and plotted the predicted expression for *MEP3 (MGG_17249)* during rice blast infection, as shown in Figure 3.3. This result shows that *MEP3* is not expressed prior to plant penetration when *M. oryzae* conidia germinate and form an appressorium. Still, the gene then peaks in expression when the pathogen grows inside host tissue, between 24-48 hours following infection. To further corroborate *MEP3* expression and localisation, I visualised *MEP3-GFP* using laser confocal microscopy. Consistent with previously published results (Yan *et al.*, 2023), at 26h following *M. oryzae* infection, the apoplastic effector gene *MEP1* shows expression and accumulation in the appressorium. In contrast, the cytoplasmic effector *MEP3* is expressed at the BIC during invasive growth, as shown in Figure 3.4. When considered together, this expression pattern categorises the *MEP3* effector gene into co-expression module 4, where many *M. oryzae* effectors are co-regulated (Yan *et al.*, 2023). This makes *MEP3* a good candidate for studying effector-gene regulation based on the hypothesis that effectors with similar expression patterns may be subject to the same regulatory mechanisms.

Secondly, the *MEP3* effector gene was selected because of its high conservation across the *Magnaporthe* pangenome. Mep2 and Mep3 protein sequences were analysed for conservation through BLAST analysis (Camacho *et al.*, 2009) among 163 *M. oryzae* isolates, including different host-infecting lineages (in collaboration with Dr. Yu Sugihara). This allowed the presence/absence annotation for these two effectors and their variants in a *Magnaporthe* phylogenetic tree, as shown in Figure

3.5. The analysis included sequence data from strains collected on rice (*Oryza* lineage), finger millet (*Eleusine* lineage), wheat (*Triticum* lineage), annual and perennial ryegrasses (*Lolium* lineage), foxtail millet (*Setaria* lineage), weeping lovegrass (*Eragrostis* lineage), teosintes (*Zea* lineage), St. Augustine grass (*Stenotaphrum* lineage), signal grass (*Brachiaria1* for *Brachiaria mutica* and *Brachiaria2* for *Brachiaria distachya*), and from close relatives *M. grisea,* and *M. pennisetigena*. Genomes were retrieved from publicly available data (Gladieux *et al.*, 2018) and combined with some additional sequences available at The Sainsbury Laboratory in Norwich (Win & Latorre, In prep). This analysis demonstrates that Mep3 was highly conserved across the queried sequences except in closely related species *M. pennisetigena* and *M. grisea*. We also used the conservation of Mep2 as a comparison because this effector was used to successfully identify Rgs1 as a regulator of effector gene expression in *M. oryzae* (Tang *et al.*, 2023). Mep2 was not universally conserved in *M. oryzae*, missing in *Setaria* and *Brachiaria1* infecting lineages, but this did not pose an issue when performing the previous forward genetic screens.

Finally, because structurally similar effectors are co-regulated during rice blast infection, Alphafold-3 was used to predict the structure of Mep3 *in silico* (Jumper *et al.*, 2021, Yan *et al.*, 2023). The Mep3 prediction showed a β-sheet sandwich conformation usually found in MAX effectors. The best-ranked model had a pLDDT score of 78/100 and a pTM score of 0.72, as shown by the confidence colouring in Figure 3.6.A. Despite their low sequence similarity, MAX effectors share a similar 3D structure characterised by a 6-stranded β-sheet sandwich (de Guillen *et al.*, 2015). In addition to the classic 6-stranded β-sheets, Mep3 is predicted to have two additional β-sheets, β7 and β8, and a C-terminal extension in a helical conformation, as shown in Figure 3.6.B, which subclassifies Mep3 into MAX effector structural subfamily A (Lahfa *et al.*, 2024).

Given that structurally conserved effectors have shown to be temporally co-regulated (Yan *et al.*, 2023), when considered together, the expression of *MEP3*,

conservation and structural prediction make this effector a good candidate for performing new forward genetic screens to identify putative regulators of effector gene expression in the rice blast fungus.

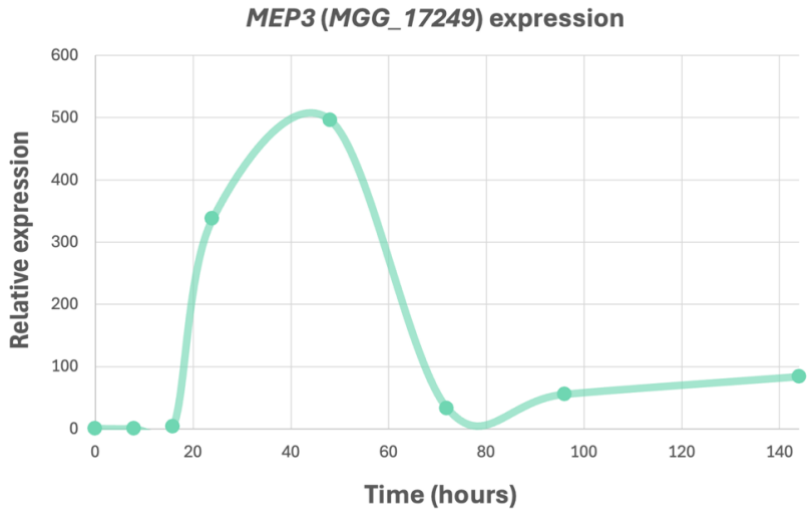

Figure 3.3 *MEP3* gene expression during rice blast infection. Data from a time course RNA-Seq experiment of infection-related development and plant infection (Yan *et al.*, 2023) was used to extract the expression profile for *MEP3 (MGG_17249)*. Relative gene expression mean values were calculated from three independent replicates extracted for eight different time points (0h, 8h, 16h, 24h, 48h, 72h, 96h, and 144h) during *M. oryzae* infection.

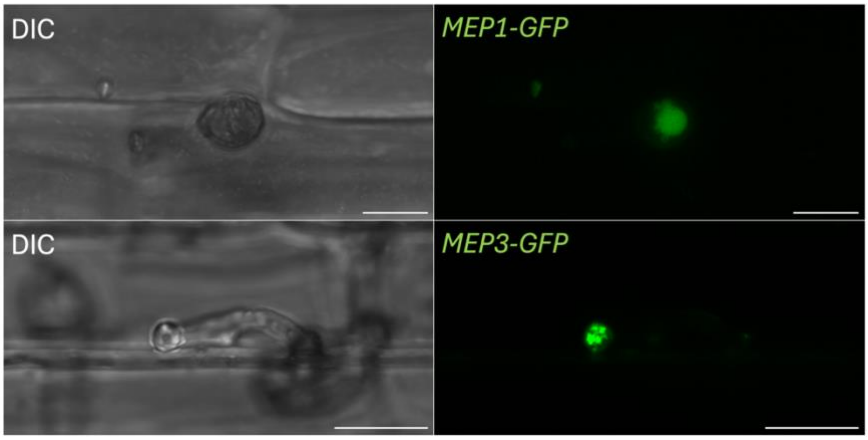

Figure 3.4 Apoplastic and cytoplasmic effectors have differentiated localisation during *M. oryzae* infection. Micrographs showing localisation of the apoplastic effector *MEP1-GFP* in the appressorium, and the cytoplasmic effector *MEP3-GFP* at the BIC. Conidia were harvested from transformants expressing *MEP1-GFP* and *MEP3-GFP*, inoculated on leaf sheaths of CO-39 rice cultivar and observed by laser confocal microscopy at 26h. Micrographs show a maximum projection of Z-stack images. Scale bar = 20 μm.

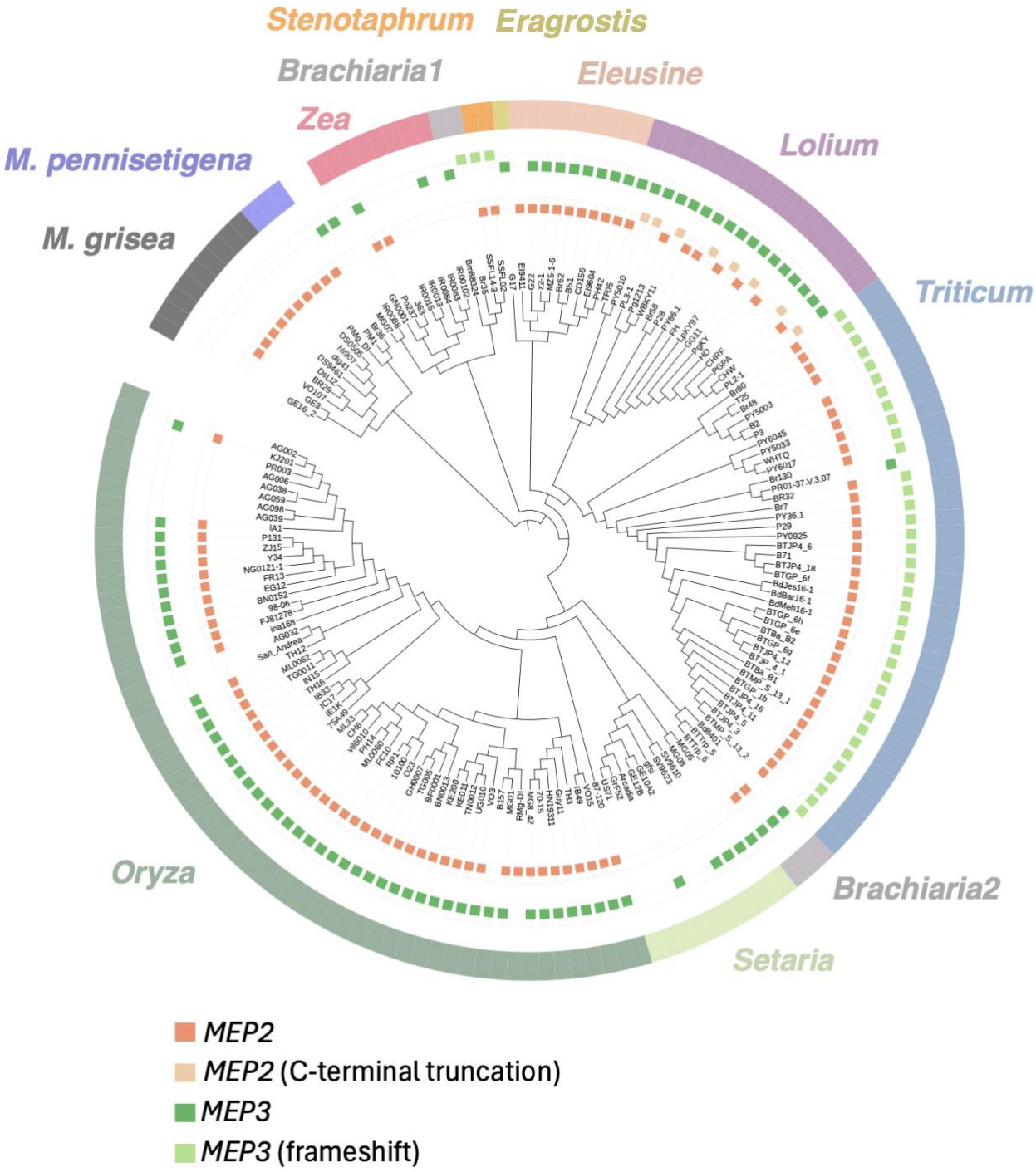
Stenotaphrum
Eragrostis
Brachiaria1
Eleusine
Zea
Lolium
M. pennisetigena
Triticum
M. grisea
Oryza
Brachiaria2
Setaria
MEP2
MEP2 (C-terminal truncation)
MEP3
MEP3 (frameshift)

Figure 3.5 Mep2 and Mep3 effector proteins are highly conserved in *M. oryzae* lineages. Mep2 and Mep3 protein sequences were analysed for conservation through BLAST analysis among 163 *M. oryzae* isolates, including different host-infecting lineages. The analysis included sequence data from strains collected on rice (dark green: referred to as *Oryza* lineage), finger millet (salmon: referred to as *Eleusine* lineage), wheat (blue: referred to as *Triticum* lineage), annual and perennial ryegrasses (lilac: referred to as *Lolium* lineage), foxtail millet (light green: referred to as *Setaria* lineage), weeping lovegrass (mustard: referred to as *Eragrostis* lineage), teosintes (pink: referred to as *Zea* lineage), St. Augustine grass (orange: referred to as *Stenotaphrum* lineage), signalgrass (grey: referred to as *Brachiaria1* for *Brachiaria mutica* and *Brachiaria2* for *Brachiaria distachya*), and from closely relatives *M. grisea* (purple) and *M. pennisetigena* (dark grey). Genomes were retrieved from publicly available data (Gladieux *et al.*, 2018), and combined with some additional sequences available at The Sainsbury Laboratory in Norwich (Win & Latorre, In prep). Phylogenetic tree was reconstructed based on the nucleotide BUSCO sequences (Manni *et al.*, 2021). Presence of the effector and their variants is indicated in orange for Mep2 and green for Mep3. Both effector proteins show high conservation among the queried sequences, although Mep2 homologues could not be detected in *Setaria* and *Brachiaria1* infecting-lineages, and Mep3 homologues could not be detected in *M. pennisetigena* and *M. grisea*.

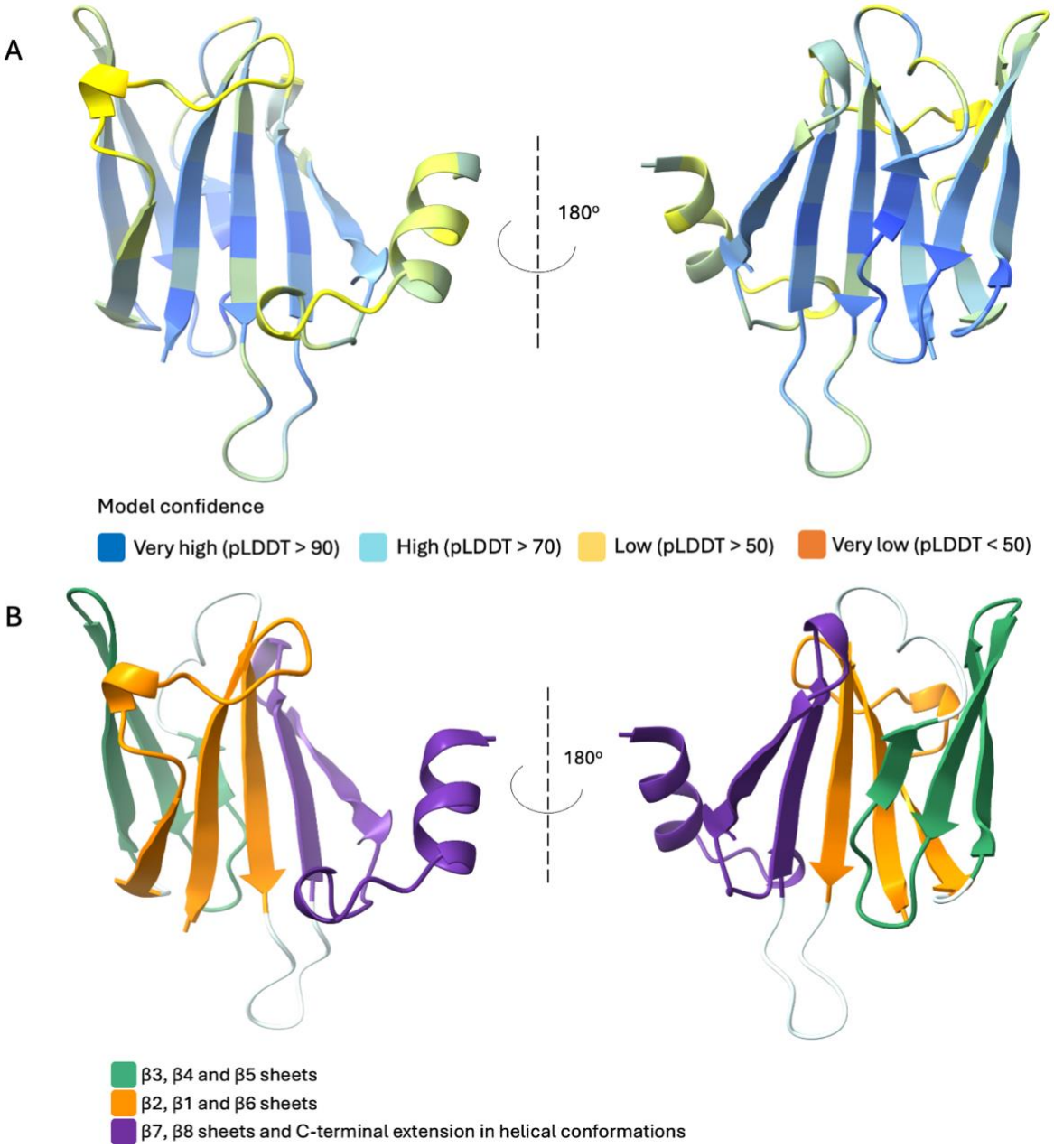

Figure 3.6 Mep3 is predicted to be a MAX effector. (A) Alphafold-3 structure prediction model for Mep3 shows canonical MAX effector fold with a pLDDT score of 78/100 as shown with the model confidence colouring. (B) In addition to the 6-stranded β-sheets sandwich (β3, β4, β5 -β2, β1, β6) coloured in green and orange, Mep3 is predicted to have 2 additional β-sheets (β7 and β8) and a C-terminal extension in helical conformation, coloured in purple. Mep3 signal peptide was cropped for visualisation purposes.

3.2.4 Identification of *CER* mutants with constitutive *MEP3-GFP* expression

Following the forward genetic screening strategy described in 3.2.1, UV mutagenesis was performed on a *M. oryzae* strain expressing *MEP3-GFP* fusion. This led to the identification of three independent *CER* mutants showing constitutive expression of *MEP3-GFP*. These were named *CER1000, CER1001,* and *CER1002*. The screening was performed on mycelium, but to verify constitutive fluorescence of candidate mutants, I observed and captured images of *M. oryzae* conidia, as shown in Figure 3.7. *M. oryzae* strain Guy11 and *MEP3-GFP* transformant prior to mutagenesis were used as negative controls because they do not show fluorescence. The *CER7* mutant, which shows constitutive expression of *MEP2-GFP* (Tang *et al.*, 2023) was used as a positive control.

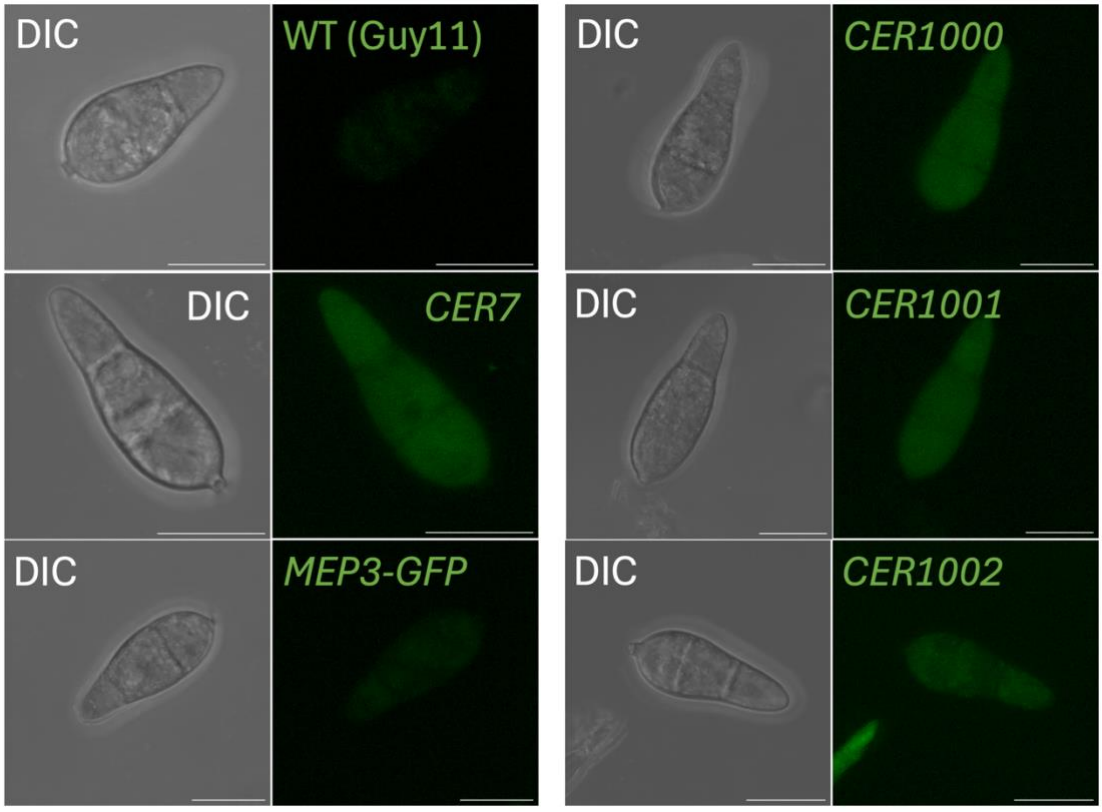

Figure 3.7 Identification of *CER* mutants showing constitutive *MEP3-GFP* expression. Micrographs show constitutive expression of *MEP3-GFP* in conidia for the *CER* mutants, *CER1000, CER1001,* and *CER1002*. The *CER7* mutant, showing constitutive expression of *MEP2-GFP,* was used as a positive control, and the Guy11 wild type and *MEP3-GFP* transformant

prior to mutagenesis were used as negative controls. Conidia were harvested from 5-day-old plate cultures and immediately observed by laser confocal microscopy. Scale bar = 20 μm.

3.2.5 q-RT-PCR analysis of constitutive *MEP3-GFP* expression in putative *CER* mutants

To ensure that the GFP fluorescence observed for the putative *CER* mutant candidates was a result of increased *MEP3* gene transcription, I carried out real-time quantitative PCR analysis (q-RT-PCR). Conidial mRNA abundance of *GFP* and *MEP3* transcripts was checked independently, as shown in Figure 3.8. Consistent with the microscopy results, *CER1000*, *CER1001,* and *CER1002* show higher transcript levels of *MEP3-GFP* when compared to the *M. oryzae MEP3-GFP* transformant prior to mutagenesis. Independent t-tests showed significance (p-value <0.05) for all three *CER* mutant candidates, confirming constitutive expression of *MEP3-GFP*.

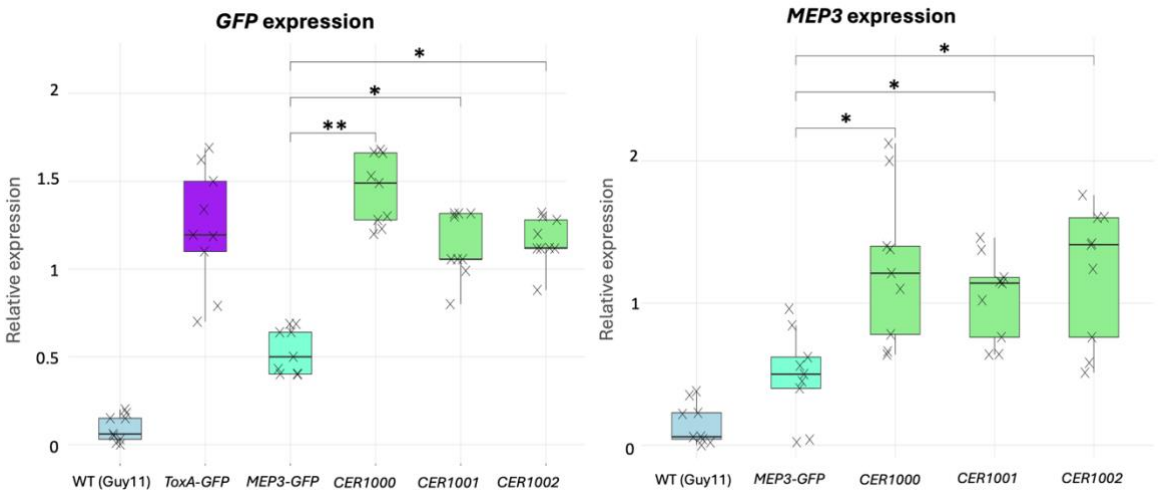

Figure 3.8 q-RT-PCR analysis confirms *CER1000, CER1001,* and *CER1002* mutants have constitutive expression of *MEP3-GFP*. Box plots showing a log2 fold change as relative transcript level of GFP and *MEP3*. *CER1000*, *CER1001,* and *CER1002* mutants have significantly higher levels of both *GFP* and *MEP3* transcripts than *M. oryzae MEP3-GFP* transformant prior to mutagenesis (t-test p-value < 0.05). *M. oryzae* Guy11 strain was used as a negative control, and *M. oryzae ToxA-GFP* transformant as a positive control of *GFP* expression. Actin (*MGG_03982*) and β-tubulin (*MGG_00604*) were used as housekeeping genes for the q-RT-PCR analysis. Results represent three biological replicates, with three technical replicates each.

3.2.6 An alternative forward genetic screen to identify effector-gene regulators in *M. oryzae*

To optimise the forward genetic screen to identify regulators of effector gene expression in *M. oryzae* a new alternative screen was designed, as shown in Figure 3.10. Following the same principles as the original screen, this newly designed pipeline overcomes the limitation posed by the previously required extensive microscopy screening.

Most *M. oryzae* effectors are co-expressed *in planta* during invasive growth and show no expression prior to plant penetration, in conidia and mycelium (Mosquera *et al.*, 2009, Yan *et al.*, 2023). The screen works with the same hypothesis; that expression of effector-encoding genes requires activation of their promoters during host colonisation and/or de-repression of these same promoters prior to plant penetration. For the new screen, effector promoter fusions to the *Hph* (hygromycin B phosphotransferase) antibiotic-resistance gene were designed. The *Hph* gene confers resistance to hygromycin B, a protein synthesis inhibitor extensively used as a selectable marker in fungi (Rao *et al.*, 1983, Kaster *et al.*, 1984, Giordano & McAllister, 1990). *M. oryzae* transformants with effector promoter-*Hph* fusions were therefore subjected to mutagenesis to identify *CER* mutants showing resistance to hygromycin B. Mutants constitutively expressing the *Hph* gene made screening possible by growth on selectable medium as shown in Figure 3.9. Constitutive expression of effectors was then confirmed by q-RT-PCR analysis and identification of putative effector candidate gene regulators achieved by whole genome sequencing, and SNP calling pipelines.

Figure 3.9 Putative *CER* mutants grow on Hygromycin B-containing medium. Images of candidate mutants *CER100, CER102, CER103, CER104,* and *CER105* growing on selection medium (CM with 800 µg/mL of Hygromycin B). *M. oryzae* effector promoter-*Hph* fusions were subjected to UV mutagenesis and then selected on Hygromycin B-containing medium. *M. oryzae* transformant prior to UV mutagenesis is used as a negative control (WT).

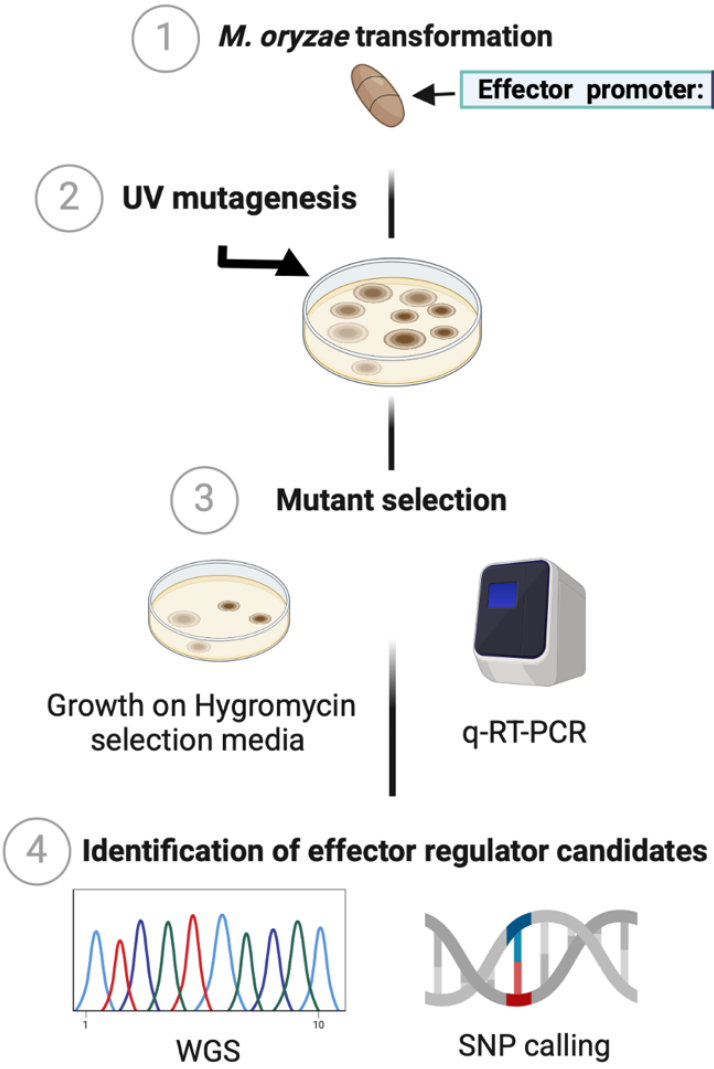

Figure 3.10 Pipeline of an alternative forward genetic screen to identify regulators of effector-gene expression in *M. oryzae*. Schematic representation of the forward genetic screen. (1) *M. oryzae* is transformed with effector promoter fusions to the *Hph* (hygromycin B phosphotransferase) gene. (2) Transformants are then subjected to UV mutagenesis. (3) Mutants with constitutive expression of effector are screened by growth on selection medium containing hygromycin B, and verified by q-RT-PCR analysis. (4) Constitutive Effector Regulator (*CER*) mutants are sent for whole genome sequencing to perform SNP calling analysis, and identify effector regulator candidates. (Image created with BioRender.com)

3.2.7 *CER* candidate mutants obtained through the alternative forward genetic screen do not show constitutive effector gene expression

To test whether *CER* mutant candidates obtained through the alternative forward genetic showed constitutive effector promoter activation, q-RT-PCR analysis was performed. *Hph* gene transcripts were analysed from conidial mRNA for the candidate mutants *CER100-CER112,* as shown in Figure 3.11. Contrary to our hypothesis, candidate mutants that grew on a Hygromycin B-containing medium did not show higher levels of *Hph* gene transcript than the original *M. oryzae* strain prior to mutagenesis. This result suggests that the selected *M. oryzae* strains are not *CER* mutants, and their ability to grow on the selection medium cannot be explained by constitutive expression of the gene fusion.

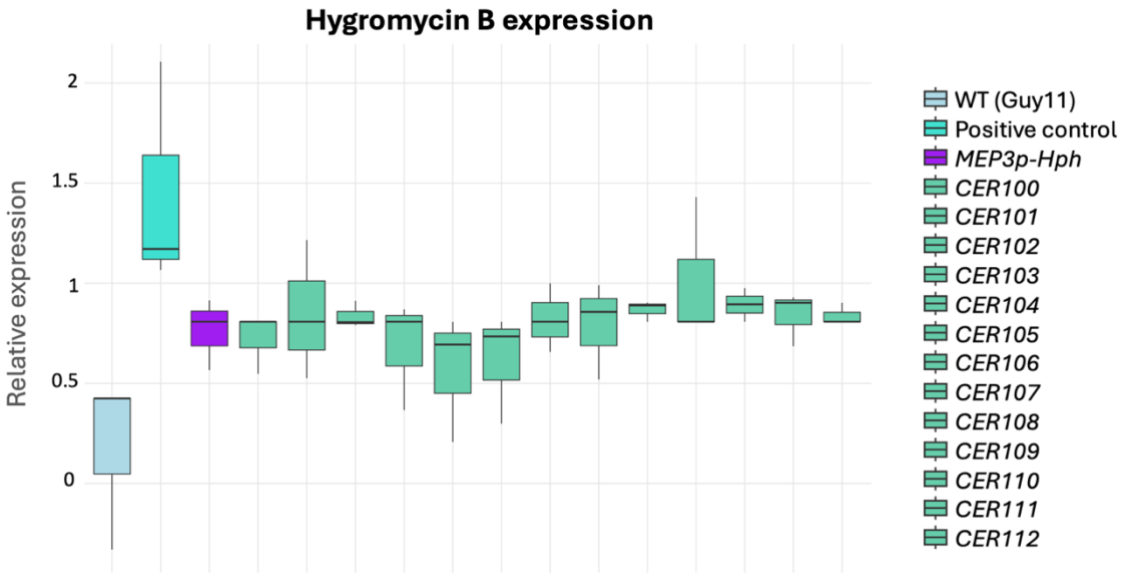

Figure 3.11 q-RT-PCR analysis reveals that *CER* mutants obtained through the alternative forward genetic screen do not show constitutive expression of the *Hph* gene. Box plot showing a log2 fold change as relative transcript level of *Hph* gene. The mean value is shown as a horizontal line inside the box. *CER100-CER112* candidate mutants have similar levels of *Hph* transcripts to the original *M. oryzae* strain prior to mutagenesis. *M. oryzae* Guy11 strain was used as a negative control and *ΔSep4* as a positive control of *Hph* expression. Actin (*MGG_03982*) and β-tubulin (*MGG_00604*) were used as housekeeping genes. Results represent three biological replicates.

3.3 Discussion

Temporal and spatial regulation of effector genes is imperative for the survival of phytopathogenic fungi and the successful colonisation of host tissue. This precise gene regulation is particularly important for hemibiotrophs, which adopt an intermediate lifestyle with a temporal switch from biotrophy to necrotrophy (Toruño *et al.*, 2016). High-throughput transcriptomic analysis of *Colletotrichum higginsianum* and *M. oryzae* evidence the meticulous orchestration of infection. In both organisms, effector genes show coordinated expression at different pathogenic stages: appressorium penetration, initial biotrophic growth, and following necrotroph switch (Kleemann *et al.*, 2012, Yan *et al.*, 2023). This suggests that these transitions are the result of sophisticated signalling that regulates effector gene expression. For *M. oryzae*, effector gene expression has been linked to regulatory pathways such as appressorium formation (Sakulkoo *et al.*, 2018, Lambou *et al.*, 2024), G-protein signalling (Tang *et al.*, 2023), and epigenetics (Soyer *et al.*, 2014, Wu *et al.*, 2021, Zhang *et al.*, 2021). However, the specific mechanisms by which these differentiated pathways regulate effector genes remain unknown.

Taking advantage of the temporal dynamics of effector gene expression, I designed and tested a series of forward genetic screens to identify effector gene regulators in *M. oryzae*. Effector genes are not expressed *ex planta* in conidia or mycelium but are highly expressed *in planta* when the pathogen is growing inside the host (Mosquera *et al.*, 2009, Yan *et al.*, 2023). Therefore, I used UV mutagenesis of an *M. oryzae* transformant expressing the effector gene fusion *MEP3-GFP* to identify *CER* mutants with constitutive effector gene expression. Under normal conditions, this strain only shows *MEP3* expression during invasive growth, so the constitutive expression of this effector in conidia and mycelium was used to select mutants. After extensive screening, I identified three putative *CER* mutants showing constitutive expression of *MEP3-GFP* named *CER1000, CER1001,* and *CER1002*. Constitutive expression of the *MEP3* effector was verified by microscopy and q-RT-PCR analysis. Potentially, these mutants have an alteration in a regulatory pathway

that governs *MEP3* transcription. Further mapping of these mutants could therefore lead to the identification of putative effector gene regulators in *M. oryzae*.

To optimise the forward genetic screen, an alternative workflow was also designed and tested. By fusing effector promoters to the hygromycin B phosphotransferase gene (*Hph*), a screen for constitutive effector-gene-expressing mutants can be facilitated directly on the selection medium. This screen follows the hypothesis that constitutive activation of the effector promoter by mutagenesis leads to constitutive expression of the *Hph* gene, making these *M. oryzae* strains resistant to the antibiotic hygromycin B. The new pipeline reduces the previous time spent on microscopy screening. In addition, by simplifying the screen, the identification of a larger number of *CER* mutants and the possibility of saturating the screen was made possible. However, all candidate *CER* mutants obtained through this alternative screen did not show expression of the *Hph* gene when checked through q-RT-PCR analysis. This result suggests that the ability of these *M. oryzae* strains to grow on a hygromycin B-containing medium must be related to mutations different from the expected alteration of effector transcription driving *Hph* gene expression.

Hygromycin B is an extensively used antibiotic which targets small ribosomal subunits affecting protein synthesis. The *Hph* resistance gene encodes for an enzyme that phosphorylates hygromycin B, rendering it inactive (Rao *et al.*, 1983). The *Hph* gene has proven highly effective and is extensively used as a selectable marker in filamentous fungi (Rao *et al.*, 1983, Kaster *et al.*, 1984, Giordano & McAllister, 1990). However, some studies may explain *M. oryzae* acquired tolerance to this antibiotic following mutagenesis. In yeast, for instance, it was shown that specific mutations of different components of the plasma membrane proton-pumping ATPase influence tolerance to hygromycin B antibiotic (Goossens *et al.*, 2000). Similarly, mutants with malfunctioning lysosomal trafficking, biogenesis, and function also show reduced hygromycin B sensitivity (Banuelos *et al.*, 2010). Additionally, a semi-synthetic yeast enhancement study reported that different genomic rearrangements specifically contribute to hygromycin antibiotic tolerance

(Ong *et al.*, 2021). Collectively, these results provide evidence that hygromycin B toxicity can be evaded in many ways in fungi, and therefore may not be the best selectable marker to perform such a forward genetic screen.

Moreover, UV mutagenesis disrupts normal base-pairing, providing a completely randomised mutagenesis method favouring point mutations and small indels (Winston, 2008). Such an unbiased mutagenesis method seemed ideal for performing forward genetic screens, and was chosen ahead of other mutagenesis methods, such as T-DNA insertion or REMI (restriction enzyme-mediated insertion), which cause loss-of-function alleles in a semi-targeted manner (Radhamony *et al.*, 2005, Kuspa, 2006). Although randomised point mutations have advantages when using the *Hph* gene for screening, impartial targeting at a relatively high frequency might have been a disadvantage. It is possible that UV mutagenesis introduced a significant number of background mutations affecting membrane composition, transporters, and/or lysosomal function, which led to adaptation or tolerance to the antibiotic. This may have also resulted from the relatively high kill rates used in UV mutagenesis, causing multiple mutations. When considered together, we can conclude that combining *Hph* gene fusions with UV mutagenesis is not a viable strategy for performing forward genetic screens in *M. oryzae*.

In the future, it may be possible to modify the screen using an alternative selectable marker. For example, BASTA (glufosinate-ammonium) resistance conferred by the *Bar* gene, has proven to have higher selective pressure than hygromycin B resistance in plant transformations (Ontiveros-Cisneros *et al.*, 2022, Ahmed *et al.*, 2024). *Bar* encodes phosphinothricin acetyltransferase (PAT) enzyme, detoxifying phosphinothricin, the active ingredient in BASTA which targets glutamine synthetase (Thompson *et al.*, 1987). This selectable marker is also widely used in filamentous fungi, including *M. oryzae* (Qin *et al.*, 2019, Li *et al.*, 2020, Garcia *et al.*, 2023). With a stronger selection efficiency directly linked to a functional *Bar* gene, BASTA resistance could overcome the tolerance problem caused by selection for hygromycin B antibiotic resistance. In addition, a pre-screen to choose the best antibiotic and best antibiotic concentration could be carried out to ensure success.

By growing *M. oryzae* on different antibiotic-containing media, for example, and selecting one in which resistance is reduced or absent after mutagenesis, acquired tolerance could potentially be avoided.

Further screen optimisation could also be achieved using antibiotic resistance gene-GFP fusion constructs. Such fusion genes, which have proven to be functional for both antibiotic resistance properties and as fluorescent markers, enable simultaneous selection and visualisation of transformants (Bennett *et al.*, 1998, Wong *et al.*, 2011, Konishi *et al.*, 2012). By using antibiotic resistance gene-GFP fusions for forward genetic screens, constitutive expression mutants could initially be screened on selection medium and then later verified through microscopy. This method would still be faster than a screen which only uses GFP fluorescence selection, and would also guarantee the selection of mutants expressing the gene fusions. The dual screening process would eliminate strains that can grow on the selection medium due to background mutations causing antibiotic tolerance. I designed and tested *Bar* gene-GFP fusion constructs in *M. oryzae* to test this idea. Fusion constructs, under a constitutive promoter, were successfully transformed, selected on BASTA-containing medium, and showed constitutive expression of GFP in conidia, as shown in Figure 3.12. This result confirms *Bar* gene-GFP constructs are functional and could be used to perform forward genetic screens in the future, presenting a new research tool to study regulatory pathways in *M. oryzae*.

In summary, in this chapter, I performed a forward genetic screen identifying three *CER* mutants showing constitutive expression of *MEP3-GFP*. Additionally, I designed an alternative faster forward genetic screen, provided reasons why it was not successful, and introduced a potential plan to overcome these limitations. Collectively, these results offer valuable resources for further studying effector gene regulation in the rice blast fungus. In Chapter 4, I describe the identification of the genes corresponding to the identified *CER* mutants.

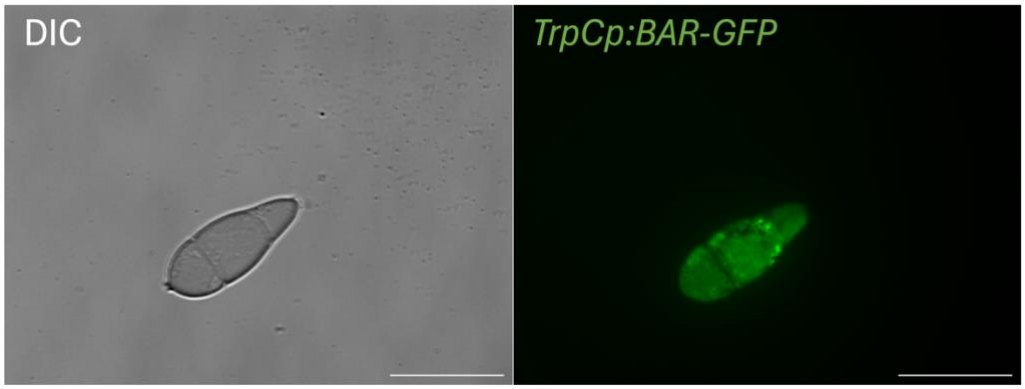

Figure 3.12 *Bar* gene-GFP construct is functional in *M. oryzae*. Micrographs of *M. oryzae* transformed with *Bar* gene-GFP fusion constructs under *TrpC* constitutive promoter (Hamer & and Timberlake, 1987) show GFP expression in conidia. Conidia were harvested from 5-day-old culture plates and immediately observed with an epifluorescence microscope. Scale bar = 10 μm.

Chapter 4: Regulatory Plasticity in Fungal Virulence: Lessons from *MEP3* and *RGS1*

4.1 Introduction

Genetic context, shaped by chromatin structure, genetic interactions and environmental signals, enables gene expression to become highly dynamic (Gibcus & Dekker, 2012). Because of this, fungal genetic regulation adapts to changing conditions, including host immunity, internal or external stressors, and nutrition availability (Gladieux *et al.*, 2018). This allows fungi to survive stresses and mutagenesis by compensatory mechanisms and redundant signalling pathways (Lehner, 2011). Although signal transduction, transcription factors (TF), and RNA editing are known to be the most critical control points, every step in the DNA-to-RNA-to-protein pathway presents an opportunity for regulation (Karin, 1991, Lynch & Conery, 2003, Noble & Andrianopoulos, 2013). Furthermore, gene regulation becomes more complex when considering the larger regulatory landscape, including chromatin remodelling, non-coding RNAs, and post-transcriptional mechanisms (Jaenisch & Bird, 2003, Gibcus & Dekker, 2012, Moore *et al.*, 2013).

Well-known documented examples of genomic plasticity exist for fungal pathogens. In *Fusarium graminearum*, deleting the MAPK Gpmk1, which controls virulence, can trigger a compensatory response that upregulates another MAPK, Mgv1, involved in cell wall integrity (Ren *et al.*, 2019). Additionally, in the human pathogen *Candida albicans*, different environmental conditions can be balanced through Hsp90 chaperones by stabilising alternative signalling pathways (O'Meara et al., 2017). Another manifestation of fungal plasticity is the epigenetic control of virulence genes, which allows pathogens to switch rapidly between different infection states. Histone changes, for instance, drive the phenotypic switching between white and opaque states in *C. albicans* and transcriptional regulators, such as Wor1, govern the transition between commensal and pathogenic forms (Zordan

et al., 2006). Additionally, effector gene expression in *M. oryzae* has been shown to be influenced by heterochromatin-dependent gene silencing, which allows the pathogen to optimise its infection strategy (Soyer *et al.*, 2014). These additional layers of regulation enable fungi to rapidly adapt their gene expression, providing a great selectable advantage to changing environments (Gladieux *et al.*, 2018).

Transcriptional and post-transcriptional gene regulation is modulated by signal transduction cascades that translate internal or external stimuli. These signalling pathways involve secondary messengers such as Ca^{2+}, cAMP, IP_3, protein-protein interactions, phosphorylation, and G-protein activation, ultimately modulating TF activity. These modifications affect TF localisation, conformational states, and protein interactions, influencing DNA-binding ability and transcriptional control (Karin, 1991).

A key component of these transduction pathways is the G-protein signalling system, which serves as a molecular switch, integrating environmental signals to regulate cellular processes. G-proteins control growth, stress response, and virulence (Gilman, 1987, Siderovski & Willard, 2005) by forming heterotrimeric complexes composed of G_α, G_β, and G_γ subunits that mediate responses to external stimuli (Gilman, 1987, Watson *et al.*, 1996). G-proteins experience conformational changes when G-protein-coupled receptors (GPCRs) are activated. They switch from an inactive GDP (guanosine diphosphate) bound state to an active GTP (guanosine triphosphate) bound state. This activation dissociates the G_α subunit from the $G_{\beta\gamma}$ dimer, triggering downstream signalling events such as phosphodiesterase activation, protein kinase cascades, adenylate cyclase stimulation, and ion channel regulation (Siderovski & Willard, 2005). Regulators of G-protein signalling (RGS) modulate these pathways by accelerating GTP hydrolysis, thereby fine-tuning cellular responses (Mukerjee *et al.*, 2011, Zhang *et al.*, 2011a, Park *et al.*, 2012a). *M. oryzae* possesses one G_γ subunit, two G_β subunits (Mgb1 and Mgb2) and three distinct G_α subunits (MagA, MagB and MagC). To regulate sexual reproduction, infection-mediated development, conidiation, and pathogenicity,

these G-proteins interact with RGS proteins (Liu & Dean, 1997, Nishimura *et al.*, 2003, Liu *et al.*, 2007). A forward genetic screen also revealed *RGS1* as a late-stage effector gene expression repressor (Tang *et al.*, 2023). This suggests that RGS proteins may also have direct roles in gene regulation in addition to their classical function in signal transduction. The capacity to activate or suppress effector genes in response to environmental cues may benefit a pathogenic fungus, as effectors are essential for host infection.

To investigate these pathways further, in Chapter 3, I described a forward genetic screen used to identify regulators of *MEP3*, a late-stage effector gene in *M. oryzae*. Three putative *CER* mutants (*CER1000, CER1001*, and *CER1002*) that showed constitutive expression of *MEP3* were identified through this screen. Following the characterisation of these mutants, the present chapter identifies the corresponding candidate gene regulating *MEP3* expression. Whole-genome sequencing and SNP analysis revealed that *CER1001* and *CER1002* carried mutations in *RGS1*, confirming its role as an effector gene repressor. However, for the *CER1000* mutant, none of the identified potential regulators could be confirmed in genetic complementation experiments. RNA sequencing analysis was performed in all three mutants, revealing additional SNPs to those initially found through WGS. This result suggests that translational regulatory mechanisms or secondary mutations may have arisen to obscure *MEP3* constitutive expression.

These results support the idea that fungal diseases have a high regulatory plasticity, enabling them to buffer genetic disruptions through redundant pathways and epigenetic modifications. The unexpected loss of *MEP3* transcripts in *CER* mutants highlights the complexity of gene regulation, raising the possibility of compensatory mutations, chromatin remodelling, or translational silencing. These results are discussed in the context of effector gene regulation, particularly highlighting the role of *RGS1* in this process.

4.2 Results

4.2.1 Bioinformatic pipeline to identify SNPs in sequenced mutants

A bioinformatic pipeline was designed to identify the candidate genes responsible for regulating *MEP3-GFP* expression in the putative *CER* mutants, as illustrated in Figure 4.1. Illumina whole genome sequencing was performed on three *CER* mutants (*CER1000*, *CER1001,* and *CER1002*) alongside the original *MEP3-GFP M. oryzae* strain prior to mutagenesis. Quality control of the raw reads was done with FastQC (Babraham Bioinformatics) to evaluate data integrity. Then, Trimmomatic was used to filter out sequences with fewer than 25 base pairs (Bolger *et al.*, 2014) and trim Illumina adapter sequences. The processed reads were aligned to the Guy11 reference genome of *M. oryzae* using the Burrows-Wheeler Aligner (BWA-MEM) program. The resulting SAM files were sorted and converted to BAM format using Samtools 1.9 (Li *et al.*, 2009), and the Genomic Analysis Toolkit (GATK) was used to find single nucleotide polymorphisms (SNPs), small insertions or deletions (indels). The resulting VCF files were filtered and annotated using HaplotypeCaller and SNPEff to determine the functional impact of the identified mutations. Identical mutations were cross-compared among all samples to exclude shared variants and focus on distinct alleles. Additionally, read coverage was analysed to ensure that no genomic regions displayed abnormally low or non-existent read counts, suggesting larger deletions in the sequences.

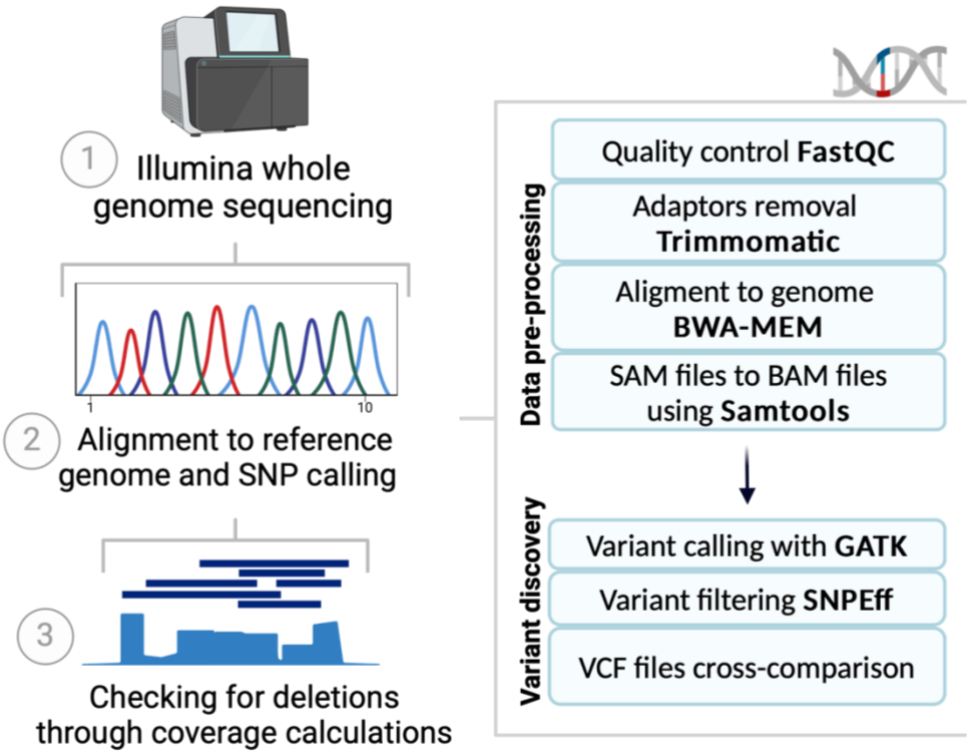

Figure 4.1 Bioinformatic pipeline for the discovery of SNPs in sequenced mutants. Schematic representation of a bioinformatic pipeline for identification of SNPs and indels in the sequenced *M. oryzae* mutants. (1) Strains were sent for the whole genome sequence using Illumina. (2) FastQC is used to assess the quality of the reads; Trimmomatic is used to remove low-quality reads, <25 base pair long reads and Illumina adapter sequences; and alignment to the reference genome is done using BWA-MEM software (Burrows-Wheeler Aligner) and Samtools 1.9. Finally, GATK (Genomic Analysis Toolkit) HaplotypeCaller and SNPEff are used for the identification of SNPs and indels, functionally annotated and finally filtered identical mutations between strains are used to generate a list of putative gene regulator candidates. (3) Large-scale genomic deletions are checked by calculating read coverage to ensure no genomic regions exhibit abnormally low or absent read counts. (Image created with Biorender.com)

4.2.2 *CER* mutant sequence analysis allows the identification of putative effector gene regulators in *M. oryzae*

Using the described bioinformatic pipeline, putative *MEP3* effector gene regulators were identified for the sequenced mutants (*CER1000, CER1001,* and *CER1002),* as shown in Table 4.1. By focusing on SNPs or indels near or within coding regions, a final list of 17 putative regulator genes was compiled: 11 for the *CER1000* mutant, 3 for the *CER1001* mutant, and 4 for the *CER1002* mutant.

Most SNPs found were missense variants, single nucleotide substitutions that change codons and result in alterations to amino acids. Nevertheless, a deletion, an early start codon mutation, and frameshift mutations were also found. Notably, in the list of putative gene regulators, *MGG_05308* and *MGG_10001* were previously found to influence virulence through high-throughput mutagenesis (Jeon *et al.*, 2007), and *MGG_06465*, a homologue of the yeast *PDS5* is known to be involved in epigenetic regulation (Goto *et al.*, 2017). The discovery of mutations in these genes supports the hypothesis that these putative regulators may control pathogenicity.

Additionally, all three *CER* mutants displayed mutations in G-protein signalling pathway components, with the G_{α} subunit MagA (*MGG_04204*) mutated in *CER1000,* and *RGS1* (*MGG_14517*) mutated in *CER1001* and *CER1002*. This finding supports previous research that connected G-protein signalling to effector regulation in the blast fungus (Tang *et al.*, 2023). However, due to the existence of a list of potential effector regulators containing different mutations for each *CER* strain, a complementation analysis was conducted to pinpoint the precise causal mutation linked to the constitutive expression of *MEP3-GFP*.

Table 4.1 Putative regulator genes identified through the *CER* mutant WGS analysis.

Mutant	Gene	Information about the SNP	Information about the gene
CER1000	*MGG_15057*	Missense variant	Membrane transporter activity domain
CER1000	*MGG_15981*	Missense variant	Uncharacterized (very small)
CER1000	*MGG_07497*	Missense variant	Averantin oxidoreductase (Pythocrome 450 family) iron binging
CER1000	*MGG_06053*	Missense variant	Regulator of phospholipase D *SRF1*
CER1000	*MGG_05308*	Missense variant	Uncharacterized (reduced virulence, sporulation, germination and appressorium formation phenotype)
CER1000	*MGG_06465*	Missense variant	*PDS5* (involved in chromosomal maintenance)
CER1000	*MGG_00690*	Missense variant	Uncharacterized (very small)
CER1000	*MGG_04204*	Missense variant	Guanine nucleotide-binding protein alpha-2 subunit (G_{α})
CER1000	*MGG_09444*	Missense variant	Methylitaconate delta2-delta3-isomerase
CER1000	*MGG_10299*	Missense variant	Heterokaryon incompatibility domain-containing protein
CER1000	*MGG_10577*	5 prime UTR premature start codon	Uncharacterized
CER1001	*MGG_14517*	Frameshift variant	*RGS1*
CER1001	*MGG_07024*	Frameshift variants	Predicted virulence factor with a signal peptide
CER1001	*MGG_16623*	Disruptive in frame deletion	Mating type protein *MAT1-2-4*
CER1002	*MGG_14517*	Missense variant	*RGS1*
CER1002	*MGG_08415*	Missense variant	*MPN1,* metalloprotease
CER1002	*MGG_12955*	Frameshift variant	Target of rapamycin complex 2 subunit *SIN1*
CER1002	*MGG_10001*	Frameshift variants	Uncharacterized (reduced virulence)

4.2.3 Genetic complementation experiment confirms *RGS1* dominantly represses *MEP3-GFP* expression in *M. oryzae* conidia

Genetic complementation experiments were performed to determine whether the SNPs found in the *RGS1* locus, after UV mutagenesis, were responsible for the constitutive expression of *MEP3-GFP* in the *CER1001* and *CER1002* mutants. *RGS1* had been previously reported to repress a subset of effectors in *M. oryzae* (Tang *et al.*, 2023), prompting us to investigate whether it also functions as a transcriptional repressor of *MEP3* expression. We reasoned that if the identified SNPs result in a malfunctioning allele, the ectopic transformation of the *CER* mutants with native *RGS1* should restore wild-type repression of *MEP3* in conidia. The workflow used to generate complementation experiments is shown in Figure 4.2.

Using this method, an ectopic copy of *RGS1* with its native promoter and 3' UTR sequences was successfully introduced into *CER1001* and *CER1002* mutants. GFP transcript levels in conidial mRNA were measured using q-RT-PCR analysis to evaluate transcriptional suppression of *MEP3-GFP*. In both mutants transformed with functional *RGS1*, *MEP3-GFP* transcript levels were comparable to those in the *M. oryzae MEP3-GFP* transformant prior to mutagenesis, as shown in Figure 4.3. Independent t-tests revealed a significant difference (p-value <0.05) in *MEP3-GFP* expression for the *CER* mutants before genetic complementation (*CER1001* and *CER1002*) but not for their respective complemented strains (*CER1001-RGS1* and *CER1002-RGS1*). These results prove that if *RGS1* is introduced *in trans,* it can dominantly repress the expression of *MEP3* in *M. oryzae* conidia.

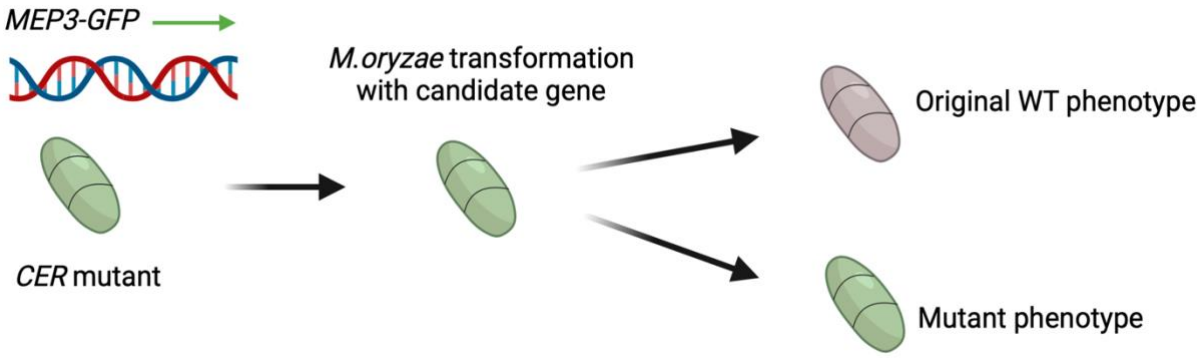

Figure 4.2 Genetic complementation workflow. A genetic complementation experiment was designed to validate that putative effector regulator candidates can transcriptionally repress *MEP3-GFP* expression. *M. oryzae CER* mutants are ectopically transformed with functional copies of putative effector genes with native promoter and 3'UTR sequences. Transformants are then analysed phenotypically for their ability to restore the wild-type *MEP3* gene expression in conidia. (Image created with Biorender.com)

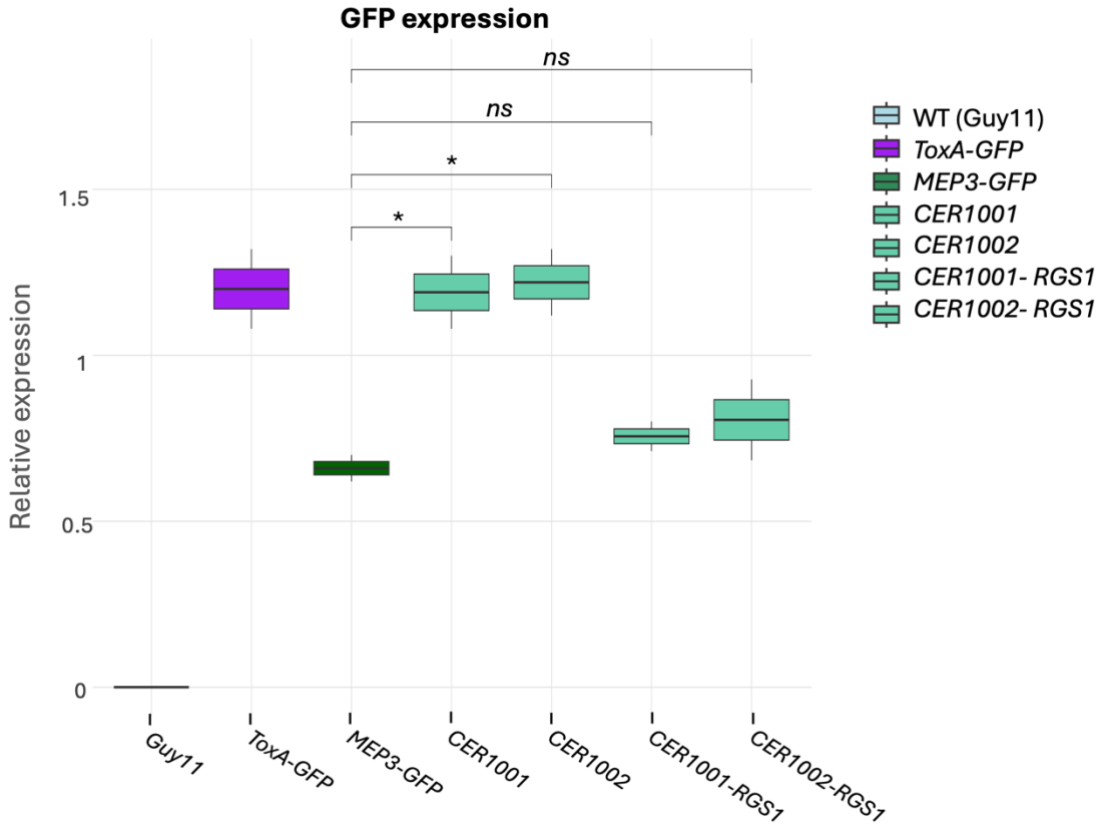

Figure 4.3 q-RT-PCR analysis confirms *RGS1* functions as a transcriptional repressor of *MEP3* expression. Box plots showing a log2 fold change as relative transcript level of GFP. Independent t-tests revealed a significant difference (p-value <0.05) in *MEP3-GFP* expression for the *CER* mutants prior to genetic complementation (*CER1001* and *CER1002*) but not for their respective complemented strains (*CER1001-RGS1* and *CER1002-RGS1*). *M. oryzae* Guy11 strain was used as a negative control, and *M. oryzae ToxA-GFP* transformant as a positive control of GFP expression. Actin (*MGG_03982*) and β-tubulin (*MGG_00604*) were used as housekeeping genes for q-RT-PCR analysis. The mean value is shown as a horizontal line inside the box, and error bars equal the standard deviation. Results represent three biological replicates.

4.2.4 Unique *RGS1* mutations identified in *CER1001* and *CER1002* mutants

Having confirmed that the *RGS1* mutations found in *CER1001* and *CER1002* are responsible for constitutive *MEP3-GFP* expression in conidia, we proceeded to analyse these mutations. For *CER7,* a previously characterised *RGS1* mutant, whole genome sequencing identified a SNP introducing a stop codon at position 289. This premature termination results in a truncated Rgs1 protein lacking predicted NLS (nuclear localisation signal) and RGS domains, impairing its functionality (Tang *et al.*, 2023). The independent *RGS1* mutations found in *CER1001* and *CER1002* mutants differ from those of *CER7*, as shown in Figure 4.4. *CER1001* presents a SNP within the RGS domain at position 648, leading to early termination of protein translation, albeit only 22 amino acids shorter. In contrast, *CER1002* carries a SNP upstream of the predicted NLS at position 361, altering a positively charged amino acid arginine to polar uncharged glutamine in the protein sequence.

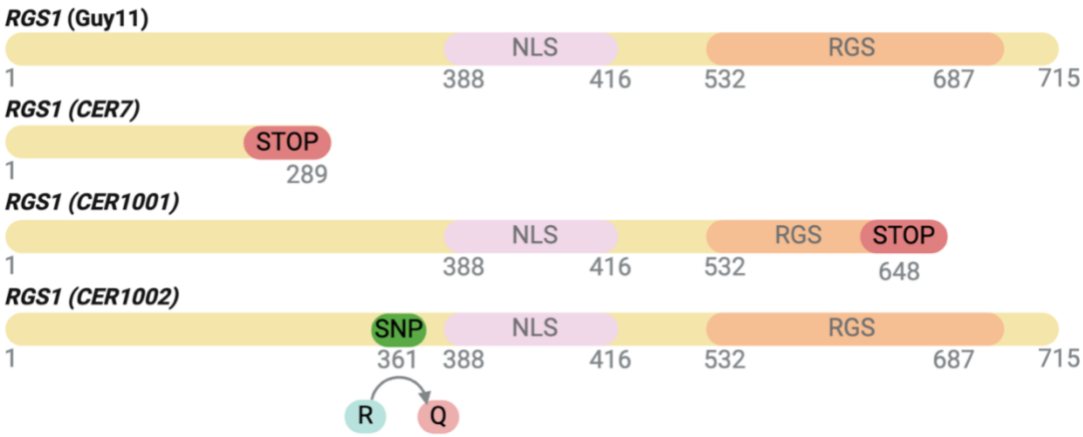

Figure 4.4 *RGS1* SNPs found in *CER1001* and *CER1002* mutants. Schematic representation of the mutations identified within the *RGS1* coding region for three independent *CER* mutants. *CER7* shows a SNP at position 289, introducing an early stop codon—the premature termination results in a truncated Rgs1 protein lacking predicted NLS and RGS domains. *CER1001* shows a SNP at position 648, which also leads to an early stop codon, but the truncated version of Rgs1 protein is only 22 amino acids shorter than native Rgs1. *CER1002* shows a missense SNP at position 361, altering a positively charged amino acid arginine to polar uncharged glutamine in the protein sequence. (Image created with Biorender.com)

4.2.5 *CER1001* and *CER1002* mutants *of M. oryzae* show reduced virulence

Leaf drop infections evaluated the pathogenicity of mutant strains *CER1000*, *CER1001*, and *CER1002*. Compared to the wild-type strain Guy11, *CER1001* and *CER1002* exhibited significantly reduced pathogenicity (p-value <0.05), as shown in Figure 4.5. According to earlier research, *RGS1* mutations and deletions demonstrate decreased virulence in leaf infection assays (Tang *et al.*, 2023). Therefore, these findings provide evidence that the *RGS1* mutations present in *CER1001* and *CER1002* may result in a malfunctioning allele, impairing the virulence of the fungus.

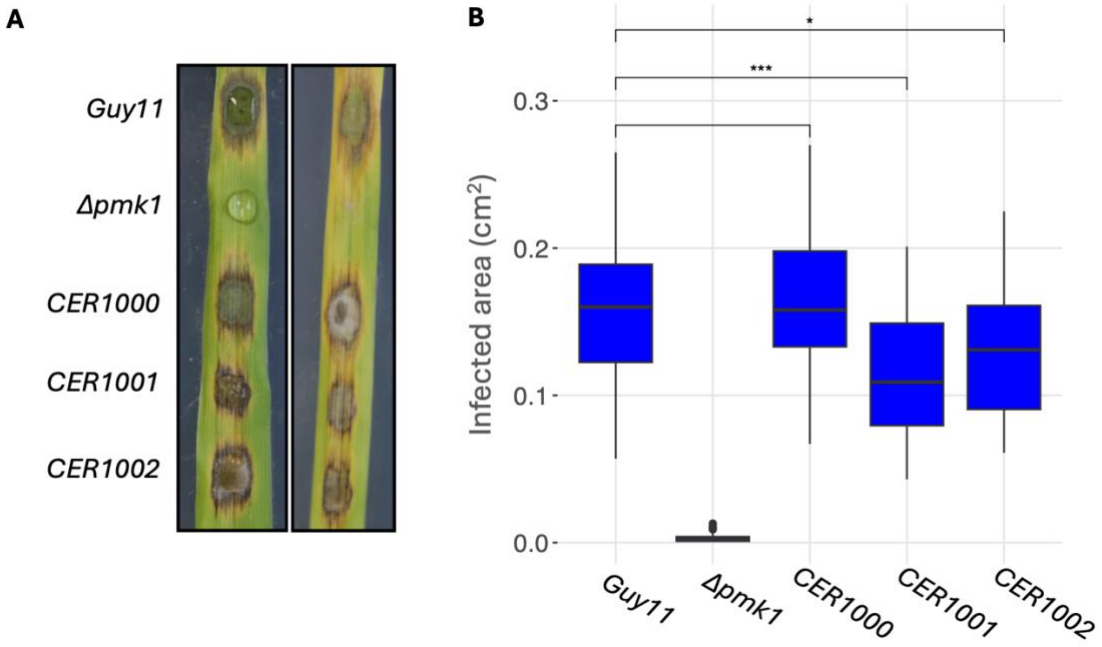

Figure 4.5 *CER1001* and *CER1002* mutant strains have reduced virulence phenotypes. (A) One-week-old seedlings of barley cultivar Golden Promise were inoculated with equal amounts of conidial suspension (5 x 10^4 conidia/mL with 0.2% (w/v) gelatin) of *M. oryzae* strains Guy11, *Δpmk1*, *CER1000, CER1001* and *CER1002*. Detached leaves were incubated on water-soaked Whatman paper at 25°C with a 12h photoperiod for 5 days before visualising and quantifying blast disease progression. (B) Box plots show the calculated area of disease lesions for each strain (n=20 lesions per replicate). The mean value is shown as a horizontal line inside the box. T-tests show significantly reduced virulence (p-value <0.05) for *CER1001* and *CER1002* mutants when compared to the infection caused by wild-type strain Guy11. Δ*pmk1* mutant was used as a negative control. Results represent three biological replicates.

4.2.6 Putative effector gene regulators found for the *CER1000* mutant are unable to suppress *MEP3* expression

To determine whether any of the 11 putative effector regulator genes identified through whole-genome sequencing of the *CER1000* mutant were responsible for *MEP3-GFP* constitutive expression, I performed genetic complementation experiments following the workflow in Figure 4.2. This approach examined whether individually adding a native allele of the putative regulators into the *CER1000* mutant background could dominantly suppress constitutive *MEP3-GFP* expression.

For complementation experiments, allele copies for each putative regulator were ectopically transformed into *M. oryzae* under the control of their native promoters and corresponding 3'UTR sequences (*CER1000-MGG_06465, CER1000-MGG_06053, CER1000-MGG_04204, CER1000-MGG_10299, CER1000-MGG_05308, CER1000-MGG_09444, CER1000-MGG_00690, CER1000-MGG_15057,* and *CER1000-MGG_07497*). To assess whether any complemented strains restored the original *MEP3* gene expression phenotype, GFP fluorescence was analysed by epifluorescence microscopy and q-RT-PCR analysis. Epi-fluorescence microscopy images were quantified for pixel intensity. As Figure 4.6 illustrates, individual t-tests (p-value <0.05) showed no significant differences in fluorescence between the *CER1000* mutant and any complemented strains.

Furthermore, to support this result, we measured *GFP* transcript levels in conidial mRNA. The *CER1000* mutant and its complemented strains did not differ significantly (p-value <0.05) according to q-RT-PCR analysis, as shown in Figure 4.7. This finding corroborates the earlier fluorescence measurement, indicating that none of the putative candidates functioned as transcriptional regulators of *MEP3* expression in the *CER1000* mutant. However, further examination is required to determine whether these potential regulators influence *MEP3* expression in *M. oryzae*.

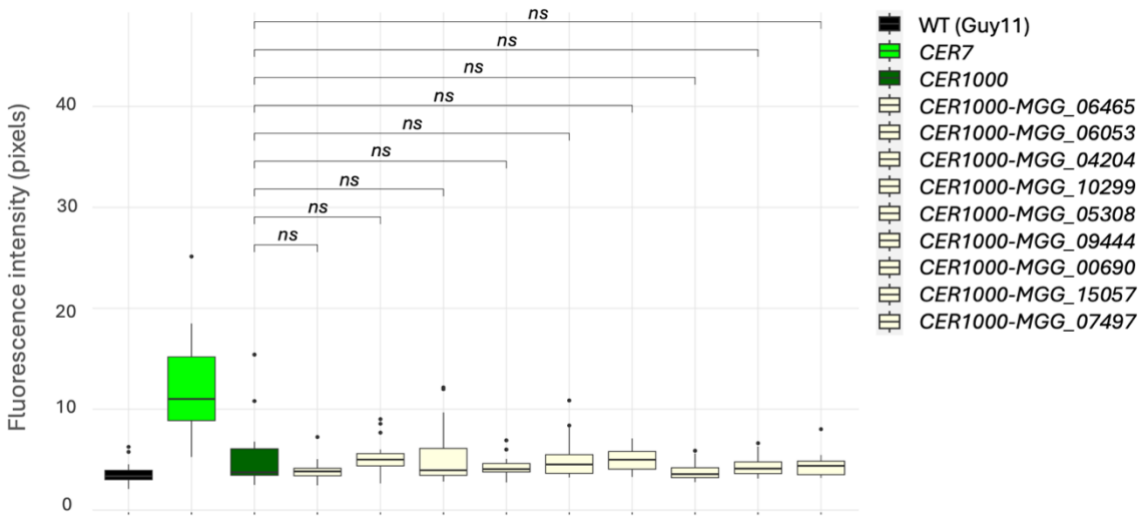

Figure 4.6 Similar fluorescence intensity was found for the *CER1000* mutant and complemented strains. Box plots show fluorescence intensity pixel quantification from epifluorescence images, calculated using ImageJ (Fiji). No significant difference (p-value <0.05) was found between *CER1000* and its complemented strains (*CER1000-MGG_06465, CER1000-MGG_06053, CER1000-MGG_04204, CER1000-MGG_10299, CER1000-MGG_05308, CER1000-MGG_09444, CER1000-MGG_00690, CER1000-MGG_15057,* and *CER1000-MGG_07497*), revealing none of these putative effector regulators can dominantly repress *MEP3* expression. *M. oryzae* Guy11 strain was used as a negative control, and the *CER7* mutant, which has constitutive *MEP2-GFP* expression, as a positive control of GFP expression. The mean value is shown as a horizontal line inside the box. Results represent three biological replicates.

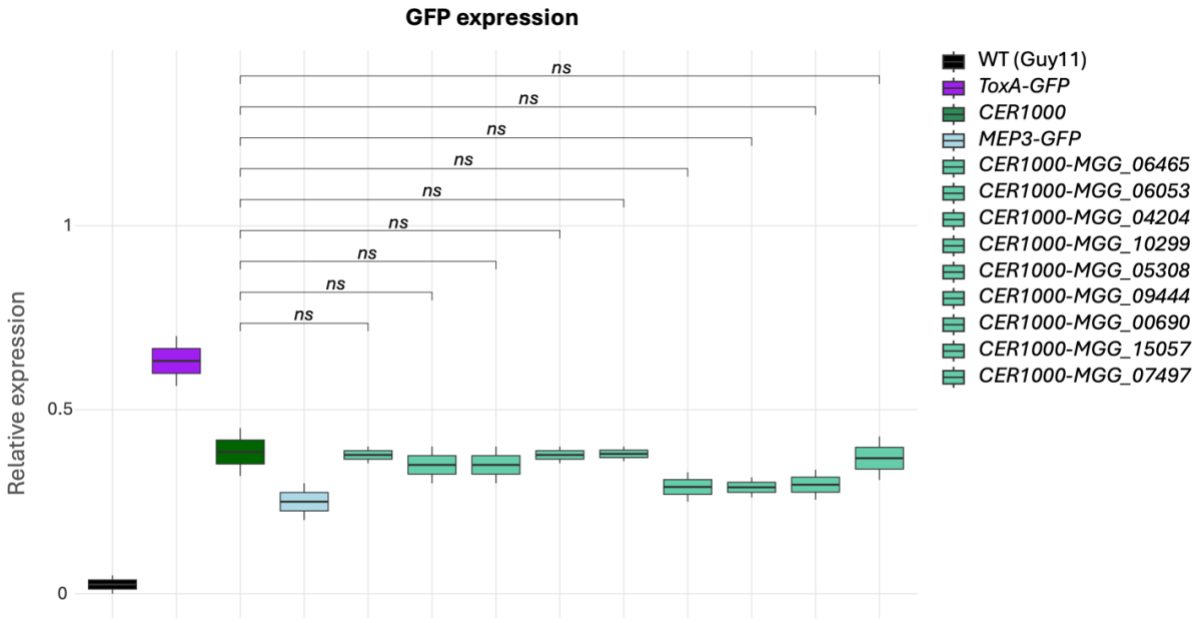

Figure 4.7 Similar *GFP* transcript levels were found for the *CER1000* mutant and complemented strains. Box plots showing a log2 fold change as relative transcript level of GFP. Independent t-tests revealed no significant difference (p value <0.05) between *CER1000* and its complemented strains (*CER1000-MGG_06465, CER1000-MGG_06053, CER1000-MGG_04204, CER1000-MGG_10299, CER1000-MGG_05308, CER1000-MGG_09444, CER1000-MGG_00690, CER1000-MGG_15057,* and *CER1000-MGG_07497*) confirming the previous fluorescence quantification results. *M. oryzae* Guy11 strain was used as a negative control, and the *CER7* mutant, which has constitutive *MEP2-GFP* expression, was used as a positive control of *GFP* expression. Actin (*MGG_03982*) and β-tubulin (*MGG_00604*) were used as housekeeping genes for the q-RT-PCR analysis. The mean value is shown as a horizontal line inside the box. Results represent three biological replicates.

4.2.7 RNA sequencing for the *CER* mutants

Following the characterisation of the *CER* mutants, we performed RNA sequencing analysis of conidial mRNA from *CER1000, CER1001,* and *CER1002*, along with the *MEP3-GFP M. oryzae* strain, prior to mutagenesis. The goal was to validate the constitutive expression of *MEP3*, investigate transcriptional similarities between *CER1001* and *CER1002* with previously characterised *RGS1* mutants, and gain further insight into *CER1000*, for which a putative effector regulator had not yet been identified.

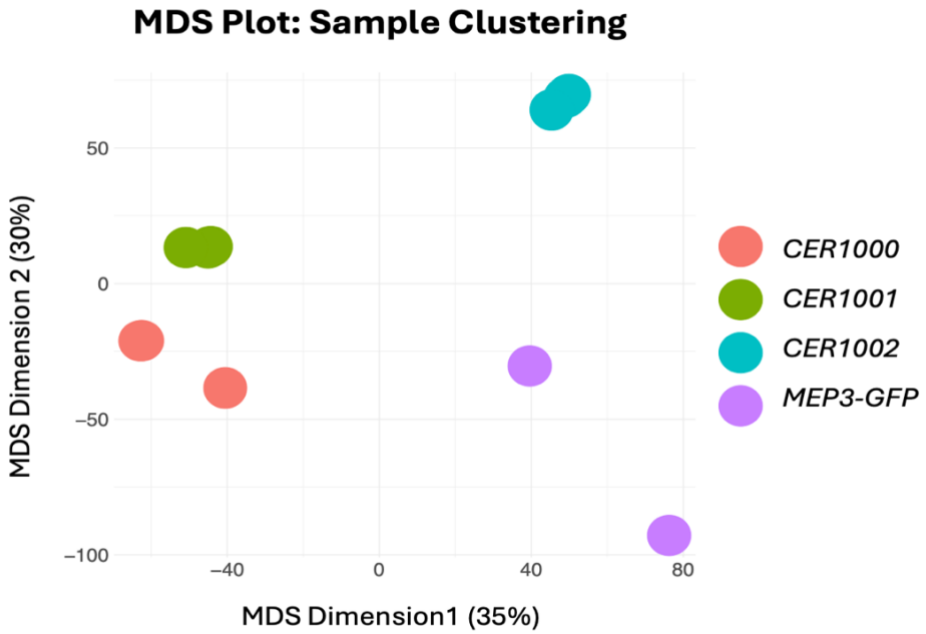

Figure 4.8 Multidimensional scaling (MDS) plot for RNA-Seq experiment of *CER1000, CER1001, CER1002,* and *MEP3-GFP M. oryzae* strains. MDS plotting was performed to analyse sample clustering based on expression value. Combining both dimensions, there is a 65% variance across samples. Biological replicates, represented by the same colours, cluster together, suggesting reproducibility of the data, and different strains show differentiated clustering. *CER1000* samples are represented in red, *CER1001* in green, *CER1002* in blue, and *MEP3-GFP M. oryzae* strain prior to mutagenesis in purple.

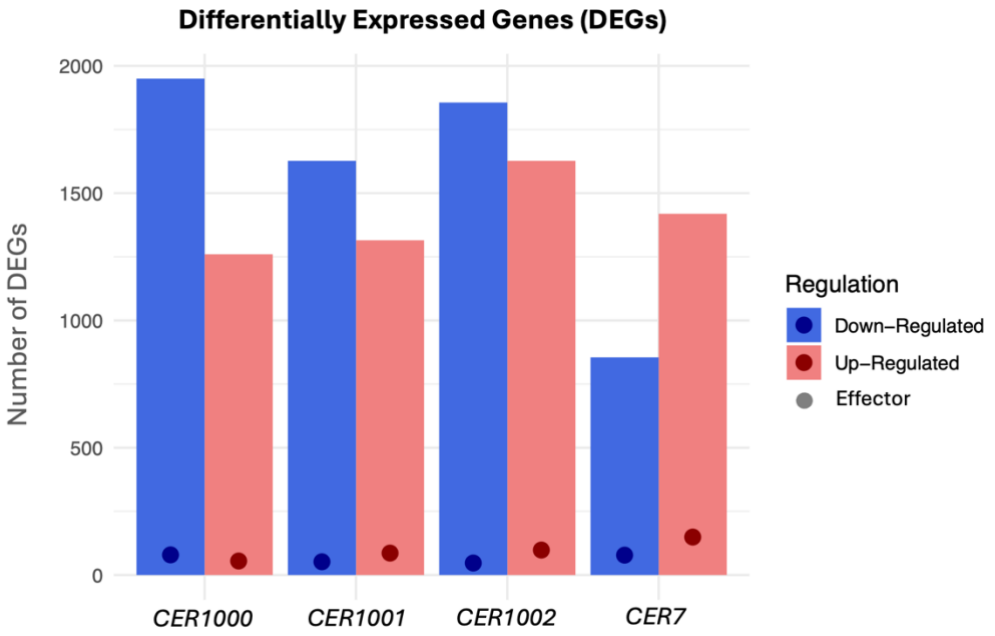

Figure 4.9 Number of DEGs across *CER* mutant. Bar chat displays the number of differentially expressed genes (DEGs) for four comparisons (*CER1000, CER1001, CER1002,* and *CER7 vs. MEP3-GFP*). Blue bars represent up-regulated genes, while red bars indicate down-regulated genes. Effector genes are marked as blue (up-regulated) and red (down-regulated) dots.

Transcriptional clustering of the RNA sequencing data was analysed using a multidimensional scaling (MDS) plot. The first MDS dimension (35%) and second MDS dimension (30%) accounted for 65% of the total variance across all eight samples, as shown in Figure 4.8. Reassuringly consistent with reproducibility of the data generated, biological replicates for each sample grouped together, while higher variance was observed among different strains.

Illumina RNA-Seq analysis was used to examine two biological replicates per strain. Trimmomatic (Bolger *et al.*, 2014) and FastQC (Babraham Bioinformatics) were used for raw read quality control and filtering. Kallisto was used to quantify the processed reads after they were mapped to the *M. oryzae* Guy11 reference genome (Bray *et al.*, 2016), and edgeR was used for differential gene expression analysis of the transcript quantifications obtained through Kallisto (Robinson *et al.*, 2009, Pimentel *et al.*, 2017). Differentially expressed genes were determined using a

threshold of $\log_2$ fold-change (>=1) and adjusted p-value (p<=0.05). Figure 4.9 shows the overall number of DEGs for each comparison, finding misregulation in effector genes.

To further investigate the similarities among different *RGS1* mutants, we compared DEGs from *CER1001* and *CER1002* to those of *CER7*, as illustrated in Figure 4.10. We hypothesised that independent *RGS1* mutations in all three strains could have comparable effects on gene expression if they all led to a malfunctioning allele. Through cross-comparison of all three mutants, we identified 93 genes commonly up-regulated, including 15 late-expression effector genes, and 41 commonly down-regulated genes. This result further supports *RGS1* function as a transcriptional repressor of late expression effectors genes in *M. oryzae*. Additionally, by examining both shared and distinct transcriptional alterations among these mutants, this data can be used to gain further insights into *RGS1* regulatory mechanisms.

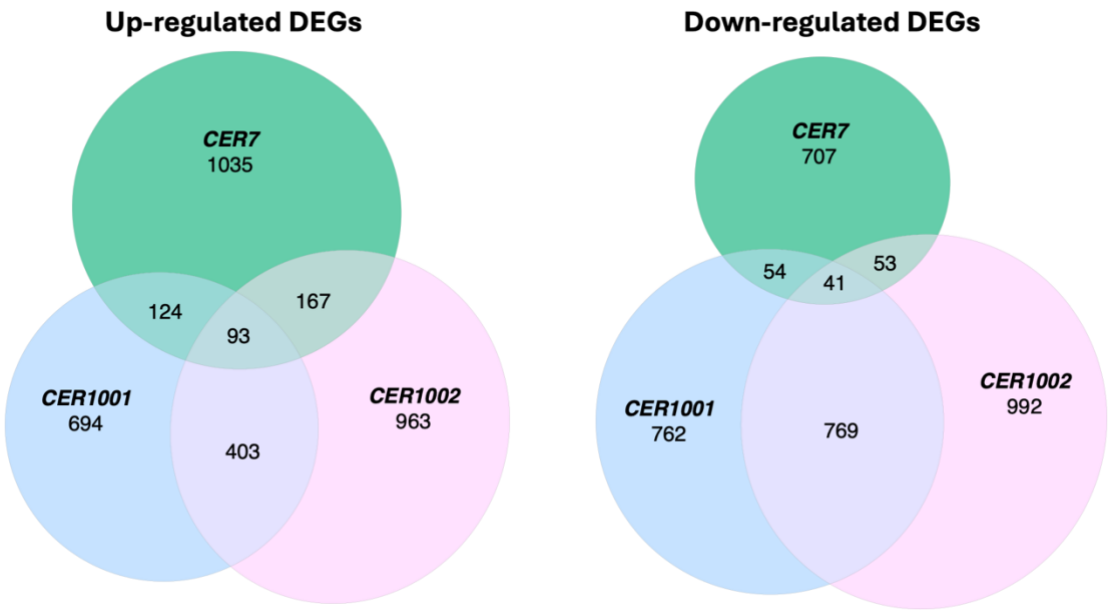

Figure 4.10 Overlapping DEGs for *CER1001, CER1002* and *CER7*. DEGs for three *RGS1* mutants—*CER1001* (blue), *CER1002* (pink), and *CER7* (green)— show overlapping genes illustrated as Euler diagrams. Among the three strains, there are 93 commonly up-regulated genes and 41 down-regulated genes.

Furthermore, multiple effector genes were misregulated in *CER1000*, according to further cross-comparison of our data with a publicly available list of 546 predicted MEPs (Yan *et al.*, 2023). This validation demonstrated that all three *CER* mutants (*CER1000, CER1001,* and *CER1002)* carried mutations affecting the regulation of effector genes in *M. oryzae*. However, contrary to our initial hypothesis, no reads corresponding to *MEP3* were detected in any transcriptomic datasets.

To verify that these transcriptomic results corresponded to the originally sequenced *CER* mutants, we performed SNP calling using the pipeline described in Section 4.1. This analysis confirmed that the same SNPs in *RGS1* were still present in *CER1001* and *CER1002*. In *CER1000*, 8 out of the 11 initially identified SNPs remained unchanged, including mutations in *MagA* (*MGG_04204*) and *PDS5* (*MGG_06465*), as shown in Table 4.2. However, new additional SNPs were found near or within coding regions for each mutant—192 in *CER1000*, 90 in *CER1001*, and 80 in *CER1002*, illustrated in Figure 4.11.

These newly discovered SNPs could explain why *MEP3* was undetectable in the RNA-Seq data if secondary mutations had compensated for the initially selected phenotype. Given this unexpected complexity and the heavily mutated background, we decided not to investigate these three *CER* mutants further.

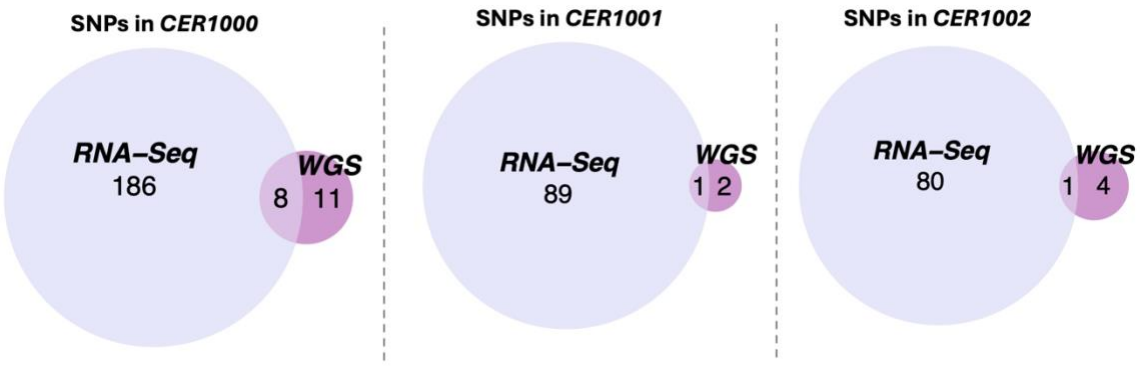

Figure 4.11 Overlapping SNPs identified through WGS and RNA-Seq analysis for *CER1000, CER1001,* and *CER1002* mutants. SNP calling pipelines were performed on each mutant strain's whole-genome sequencing and RNA-Seq datasets. Euler diagrams show the number of overlapping SNPs among both sequencing methods.

Table 4.2. Putative regulator genes identified through WGS and RNA-Seq analysis.

Mutant	Gene	Information about the SNP	Information about the gene
CER1000	*MGG_15057*	Missense variant	Membrane transporter activity domain
CER1000	*MGG_06053*	Missense variant	Regulator of phospholipase D *SRF1*
CER1000	*MGG_06465*	Missense variant	*PDS5* (involved in chromosomal maintenance)
CER1000	*MGG_00690*	Missense variant	Uncharacterized (very small)
CER1000	*MGG_04204*	Missense variant	Guanine nucleotide-binding protein alpha-2 subunit (G_{α})
CER1000	*MGG_09444*	Missense variant	Methylitaconate delta2-delta3-isomerase
CER1000	*MGG_10299*	Missense variant	Heterokaryon incompatibility domain-containing protein
CER1000	*MGG_10577*	5 prime UTR premature start codon	Uncharacterized
CER1001	*MGG_14517*	Frameshift variant	*RGS1*
CER1002	*MGG_14517*	Missense variant	*RGS1*

4.3 Discussion

Heterotrimeric G-proteins regulate fungal development and pathogenicity by linking cell surface receptors to cytoplasmic responses (Bölker, 1998). Disruption of G-protein regulators (RGS) has revealed various roles in fungi. For instance, it was discovered that the *RGS1* homolog *SST2* controls pheromone and mating responses in *Saccharomyces cerevisiae* (Dohlman *et al.*, 1996, Chasse Scott *et al.*, 2006). In pathogenic fungi such as *F. graminearum* and *M. oryzae, RGS1* contributes to full virulence, affecting vegetative growth, vesicle fusion and autophagy (Zhang *et al.*, 2011a, Yuan *et al.*, 2022). Though RGS proteins primarily regulate gene expression indirectly via cAMP signalling, *SST2* contains a proteolytic cleavage site that produces different translational products with distinct localisations and functions (Hoffman *et al.*, 2000), raising the possibility of direct gene regulation.

4.3.1 Forward genetic screens identify *RGS1* as a repressor of *MEP3*

Functional genomic screens, which associate phenotypic traits with genetic regulators, occasionally rely on understanding dynamic gene expression in specific contexts, such as developmental stages or disease progression. These screens have successfully identified key modulators of gene expression, including epigenetic regulators, transcriptional repressors, activators, and kinases (Pfannenstiel *et al.*, 2017, Reilly *et al.*, 2018, Huang *et al.*, 2020, Tang *et al.*, 2023). However, most traits are polygenic, challenging genetic research to establish direct genotype-to-phenotype relationships (O'Meara, 2024).

A forward genetic screen in *M. oryzae* identified *RGS1* as a repressor of late-expression effector genes (Tang *et al.*, 2023). Expanding on this approach, this chapter characterises Constitutive Effector Regulator (*CER*) mutants, which exhibit *MEP3-GFP* constitutive expression in conidia. Whole-genome sequencing (WGS) of *CER1000, CER1001,* and *CER1002* mutants identified SNPs near or within coding genomic regions for each mutant strain, offering a comprehensive list of putative effector regulators. For *CER1001* and *CER1002* mutants, SNPs were identified

within the *RGS1* gene. The Rgs1 protein was truncated in *CER1001* due to a SNP introducing an early stop codon in the protein sequence, while in *CER1002*, a missense mutation changed a positively charged arginine to an uncharged glutamine in the protein sequence. In contrast, the *CER1000* mutant exhibited mutations in 11 different putative effector regulators, including *MGG_05308* and *MGG_10001,* previously linked to pathogenicity (Jeon *et al.*, 2007), *MGG_06465*, a putative epigenetic regulator homologous to yeast *PDS5* (Goto *et al.*, 2017), and *MGG_04204,* the G-protein G_{α} subunit MagA (Liu *et al.*, 2007).

Genetic complementation experiments found that *RGS1* repressed *MEP3* gene expression in *M. oryzae* conidia. The result validates previous findings linking Rgs1 to effector gene regulation (Tang *et al.*, 2023). Furthermore, virulence assays confirmed that the *RGS1* mutants, *CER1001* and *CER1002,* exhibited reduced pathogenicity in barley leaf drop assays. Once again reinforcing previous findings which propose *RGS1* mutations and deletion strains show reduced pathogenicity (Zhang *et al.*, 2011a). Altogether, through forward genetics, *RGS1* has again proven to be involved in effector gene regulation, playing an essential role in disease progression. Furthermore, identifying new key mutations within the *RGS1* coding region that may modulate gene expression directly or indirectly offers new valuable resources to comprehend this regulatory system.

4.3.2 Unexpected loss of *MEP3* transcripts suggests compensatory regulatory mechanisms

Despite identifying *RGS1* as a dominant repressor of the *MEP3* gene, none of the potential effector regulator candidates could be verified as regulatory determinants for the *CER1000* mutant. This was seen through genetic complementation experiments, which demonstrated no phenotypic differences between *CER1000* or any of its complemented strains. Furthermore, *MEP3* transcripts were not detectable through RNA-Seq analysis in any of the three *CER* mutants, a finding that contradicted the initial GFP expression observations and complicated the

investigation further. SNP calling was performed on RNA-Seq data to establish the sample's identity, confirming the presence of the *RGS1* SNPs in *CER1001* and *CER1002*, and 8 out of 11 original *CER1000* SNPs. However, further SNPs were found in all three *CER* mutants, suggesting additional mutational changes beyond those initially found by WGS analysis.

These extra mutations found by RNA-seq may explain the loss of *MEP3* constitutive expression in the *CER* mutants. For instance, these secondary mutations might have occurred to lower *MEP3* transcription, obscuring the initial constitutive expression, if *M. oryzae* is disadvantaged by the misregulation of this effector. In many eukaryotic systems, it has been observed that the loss of a single regulatory gene often sets off compensatory signalling pathways that restore the balance of gene expression (Lehner, 2011). It is commonly known that fungal pathogens exhibit this regulatory buffering. In *M. oryzae*, for instance, cAMP levels regulated by *RGS1* can be counterbalanced by other RGS proteins in the event of *RGS1* mutations (Zhang *et al.*, 2011a). In *F. graminearum*, deleting the virulence-controlling MAPK Gpmk1 prompts compensatory activation of Mgv1, another MAPK that plays a role in maintaining cell wall integrity, providing another illustration of this adaptation (Ren *et al.*, 2019). These genetic alterations show how well fungal pathogens respond and can overcome various challenges.

Furthermore, the absence of *MEP3* transcripts in the RNA data could also be explained by post-transcriptional regulation, mRNA inhibition, or destruction. Western blot analysis could detect protein levels in conidia and mycelium, and ribosome profiling (Ingolia *et al.*, 2009) could clarify whether *MEP3* mRNA is actively translated.

4.3.3 Implications of fungal virulence and antifungal resistance

The possibility of secondary mutations compensating for effector gene misregulation has broader implications for understanding fungal virulence. This suggests a high degree of regulatory plasticity which could have a concerning impact

on antifungal resistance (Fisher *et al.*, 2012). Antimicrobial resistance (AMR) has been documented to occur through genetic alterations that activate cellular defence mechanisms, including drug efflux and stress response pathways (Lee *et al.*, 2023). Resistance has been reported for all significant antifungal drug classes. For example, echinocandins, which target β-glucan synthase (*FKS1* and *FKS2* genes) weakening the fungal cell wall (Zhao *et al.*, 2023), can be evaded in *Candida* and *Aspergillus* species through *FKS* mutation which affects the fungicide binding (Lewis *et al.*, 2011, Chowdhary *et al.*, 2018). Polyenes, which act by extracting ergosterol from fungal membranes, can be resisted through mutations in the ergosterol biosynthesis pathway (Carolus *et al.*, 2021). Furthermore, azole antifungals, which also disturb cell membranes, can be evaded through mutations in the *ERG11* gene, which encodes the target enzyme lanosterol 14α-demethylase, or through overexpression of efflux pumps (Marichal *et al.*, 1999). Examples of these resistance mechanisms are known for many plant pathogenic fungi (Cools *et al.*, 2013). These parallels suggest that targeting *RGS1* or its downstream targets as a disease control strategy may be less effective if compensatory mutations bypass its regulatory function.

This chapter presents novel insights into the function of *RGS1* in effector gene regulation and fungal virulence. Although *RGS1* is involved in regulating late-expression *M. oryzae* effectors, including *MEP3*, the unexpected absence of *MEP3* transcripts in the *CER* mutants suggests additional levels of regulation. These might include translational control and/or chromatin remodelling. By investigating these processes further, we can better understand fungal adaptability and create strategies to combat antifungal resistance.

Chapter 5: The Bip1 transcriptional regulator is controlled by the Pmk1 MAPK/Mst12 signalling pathway

5.1 Introduction

Plant pathogens rely on timely and fine-tuned effector gene expression to establish successful infections (Giraldo & Valent, 2013, Toruño *et al.*, 2016, Nobori *et al.*, 2020, Molloy *et al.*, 2024). In filamentous fungi such as *M. oryzae*, this regulation is controlled by multiple interconnected signalling pathways, including the cAMP-dependent protein kinase A (PKA) pathway, Pmk1 MAPK signalling pathway, the cell wall integrity pathway, and epigenetic modifications (Michielse *et al.*, 2009, Soyer *et al.*, 2014, Soyer *et al.*, 2015, Li *et al.*, 2016, Tollot *et al.*, 2016, Zhang *et al.*, 2021, Tang *et al.*, 2023). These pathways integrate environmental cues to coordinate morphogenesis with effector gene expression, highlighting a sophisticated regulatory network essential for host colonisation.

Some key signalling pathways involved in pathogenesis are conserved across filamentous fungi and have been characterised in *M. oryzae* (Wang *et al.*, 2024). For example, the Mps1 MAPK pathway, which controls cell wall integrity, conidiation, penetration, and host infection, also regulates a subset of effector genes, either directly or through the phosphorylation of the Gti1 transcription factor (TF) (Xu *et al.*, 1998, Li *et al.*, 2016). Highlighting the importance of morphogenetic changes connecting fungal development and virulence, the homologue of Git1 in *Candida albicans* is essential for phenotypic changes that allow the switch between commensal and pathogenic states (Huang *et al.*, 2006). Additionally, transcriptomic and functional studies of the Pmk1 MAPK pathway—required for appressorium formation, penetration, and invasive growth—have identified subsets of effectors regulated by this cascade (Sakulkoo *et al.*, 2018). Pmk1 can phosphorylate TFs, such as Mst12, involved in penetration and invasive growth, potentially regulating these functions (Park *et al.*, 2002, Osés-Ruiz *et al.*, 2021). Homologues of Mst12, such as

Ste12 in yeast and Ste12-like in other filamentous fungi, are well-known regulators of mating, growth, and virulence (Wong Sak Hoi & Dumas, 2010); they control numerous biological processes that often lead to complex biological development. Furthermore, in this study and previous research, *RGS1*, a G-protein regulator originally linked to appressorium formation via cAMP signalling (Zhang *et al.*, 2011a), has also been shown to play a role in effector gene regulation (Tang *et al.*, 2023). These findings suggest that the regulation of disease progression connects virulence-determinant morphological changes and transcriptional control of effector genes. With several examples supporting this hypothesis, we decided to take a reverse genetics approach to further understand the regulation of effector gene expression.

Using *M. oryzae* to characterise effector regulation; we focused on characterised transcription factors that contribute to infection-related development, particularly those that may act on appressorium formation and host penetration. As a result of this analysis, we identified **B**-ZIP **I**nvolved in **P**athogenesis-**1**, Bip1, a recently reported TF in *M. oryzae* (Lambou *et al.*, 2024). *BIP1* deletion mutants can form an appressorium but do not penetrate host tissue, suggesting a critical role in penetration and/or blast disease progression. Furthermore, by microarray analysis, Bip1 was found to be a regulator of a subset of effector-encoding genes (Lambou *et al.*, 2024). This finding suggests a possible connection between effector gene expression and host penetration. *MST12* deletion mutants and other non-penetrating *M. oryzae* mutant strains also exhibit such a correlation (Park *et al.*, 2002, Osés-Ruiz *et al.*, 2021). However, because the promoter of *BIP1* was not detected among the targets of Mst12 in a mycelium ChIP-sequencing experiment (Osés-Ruiz *et al.*, 2021), it was proposed that Bip1 functions independently from Mst12 and other known *M. oryzae* signalling pathways, leaving its precise regulatory role unknown. Given the importance of bZIP TFs in fungal biology and the potential role of Bip1 in *M. oryzae* pathogenicity, we decided to investigate this TF in the context of effector regulation.

Bip1 is a basic leucine zipper (bZIP) TF, a family which is widely conserved across eukaryotes (Vinson *et al.*, 2006). The protein sequence of bZIP TFs is characterised by a DNA-binding basic region and a leucine zipper domain that mediates dimerisation (McLachlan & Stewart, 1975). In pathogenic fungi, such as *Neurospora crassa*, *Fusarium graminearum* and *M. oryzae,* bZIP networks regulate cell cycle progression, growth development, stress responses, and metabolism (Son *et al.*, 2011, Tian *et al.*, 2011, Kong *et al.*, 2015, Tang *et al.*, 2015). In *M. oryzae*, systematic characterisation of bZIPs has linked most of them to regulating pathways that ultimately affect pathogenicity (Kong *et al.*, 2015, Tang *et al.*, 2015, Liu *et al.*, 2022a). For example, *MoAP1,* an ortholog of the yeast *YAP1*, controls genes involved in the oxidative stress response necessary for host infection (Guo *et al.*, 2011). It was also reported that *MoAP1* regulates Git1, connecting bZIP TFs to other pathogenicity regulators (Chen *et al.*, 2014). *BZIP3* has been shown to regulate glycerol biosynthesis genes to control appressorium turgor pressure (Liu *et al.*, 2022a), which connects this TF to the turgor-sensing kinase Sln1 (Ryder *et al.*, 2019). Additionally, marking one of the first known examples of a TF directly regulating effector genes in *M. oryzae, MoEITF2* was shown to directly bind the promoter of the early-expressed cytoplasmic effector gene *T2REP* (Cao *et al.*, 2022). These findings connect bZIP TFs with characterised regulatory pathways in *M. oryzae*. However, the research remains very limited, with most results relying on RT-PCR experiments and a single microarray analysis of the *BIP1* mutant. With no large-scale transcriptomic studies performed on this family of TFs in *M. oryzae*, it is difficult to draw robust conclusions regarding the regulatory role of Bip1. Therefore, it is apparent that further investigation is needed to understand the regulatory role of Bip1 in blast disease.

This chapter presents transcriptomic analysis showing that Bip1 and Mst12 co-regulate a shared subset of genes, including effector-encoding genes, during pathogenesis. Additionally, we report that Bip1 is phosphorylated during plant infection, *BIP1* expression is Pmk1 and Mst12 dependent, and Mst12 and Bip1 TFs physically interact, consistent with heterodimer formation. Collectively, these findings provide evidence that Bip1 is controlled by the Pmk1 MAPK/Mst12 signalling

pathway and suggest a hierarchy of co-ordinately regulated TFs deployed by *M.oryzae* during infection. Together, these results offer new insight into the molecular mechanisms that control *M. oryzae* virulence and expand our understanding of how bZIP TFs contribute to fungal pathogenesis.

5.2 Results

5.2.1 Overlapping genes among Pmk1, Mst12 and Bip1 datasets

Time-course RNA sequencing analysis of Δ*pmk1* and Δ*mst12* deletion mutants identified 6333 Pmk1-dependent DEGs and 2512 Mst12-dependent DEGs (Osés-Ruiz *et al.*, 2021). By cross-comparing these lists against the Bip1 microarray data (Lambou *et al.*, 2024), we found 33 of 42 Bip1-dependant DEGs were also among Pmk1 and Mst12 regulated genes, as shown in Figure 5.1. Among the overlapping genes, all Bip1-regulated effectors were also controlled by Pmk1 and Mst12. Furthermore, FIMO 'Find Individual Motif Occurrences' analysis was performed to identify promoter regions containing a Bip1 DNA-interacting motif (Lambou *et al.*, 2024). This resulted in a list of 1264 putative Bip1-regulated genes, of which half, 629 genes, could also be found among Pmk1 and Mst12 DEGs, as illustrated in Figure 5.1.

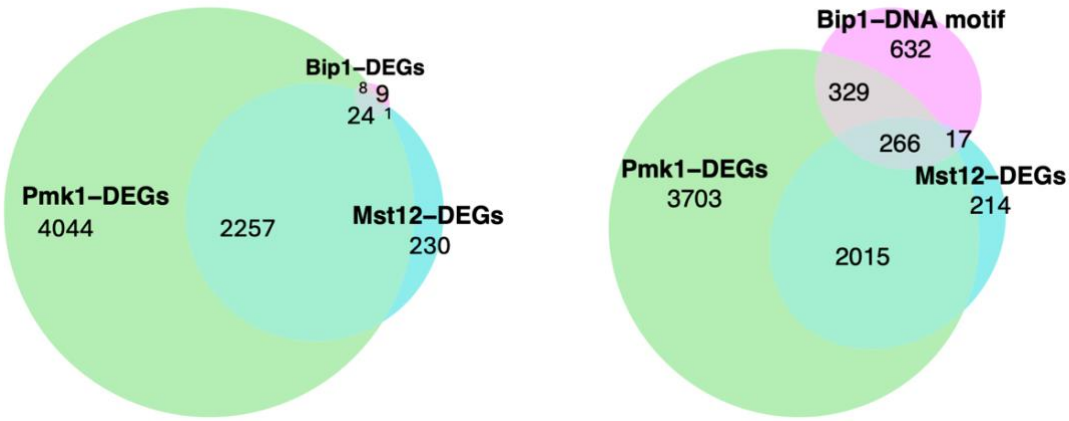

Figure 5.1 Overlapping genes found among Pmk1, Mst12 and Bip1 datasets. DEGs for Δ*pmk1* and Δ*mst12* deletion mutants were cross-compared to the Bip1 microarray dataset (Osés-Ruiz *et al.*, 2021, Lambou *et al.*, 2024), finding 33 of 42 Bip1-dependant DEGs among Pmk1 and Mst12 regulated gene set, shown in the left Euler diagram. Genes identified through FIMO analysis to have a Bip1 DNA-binding motif were also found among the Pmk1 and Mst12 DEGs, the overlap is shown in the Euler diagram on the right.

5.2.2 Expression of *BIP1* is Pmk1 and Mst12-dependent

To gain further insight into the relation of Bip1 to the Pmk1 MAKP signalling pathway, we analysed *BIP1* expression among publicly transcriptomic datasets. Mean values for *BIP1* (*MGG_08118*) reads were extracted from a time-course RNA sequencing experiment of Δ*pmk1* and Δ*mst12* deletion mutant strains (Osés-Ruiz *et al.*, 2021). For every measured time-point (0h, 8h, 14h, 16h, and 24h), the expression of *BIP1* is repressed in both Δ*pmk1* and Δ*mst12* deletion mutants compared to reads in the isogenic wild-type strain Guy11, as shown in Figure 5.2. This RNA-Seq data suggests that Pmk1 and Mst12 are necessary for regulating *BIP1* during appressorium development of *M. oryzae*, perhaps positioning this bZIP regulator downstream of the Pmk1 MAKP signalling cascade, in contradiction to the conclusion of Lambou et al., 2024.

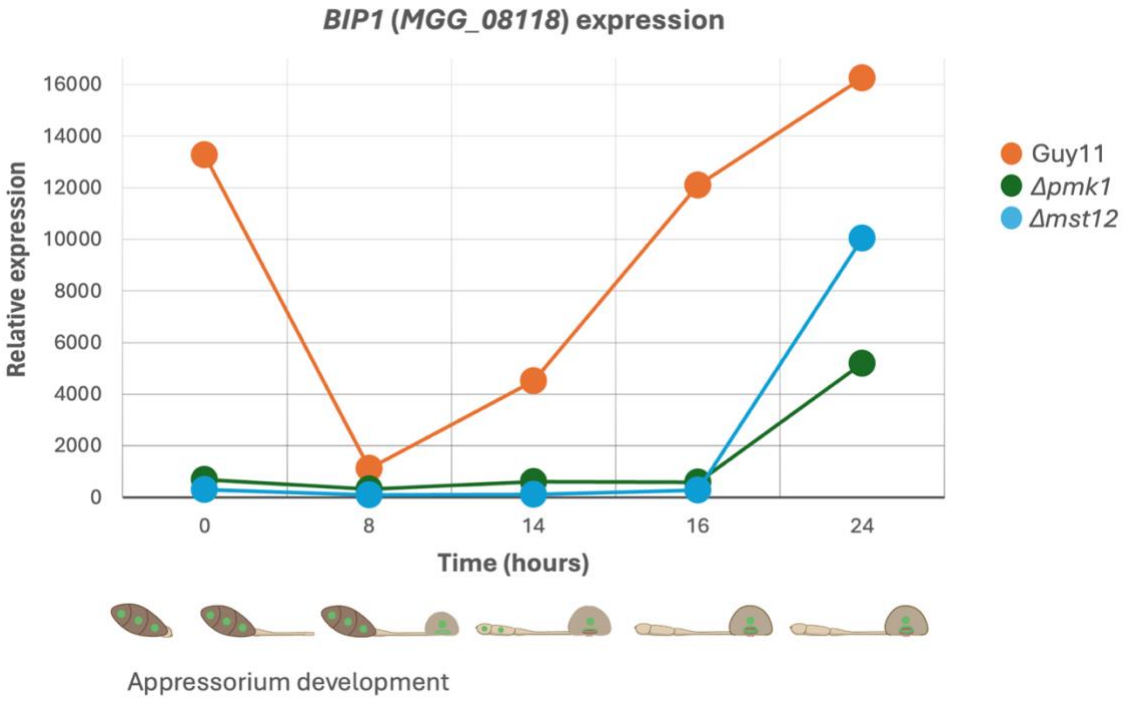

Figure 5.2 *BIP1* expression during appressorium development. Mean values for *BIP1* reads are represented for five different time points (0h, 8h, 14h, 16h, and 24h) during the appressorium development of *M. oryzae* for three distinct strains: wild-type Guy11 (orange), Δ*pmk1* deletion mutant (green), and Δ*mst12* deletion mutant (blue). Compared to the isogenic wild-type, *BIP1* reads show lower expression in deletion mutants for every represented time point. Information was extracted from publicly available transcriptomic datasets (Osés-Ruiz *et al.*, 2021).

5.2.3 Bip1 is phosphorylated during appressorium development

Large-scale discovery phosphoproteomics identified approximately 2,000 proteins phosphorylated during appressorium development of *M. oryzae* (Cruz-Mireles *et al.*, 2024). Furthermore, through comparative phosphosite abundance analysis between the isogenic wild-type Guy11 and Δ*pmk1* deletion mutant, these phosphorylated proteins can be related to Pmk1 control. Therefore, by analysing this dataset, we identified a putative phosphorylation site in a serine in position 32, just before the bZIP domain of Bip1, as shown in Figure 5.3. Additionally, through abundance analysis for this phosphosite, we found that Bip1 phosphorylation is Pmk1-dependant at 4 and 6 hours post-infection (hpi). This regulation could occur at the transcriptional level, either by controlling *BIP1* gene expression or the expression of a kinase responsible for Bip1 phosphorylation. Alternatively, Pmk1 may directly regulate Bip1 through phosphorylation, either by phosphorylating Bip1 itself or by activating another kinase that subsequently modifies Bip1.

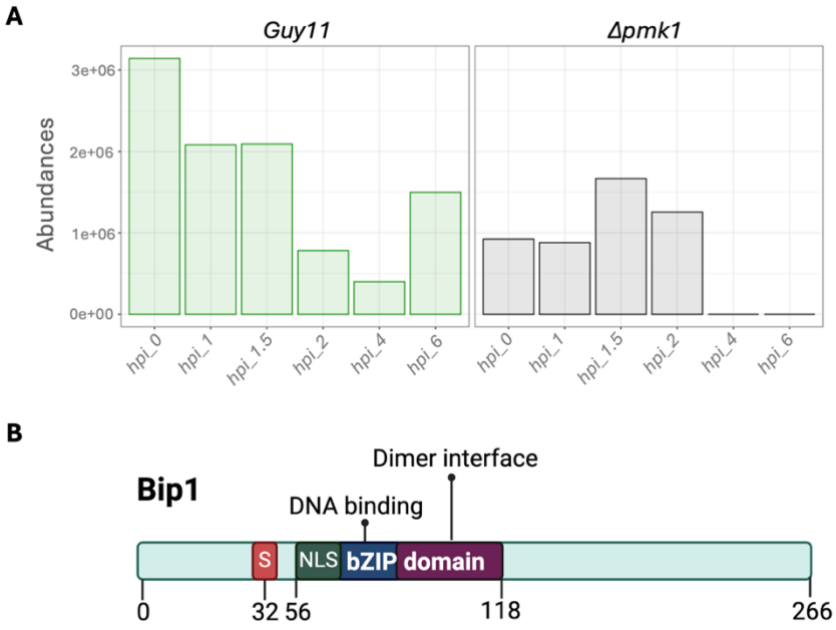

Figure 5.3 Bip1 is phosphorylated during appressorium development. (A) Bip1 phosphosite (serine in position 32) abundances from a discovery phosphoproteomics analysis performed during appressorium development of *M. oryzae* (0h, 1h, 1.5h, 2h, 4h ,and 6h) for wild type Guy11 and Δ*pmk1* deletion mutant. (B) Bip1 protein showing phosphorylation site (serine in position 32) and bZIP domain from position 56 to 118, comprising an NLS, DNA-binding domain and dimer interfaces. (Image created using Biorender.com)

5.2.4 Mst12 DNA-binding motif discovered within the promoter of *BIP1*

A ChIP-seq analysis performed on *M. oryzae* mycelium previously identified five putative Mst12 DNA-binding motifs (Osés-Ruiz *et al.*, 2021). To further investigate the relationship between Bip1 and Mst12, we decided to scan the *BIP1* promoter for these DNA-interacting sites. Using FIMO, motif one was identified within the promoter region of *BIP1*, 661 base pairs upstream of the start codon. Additionally, Alphafold-3 (Abramson *et al.*, 2024) was used to predict the *in silico* interaction between Mst12 protein and 50 base pairs of *BIP1* promoter region, containing the identified putative Mst12 DNA-binding motif. The Mst12 protein possesses a conserved DNA-binding Pmk1-interacting homeodomain and two C-terminal C_2H_2 zinc finger domains, absent in ascomycete yeasts (Wong Sak Hoi & Dumas, 2010). The best-ranked model, with a pLDDT score of 57/100, predicted contact to occur between the second C_2H_2 zinc finger domain of Mst12 and the putative DNA-binding motif found within the *BIP1* promoter, as illustrated in Figure 5.4. A further prediction of the interacting parts of this complex, the second C_2H_2 zinc finger domain of Mst12 and the putative Mst12 DNA-binding motif (“CCTGTAAT”) found within the *BIP1* promoter had a higher ranking value with a pLDDT score of 75/100, an ipTM score of 0.67, and a pTM score of 0.74, suggesting the interaction is better predicted when distorted regions of both Mst12 protein and *BIP1* promoter are removed.

As a proof of concept, we also predicted the known interaction between the Bip1 protein sequence and Bip1 DNA-binding motif (“TGACTC”) found within the promoter of *MGG_08381* (avirulence gene cluster 1, *ACE1*) gene (Lambou *et al.*, 2024). The best-ranked model for this *in silico* prediction had a pLDDT score of 65/100, an ipTM score of 0.25, and a pTM score of 0.29, lower values than those predicted for the Mst12-*BIP1* promoter interaction. Furthermore, we also tested variations of the Mst12 and *BIP1* promoter interaction. Two of these modified the DNA-binding motif, including completely removing the motif and swapping the motif with a sequence of thymine residues. The third prediction tested the interaction using an Mst12 splice variant lacking the second C_2H_2 zinc finger domain (Hoi *et al.*, 2007, Schamber *et al.*, 2010). All these predictions demonstrated lower ranks (Table

5.1), thereby supporting the idea that the second C_2H_2 zinc finger domain of Mst12 binds to the ChIP-seq predicted DNA-binding motif identified in the promoter of *BIP1*.

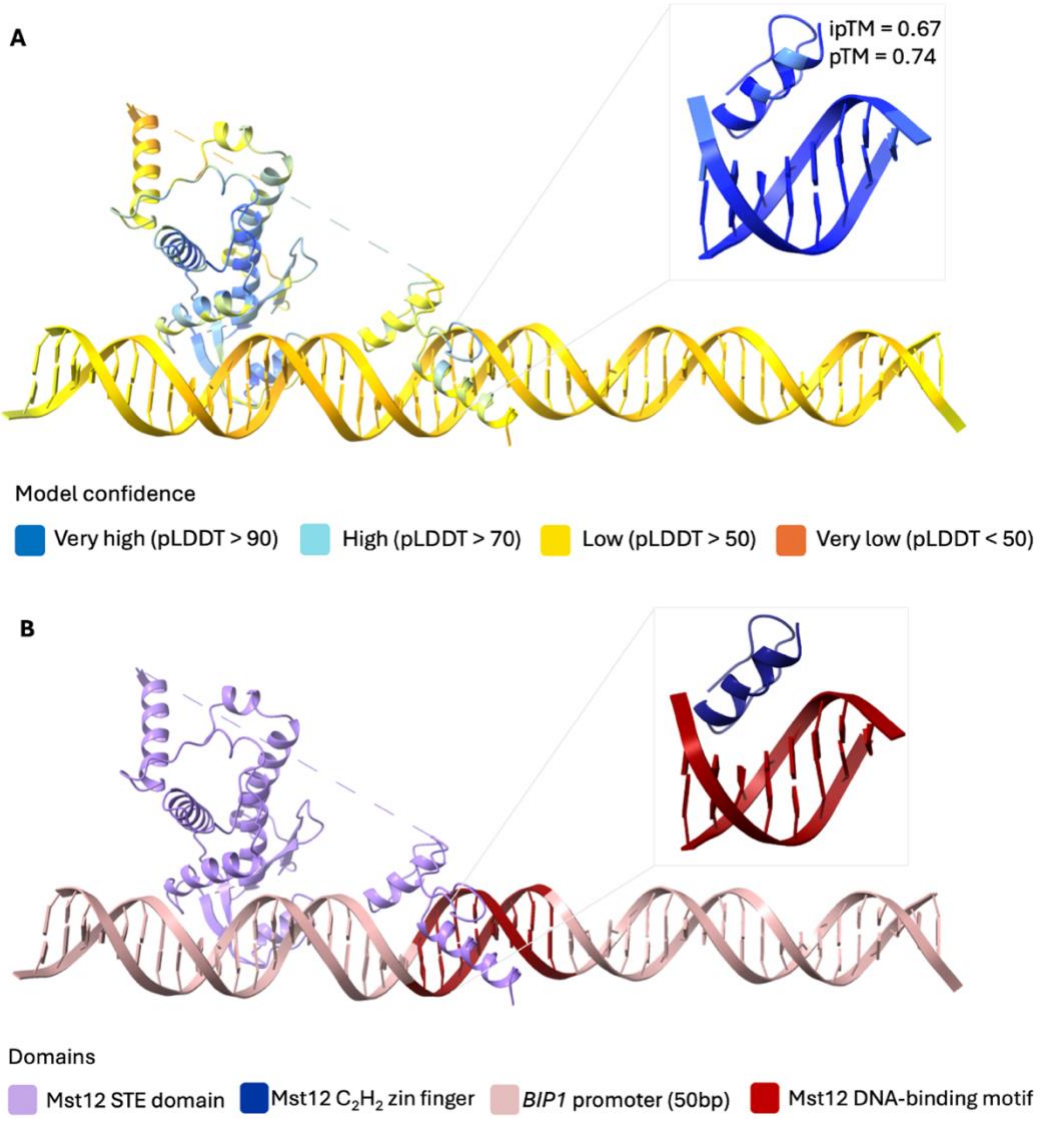

Figure 5.4 *In silico* prediction of Mst12 and *BIP1* promoter interaction. (A) Alphafold-3 prediction of Mst12 protein with 50bp of the *BIP1* promoter, containing a putative Mst12 DNA-binding motif (Osés-Ruiz *et al.*, 2021). Contact is predicted to occur through the second C_2H_2 zinc finger domain of Mst12 and the predicted DNA-binding site on the *BIP1* promoter. pLDDT scores are shown with the model confidence colouring. Distorted regions have been cropped for visualisation purposes. (B) The Mst12- *BIP1* promoter interacting prediction coloured by domains: Mst12 STE domain (purple), Mst12 C_2H_2 zinc finger domains (blue), 50bp of *BIP1* promoter (pink) and Mst12 DNA-binding domain (red).

Table 5.1 Alphafold-3 scores for Mst12-*BIP1* promoter intercations.

AF3 predicted model	plDDT	ipTM	pTM
Mst12-BIP1 promoter no DNA binding motif	62/100	0.29	0.32
Mst12-BIP1 promoter DNA binding motif Thymines swap	23/100	0.19	0.38
Mst12 splice variant - BIP1 promoter	34/100	0.34	0.36

5.2.5 Bip1 is conserved in pathogenic fungi

To understand the evolution of Bip1 and potentially gain further insight into its function, we examined its conservation across a selection of filamentous fungal species (with Dr Neha Sahu). For this analysis, we used a publicly available set of fungal species based on a previous study (Cruz-Mireles *et al.*, 2024), including plant pathogens, mutualists, saprophytes, human pathogens, and two model yeast species, *Saccharomyces cerevisiae* and *Schizosaccharomyces pombe*. Proteomes for these 41 fungal species were sourced from NCBI and JGI Mycocosm, and orthology relationships were inferred using OrthoFinder (Emms & Kelly, 2019). Through this analysis, we identified 61 orthologues of Bip1 conserved across hemibiotrophs, necrotrophs, biotrophs, and saprophytes, with a notable expansion within the *Fusarium* genus, as illustrated in Figure 5.5. The absence of Bip1 among the queried yeasts, symbionts, commensal, and endophyte species is consistent with conservation of this TF to be restricted to pathogenic fungi. This finding further supports the role of Bip1 in host infection.

Additionally, in order to compare the conservation of Bip1 and Mst12 across these fungal species, we chose to include both TFs in the OrphoFinder analysis. Unlike Bip1, orthologues of Mst12 are found in most queried fungal species, with the exception of *S. cerevisiae* and *S. pombe*, as illustrated in Figure 5.5. This analysis supports previous studies suggesting that Mst12 is highly conserved across filamentous ascomycete fungi, regardless of their lifestyle (Wong Sak Hoi & Dumas, 2010). Furthermore, upon examining both TFs in these fungal species, we discovered a correlation between species which possess a Bip1 orthologue and those exhibiting better conservation of the Mst12 domains, including the two C-terminal C_2H_2 zinc finger domains, Figure 5.6. This result reinforces the *in silico* prediction of Mst12-*BIP1* promoter interaction via the second C_2H_2 zinc finger domain of Mst12, and it further supports previous findings linking the C_2H_2 zinc finger domains of Ste12 proteins to pathogenicity-related functions (Hoi *et al.*, 2007, Schamber *et al.*, 2010).

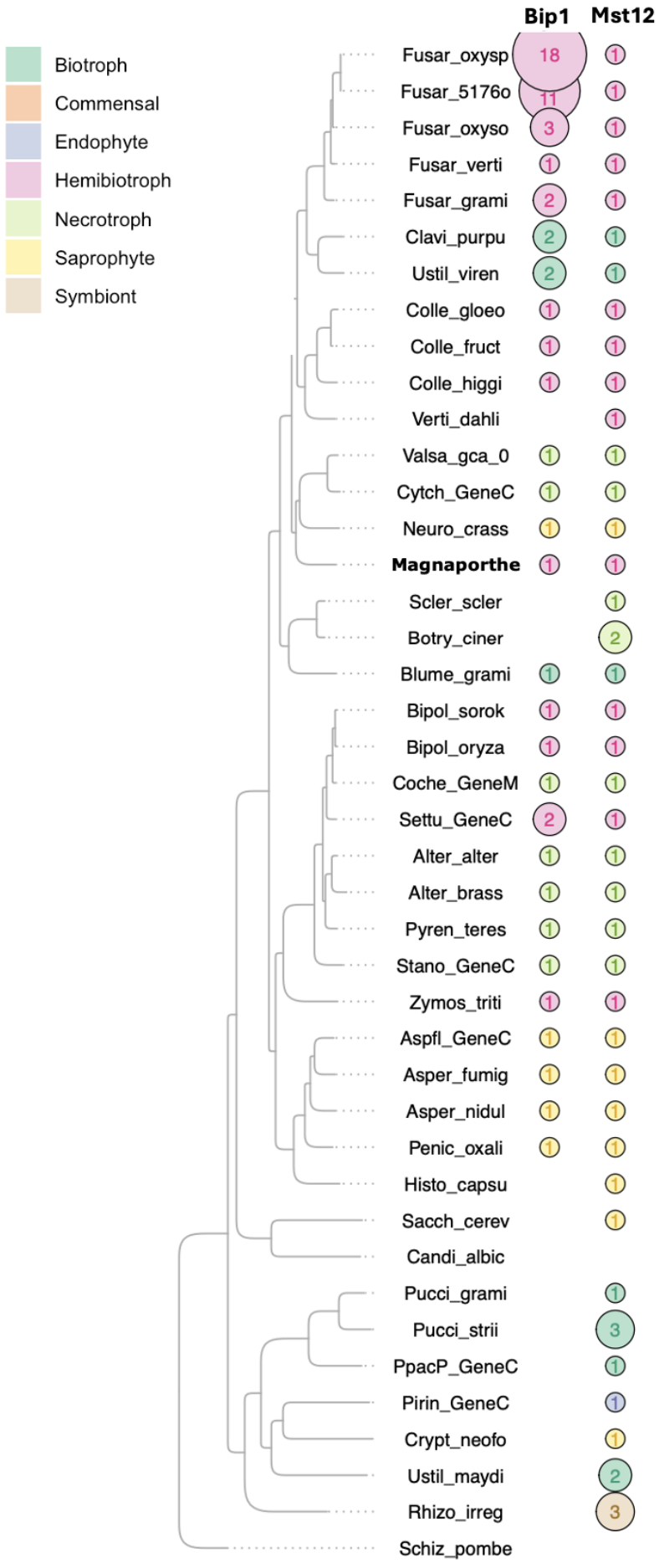
Bip1
Mst12
Biotroph
Commensal
Endophyte
Hemibiotroph
Necrotroph
Saprophyte
Symbiont
Fusar_oxysp 18 1
Fusar_5176o 11 1
Fusar_oxyso 3 1
Fusar_verti 1 1
Fusar_grami 2 1
Clavi_purpu 2 1
Ustil_viren 2 1
Colle_gloeo 1 1
Colle_fruct 1 1
Colle_higgi 1 1
Verti_dahli 1
Valsa_gca_0 1 1
Cytch_GeneC 1 1
Neuro_crass 1 1
Magnaporthe 1 1
Scler_scler 1
Botry_ciner 2
Blume_grami 1 1
Bipol_sorok 1 1
Bipol_oryza 1 1
Coche_GeneM 1 1
Settu_GeneC 2 1
Alter_alter 1 1
Alter_brass 1 1
Pyren_teres 1 1
Stano_GeneC 1 1
Zymos_triti 1 1
Aspfl_GeneC 1 1
Asper_fumig 1 1
Asper_nidul 1 1
Penic_oxali 1 1
Histo_capsu 1
Sacch_cerev 1
Candi_albic
Pucci_grami 1
Pucci_strii 3
PpacP_GeneC 1
Pirin_GeneC 1
Crypt_neofo 1
Ustil_maydi 2
Rhizo_irreg 3
Schiz_pombe

Figure 5.5 Bip1 and Mst12 conservation across fungal species. Fungal species tree illustrates the number of orthologues identified for Bip1 and Mst12 using OrthoFinder (Emms & Kelly, 2019). For the analysis, a list of fungal species, including biotrophs (green), commensal (orange), endophytes (blue), hemibiotrophs (pink), necrotrophs (light green), saprophytes (yellow) and symbionts (brown) was used. The full list includes, *Fusarium oxysporum-2, Fusarium oxysporum-5176, Fusarium oxysporum-C. alt, Fusarium verticillioides, Fusarium graminearum, Claviceps purpurea, Ustilago virens, Colletotrichum gloeosporioides, Colletotrichum fructicola, Colletotrichum higginsianum, Verticillium dahliae, Valsa mali, Cytospora chrysosperma, Neurospora crassa, Magnaporthe oryzae, Sclerotinia sclerotiorum, Botrytis cinerea, Blumeria graminis, Bipolaris sorokiniana (Cochliobolus sativus), Bipolaris oryzae, Cochliobolus heterostrophus, Setosphaeria turcica, Alternaria alternata, Alternaria brassicicola, Pyrenosphora teres, Stagonospora nodurum, Zymoseptoria tritici, Aspergillus flavus, Aspergillus nidulans, Aspergillus fumigatus, Penicillium oxalicum, Histoplasma capsulatum, Saccharomyces cerevisae, Candida albicans, Puccinia graminis, Puccinia striiformis, Phakopsora pachyrhizi, Piriformospora indica, Cryptococcus neoformas, Ustilago maydis,* and *Rhizophagus irregularis*. For Bip1, a total of 61 orthologues were identified across hemibiotrophs, necrotrophs, biotrophs, and saprophytes, with a notable expansion within the *Fusarium* genus, and no orthologues were found among the queried yeasts, symbionts, commensal, and endophyte species. For Mst12, 41 orthologues were present across all queried species except for the yeasts, *S. cerevisiae* and *S. pombe,* suggesting high conservation of this TF. For *M. oryzae* there is only one Bip1 orthologue and one Mst12 orthologue.

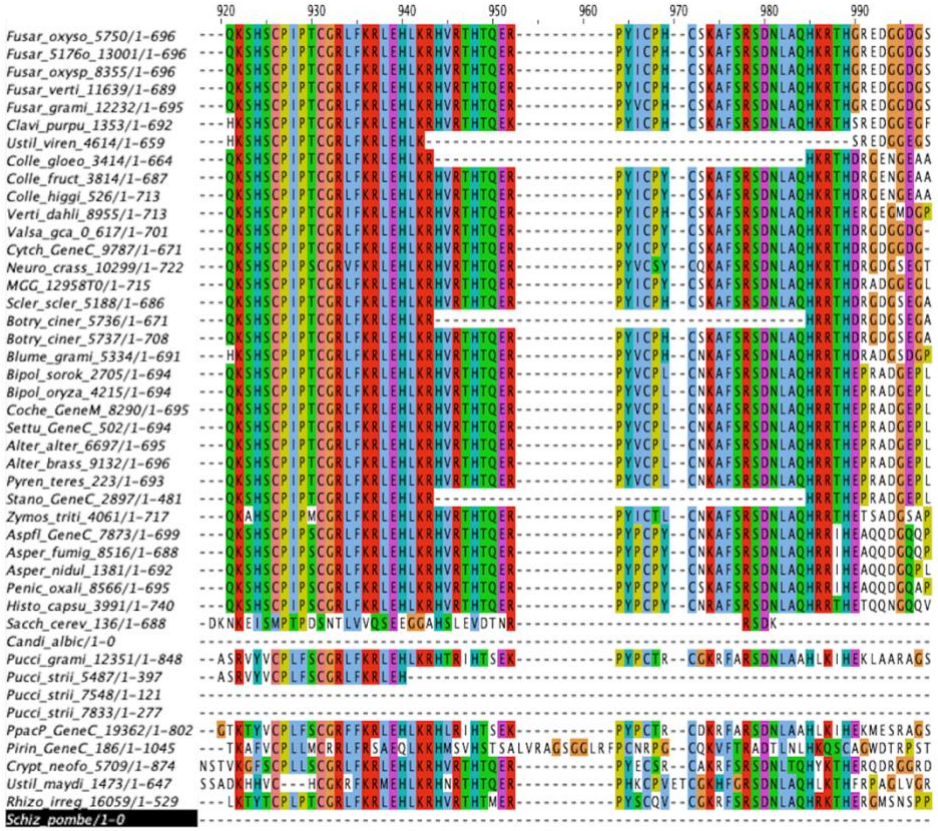

Figure 5.6 Conservation of Mst12 C_2H_2 zinc finger domains in fungal species. Snapshot of Mst12 C_2H_2 zinc finger domains alignment (Clustal) for 41 fungal species including, *Fusarium oxysporum-2, Fusarium oxysporum-5176, Fusarium oxysporum-C. alt, Fusarium verticillioides, Fusarium graminearum, Claviceps purpurea, Ustilago virens, Colletotrichum gloeosporioides, Colletotrichum fructicola, Colletotrichum higginsianum, Verticillium dahliae, Valsa mali, Cytospora chrysosperma, Neurospora crassa, Magnaporthe oryzae, Sclerotinia sclerotiorum, Botrytis cinerea, Blumeria graminis, Bipolaris sorokiniana (Cochliobolus sativus), Bipolaris oryzae, Cochliobolus heterostrophus, Setosphaeria turcica, Alternaria alternata, Alternaria brassicicola, Pyrenosphora teres, Stagonospora nodurum, Zymoseptoria tritici, Aspergillus flavus, Aspergillus nidulans, Aspergillus fumigatus, Penicillium oxalicum, Histoplasma capsulatum, Saccharomyces cerevisae, Candida albicans, Puccinia graminis, Puccinia striiformis, Phakopsora pachyrhizi, Piriformospora indica, Cryptococcus neoformas, Ustilago maydis,* and *Rhizophagus irregularis*.

5.2.6 Generation of a Δ*bip1* mutant by targeted gene replacement

To investigate the role of Bip1 in the context of effector gene regulation, we generated a null Δ*bip1* mutant in the wild-type Guy11 strain of *M. oryzae*. For this, I designed a DNA fragment for homologous recombination (Bird & Bradshaw, 1997, Weld *et al.*, 2006), which included a 1.5kb 5' flanking region of the *BIP1* ORF, followed by a *BASTA* resistance gene under a constitutive promoter, and then another 1.5kb 3' flanking region of the *BIP1* gene, as shown in Figure 5.7.A. The DNA fragment was amplified by PCR and used to transform *M. oryzae* protoplasts. PCR and Sanger sequencing verified positive colonies growing on the selection medium. Two *BIP1* deletion mutants, Δ*bip1_2* and Δ*bip1_3*, were confirmed through Illumina whole genome sequencing and infection assays, as illustrated in Figure 5.7.B and Figure 5.8. Read coverage for *BIP1* (*MGG_08118*) was mostly absent for both mutants, and neither of them could penetrate when tested in barley leaf drop infection assays, confirming the previously reported Δ*bip1* mutant phenotype (Lambou *et al.*, 2024).

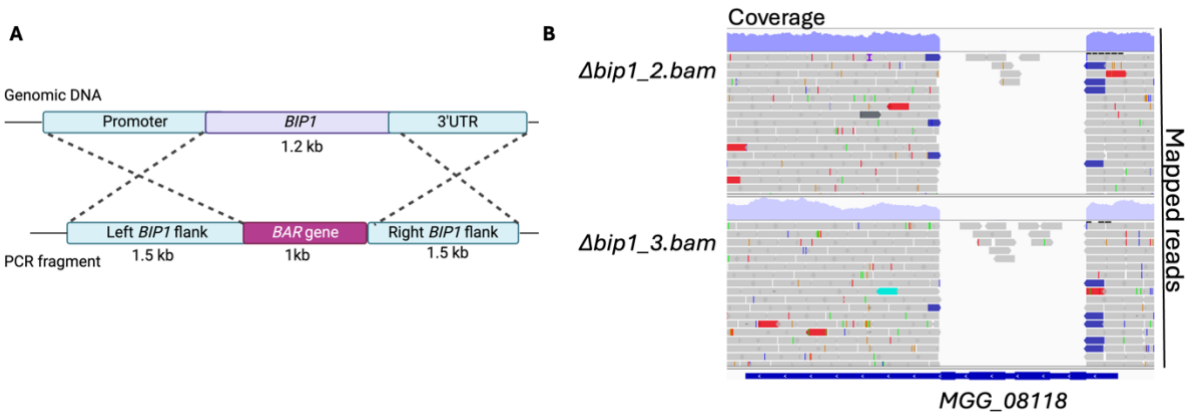

Figure 5.7 Δ*bip1* mutant generation. (A) DNA fragment designed to generate Δ*bip1* mutant through homologous recombination; 1.5kb 5' flanking region of the *BIP1* gene, followed by a *BASTA* resistance gene under a constitutive promoter, and then another 1.5kb 3' flanking region of the *BIP1* gene. (B) IVG snapshot of gene deletion mutants (Δ*bip1_2* and Δ*bip1_3)* coverage for the *BIP1* (MGG_08118) gene. Both mutants show low reads due to the presence of the *BASTA* gene inserted by homologous recombination.

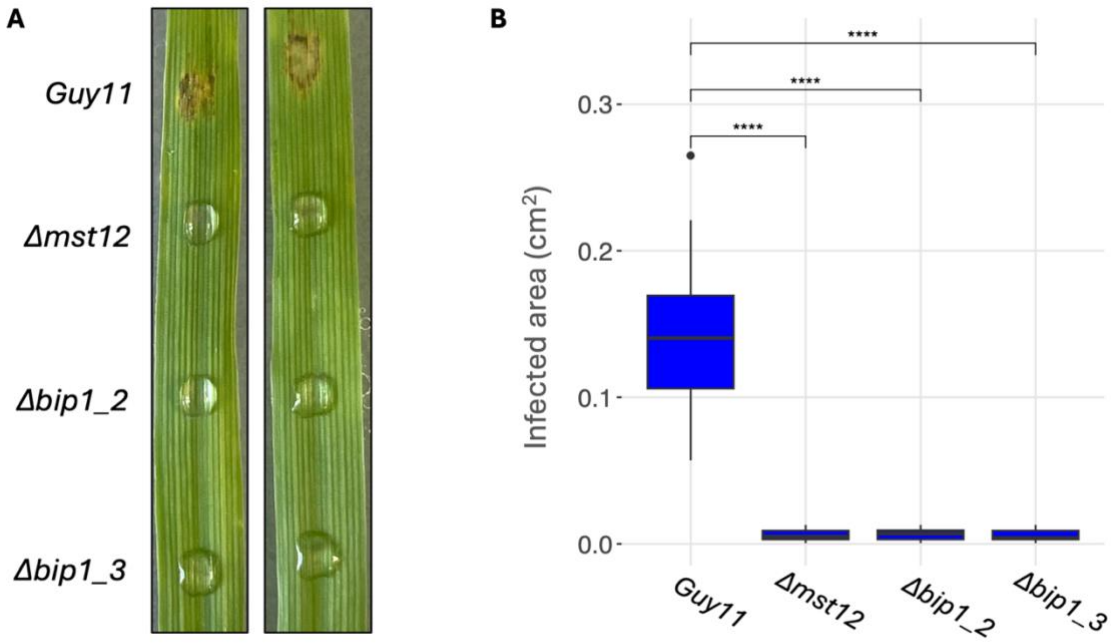

Figure 5.8 Δ*bip1* mutants are non-pathogenic. (A) One-week-old seedlings of barley cultivar Golden Promise were inoculated with equal amounts of conidial suspension (5 x 10^4 conidia/mL with 0.2% (w/v) gelatin) of *M. oryzae* strains Guy11, Δ*mst12*, Δ*bip1_2,* and Δ*bip1_3*. Detached leaves were incubated on water-soaked Whatman paper at 25°C with a 12h photoperiod for 5 days before visualising and quantifying blast disease progression. (B) Box plots show the calculated area of disease lesions for each strain (n=20 lesions per replicate). The mean value is shown as a horizontal line inside the box. T-tests show significantly reduced virulence (p-value <0.05) for all mutant strains compared to wild-type infection. Results represent three biological replicates.

5.2.7 Bip1 is required for septin localisation during appressorium development of *M. oryzae*

Previous studies have demonstrated how cytoskeletal organisation is affected in non-penetrating mutants of *M. oryzae* (Gupta *et al.*, 2015, Sakulkoo *et al.*, 2018, Ryder *et al.*, 2019, Osés-Ruiz *et al.*, 2021). For example, deletion of *MST12* mislocalises septin 3, septin 6, F-actin, β-tubulin, and the Chm1 kinase (Gupta *et al.*, 2015, Osés-Ruiz *et al.*, 2021). Chm1 kinase is the yeast Cla4 homologue, a member of the PAK (p21-activated kinase) family responsible for septin

phosphorylation (Li *et al.*, 2004). Additionally, in Δ*sln1* deletion mutants, septin 3, septin 5, F-actin, gelsolin, and Chm1 were also mis-localised, impairing appressorium maturation and host penetration (Ryder *et al.*, 2019).

I reasoned that because Δ*bip1* mutants can form an appressorium but are impaired in host penetration, this might also be due to disrupted cytoskeletal components. To investigate this, I transformed Guy11 and Δ*bip1* with fluorescently labelled Chm1, actin, septin 3, and septin 5 plasmids (from Dr Lauren Ryder and Dr Iris Eiresmann) to visualise and compare their expression in appressoria. In the wild-type, Chm1, actin, septin 3 and septin 5 organise into a ring structure at the base of the appressorium, as previously reported (Dagdas *et al.*, 2012). For the Δ*bip1* mutant, while actin and Chm1 exhibited wild-type-like localisation, septins 3 and 5 displayed distinct localisations. Septin 3 formed a ring, although it was not as distinctly organised as seen in the wild-type Guy11. In the case of septin 5, the difference was particularly evident, as the Δ*bip1* mutant failed to form a ring at the base of the appressorium, as illustrated in Figure 5.9. This result suggests that Bip1 is required for the localisation of septins at the appressorium and therefore is necessary for cytoskeletal reorganisation that enables plant penetration by *M. oryzae*.

Furthermore, considering this result in the context of the Pmk1 MAPK signalling pathway, we observe differences in cytoskeletal localisation for Δ*mst12* (Gupta *et al.*, 2015, Osés-Ruiz *et al.*, 2021) and Δ*bip1* mutants, with fewer components showing mislocalisation in Δ*bip1* compared to Δ*mst12*. This finding further supports the idea that Bip1 is a component of this pathway that acts downstream of the Mst12 regulator.

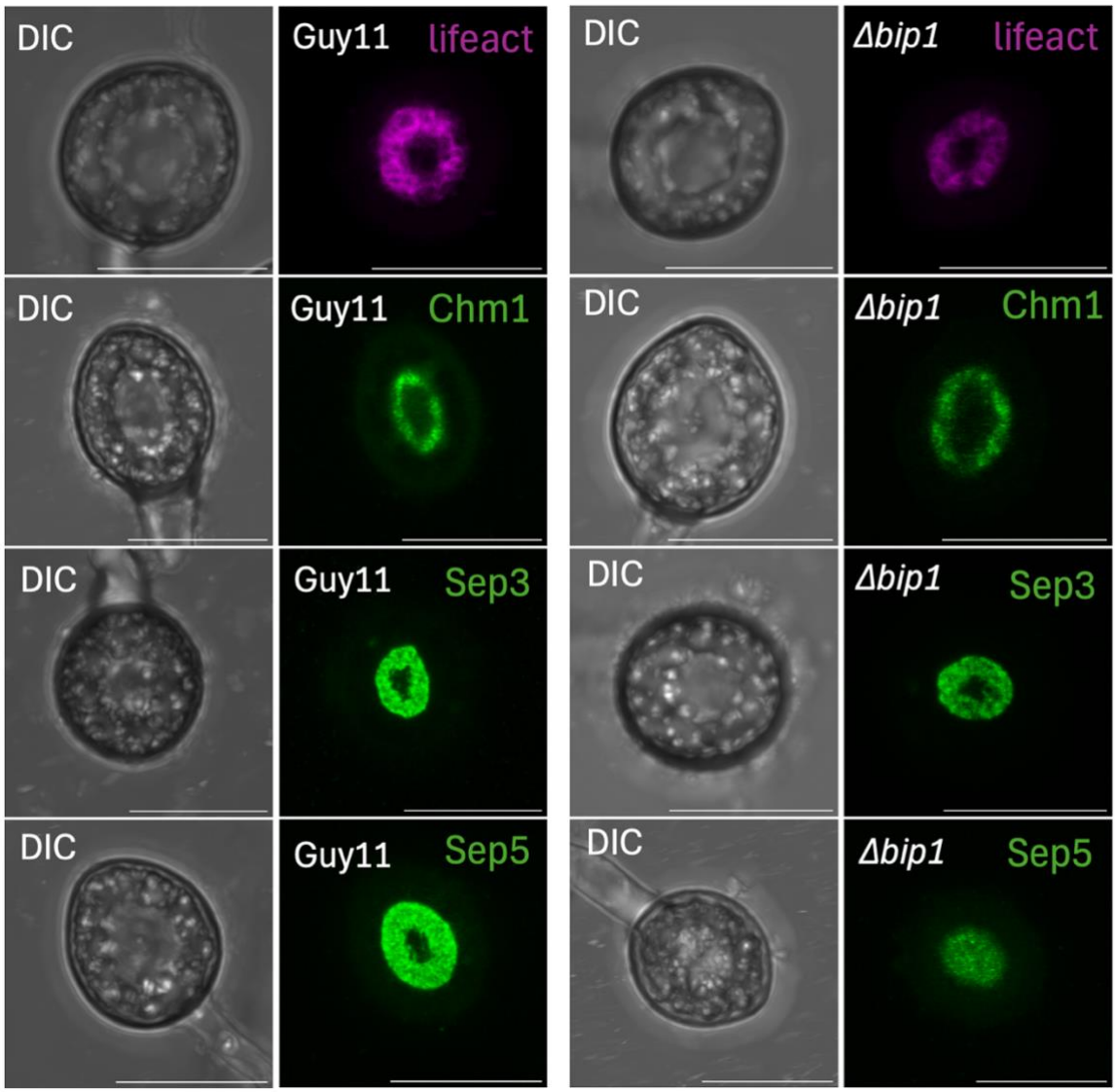

Figure 5.9 Bip1 is required for septin localisation during appressorium development of *M. oryzae*. Micrographs show actin, Chm1 kinase, septin 3 and septin 5 in ring organisation for wild-type Guy11 and Δ*bip1* mutant during appressoria development of *M. oryzae*. The Δ*bip1* mutant shows wild-type-like localisations for actin and Chm1. However, septins are mis-localised; septin 3 forms a ring, but this is not as distinctively formed as for the wild-type, while septin 5 fails to form its classical ring organisation. Conidia were harvested from Guy11 and Δ*bip1* transformants expressing Lifeact-RFP, Chm1-GFP, Sep3-GFP, and Sep5-GFP, inoculated on hydrophobic coverslips and observed by laser confocal microscopy at 24h. Micrographs show a maximum projection of Z-stack images. Representative images from three biological replicates. Scale bar = 10 μm.

5.2.8 Constitutive *BIP1* expression affects appressorium formation and pathogenicity

Continuing the characterisation of Bip1 function, we generated *M. oryzae* transformants with constitutive *BIP1* expression. To achieve this, a plasmid was constructed with the *TrpC* constitutive promoter (Hamer & and Timberlake, 1987) driving the *BIP1* gene, which was fused to GFP for visualisation purposes. This plasmid was used to transform *M. oryzae* wild-type Guy11 and Δ*mst12* mutant protoplasts. Using fluorescently labelled *BIP1-GFP*, we confirmed that the transcription factor localises to the nucleus during appressorium development in conidia and fully formed appressoria, as shown in Figure 5.10 (with Dr Lauren Ryder). This finding is consistent with previous studies documenting Bip1 localisation to the appressorium nucleus (Lambou *et al.*, 2024).

Constitutive *BIP1*-expressing *M. oryzae* strains were used to conduct detailed phenotypic examinations. Through barley leaf drop infection assays, we observed that constitutive expression of *BIP1* significantly reduces pathogenicity (t-test, p-value < 0.05), as illustrated in Figure 5.11. These results imply that changes in *BIP1* expression might also influence appressorium-mediated infection, aligning with the need for homeostatic regulation of Bip1 for its baseline function—where both insufficient and excessive expression can impact its function. Additionally, we decided to visualise the morphology of the appressoria in the constitutive *BIP1*-expressing strains, hypothesising that reduction in pathogenicity could be related to malfunctioning appressoria. In contrast to the Δ*mst12* and Δ*bip1* mutants, which exhibit wild-type appressorium morphology, constitutively expressing *BIP1* strains displayed a range of phenotypes, including the presence of two appressoria, long germ tubes, enlarged germ tubes, or non-germinating conidia Elongated and unusually large germ tubes were the predominant phenotype observed (57%), while only 30% of appressoria exhibited a wild-type appearance, as shown in Figure 5.12. Furthermore, we found that overexpressing *BIP1* in an Δ*mst12* mutant background enhanced appressorial dysmorphia. Only 9% of the visualised appressoria appeared to have a wild-type phenotype, with an increase in long germ tubes (44%)

and two-appressoria (23%). Therefore, the appressoria defect shown for constitutive expression of *BIP1* is only exacerbated when Mst12 is not present, suggesting regulation of Bip1 homeostasis by Mst12. This result further supports the hypothesis that Bip1 functions downstream of the Pmk1 MAPK signalling pathway during *M. oryzae* appressorium formation.

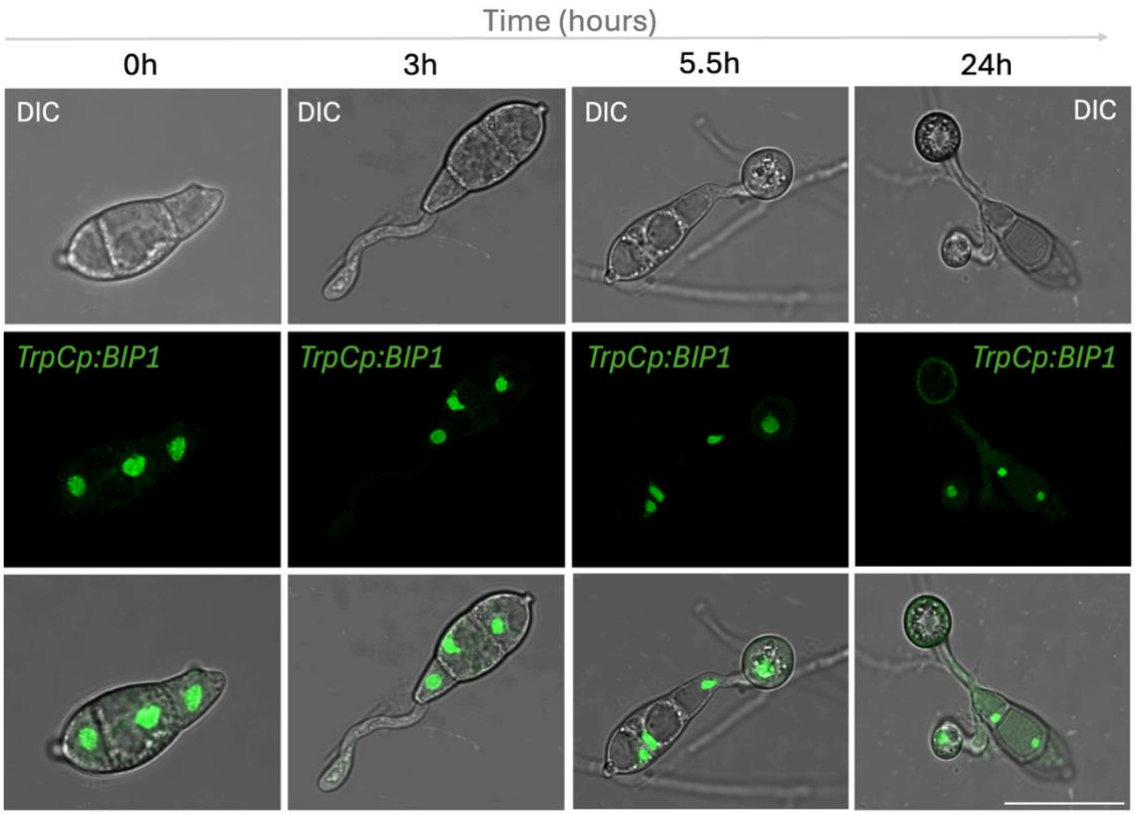

Figure 5.10 Bip1 localises to the nucleus during appressorium development of *M. oryzae*. Micrographs show Bip1 localisation to the nucleus during different time points of appressorium development, including conidia (0h), germination (3h), appressorium differentiation (5.5h), and appressorium maturation (24h). *BIP1* constitutive-expression strains (Guy11 ectopically transformed with *TrpC:BIP1:GFP* constructs) were used for visualisation. Conidia were harvested, inoculated on hydrophobic coverslips, and observed by laser confocal microscopy at the indicated time points. Micrographs show a maximum projection of Z-stack images. Representative images from three biological replicates. Scale bar = 20 μm.

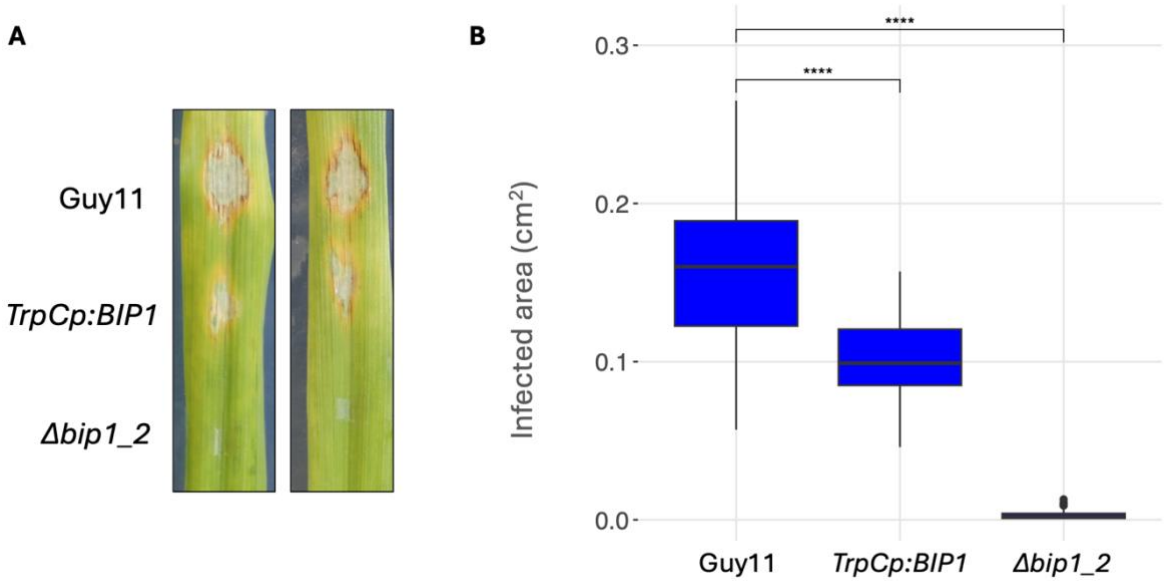

Figure 5.11 Constitutive expression of *BIP1* affects virulence of *M. oryzae*. (A) One-week-old seedlings of barley cultivar Golden Promise were inoculated with equal amounts of conidial suspension (5 x 104 conidia/mL with 0.2% (w/v) gelatin) of *M. oryzae* strains Guy11, Guy11:*TrpCp:BIP1,* and Δ*bip1_2*. Detached leaves were incubated on water-soaked Whatman paper at 25°C with a 12h photoperiod for 5 days before visualising and quantifying blast disease progression. (B) Box plots show the calculated area of disease lesions for each strain. The mean value is shown as a horizontal line inside the box, and error bars equal the standard deviation. T-tests show significantly reduced virulence (p-value <0.05) for Guy11:*TrpCp:BIP1* and Δ*bip1_2* strains compared to wild-type infection. Results represent three biological replicates.

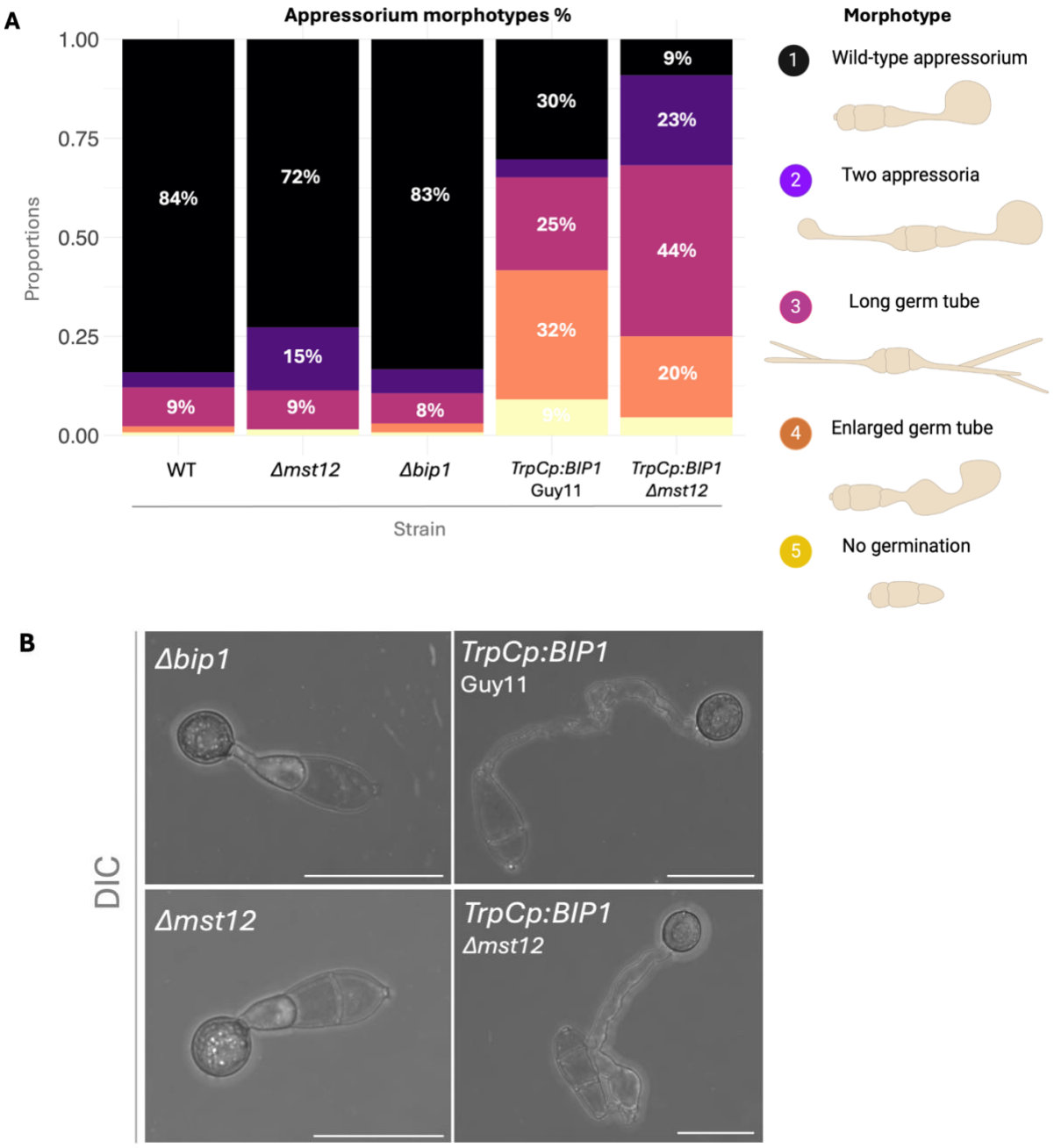

Figure 5.12 Constitutive expression of BIP1 affects M. oryzae appressoria formation. (A) Proportions of appressoria morphotypes observed for wild-type *Guy11*, *Δmst12*, *Δbip1*, *Guy11:TrpCp:BIP1*, and *Δmst12 :TrpCp:BIP1 M. oryzae* strains. Morphotypes illustrated on the right include wild-type (black), two-appressoria (purple), long germ tube (pink), enlarged germ tube (orange), and no germination (yellow). For both Δ*mst12* and Δ*bip1* mutants, the quantified appressoria mostly presented wild-type morphology. In contrast, Guy11:*TrpCp:BIP1 and* Δ*mst12*:*TrpCp:BIP1* strains exhibited two appressoria, long germ tubes or enlarged appressoria morphology, which was increased in Δ*mst12*:*TrpCp:BIP1*. (B) Micrographs show a representative

example of the observed morphologies for Δ*mst12*, Δ*bip1*, Guy11:*TrpCp:BIP1, and* Δ*mst12* :*TrpCp:BIP1 M. oryzae* strains. Conidia were harvested, inoculated on hydrophobic coverslips, and observed by laser confocal microscopy at 24h. Micrographs show a maximum projection of Z-stack images. Scale bar = 20 μm.

5.2.9 Bip1 can form homodimers and interacts with Mst12

In the regulation of distinct molecular functions, Mst12 and its homologues have been shown to form protein complexes with other TFs (Mueller & Nordheim, 1991, Dohlman & Thorner, 2001, Zhou *et al.*, 2011). Consequently, to identify potential interactions between Mst12 and Bip1 proteins, a Yeast-Two-Hybrid (Y2H) experiment was conducted. For this, I utilised Y2H vectors pGBKT7-BD (bait) and pGADT7-AD (prey) for Mst12, Pmk1, and Hox7 TFs previously generated in the laboratory (Osés-Ruiz *et al.*, 2021) and constructed Bip1 prey and bait vectors through CDS sequence amplification from *M. oryzae* cDNA. Co-transformed yeast was grown on selection medium, showing unrestricted growth for the positive control (T-AD/35-BD), Bip1-AD/Bip1-BD and Mst12-AD/Bip1-BD, as presented in Figure 5.13. While negative control (T-AD/Lam-BD), Pmk1-AD/Bip1-BD and Hox7-AD/Bip1-BD did not show any growth, indicating no interaction among these proteins.

Furthermore, reinforcing these results, positive interactions among Bip1-Bip1 and Mst12-Bip1 exhibited high-ranking confidence models when predicted *in silico*, as shown in Figure 5.14. These experiments provide evidence that Bip1 can form homodimers, a result commonly found for bZIP TFs (McLachlan & Stewart, 1975), and that Mst12 and Bip1 proteins can physically interact, providing new insight into their potential molecular interplay in *M. oryzae*.

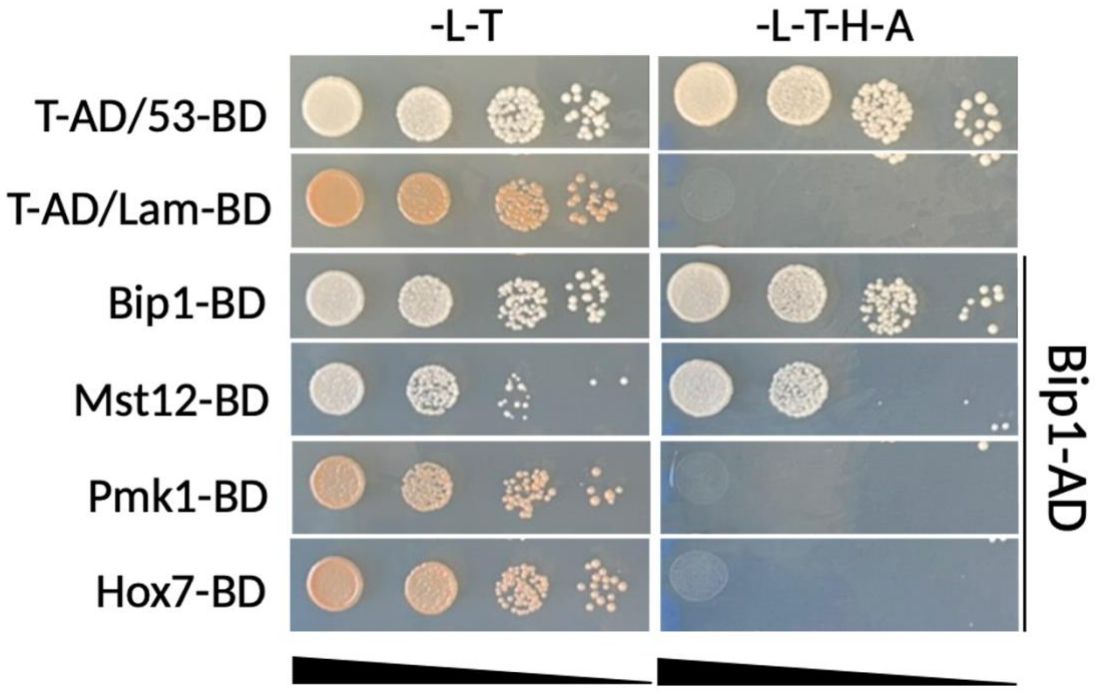

Figure 5.13 Bip1 can form homodimers and interacts with Mst12. Yeat-Two-Hybrid (Y2H) assay shows co-transformed yeast can grow on SD medium (-Leu -Trp -His -Ade) for the positive control (T-AD/35-BD), Bip1-AD/Bip1-BD and Mst12-AD/Bip1-BD. No growth is shown for the negative control (T-AD/Lam-BD), Pmk1-AD/Bip1-BD, and Hox7-AD/Bip1-BD. Serial dilutions (1, 0.1, 0.01, and 0.001 DO_{600}) go from left to right in each panel. The viability of co-transformed cells is shown by growth on SD medium (-Leu -Trp).

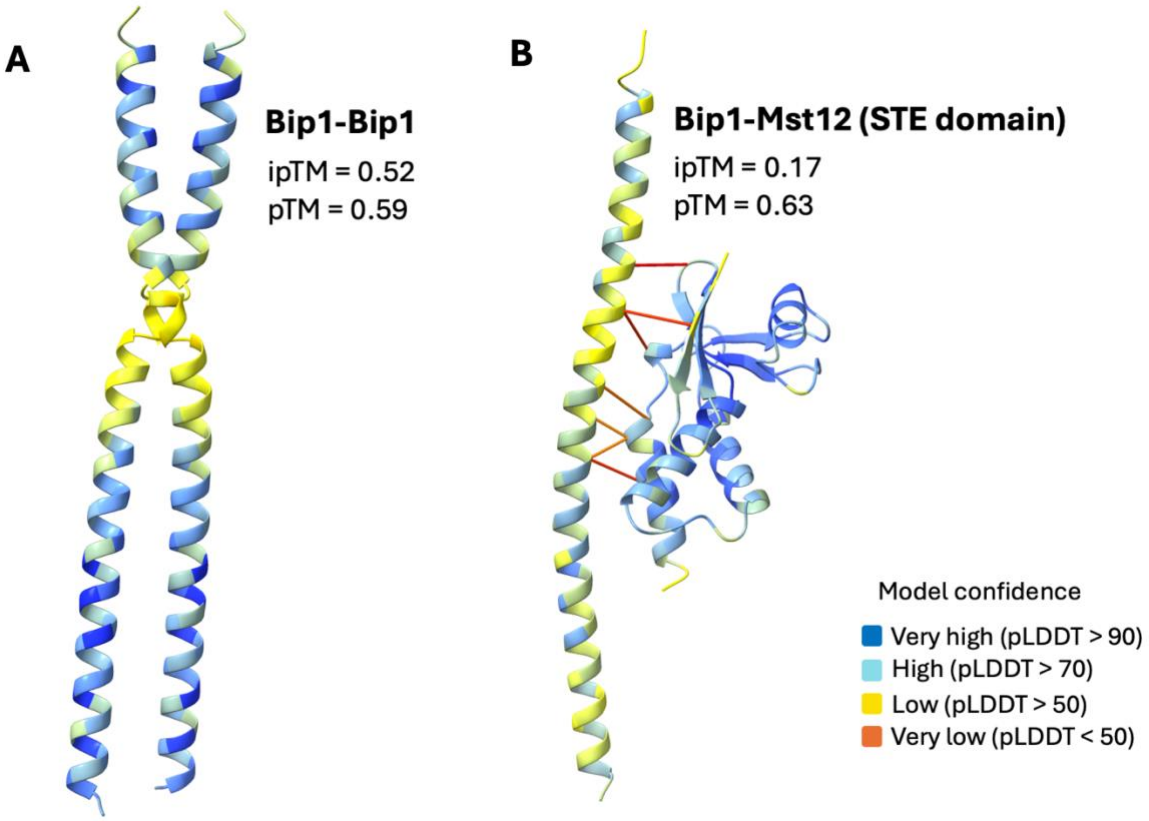

Figure 5.14 *In silico* prediction of Bip1 and Mst12 interactions. Alphafold-3 predictions of (A) Bip1-Bip1 interaction and (B) Bip1-Mst12 (STE domain) interaction. pLDDT scores are shown with the model confidence colouring. Distorted regions are cropped for visualisation purposes.

5.2.10 Time-course RNA-Seq analysis reveals overlapping gene regulation for Bip1 and Mst12

To further investigate the regulatory role of Bip1 in relation to the Pmk1 MAPK signalling pathway, we performed a global transcriptomic analysis during appressorium development of *M. oryzae*. The objective of this experiment was to compare transcriptomic profiles of *M. oryzae* strains—wild-type Guy11, Δ*mst12*, Δ*bip1* mutants and *TrpCp:BIP1* overexpression strain—across three different time points (0h, 4h, and 24h) of appressorium development. A total of 36 samples were analysed, comprising three biological replicates per strain and time point (in collaboration with Dr Neha Sahu).

Sample relationships and transcriptional fingerprints were examined through a multidimensional scaling (MDS) plot. The first MDS dimension (36%) and second MDS dimension (17%) accounted for 53% of the total variance across samples. The biological replicates for each sample were consistently grouped together, ensuring reproducibility of the generated data. Further sample clustering was observed for different analysed time points (0h, 4h, and 24h of appressorium development of *M. oryzae*), suggesting less transcriptomic variation between samples across developmental stages, as illustrated in Figure 5. 15.

Given the MDS analysis, we analysed differentially expressed genes for each sample and time point. Following raw read quality control and filtering with Trimmomatic (Bolger *et al.*, 2014) and FastQC (Babraham Bioinformatics), we used Kallisto to map and quantify processed reads (Bray *et al.*, 2016). Differential gene expression was calculated using edgeR (Robinson *et al.*, 2009, Pimentel *et al.*, 2017), and ultimately, the selection of differentially expressed genes was determined using a threshold of $\log_2$ fold-change (>=1) and adjusted p-value (p<=0.05). The total number of DEGs is presented in Figure 5.16.A and the overlap of RNA-Seq samples is represented by Euler diagrams (Micallef & Rodgers, 2014) in Figure 5.16.B. The greatest overlap was observed among Δ*bip1* and Δ*mst12* mutant transcriptomes, suggesting similarities among differentially expressed genes. However, non-overlapping areas also indicate that unique gene expression may be associated with each individual TF during *M. oryzae* appressorium development.

The distribution of up and down-regulated genes was plotted as heatmaps for every sample and time point to investigate global transcriptomic expression patterns further. Through this analysis, we could observe that Δ*bip1* and Δ*mst12* mutants exhibited similar gene expression patterns, showing blocks of genes commonly up or down-regulated for every plotted time point, as seen in Figure 5.17.A and Figure 5.17.B. This was further supported by a Pearson correlation matrix (Friendly, 2002), finding higher correlation values among Δ*bip1* and Δ*mst12* transcriptomes, sharing

the highest correlation, especially at 0h and 4h, as shown in Figure 5.17.C. However, some differences observed for these mutant strains among Euler plots and heatmaps suggest both TF have unique differential gene expression as well as the observed commonalities.

For the constitutive *BIP1*-overexpressing *M. oryzae* strain (*TrpCp:BIP1*), Euler plots and heatmaps revealed different transcriptomic signatures to those found in Δ*bip1* and Δ*mst12* mutants, mostly presenting similarity to the wild-type Guy11. However, for some sections, it also displayed signatures that were opposite to those found in Δ*bip1* and Δ*mst12* mutants, further reinforcing the analysis and the putative regulatory function of Bip1.

Transcriptomic results suggest that while Bip1 and Mst12 have unique regulatory roles, they also share a subset of co-regulated genes during appressorium development. This analysis further supports the hypothesis that these TFs act downstream of the Pmk1 MAPK signalling pathway, regulating pathogenic gene expression in *M. oryzae*.

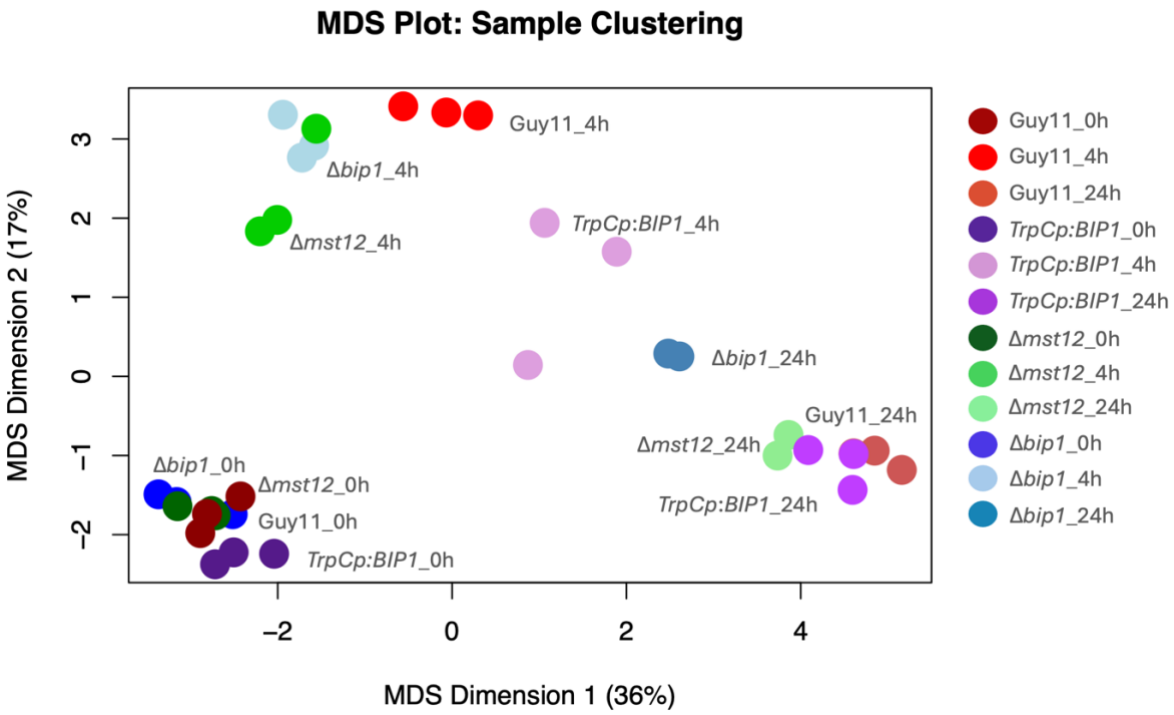

Figure 5.15 Multidimensional scaling (MDS) plot for the time-course RNA-Seq analysis. MDS plotting was performed to analyse sample clustering based on expression value. Combining both dimensions, there is a 53% variance across samples. Biological replicates, represented by the same colours, cluster together, suggesting reproducibility of the data. Grouping is also observed by time point (0h, 4h, 24h) of appressorium development. Guy11 samples are represented in red tones, *BIP1* overexpression (*TrpCp:BIP1)* is represented in purple tones, Δ*mst12* mutant is represented in green tones, and Δ*bip1* mutant is represented in blue tones.

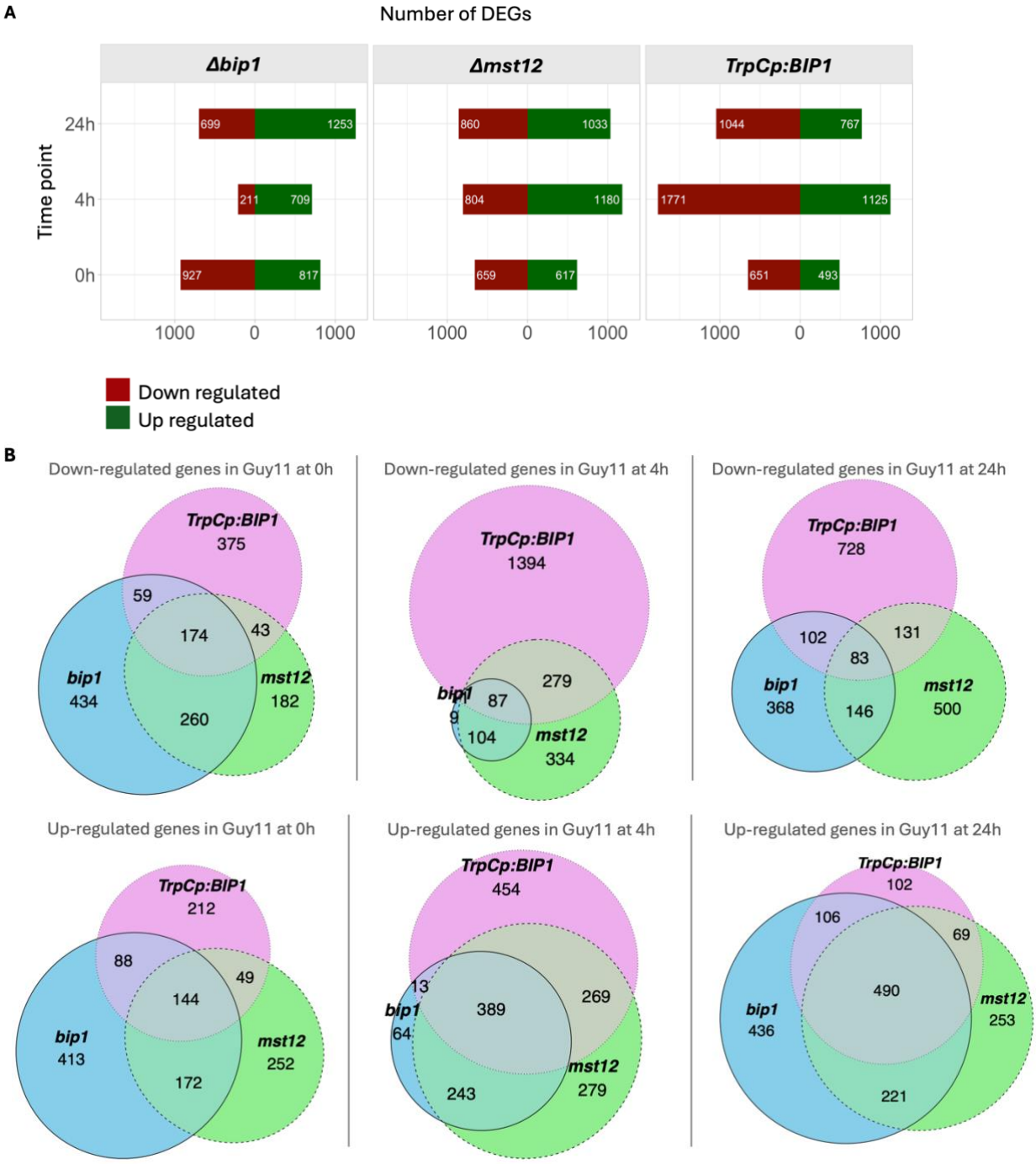

Figure 5.16 Number of DEGs identified during appressorium development for Δ*mst12*, Δ*bip1* mutants, and *BIP1* overexpression (*TrpCp:BIP1*) *M. oryzae* strains. (A) Number of up-regulated (green) and down-regulated (red) genes for Δ*mst12*, Δ*bip1* mutants, and *BIP1* overexpression (*TrpCp:BIP1*) *M. oryzae* strains compared with wild type Guy11 at different time points of appressorium development (0h, 4h, and 24h). (B) Euler plots show overlapping genes across samples and time points. *TrpCp:BIP1* is represented in pink, Δ*bip1* mutant is represented in blue and Δ*mst12* mutant is represented in green.

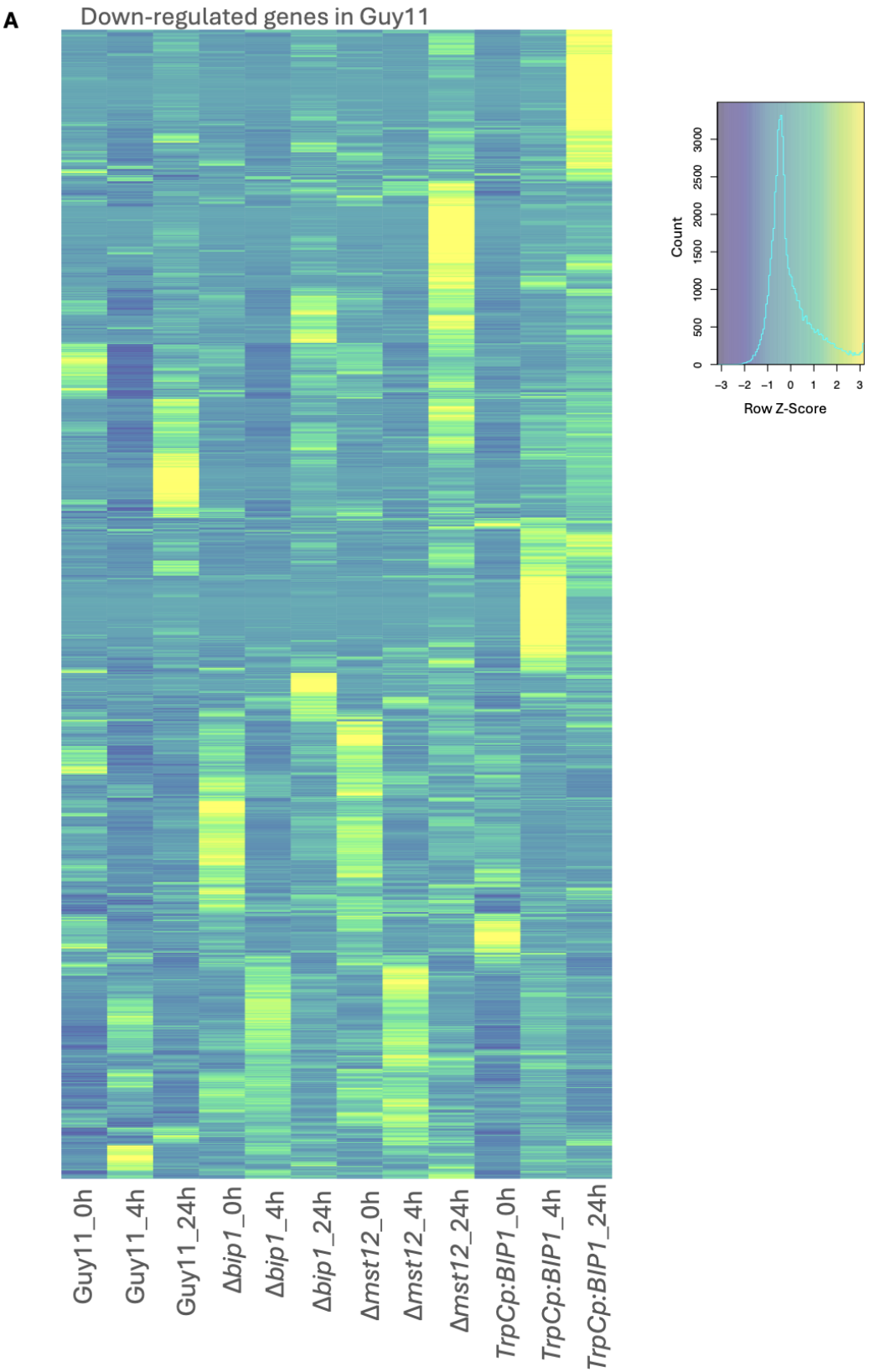

Figure 5.17.A Heatmap of down-regulated genes in Guy11. Down-regulated genes in Guy11 from global transcriptomic analysis for Δ*mst12*, Δ*bip1* mutants, and *BIP1* overexpression (*TrpCp:BIP1) M. oryzae* strains during appressorium development of *M. oryzae*. Row Z score = (tpm for a single gene) – mean/standard deviation.

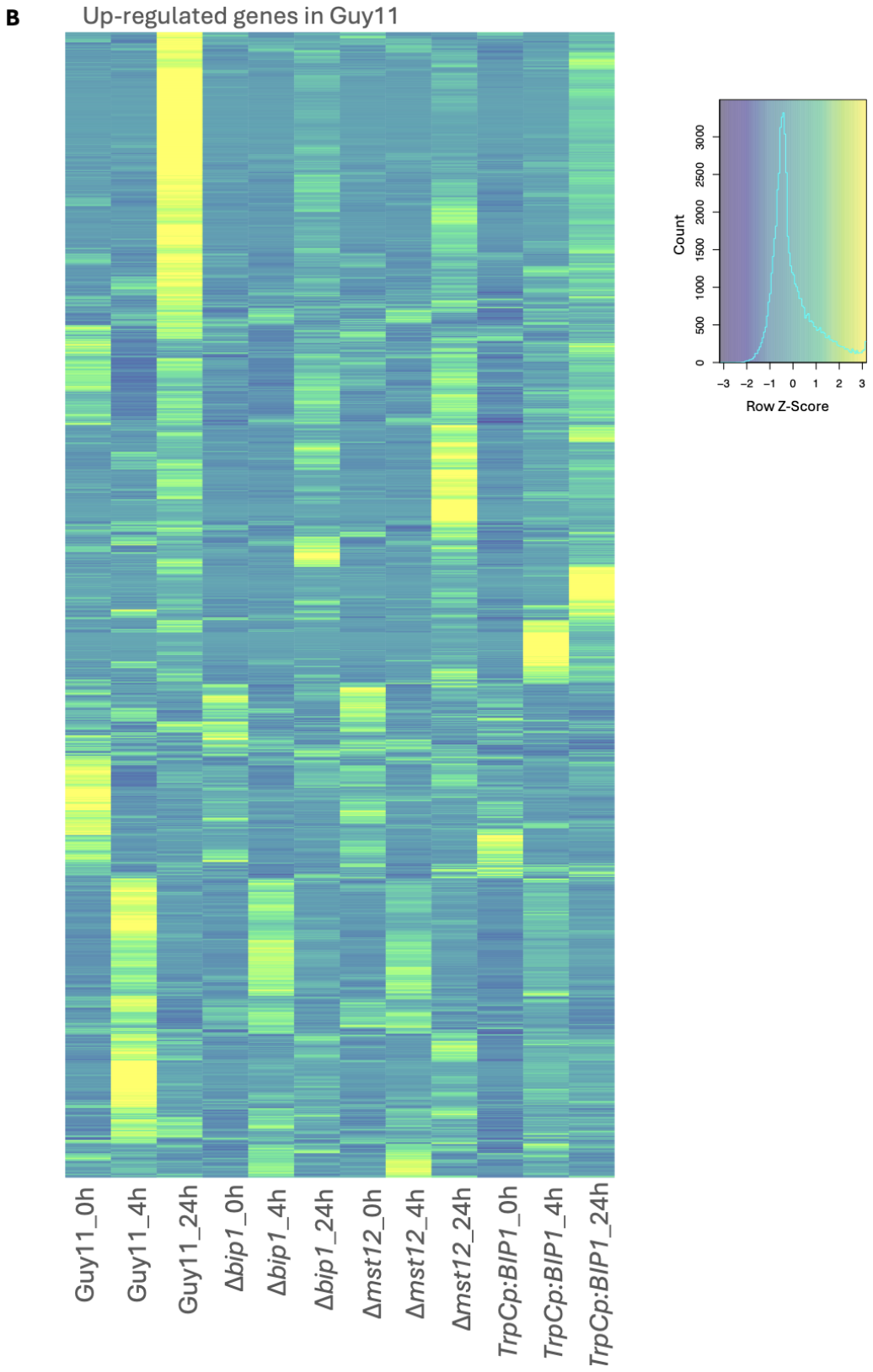

Figure 5.17.B Heatmap of up-regulated genes in Guy11. Up-regulated genes in Guy11 from global transcriptomic analysis for Δ*mst12*, Δ*bip1* mutants, and *BIP1* overexpression (*TrpCp:BIP1) M. oryzae* strains during appressorium development of *M. oryzae*. Row Z score = (tpm for a single gene) – mean/standard deviation.

C

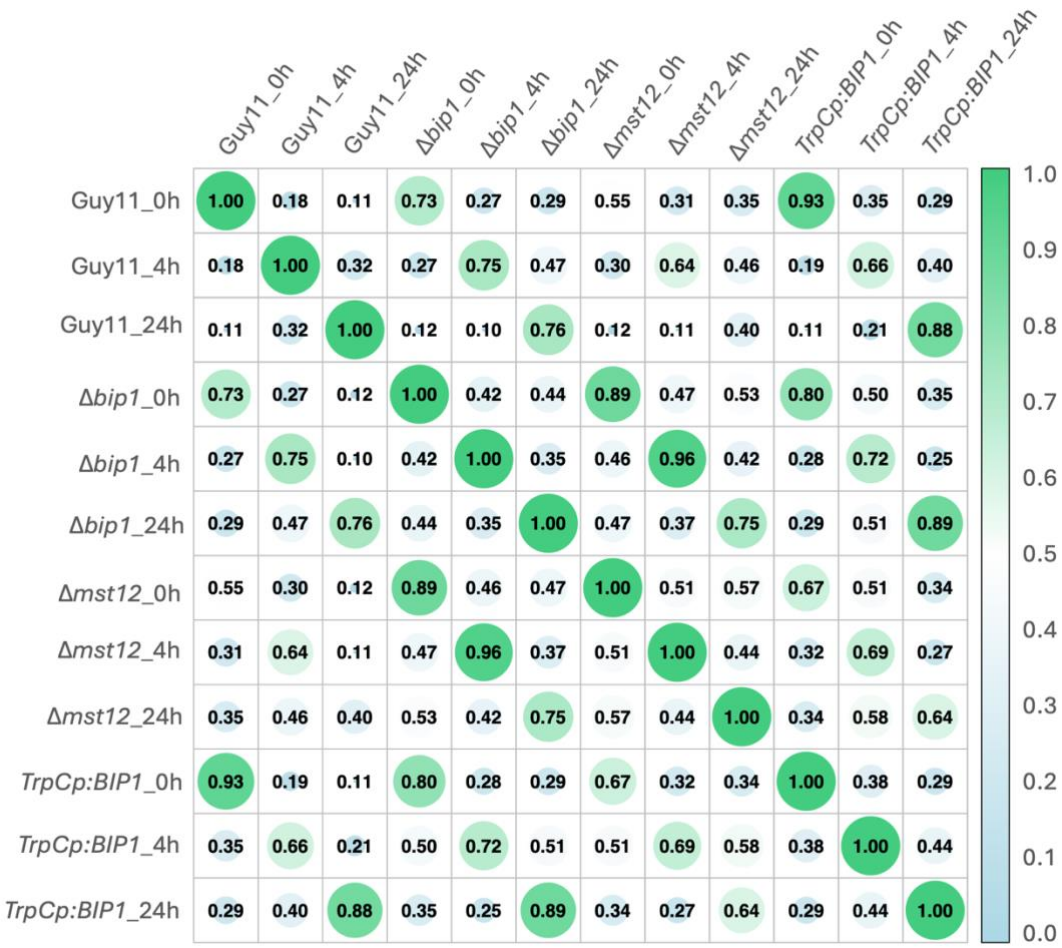

Figure 5.17.C Pearson correlation matrix to compare gene expression between analysed *M. oryzae* mutant strains. Pearson correlation matrix based on gene expression of global transcriptomic analysis for Δ*mst12*, Δ*bip1,* and *BIP1* overexpression (*TrpCp:BIP1) M. oryzae* strains during appressorium development. High correlation is represented in green and lower correlation is represented in light blue.

5.2.11 GO enrichment analysis of Bip1 and Mst12 regulated genes

Having established that Bip1 and Mst12 have similar gene expression patterns during appressorium development of *M. oryzae*, the next step was to investigate common and distinctly regulated genes. For this, we performed Gene Ontology (GO) enrichment analysis for up and down-regulated genes at every sequenced time point. In filamentous fungi, the majority of genes lack annotations or known molecular functions. To maximise available information, we used a script to annotate GO-enrichment plots based on biological processes (BC) and molecular function (MF) domains. Investigating commonly enriched genes (Figure 5.18), we identified growth-related metabolic processes (including sulphate assimilation, cellular oxidant detoxification, hydrogen sulphide biosynthesis, and carbohydrate metabolisms), cytoskeletal organisation, chromatin remodelling, RNA maturation, RNA binding, DNA binding, ribosome binding, and methylation at the earlier time points. Enrichment in metabolic and biosynthetic processes, transmembrane transport activity, and intracellular homeostasis regulation were overrepresented at 24h. For instance, among commonly regulated genes, a family of membrane-associated fasciclin glycoproteins Flp1 (*MGG_02884*), Flp2 (*MGG_09372*), and Flp3 (*MGG_05483*) involved in cell adhesion (Johnson *et al.*, 2003, Seifert, 2018) previously reported to be regulated by both Pmk1 MAPK and Mst12 (Osés-Ruiz *et al.*, 2021), could be found among Δ*bip1* and Δ*mst12* downregulated genes. Suggesting *BIP1* is also required for their expression and providing further evidence that this TF acts downstream of the Pmk1 MAPK/Mst12 signal transduction pathway.

Additionally, there were some differentiated enrichments for each transcription factor; for instance, Δ*mst12* presented enrichment in genes related to nucleotide binding and chitin-binding, while Δ*bip1* showed enrichment for genes involved in cell division, translation, nucleocytoplasmic transport, cortical actin organisation, and iron binding.

Figure 5.18.A Biological processes GO-enrichment for up-regulated genes. GO-enrichment subject to biological procesess of up-regulated DEGs in Guy11. Transcriptomic data for Δ*mst12*, Δ*bip1* mutants, and *TrpCp:BIP1 M. oryzae* strains during appressorium development (0h, 4h, 24h) of *M. oryzae*.

B

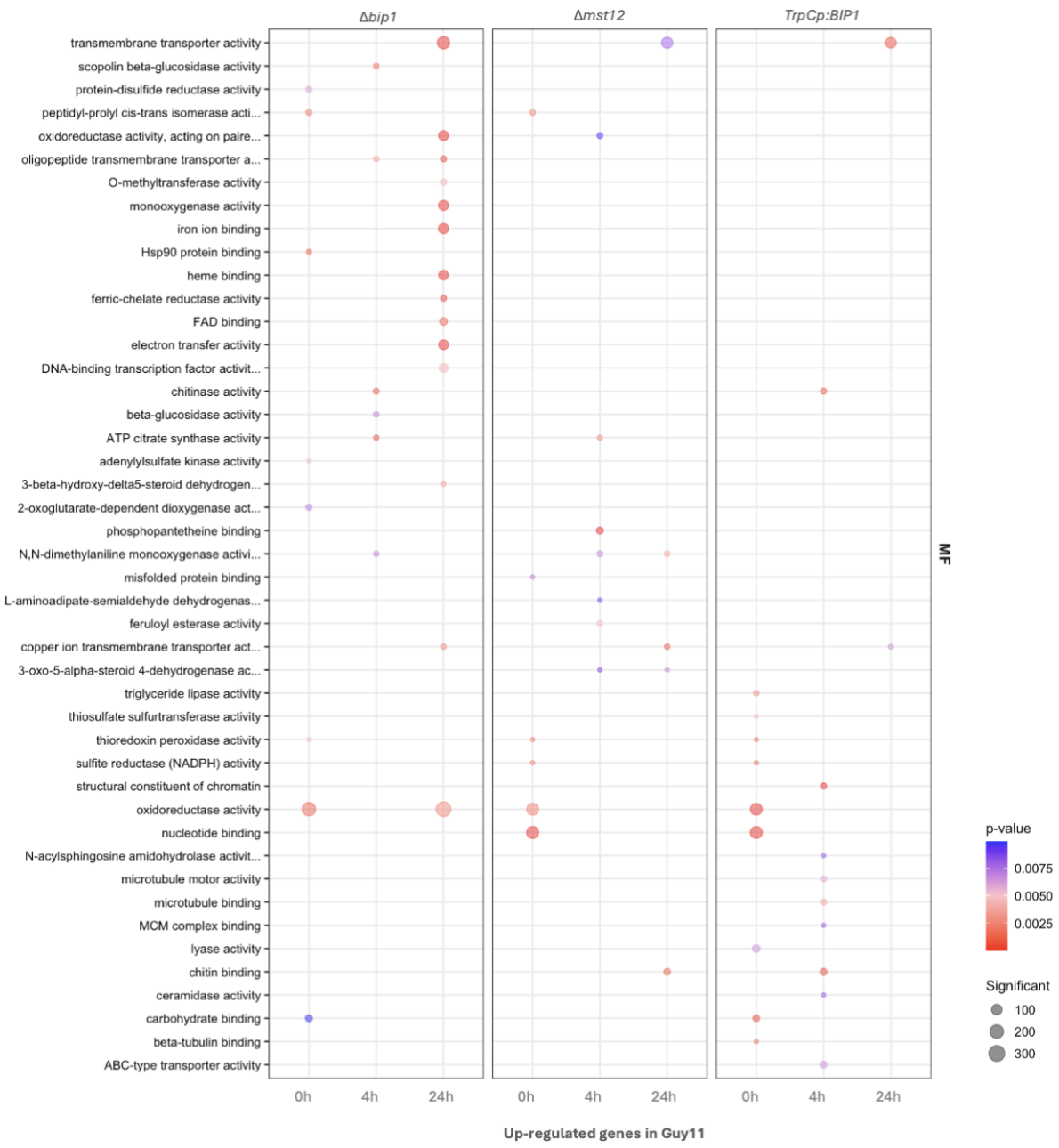

Figure 5.18.B. Molecular function GO-enrichment for up-regulated genes. GO-enrichment subject to molecular functions of up-regulated DEGs in Guy11. Transcriptomic data for Δ*mst12*, Δ*bip1* mutants, and *TrpCp:BIP1 M. oryzae* strains during appressorium development (0h, 4h, 24h) of *M. oryzae*.

C

Figure 5.18.C Biological processes GO-enrichment for down-regulated genes. GO-enrichment subject to biological processes of down-regulated DEGs in Guy11. Transcriptomic data for Δ*mst12*, Δ*bip1* mutants, and *TrpCp:BIP1 M. oryzae* strains during appressorium development (0h, 4h, 24h) of *M. oryzae*.

D

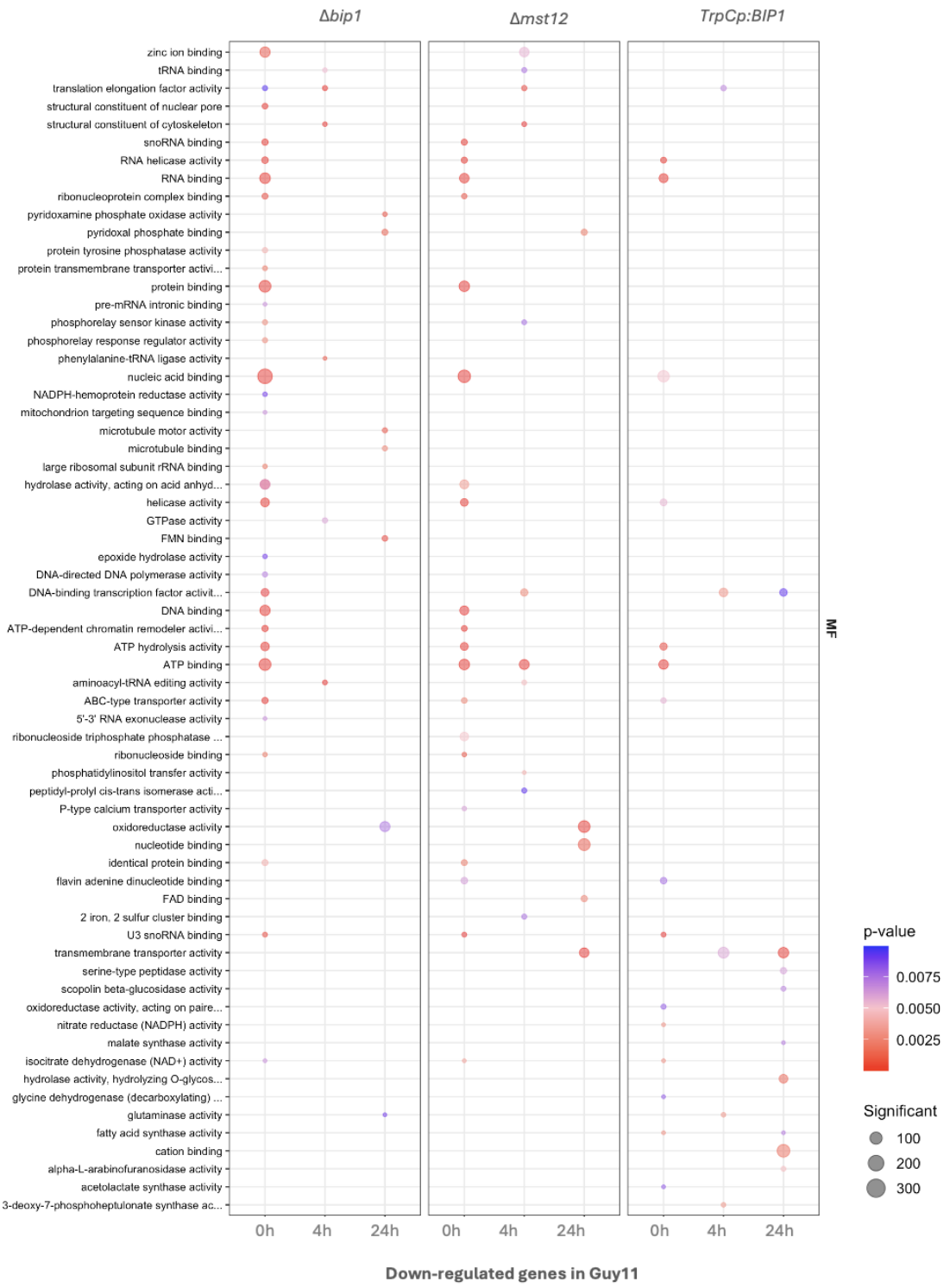

Figure 5.18.D Molecular function GO-enrichment for down-regulated genes. GO-enrichment subject to molecular functions of down-regulated DEGs in Guy11. Transcriptomic data for Δ*mst12*, Δ*bip1* mutants, and *TrpCp:BIP1 M. oryzae* strains during appressorium development (0h, 4h, 24h) of *M. oryzae*.

5.2.12 Mst12 and Bip1 co-regulate a hierarchy of transcription factors required for appressorium development

Transcriptomic analysis previously identified a hierarchy of transcriptional regulators dependent on both Pmk1 MAPK and Mst12 TF (Osés-Ruiz *et al.*, 2021). These included a combination of characterised and uncharacterised TFs expressed during the appressorium development of *M. oryzae*. To further validate that Bip1 is downstream of the Pmk1 MAPK/ Mst12 signalling cascade, we searched for these TFs in our newly generated dataset. Through this analysis, we identified that all nine Zn_2Cys_6 TFs reported to be Pmk1 and Mst12 dependent (Osés-Ruiz *et al.*, 2021) were also Bip1 dependent. These included Fzc30, Fzc41, Fzc52, and Fzc64, previously reported to be implicated in stress responses; Fzc50, implicated in conidial germination; and Fzc75, related to appressorium development (Lu *et al.*, 2014, Osés-Ruiz *et al.*, 2021). Additionally, every **R**elated to **P**mk1 **P**athway TF, termed RPP (RPP1, RPP2, RPP3, RPP4, and RPP5) and the homeobox-domain TF Hox7, which is phosphorylated by Pmk1 to regulate appressorium development (Kim *et al.*, 2009, Osés-Ruiz *et al.*, 2021), were also found to be regulated by Bip1. These findings are consistent with Bip1 acting downstream of the Pmk1 MAPK/ Mst12 pathway, required for appressorium development and pathogenicity of *M. oryzae*.

5.2.13 Effector genes regulated by Bip1 and Mst12

Focusing on effector gene regulation, we decided to cross-compare our datasets with a list of 546 predicted MEP effectors (Yan *et al.*, 2023). This allowed identification of 80 Bip1 and Mst12 dependent effectors across all time points; 66 were up-regulated, suggesting Bip1 and Mst12 are both required for their expression, while 14 were down-regulated, suggesting repression of these genes by the TFs. Bip1 and Mst12 regulated effectors showed diverse expression patterns, peaking at different time points of *M. oryzae* infection. However, most showed a peak between 16h and 48h, as illustrated in Figure 5.19. They represented effectors from 33 different structural groups (Seong & Krasileva, 2021) shown in Table 5.2, and among them, Bas3 had been previously reported to be transcriptionally regulated by Pmk1

MAPK (Sakulkoo *et al.*, 2018). This result further suggests that Bip1 is part of the Pmk1 MAPK signal transduction pathway.

Additionally, across the analysed time points, we identified 231 effectors (170 up-regulated and 61 down-regulated) exclusively Bip1-dependent and 263 effectors (115 up-regulated and 148 down-regulated) exclusively Mst12-dependent. This finding suggests that both Bip1 and Mst12 may act individually as transcriptional activators and transcriptional repressors of a different subset of effectors.

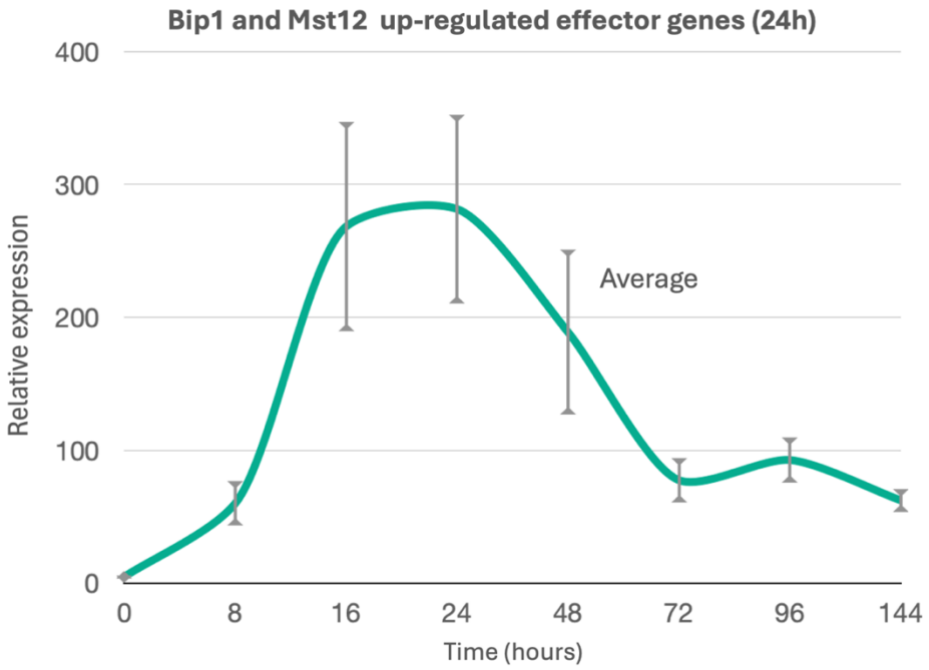

Figure 5.19 Average expression of Bip1 and Mst12 regulated effector genes. The average relative expression pattern for 52 Bip1 and Mst12-dependent effectors during the time course of *M. oryzae* infection development. Genes were up-regulated in Guy11 at 24h when compared to Δ*bip1* and Δ*mst12* mutants. The green line represents the moving average, and the error bars equal the standard deviation.

Table 5.2. Mst12 and Bip1 up-regulated effectors at 24h of appressorium development.

Gene	Gene name	Expression Module	Structural cluster	Structural description	Description
MGG_10477	MEP499	NA	1	Rossmann fold	SGNH hydrolase
MGG_00110	MEP583	Module 9	1	Rossmann fold	NAD(P)-binding Rossmann-fold domains
MGG_02814	MEP684	Module 2	1	Rossmann fold	alpha/beta-Hydrolases
MGG_13429	MEP756	Module 8	2	TIM Barrel	(Trans)glycosidases
MGG_10423	MEP713	Module 2	2	TIM Barrel	(Trans)glycosidases
MGG_09439	MEP533	Module 9	5	Coagulation Factor XIII; Chain A, domain 1	E set domains
MGG_00703	MAS3 (MEP64)	Module 5	5	Immunoglobulin-like	Galactose-binding domain-like
MGG_14793	MEP487	Module 4	8	Complement Module; domain 1	insert domain,N-utilization substance G protein NusG
MGG_11599	MEP413	Module 3	9	Glycosyltransferase	Seven-hairpin glycosidases
MGG_02273	MEP486	Module 8	11	Jelly Rolls	PA14-like
MGG_09351	MEP456	Module 2	13	Cathepsin D, subunit A; domain 1	Acid proteases
MGG_16603	MEP50	Module 5	14	Glutaredoxin	lambda repressor-like DNA-binding domains
MGG_17205	MEP331	Module 4	14	hfbii hydrophobin	Defensin-like
MGG_09322	MEP404	Module 8	16	Rossmann fold	Subtilisin-like
MGG_03056	MEP497	Module 4	16	Rossmann fold	Subtilisin-like
MGG_07404	MEP197	Module 2	16	Rossmann fold	Subtilisin-like
MGG_13868	MEP288	Module 4	20	Alpha-Beta Plaits	ACT-like
MGG_07810	MEP153	Module 4	20	Alpha-Beta Plaits	MTH1187/YkoF-like
MGG_10796	MEP548	Module 3	21	AOC barrel-like	C2 domain (Calcium/lipid-binding domain
MGG_10237	MEP407	Module 6	24	Pectate Lyase C-like	Pectin lyase-like
MGG_06798	MEP443	Module 5	25	Farnesyl Diphosphate Synthase	TROVE domain-like
MGG_02778	SVP (MEP161)	Module 3	26	Tetracycline Repressor; domain 2	MukF C-terminal domain-like
MGG_07704	MEP697	Module 7	30	Aminopeptidase	Zn-dependent exopeptidases
MGG_03456	MEP126	Module 9	32	Collagenase (Catalytic Domain)	Metalloproteases ("zincins")
MGG_07424	MEP283	Module 2	39	Thaumatin	Cytolysin/lectin
MGG_00721	MEP719	Module 3	42	Phosphatidylethanolamine-binding Protein	E set domains
MGG_06844	MEP393	Module 2	42	Phosphatidylethanolamine-binding Protein	PEBP-like
MGG_11610	BAS3 (MEP88)	Module 5	51	Phosphorylase Kinase; domain 1	Interleukin 8-like chemokines

MGG_03946	MEP586	Module 3	53	Immunoglobulin-like	Cupredoxins
MGG_08291	MEP498	Module 3	53	Immunoglobulin-like	Cupredoxins
MGG_08515	MEP15	Module 4	56	de novo design (two linked rop proteins)	FAT domain of focal adhesion kinase
MGG_09387	HEG8/BAS (MEP103)	Module 4	56	Four Helix Bundle (Hemerythrin (Met), subunit A)	Aspartate receptor
MGG_09763	MEP437	Module 3	56	Four Helix Bundle (Hemerythrin (Met), subunit A), Aspartate receptor	Aspartate receptor
MGG_17582	MEP349	Module 6	59	Single alpha-helices involved in coiled-coils or other helix-helix interfaces	Myosin S1 fragment
MGG_02884	MFP1	Module 8	73	Rossmann fold	Acyl-CoA dehydrogenase NM domain-like
MGG_08300	MEP250	Module 5	93	Methane Monooxygenase Hydroxylase; Chain G, domain 1	Hyaluronidase post-catalytic domain-like
MGG_05539	MEP706	Module 5	98	Aminopeptidase	Zn-dependent exopeptidases
MGG_03671	MEP816	Module 5	107	Cyclin-Dependent Kinase Subunit Type 2,Cyclin-dependent kinase	Cell cycle regulatory proteins
MGG_08647	MEP501	Module 8	175	Leucine-rich repeat, LRR (right-handed beta-alpha superhelix)	Ankyrin repeat
MGG_03585	MEP472	Module 4	211	Four Helix Bundle (Hemerythrin (Met), subunit A)	Plant invertase/pectin methylesterase inhibitor
MGG_00511	MEP655	Module 3	271	Methane Monooxygenase Hydroxylase; Chain G, domain 1	GAT-like domain
MGG_05818	MEP433	Module 3	288	Ubiquitin-like (UB roll)	RNA-binding domain
MGG_07656	CSN1 (MEP77)	Module 2	296	Rossmann fold	Metalloproteases ("zincins")
MGG_12748	GTR1 (MEP67)	Module 3	299	Single alpha-helices involved in coiled-coils or other helix-helix interfaces	Troponin coil-coiled subunits
MGG_16353	MEP1	Module 4	336	Cytochrome C Oxidase; Chain M,Cytochrome c oxidase	Mitochondrial cytochrome c oxidase subunit VIIIb (aka IX)
MGG_02851	MEP822	Module 5	805	Glycoprotein D; Chain: A	Immunoglobulin

5.3 Discussion

Many plant pathogenic fungi, including *M. oryzae*, gain entry to their host using a specialised cell known as an appressorium (Ryder *et al.*, 2022). These infection structures accumulate sufficient turgor pressure to breach the leaf cuticle by forming a rigid penetration peg (Ryder *et al.*, 2019, Ryder *et al.*, 2023). Infection-related development is known to be controlled by signal transduction pathways, including the cAMP-dependent protein kinase A (PKA) pathway and the Pmk1 MAPK pathway (Xu & Hamer, 1996, Choi & Dean, 1997). Through the regulation of downstream TFs, these conserved cascades orchestrate timely morphogenesis transitions. Among these TFs, Hox7, Znf1, and Sfl1 regulate spore germination, appressorium differentiation and maturation, while Mst12, Git1, and Mig1 regulate penetration, invasive growth and effector expression in *M. oryzae* (Park *et al.*, 2002, Mehrabi *et al.*, 2008, Kim *et al.*, 2009, Li *et al.*, 2011, Yue *et al.*, 2015, Li *et al.*, 2016). Although each of these TFs has a distinct function, some regulatory overlap indicates sophisticated coordination of transcriptional regulation to facilitate blast infection (Wang *et al.*, 2024).

Previous studies have found that mutants with penetration deficiency, such as Δ*git1* or Δ*mst12* mutants, also exhibit altered effector gene expression (Park *et al.*, 2002, Li *et al.*, 2016, Osés-Ruiz *et al.*, 2021). The connection between morphogenesis control and effector gene regulation, along with the established regulatory redundancy, prompted the investigation of non-penetrating *M. oryzae* mutants in this study. This chapter describes the bZIP TF Bip1 and provides evidence that it is a component of the conserved Pmk1 MAPK signalling pathway, which is crucial for appressorium development, penetration, and effector gene expression (Xu & Hamer, 1996, Park *et al.*, 2002, Sakulkoo *et al.*, 2018, Osés-Ruiz *et al.*, 2021). Bip1 was previously described to regulate a subset of appressorium-related genes and early expression effector genes independently from any known signalling pathway in *M. oryzae* (Lambou *et al.*, 2024). These observations were based on microarray data performed on Bip1 and comparisons among publicly available Pmk1 and Mst12 transcriptomic and ChIP-Seq datasets (Osés-Ruiz *et al.*, 2021,

Lambou *et al.*, 2024). However, our observations and follow-up experiments demonstrate that Bip1 is downstream of Pmk1 MAPK and Mst12, providing new insights into this established pathogenicity-related cascade and how it governs effector gene expression.

Initial considerations prompting the investigation of Bip1 included the identification of numerous Pmk1 and Mst12-dependent genes within putative Bip1-dependent gene datasets. A total of 80% of genes identified in a Bip1 microarray dataset and 50% of genes highlighted through FIMO as possessing a Bip1 DNA-binding motif were also among Pmk1 and Mst12 DEGs, including all of the effector genes. Additionally, we discovered that *BIP1* gene expression is down-regulated in Δ*pmk1* and Δ*mst12* mutant RNA-Seq data, suggesting that *BIP1* expression depends on *PMK1* and *MST12*. Furthermore, discovery phosphoproteomics facilitated the identification of a Bip1 putative phosphorylation site (Cruz-Mireles *et al.*, 2024). This phosphorylation exhibited reduced abundance at later stages of appressorium development in a Δ*pmk1* mutant. A result that suggests Bip1 phosphorylation may be regulated by Pmk1 either transcriptionally or through direct/indirect phosphorylation of the protein. Although Y2H did not reveal any interaction between Pmk1 and Bip1, quantitative phosphoproteomics experiments, such as parallel reaction monitoring (PRM), should be used to test whether this phosphorylation is directly Pmk1-dependent.

Further supporting the connection of Bip1 to the Pmk1 MAPK signalling pathway, we discovered an Mst12 DNA-binding motif within the *BIP1* promoter. High-ranking *in silico* models predicted binding to occur through the second C_2H_2 zinc finger domain of Mst12, aligning with the reported pathogenicity-related function of Mst12 homologues C_2H_2 zinc finger domains (Wong Sak Hoi & Dumas, 2010). In both *Botrytis cinerea* and *Colletotrichum lindemuthianum*, the Ste12 transcription factor is shown to have splice variants lacking the second C_2H_2 zinc finger domain, which exerts an inhibitory effect on pathogenicity (Hoi *et al.*, 2007, Schamber *et al.*, 2010).

Additionally, we confirmed that Bip1 homodimerises and Mst12 and Bip1 can physically interact through Y2H experiments, suggesting their heterodimer formation may occur in *M. oryzae*. In yeast, for instance, Ste12 forms a heterodimer with TF Tec1 to regulate filamentation (Bao *et al.*, 2004), and forms heteromultimeric dimers with Mcm1 MADS-box protein to regulate pheromone responses (Mueller & Nordheim, 1991, Dohlman & Thorner, 2001). Furthermore, Mst12-Mcm1 interaction was further investigated and proposed to regulate germ tube and appressorium formation in *M. oryzae* (Zhou *et al.*, 2011). Therefore, Mst12-Bip1 complex formation is possible and may involve a specific regulatory mechanism that is distinct from individual regulation. However, the Mst12-Bip1 interaction requires further validation, achievable through co-immunoprecipitation or isothermal titration calorimetry (ITC) experiments to provide stronger *in vivo* and *in vitro* evidence, respectively. Validating an interaction between these proteins and the predicted binding interface would allow the analysis of their individual and in-complex regulatory roles in fungal pathogenesis.

To investigate Bip1 function further, we examined the organisation of the appressorium cytoskeleton. In Δ*mst12* mutants, septins, actin, and the Chm1 septin kinase exhibit mislocalisation, suggesting Mst12 is required for their organisation (Gupta *et al.*, 2015, Osés-Ruiz *et al.*, 2021). In the case of Δ*bip1* mutant, actin and Chm1 kinase showed wild-type organisation. However, septin 3 and septin 5 exhibited mislocalisation in the appressorium. This was particularly evident for septin 5 which failed to form its characteristic ring shape—essential for host infection (Gupta *et al.*, 2015). This result is consistent with the role of Bip1 being downstream of Mst12. Additionally, constitutively expressing *BIP1* affected pathogenicity and appressorium morphogenesis, showing enlarged germ tubes, long germ tubes, and the formation of two appressoria. This result suggests Bip1 homeostatic balance is necessary for proper development and infection. In a Δ*mst12* mutant background, appressorium dysmorphia associated with overexpressing *BIP1* was increased, providing further evidence of the hierarchic relationship between these transcriptional regulators. Taken together, these results

establish Bip1 as a transcriptional regulator that likely acts downstream of Mst12 but is necessary for appressorium penetration.

Finally, transcriptional analysis for Δ*mst12* and Δ*bip1* mutants revealed highly correlated gene expression patterns during appressorium development (0h, 4h, and 24h). Among these, we found a family of membrane-associated fasciclin glycoproteins Flp1, Flp2 and Flp3 involved in cell adhesion (Johnson *et al.*, 2003, Seifert, 2018). Additionally, we identified that the Pmk1 MAPK and Mst12 controlled hierarchy of TFs, which has been previously reported to be utilised by *M. oryzae* during appressorium development (Osés-Ruiz *et al.*, 2021), are also regulated by Bip1. Including Zn_2Cys_6 TFs Fzc30, Fzc41, Fzc52, and Fzc64, involved in stress response; Fzc50, implicated in conidial germination; Fzc75, related to appressorium development; homeobox-domain TF Hox7, which is phosphorylated by Pmk1 to regulate appressorium development; and all five **R**elated to **P**mk1 **P**athway TFs, (RPP1, RPP2, RPP3, RPP4, and RPP5) (Kim *et al.*, 2009, Lu *et al.*, 2014, Osés-Ruiz *et al.*, 2021). Furthermore, we found commonly regulated effector genes, including BAS3, previously identified to be regulated by Pmk1 MAPK (Sakulkoo *et al.*, 2018) , which is suggested to be crucial for cell-to-cell movement in the host (Mosquera *et al.*, 2009).

Taken together, these results suggest that Mst12 and Bip1 TFs may function cooperatively or through the formation of a complex, as presented in a model in Figure 6.1 in Chapter 6, to regulate development and disease progression in the blast fungus. Moreover, these findings establish that Bip1 is regulated by the Pmk1 MAPK/Mst12 signalling pathway and highlight that Mst12 and Bip1 are components of a hierarchical network of TFs that coordinate *M. oryzae* infection-related development.

Chapter 6: General discussion

The rice blast fungus, *M. oryzae,* produces a battery of effectors that are either secreted to the apoplast or internalised into the host cytoplasm during plant infection (Valent & Khang, 2010, Oliveira-Garcia *et al.*, 2024). Consistent with many plant pathogenic fungi, effector proteins are deployed to enable adaptation to the newly colonised environment by manipulating host cell biology and thereby protecting the fungus from plant immunity responses (Abramovitch *et al.*, 2006, Kamoun, 2006, Hogenhout *et al.*, 2009, Toruño *et al.*, 2016, Oliveira-Garcia *et al.*, 2024). Most apoplastic effectors target host enzymes, cell wall components, and extracellular immunity (De Wit *et al.*, 2009, Hogenhout *et al.*, 2009, Buscaill & van der Hoorn, 2021). For example, *M. oryzae* Slp1 binds chitin fragments to compete with the plant chitin-binding protein pattern recognition receptor CEBiP and prevent pathogen recognition (Mentlak *et al.*, 2012). By contrast, cytoplasmic effectors have been shown to target host immunity pathways, transcriptional regulation, and plant metabolism to promote biotrophic growth (Oliveira-Garcia *et al.*, 2024). For instance, the *M. oryzae* Avr-Pik effector binds HMA proteins to manipulate their function (Oikawa *et al.*, 2024), whereas HTR1 and HTR2 (Host Transcription Reprogramming Proteins 1 and 2) can modify host immunity-related transcription (Kim *et al.*, 2020). Furthermore, effector Avr-Piz-t targets plant ubiquitination and potassium uptake (Park *et al.*, 2012b, Shi *et al.*, 2018), MoPte1 targets host peroxisomes (Ning *et al.*, 2022), Avr-Pita targets host mitochondria (Han *et al.*, 2021a), and Avr-Pii targets the host exocyst complex (De la Concepcion *et al.*, 2022), exemplifying the array of strategies and effector targets employed by the blast fungus.

Through transcriptomic analysis, a total of 546 host-induced genes have been predicted to encode effectors in *M. oryzae* (Yan *et al.*, 2023). However, experimental validation has been limited due to the challenges of characterising such a large population of effectors, given their varied expression patterns, localisation, structures, and functions (Seong & Krasileva, 2021, Yan *et al.*, 2023, Le Naour--

Vernet *et al.*, 2025). Therefore, high-throughput analyses will be required to gain a comprehensive understanding of the role of effectors in fungal pathogenesis. For instance, it has been proposed that *M. oryzae* mutants may be bar-coded and utilised for large-scale infection assays aimed at determining the relative fitness conferred by each effector (Oliveira-Garcia *et al.*, 2024). In this context, investigating the regulation of effector genes could provide an alternative systematic and unifying approach for their study.

6.1 Gene regulation in filamentous plant pathogenic fungi

In filamentous fungi, many transcriptional regulators that drive disease progression also control effector gene expression (Tan & Oliver, 2017, John *et al.*, 2021, Wang *et al.*, 2024). For example, the Zn_2Cys_6 Pf2 TF can positively regulate effectors in Brassicaceae and necrotrophic wheat-infecting fungi (Cho *et al.*, 2013, Rybak *et al.*, 2017, Jones *et al.*, 2019), and has also been found to control virulence, infection-related morphogenesis, sporulation, stress tolerance, and carbohydrate metabolism in *M. oryzae, Zymoseptoria tritici,* and *Fusarium graminearum* (Chung *et al.*, 2013, Oh *et al.*, 2016, Habig *et al.*, 2020). Likewise, conserved fungal morphogenesis regulators such as Git1, Mst12, Con7, and StuA play roles in both development and effector gene expression in filamentous fungi (John *et al.*, 2021). Fungi possess 80 TF families, including homeodomain-like, Zn_2Cys_6 (C6 zinc cluster), C_2H_2-like zinc finger proteins, GATA proteins, basic leucine-zipper and basic helix-loop-helix regulators, and the Velvet family (Shelest, 2017). Such significant TF diversification potentially explains the high regulatory redundancy and complexity of gene expression in fungal plant pathogens (Raffaele & Kamoun, 2012, Shelest, 2017); however, it also complicates regulatory investigations. Additionally, TF neofunctionalisation and TF complex formation further influence gene regulation. An example of neofunctionalisation is the Zn_2Cys_6 Ftf1/2 TF pair, which are virulence determinants in *Fusarium oxysporum* (Ma *et al.*, 2010, de Vega-Bartol *et al.*, 2011) but do not affect pathogenicity in *Fusarium graminearum* (Son *et al.*, 2011). While demonstrating complex formation, the well-characterised GATA factor AreA regulates nitrogen assimilation through complex formation with the GATA TF AreB,

the bZIP TF MeaB, and the Zn_2Cys_6 TF NirA in many filamentous fungi (Bolton & Thomma, 2008, Michielse *et al.*, 2014). Another example is the *Aspergillus nidulans* Velvet complex VelB/VeA/LaeA that coordinates light perception, fungal development, and secondary metabolism (Bayram *et al.*, 2008).

Furthermore, outside of TF control, gene regulation is also shaped by environmental cues, signal transduction cascades, RNA editing, post-transcriptional mechanisms, and epigenetic changes (Karin, 1991, Jaenisch & Bird, 2003, Lynch & Conery, 2003, Gibcus & Dekker, 2012, Noble & Andrianopoulos, 2013). For instance, in *M. oryzae,* effector-encoding genes have been reported to be regulated through MAPK signal transduction pathways and via G-protein signalling (Sakulkoo *et al.*, 2018, Tang *et al.*, 2023). Additionally, methylation and chromatin dynamics are involved in epigenetically controlling effector gene expression in *M. oryzae*, *Ustilaginoidea virens, Leptosphaeria maculans,* and *Fusarium spp.* (Soyer *et al.*, 2014, Dallery *et al.*, 2019, Meng *et al.*, 2021, Tang *et al.*, 2021). Taken together, these examples highlight the numerous layers of genetic regulation and the complexity of gene regulation in plant pathogenic fungi (Gibcus & Dekker, 2012). Therefore, the study of effector gene expression must consider all regulatory mechanisms, including the significant fungal genomic plasticity that continues to drive pathogen survival and evolution (Fisher *et al.*, 2012, Gladieux *et al.*, 2018).

6.2 Understanding effector gene regulation in *M. oryzae*

To gain further knowledge of transcriptional control of effector gene expression, in this study, we investigated effector gene regulation in *M. oryzae*. Previous studies have connected effector gene regulation in *M. oryzae* with various TFs, epigenetic modifications, MAPK, and G-protein signalling pathways (Xu *et al.*, 1998, Mehrabi *et al.*, 2008, Li *et al.*, 2016, Sakulkoo *et al.*, 2018, Osés-Ruiz *et al.*, 2021, Cao *et al.*, 2022, Tang *et al.*, 2023, Lambou *et al.*, 2024, Wang *et al.*, 2024). The previously identified TFs include the penetration and virulence regulator Mst12, which acts downstream of the Pmk1 MAPK signalling pathway (Park *et al.*, 2002, Osés-Ruiz *et al.*, 2021); the cell wall integrity regulators Mig1 and Git1, which act downstream of

the Mps1 kinase cascade (Xu *et al.*, 1998, Mehrabi *et al.*, 2008, Li *et al.*, 2016); the penetration and virulence regulators Eitf1 (Zn_2Cys_6) and Eitf2 (bZIP) (Cao *et al.*, 2022); and the newly described appressorium and penetration regulator Bip1 (Lambou *et al.*, 2024). G-protein signalling also regulates effector gene expression acting via the cAMP-dependent protein kinase A (PKA) pathway (Zhang *et al.*, 2011a) or through repression of transcription by the G-protein regulator Rgs1 (Tang *et al.*, 2023). Meanwhile, epigenetic modifications enhance virulence gene transcription through histone and heterochromatin modification (Wu *et al.*, 2021, Zhang *et al.*, 2021). These examples highlight regulatory redundancy with many pathways controlling effector gene expression in *M. oryzae*. They also pinpoint some key knowledge gaps, such as the molecular interplay between these regulation strategies (Wang *et al.*, 2024). In this context, we employed two complementary approaches to investigate these regulatory networks: a forward genetic screen to identify novel regulatory components, and a reverse genetic approach to further characterise known regulatory pathways.

6.3 Investigating effector gene regulation in *M. oryzae* using genetic screens and mutagenesis

Most *M. oryzae* effector genes are not expressed prior to host penetration and are highly expressed when the pathogen grows inside the plant (Mosquera *et al.*, 2009). High-throughput transcriptomic analysis of *M. oryzae* has demonstrated coordinated gene expression during blast infection, with most effector genes expressed between 24h and 48h during invasive growth (Yan *et al.*, 2023). Therefore, to further investigate the temporal dynamics of effector gene expression, we conducted a series of forward genetic screens aimed at identifying regulators of effector genes in *M. oryzae,* as explained in Chapter 3.

For this screen, we selected *MEP3*, which encodes a conserved, MAX-fold predicted cytoplasmic effector, fused the promoter and coding region of the gene to GFP, carried out UV mutagenesis, and screened for Constitutive Effector Regulators (*CER*) mutants. By selecting mutants that constitutively express *MEP3-GFP*, we

hypothesised that they may carry a mutation in a regulatory gene, resulting in constitutive effector gene expression. The G-protein regulator Rgs1, for example, was previously identified to repress late-expression effectors in *M. oryzae* through a similar screen (Tang *et al.*, 2023). After extensive screening, three *CER* mutants showing constitutive expression of *MEP3-GFP* were identified and named *CER1000*, *CER1001,* and *CER1002*. Their *MEP3-GFP* expression was confirmed through microscopy and q-RT-PCR analysis before they were sent for Illumina WGS.

An alternative forward genetic screen was also designed and tested to optimise microscopy screening time. This new screen fused effector promoters to the hygromycin B phosphotransferase gene (*Hph*), to test the hypothesis that constitutive effector-gene-expressing mutants could be selected based on hygromycin B antibiotic resistance. However, candidate mutants, which grew on selection medium, did not show constitutive expression of the *Hph* gene. This result suggested that these mutants were evading antibiotic toxicity through a different mechanism rather than constitutive expression of the *Hph* resistance gene. Looking at previous reports, we found many examples where fungi have acquired tolerance to hygromycin B, including modifications in plasma membrane proton-pumping ATPase (Goossens *et al.*, 2000), malfunctioning lysosomal trafficking (Banuelos *et al.*, 2010), and different genomic rearrangements (Ong *et al.*, 2021). Therefore, we concluded that employing randomised and high mutagenesis methods, such as UV mutagenesis (Winston, 2008) combined with *Hph* gene fusions, was not a viable strategy for conducting forward genetic screens in *M. oryzae*. However, to overcome this limitation, we have proposed an alternative strategy using the *Bar* gene-GFP fusion to perform a dual screening process. In various studies, these constructs have been shown to be functional for both antibiotic resistance properties and fluorescent markers (Bennett *et al.*, 1998, Wong *et al.*, 2011, Konishi *et al.*, 2012). By using a stronger selectable antibiotic resistance gene (Ontiveros-Cisneros *et al.*, 2022, Ahmed *et al.*, 2024) fused to GFP, we could initially pre-screen candidate mutants on selection medium and then confirm gene expression visually with GFP fluorescence.

6.4 Fungal genomic plasticity complicates the characterisation of *CER* mutants

In Chapter 4, continuing the characterisation of constitutively *MEP3-GFP* expressing mutants, *CER1000*, *CER1001*, and *CER1002*, we performed variant calling of their sequenced genomes. This allowed identification of putative effector regulators that possessed a mutation near or within their coding region. For *CER1001* and *CER1002,* SNPs were identified within the *RGS1* gene, which were predicted to generate a truncated Rgs1 protein in *CER1001*, while in *CER1002*, a missense mutation changed a positively charged arginine to an uncharged glutamine in the protein sequence. Through genetic complementation experiments, we found that *RGS1* repressed *MEP3* gene expression in *M. oryzae* conidia. This result, and a reduction in virulence observed for *CER1001* and *CER1002* mutants in leaf drop assays, validated previous findings that implicated Rgs1 in control of effector gene expression (Tang *et al.*, 2023) and fungal pathogenicity (Zhang *et al.*, 2011a).

For the *CER1000* mutant, 11 different putative effector regulators were identified through WGS and variant calling. These included *MGG_05308* and *MGG_10001,* previously linked to pathogenicity (Jeon *et al.*, 2007), *MGG_06465*, a putative epigenetic regulator homologous to yeast *PDS5* (Goto *et al.*, 2017), and *MGG_04204,* the G-protein G_{α} subunit MagA (Liu *et al.*, 2007). However, genetic complementation experiments could not unambiguously confirm any of these putative regulator candidates. Further complicating the characterisation of these *CER* mutants, RNA-Seq analysis failed to detect initial *MEP3* transcript observations from the mutant screen, contradicting the visualisation of *MEP3-GFP* expression. We then confirmed sample identity by identifying initially detected SNPs, including *RGS1*, *PDS5*, and *MagA* mutations. However, through this analysis, we also discovered new mutations for each *CER* mutant. We hypothesised that these secondary mutations might compensate for the original effector gene misregulation. Examples of regulatory buffering are not uncommon in filamentous fungi, such as different RGS proteins balancing cAMP levels when *RGS1* is mutated in *M. oryzae*

(Zhang *et al.*, 2011a) or the MAPK Mgv1 compensating for MAPK Gpmk1 in maintaining cell wall integrity in *F. graminearum* (Ren *et al.*, 2019). Furthermore, in the context of AMR, fungal genomes exhibit high regulatory plasticity, demonstrating genetic alterations as survival strategies (Fisher *et al.*, 2012, Lee *et al.*, 2023). Given these complications, we decided not to continue with the characterisation of these *CER* mutants. However, the finding of different *RGS1* mutations leading to effector gene repression in *CER1001* and *CER1002*, plus the new putative effector regulator candidates found for *CER1000*, could be further explored in the context of effector gene regulation in *M. oryzae*.

6.5 Hierarchical transcriptional control of blast infection: the role of Bip1 in *M. oryzae*

Although the forward genetic screens reported here presented limitations in studying effector gene regulation, they did provide further evidence for the role of Rgs1 as a repressor of effector gene expression in *M. oryzae* (Tang *et al.*, 2023). Rgs1 contributes to full virulence in pathogenic fungi, affecting vegetative growth, vesicle fusion, and autophagy (Zhang *et al.*, 2011a, Yuan *et al.*, 2022). Furthermore, in *M. oryzae*, it has been shown to regulate appressorium formation via cAMP modulation (Zhang *et al.*, 2011a). Therefore, this finding further supports the connection between the regulation of infection-related morphological development and transcriptional control of effector-encoding genes. Based on this conclusion, in Chapter 5, we decided to take a reverse genetic approach to investigate this correlation in more detail.

By focusing on TFs that contribute to infection-related development, we decided to explore those that may act on appressorium formation and host penetration in *M. oryzae*. We focused on **B**-ZIP **I**nvolved in **P**athogenesis-**1**, Bip1, a recently reported TF in *M. oryzae*. This TF was of interest because *BIP1* deletion mutants are non-pathogenic, exhibit host penetration deficiency, and are also linked to regulating a number of effectors identified through microarray analysis (Lambou *et al.*, 2024).

Through analysis of published global transcriptomic profiles, we discovered that many reported Bip1-dependent genes were also found in RNA-Seq datasets that investigated control of gene expression by Pmk1 and Mst12 (Osés-Ruiz *et al.*, 2021), suggesting a link between these regulators and Bip1. Additionally, looking at these same datasets, we found that *BIP1* expression was down-regulated during appressorium development in both *Δpmk1* and *Δmst12* mutants, suggesting transcriptional regulation of Bip1 required both of these upstream regulators. Upon further investigation, I found that Bip1 possesses a phosphorylation site that may be Pmk1-dependent at later stages of appressorium development (Cruz-Mireles *et al.*, 2024), and an Mst12 DNA-binding motif within the *BIP1* promoter (Osés-Ruiz *et al.*, 2021). *In silico* prediction of the Mst12-*BIP1* promoter showed the interaction to occur through the second C_2H_2 zinc finger domain of Mst12. For Mst12 homologues in *Botrytis cinerea* and *Colletotrichum lindemuthianum*, splice variants lacking a second C_2H_2 zinc finger domain have been reported to inhibit pathogenicity (Hoi *et al.*, 2007, Schamber *et al.*, 2010). Therefore, the predicted interaction between Mst12 and the *BIP1* promoter through this pathogenicity-related domain is consistent with previous reports. Moreover, conservation analysis of these TFs suggested a correlation between Bip1 (which is widely conserved among pathogenic fungi) and better conservation of Mst12 C_2H_2 zinc finger domains, further supporting the predicted interactions.

Through Y2H, we confirmed that Bip1 can form homodimers, consistent with the typical topology of bZIP TFs (McLachlan & Stewart, 1975), and that it can also physically interact with Mst12, suggesting that heterodimer formation is also possible. It has been previously found that Ste12 proteins form complexes with TFs to regulate differentiated processes. For instance, binding with Tec1 regulates filamentation (Bao *et al.*, 2004), wherease binding with Mcm1 regulates pheromone responses (Mueller & Nordheim, 1991, Dohlman & Thorner, 2001). Consequently, formation of the Mst12-Bip1 complex is possible and may entail a regulatory mechanism that is specific and distinct from their individual regulation. An example of this molecular interplay is seen for the master regulator of white-opaque switching in *Candida albicans*, Wor1, known to interact with TFs that inhibit or

enhance its activity through positive feedback loops, showcasing unique outcomes from differentiated TF complexes (Hernday *et al.*, 2013).

To gain further insight into the role of Bip1, we investigated appressorium cytoskeleton organisation. In *Δmst12* mutants, there is mislocalisation of septins, actin, and the Chm1 septin kinase, indicating that Mst12 is essential for their proper organisation (Gupta *et al.*, 2015, Osés-Ruiz *et al.*, 2021). There is also mislocalisation of septin 3 and septin 5 in Δ*bip1* mutants, while actin and Chm1 kinase showed wild-type organisation. This result is consistent with Bip1 acting downstream of Mst12 and demonstrates that Bip1 is also necessary for septin organisation in the appressorium of *M. oryzae*. Additionally, we generated a *M. oryzae* strain overexpressing *BIP1*. This revealed that constitutive expression of *BIP1* affects pathogenicity and appressorium morphogenesis. We saw that appressoria dysmorphia was enhanced if *BIP1* is overexpressed in an *Δmst12* background. Taken together, these findings provide further evidence that Bip1 functions downstream of the Pmk1 MAPK/Mst12 signalling pathway and that its timely expression is fundamental for infection-related development and infection by the blast fungus.

We then performed a transcriptomic analysis of Bip1 and Mst12 during appressorium development (0h, 4h, and 24h). This experiment confirmed that both regulators exhibit very similar transcriptional signatures, suggesting they are part of the same signalling pathway that commonly regulates a subset of genes. Among these, we identified a family of fasciclin glycoproteins (Flp1, Flp2, and Flp3) involved in cell adhesion and a network of TFs involved in appressorium development, conidial germination, and stress responses, which had been previously reported to be Pmk1 MAPK and Mst12-dependent (Johnson *et al.*, 2003, Seifert, 2018, Osés-Ruiz *et al.*, 2021). Furthermore, we identified 80 commonly regulated effectors with diverse expression patterns and structural conservation, including the Pmk1-regulated effector BAS3 (Sakulkoo *et al.*, 2018). However, RNA-Seq analysis suggested that each TF also possesses individualised patterns of genetic regulation,

including exclusively regulated effector genes. This result suggests that Bip1 and Mst12 may operate independently, collaboratively, or through the formation of complexes, as illustrated in Figure 6.1. These findings establish Bip1 to act downstream of the Pmk1 MAPK/Mst12 signalling pathway and highlights that both Mst12 and Bip1 are components of a hierarchical TF network deployed by *M. oryzae* to coordinate blast infection.

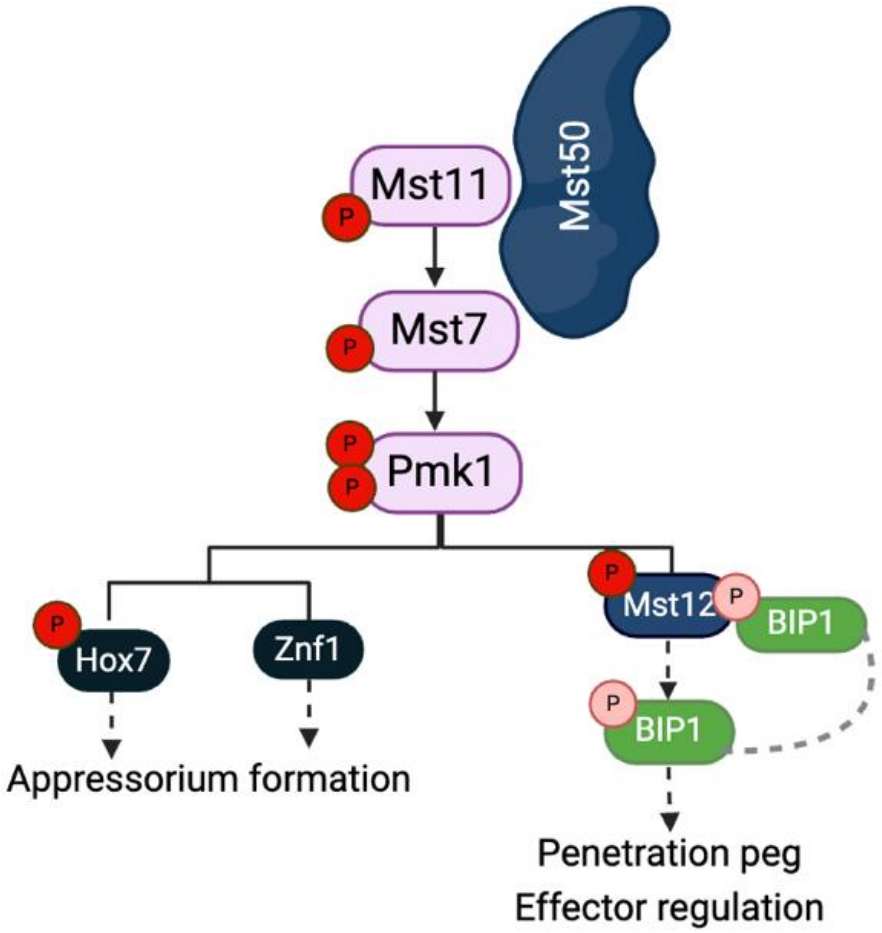

Figure 6.1. New model of the Pmk1 MAPK/Mst12 signalling pathway featuring the Bip1 regulator. Schematic representation of the Pmk1 MAPK cascade. Phosphorelay of Mst11, Mst7, and Pmk1, is scaffolded by Mst50. Downstream, Pmk1 regulates appressorium formation through phosphorylation of Hox7 and through the Znf1 TF, and it also controls penetration peg formation and effector regulation via Mst12 phosphorylation. Bip1 acts downstream of Mst12, has a putative Pmk1-dependant phosphorylation site, and can form a complex with Mst12 to regulate host penetration, disease progression, and effector-encoding genes (Adapted from Wilson & Talbot, 2009). (Image created using Biorender.com)

6.6 Relationship between Rgs1, Mst12, and Bip1 regulated effectors

To further understand crosstalk between *M. oryzae* signalling pathways that govern effector gene regulation, we decided to compare Rgs1 repressed effector genes with those found among Mst12 and Bip1 datasets. Through RNA-Seq analysis of the *RGS1* deletion mutant, it was found that 60 late-expression effector genes were repressed by this transcriptional regulator in *M. oryzae* conidia (Tang *et al.*, 2023). Though RGS proteins are known to regulate gene expression indirectly via cAMP signalling (Zhang *et al.*, 2011a), the yeast Rgs1 homologue, Sst2, contains a proteolytic cleave site that forms two distinct proteins with different functions (Hoffman *et al.*, 2000). Endoproteolytic cleavage has also been reported for *M. oryzae* Rgs1 (Liu *et al.*, 2007), raising the possibility that it can carry out direct gene regulation. However, the precise mechanisms governing the role of Rgs1 in regulating effector genes requires further investigation.

In this context, previous research has demonstrated crosstalk between the cAMP-dependent pathway, which is regulated by Rgs1, and the Pmk1 MAPK cascade (Park *et al.*, 2006, Wilson & Talbot, 2009). This cross-talk is thought to occur through the protein complex Mst11-Mst7-Mst50, which activates Pmk1 MAPK, integrating signalling from the G-protein coupled receptor Pth11 (DeZwaan *et al.*, 1999) and the G-protein subunit Mgb1 (Nishimura *et al.*, 2003). Therefore, to gain further insight, we compared 60 effector-encoding genes repressed by Rgs1 with the Mst12, Bip1, and Mst12-Bip1 regulated effector genes found in this study.

This analysis revealed some overlap in the regulation of effector-encoding genes across datasets, as illustrated in Figure 6.2. A total of 2 effector-encoding genes were identified to be repressed by Rgs1 and potentially activated (up-regulated) by Mst12 and Bip1. These include the Pmk1-regulated effector BAS3 (Sakulkoo *et al.*, 2018) and a predicted methylesterase inhibitor (*MGG_03585*), which are two structurally distinct effectors that exhibit peaks in expression at 48h and 96h of rice blast infection, as shown in Figure 6.3. Additionally, we identified 14 effector-encoding genes repressed by Rgs1 which are Bip1-dependent—potentially activated by Bip1.

These were also structurally distinct and are late expression effectors peaking at 48h and 96h of *M. oryzae* infection (as illustrated in Figure 6.4.A), including apoplastic effector BAS113 (*MGG_05785*) (Giraldo *et al.*, 2013). The last subset of commonly regulated effectors were 14 effectors repressed by Rgs1 and Mst12 (down-regulated). This group of effector genes present an earlier expression pattern peaking *in planta* between 16h and 24h of infection, as shown in Figure 6.4.B. Again, these effectors were not structurally conserved but included biotrophy-associated effectors BAS3b (*MGG_16382*), BAS4 (*MGG_02154*), BAS5 (*MGG_02154*), and BAS162b (*MGG_16026*). These observations may provide evidence that Rgs1 and Mst12 act as transcriptional repressors of a subset of early expression-biotrophy-related effectors, while Bip1 and Mst12-Bip1 act as transcriptional activators of later expression effectors in *M. oryzae*. This further supports the idea of effector genes being regulated by orchestration of signalling pathways and a network of coordinated TFs during rice blast infection. Further studies should examine the potential molecular interactions among these regulators and establish whether their shared regulation occurs directly or indirectly.

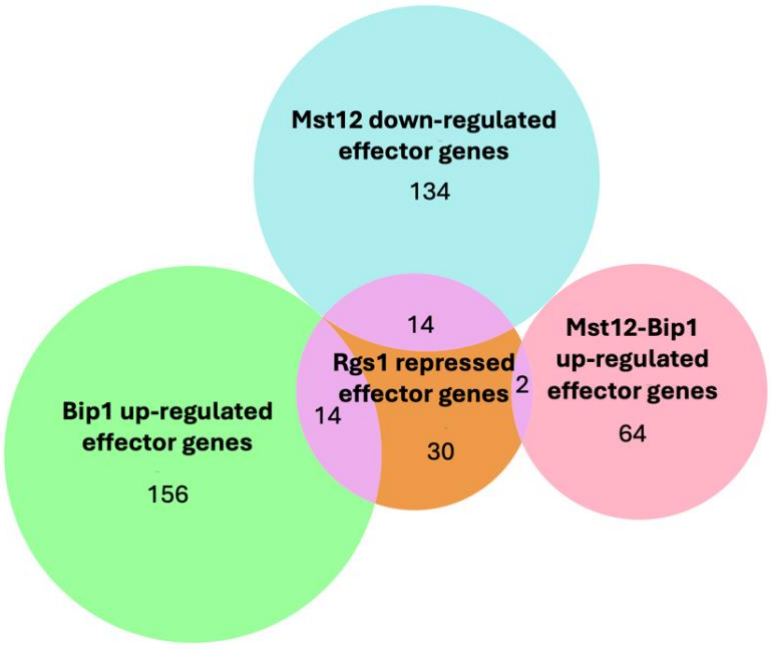

Figure 6.2. Overlap in Rgs1, Bip1 and Mst12 regulated effector-encoding genes. Euler diagrams show the overlap between 60 Rgs1 repressed effectors (orange), 66 Mst12-Bip1 up-regulated effectors (pink), 156 Bip1 up-regulated effectors (green) and 148 Mst12 down-regulated effectors (blue). Overlap is shown in violet.

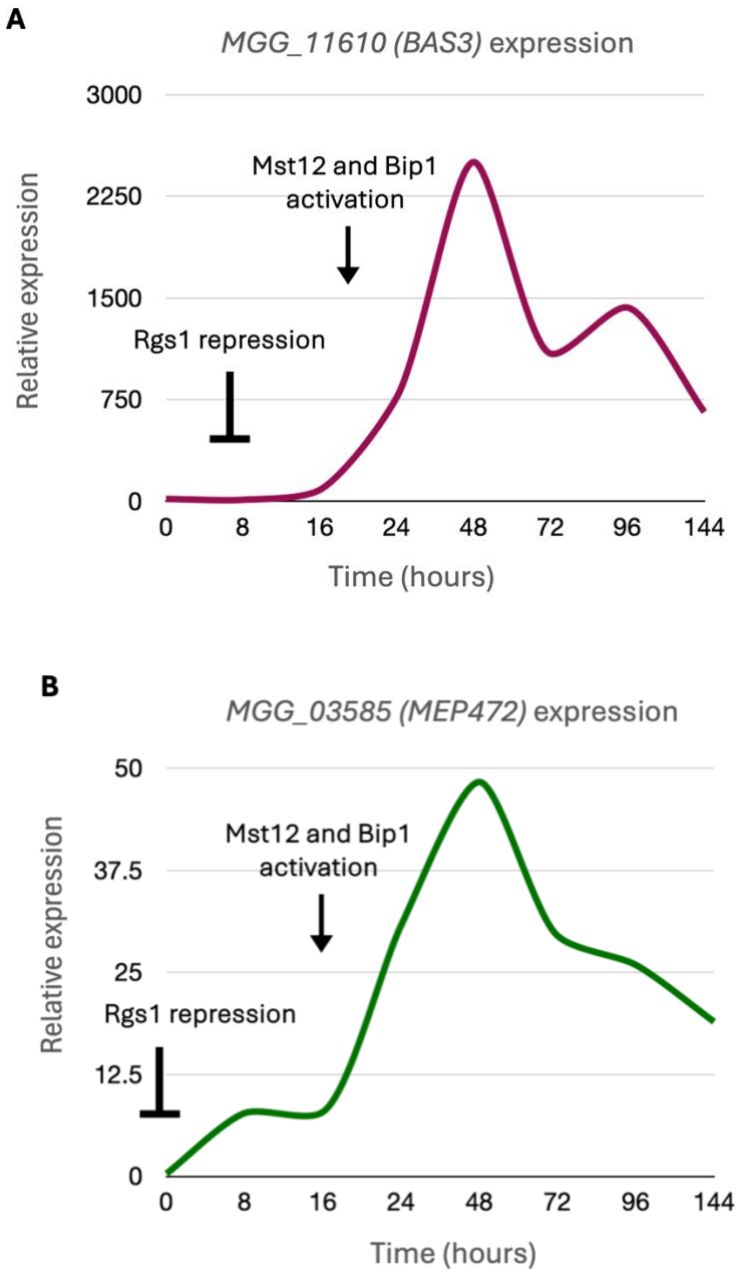

Figure 6.3. Gene expression of two effector-encoding genes regulated by Rgs1, Mst12, and Bip1. Data from a time-course RNA-Seq experiment of infection-related development and plant infection (Yan *et al.*, 2023) was used to extract the expression profile for *MGG_11610 (BAS3)* in panel A, and *MGG_03585 (MEP472)* in panel B. Relative gene expression mean values were calculated from three independent replicates extracted for eight different time-points (0h, 8h, 16h, 24h, 48h, 72h, 96h, and 144h) during rice blast infection. Rgs1 potentially represses these two effectors at earlier stages of infection, and then later on Mst12 and Bip1 may be responsible for their expression peaking at 48h and 96h of *M. oryzae* infection.

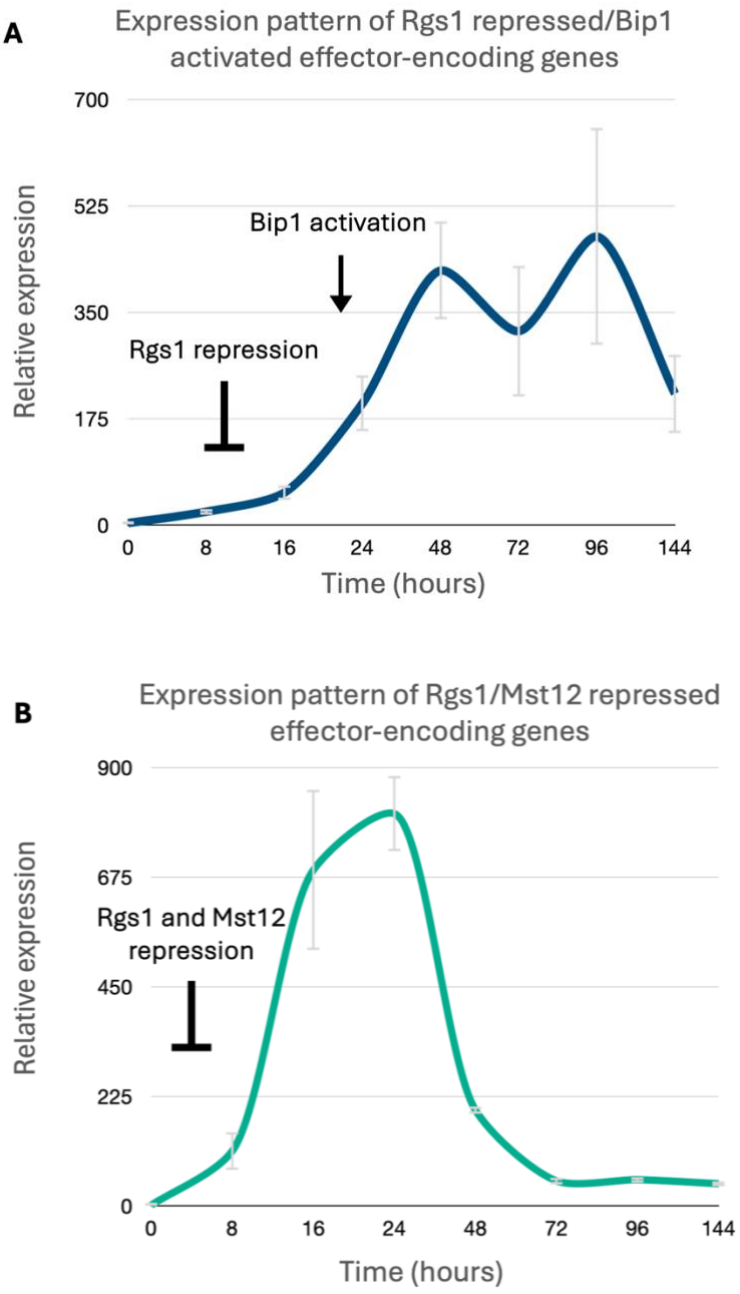

Figure 6.4. Expression pattern of effector-encoding genes during *M. oryzae* infection. Data from a time-course RNA-Seq experiment of infection-related development and plant infection (Yan *et al.*, 2023) was used to extract the expression profile for a subset of Rgs1 repressed/Bip1 activated effector-encoding genes in panel A, which peak at 48h and 96h of infection and a subset of Rgs1- Mst12 repressed effector-encoding genes in panel B, which peak between 16h and 24h of *M. oryzae* infection. Relative gene expression mean values were calculated from three independent replicates extracted for eight different time-points (0h, 8h, 16h, 24h, 48h, 72h, 96h, and 144h) during rice blast infection.

6.7 Concluding remarks and future directions

The overall aim of this study was to expand our understanding of how effector genes are regulated in *M. oryzae*. Through forward genetic screens, we were able to confirm the role of Rgs1 as a transcriptional repressor of effector-encoding genes in *M. oryzae* and gain further insight into the genomic regions responsible for this regulatory function. Furthermore, we learned that genetic screens to select effector regulators are challenging in fungal systems due to genomic plasticity and regulatory redundancy (Fisher *et al.*, 2012, Gladieux *et al.*, 2018). Through a reverse genetic approach, we then identified Bip1 as a component of the Pmk1 MAPK/Mst12 signalling pathway regulating host penetration, TFs that are important for infection-related development and effector-encoding genes. Bip1 is potentially regulated by Pmk1 MAPK transcriptionally and/or through direct or indirect phosphorylation and regulated by Mst12 transcriptionally via binding to the Mst12 DNA binding motif found in the *BIP1* promoter and/or through the formation of a protein complex. These results provide evidence of a sophisticated TF hierarchy deployed by *M. oryzae* to co-ordinately onset blast disease. Furthermore, these findings highlight the complex transcriptional control that drives infection and regulates effector genes of the blast fungus and raises many questions that need further investigation. For example, how does Rgs1 repress late-expression effectors? Is this regulation indirect or through direct DNA binding? Are there any molecular connections between Rgs1, Mst12, and Bip1? Can Mst12 bind to the promoter of *BIP1,* and is this interaction required for *BIP1* expression, as suggested by structural modelling? Is Bip1 phosphorylation required for host penetration and effector gene expression? Is Bip1 phosphorylated by the Pmk1 MAPK? Do Mst12 and Bip1 interact with each other during appressorium development? Does the putative Mst12-Bip1 interaction regulate a different subset of genes as suggested by RNA-seq analysis, or is it part of a negative feedback loop to fine-tune *BIP1* expression? What offsets this form of gene regulation? What are the external and internal cues? Is this regulation conserved across pathogenic fungi? Addressing these fundamental questions will enhance our understanding of the orchestration of effector gene expression that facilitates rice blast disease.

Appendix

Table 1. List of *Magnaporthe oryzae* strains used in this study.

Strain	Genotype	Source
Guy11	Wild type	Laboratory stock
ToxA-GFP	Wild-type strain Guy11 transformed with *ToxA-GFP* (Hygromycin B resistance)	Laboratory stock
Δpmk1	*PMK1* null mutant (Hygromycin B resistance)	Laboratory stock
Δrgs1	*RGS1* null mutant (Hygromycin B resistance)	Laboratory stock
Δmst12	*MST12* null mutant (Hygromycin B resistance)	Laboratory stock
Δbip1	*BIP1* null mutant (BAR resistance)	This study
ΔSep4	*SEP4* null mutant (Hygromycin B resistance)	Laboratory stock
MEP1-GFP	Wild-type strain Guy11 transformed with *MEP1-GFP* (SUR resistance)	Laboratory stock
MEP3-GFP	Wild-type strain Guy11 transformed with *MEP3-GFP* (SUR resistance)	Laboratory stock
MEP3p-HPH	Wild-type strain Guy11 transformed with *MEP3p-HPH* (SUR resistance)	This study
CER7	Guy11 background UV Constitutive Effector Regulator mutant 7	Laboratory stock
CER100	Guy11 background UV Constitutive Effector Regulator mutant 100	This study
CER101	Guy11 background UV Constitutive Effector Regulator mutant 101	This study
CER102	Guy11 background UV Constitutive Effector Regulator mutant 102	This study
CER103	Guy11 background UV Constitutive Effector Regulator mutant 103	This study
CER104	Guy11 background UV Constitutive Effector Regulator mutant 104	This study
CER105	Guy11 background UV Constitutive Effector Regulator mutant 105	This study

CER106	Guy11 background UV Constitutive Effector Regulator mutant 106	This study
CER107	Guy11 background UV Constitutive Effector Regulator mutant 107	This study
CER108	Guy11 background UV Constitutive Effector Regulator mutant 108	This study
CER109	Guy11 background UV Constitutive Effector Regulator mutant 109	This study
CER110	Guy11 background UV Constitutive Effector Regulator mutant 110	This study
CER111	Guy11 background UV Constitutive Effector Regulator mutant 111	This study
CER112	Guy11 background UV Constitutive Effector Regulator mutant 112	This study
TrpC:BAR-GFP	Wild-type strain Guy11 transformed with *TrpC:BAR-GFP*	This study
CER1000	Guy11 background UV Constitutive Effector Regulator mutant 1000	This study
CER1001	Guy11 background UV Constitutive Effector Regulator mutant 1001	This study
CER1002	Guy11 background UV Constitutive Effector Regulator mutant 1002	This study
CER1001-RGS1	*CER1001* transformed with native *RGS1* (BAR resistance)	This study
CER1002-RGS1	*CER1002* transformed with native *RGS1* (BAR resistance)	This study
CER1000-MGG_06465	*CER1000* transformed with native *MGG_06465* (BAR resistance)	This study
CER1000-MGG_06053	*CER1000* transformed with native *MGG_06053* (BAR resistance)	This study
CER1000-MGG_04204	*CER1000* transformed with native *MGG_04204* (BAR resistance)	This study
CER1000-MGG_10299	*CER1000* transformed with native *MGG_10299* (BAR resistance)	This study

CER1000-MGG_05308	*CER1000* transformed with native *MGG_05308* (BAR resistance)	This study
CER1000-MGG_09444	*CER1000* transformed with native *MGG_09444* (BAR resistance)	This study
CER1000-MGG_00690	*CER1000* transformed with native *MGG_00690* (BAR resistance)	This study
CER1000-MGG_15057	*CER1000* transformed with native *MGG_15057* (BAR resistance)	This study
CER1000-MGG_07497	*CER1000* transformed with native *MGG_07497* (BAR resistance)	This study
Lifeact-mCherry	Wild-type strain Guy11 transformed with *Lifeact-mCherry* (SUR resistance)	Laboratory stock
Chm1-GFP	Wild-type strain Guy11 transformed with *Chm1-GFP* (SUR resistance)	Laboratory stock
Sep3-GFP	Wild-type strain Guy11 transformed with *Sep3-GFP* (SUR resistance)	Laboratory stock
Sep5-GFP	Wild-type strain Guy11 transformed with *Sep5-GFP* (SUR resistance)	Laboratory stock
Δbip1:Lifeact-mCherry	*Δbip1* strain transformed with *Lifeact-mCherry* (SUR and BAR resistance)	This study
Δbip1:Chm1-GFP	*Δbip1* strain transformed with *Chm1-GFP* (SUR and BAR resistance)	This study
Δbip1:Sep3-GFP	*Δbip1* strain transformed with *Sep3-GFP* (SUR and BAR resistance)	This study
Δbip1:Sep5-GFP	*Δbip1* strain transformed with *Sep5-GFP* (SUR and BAR resistance)	This study
TrpCp:BIP1-GFP	*Δbip1* strain transformed with *TrpCp:BIP1-GFP* (BAR resistance)	This study
Δmst12:TrpCp:BIP1-GFP	*Δmst12* strain transformed with *TrpCp:BIP1-GFP* (Hygromycin B and BAR resistance)	This study

Table 2. List of plasmids used in this study.

Gene ID	Gene Name	Plasmid name	Assay	Source
MGG_17249	*MEP3*	MEP3-GFP pscSUR	GFP localisation and UV mutagenesis	Laboratory stock
MGG_16353	*MEP1*	MEP1-GFP pscSUR	GFP localisation	Laboratory stock
	ToxAp	ToxAp-GFP pscSUR	GFP localisation	Laboratory stock
MGG_17249	*MEP3p*	MEP3p-HPH pscSUR	UV mutagenesis	This study
	TrpCp -BAR	TrpCp-BAR-GFP pscBAR	GFP localisation and UV mutagenesis	This study
MGG_06465	PDS5 (yeast)	MGG_06465 pscBAR	Genetic complementation	This study
MGG_06053		MGG_06053 pscBAR	Genetic complementation	This study
MGG_04204	*MagA*	MGG_04204 pscBAR	Genetic complementation	This study
MGG_10299		MGG_10299 pscBAR	Genetic complementation	This study
MGG_05308		MGG_05308 pscBAR	Genetic complementation	This study
MGG_09444		MGG_09444 pscBAR	Genetic complementation	This study
MGG_00690		MGG_00690 pscBAR	Genetic complementation	This study
MGG_15057		MGG_15057 pscBAR	Genetic complementation	This study
MGG_07497		MGG_07497 pscBAR	Genetic complementation	This study
MGG_14517	*RGS1*	RGS1 pscBAR	Genetic complementation	This study

MGG_08118	*Δbip1*	BIP1_KO pscBAR	Plasmid for the generation of *Δbip1*	This study
	Yeast ABP140	Lifeact-mCherry pscSUR	mCherry localisation	Laboratory stock
MGG_06320	*CHM1*	Chm1-GFP pscSUR	GFP localisation	Laboratory stock
MGG_01521	*SEP3*	Sep3-GFP pscSUR	GFP localisation	Laboratory stock
MGG_03087	*SEP5*	Sep5-GFP pscSUR	GFP localisation	Laboratory stock
MGG_08118	*BIP1*	TrpCp:BIP1:GFP pscBAR	GFP localisation, phenotypic examination and RNA-Seq	Laboratory stock
MGG_09565	*PMK1*	Pmk1 bait	Y2H	Laboratory stock
MGG_12958	*MST12*	MST12 bait	Y2H	Laboratory stock
MGG_12865	*HOX7*	HOX7 bait	Y2H	Laboratory stock
MGG_08118	*BIP1*	BIP1 bait	Y2H	This study
MGG_08118	*BIP1*	BIP1 prey	Y2H	This study
	Y2H prey	T-pGADT7	Y2H	Laboratory stock
	Y2H bait	53-pGBKT7	Y2H	Laboratory stock
	Y2H bait	Lam-pGBKT7	Y2H	Laboratory stock

Table 3. List of oligonucleotide primers used in this study.

Oligonucleotide	Sequence (5' to 3')
Tubulin_ QPCR_F	CGACAACGAGGCTATTTACGATATTT
Tubulin_ QPCR _R	GGAGTAGGCGACCAGAGGGAAGT
GFP_F	ATGGTGAGCAAGGGCGAGGA
GFP_R	CTTGTACAGCTCGTCCATGCC
Mep3_ QPCR _F	TTGTGGAGAATTGGGGTGGT
Mep3_QPCR_R	CATCCCCTTTAGTTGCGTCG
GFP_QPCR _F	CACATGAAGCAGCACGACTT
GFP_QPCR _R	TCCTTGAAGTCGATGCCCTT
HPH_QPCR _F	ATGTGTATCACTGGCAAACTGT
HPH_QPCR _R	GGAATCCCCGAACATCGC
TrpcP_pscF	TGCAGCCCAATGTGGAATTCGATATTGAAGGAGCATTTTTGGG
TrpcT_psc_R	TCGACGGTATCGATAAGCTTAGTGGAGATGTGGAGTGGGCGC
Mep3p_psc_F	TGCAGCCCAATGTGGAATTCGTGTTCCAGATCTTGTCAGTGCC
Mep3p_Hph_R	CGGTGAGTTCAGGCTTTTTCATACCATAATGCCGATGATTTAA
HPH_psc_R	TCGACGGTATCGATAAGCTTCTATTCCTTTGCCCTCGGACGA
HPH_F	ATGAAAAAGCCTGAACTCACCG
HPH_F	TCGACGGTATCGATAAGCTTC
Mep3p_GFP_R	CTCCTCCGCCCTTGCTCACCATAATGCCGATGATTTAA
Bar_TrpC_F	TACCCAAGCATCCAAATGAGCCCAGAACGACGC
Bar_eGFP_R	GCCCTTGCTCACCACTAAATCTCGGTGACGGGCAG
Rgs1p_psc_F	TGCAGCCCAATGTGGAATTCTGGTAAAGGAATAGAGGGGA
Rgs1_GFP_R	TCGCCCTTGCTCACCATTCATAACCGTTGCGAGCGGC
MGG_06465_psc_F	TGCAGCCCAATGTGGAATTCGGCATGCCTCGCTGTCCCGGAT
MGG_06465_psc_R	TCGACGGTATCGATAAGCTTTAGATGACGAGCTTGTAGCCCTT
MGG_00690_psc_F	TGCAGCCCAATGTGGAATTCATGCCATTCGCGCTGGTGAC
MGG_00690_psc_R	TCGACGGTATCGATAAGCTTGCAATGTTGTGGGCCTGCTA
MGG_04204_psc_F	TGCAGCCCAATGTGGAATTCTAGTTTTTTTTTTCTCCCT
MGG_04204_psc_R	GTACCCGGGGATCCTCTAGACCCGAACGTCGAATAAAGTC
MGG_05308_psc_F	TGCAGCCCAATGTGGAATTCCGAGGAGGAGGACAAGAGCA
MGG_05308_psc_R	TCGACGGTATCGATAAGCTTGTGTCCCGCGTTCGCCTCAAGG
MGG_06053_psc_F	TGCAGCCCAATGTGGAATTCTTCCGTATCCGACCACCAGC

MGG_06053_psc_R	TCGACGGTATCGATAAGCTTTGGGAAACTCGTTGTAGAAA
MGG_07497_psc_F	TGCAGCCCAATGTGGAATTCATGGTCATTTCCTCGCAAGCATC
MGG_07497_psc_R	TCGACGGTATCGATAAGCTTCCGTAGTTGGGCCCTCGCTATA
MGG_09444_psc_F	TGCAGCCCAATGTGGAATTCGCCTCACGTGCTTAGTCTTCAG
MGG_09444_psc_R	TCGACGGTATCGATAAGCTTAATCGACGTATTCCTGGTTCGT
MGG_10299_psc_F	TGCAGCCCAATGTGGAATTCGCTAGACCAAGTTCGGGACG
MGG_10299_psc_R	TCGACGGTATCGATAAGCTTTTGCCGCGCCCGGACCAGCT
MGG_15057_psc_F	TGCAGCCCAATGTGGAATTCCGAGACACATCAATGTAGCTCGA
MGG_15057_psc_R	TCGACGGTATCGATAAGCTTTCAGGTCTACGTCGCGCCCAAGC
MGG_16064_psc_F	TGCAGCCCAATGTGGAATTCTGCTGGATACGGCGGTTTCA
MGG_16064_psc_R	TCGACGGTATCGATAAGCTTTTATGGAGAACCAAGAACCA
BIP1_bait_F	CATGGAGGCCGAATTCATGGCAATGTATATGCCCTC
BIP1_bait_R	GCAGGTCGACGGATCCTCAGAGAGCCGGCGATTG
BIP1_prey_F	GGAGGCCAGTGAATTCATGGCAATGTATATGCCCTC
BIP1_prey_R	CGAGCTCGATGGATCCTCAGAGAGCCGGCGATTG
BIP1_TrpCp_F	TCTACCCAAGCATCCAAATGGCAATGTATATGCCCTCAAC
BIP1_GFP_R	CGCCCTTGCTCACCATGAGAGCCGGCGATTG
BIP1_LF_psc_F	TGCAGCCCAATGTGGAATTCTCTATGTAGGTCCGGGAAGAAGC
BIP1_BAR_R	CAATATCATCTTCTGTCGACCGGTTGGAGATGGTTATGATG
BIP1_RF_BAR_F	GTCACCGAGATTTAGAGGGTCATTTGGCTCCCCTCC
BIP1_RF_psc_R	TCGACGGTATCGATAAGCTTTGTTTTGTTTGCTGCACCGTTA
BAR_F	GTCGACAGAAGATGATATTGAAGGA
BAR_R	GTCGACCTAAATCTCGGTGA
BIP1_upstream_F	TGCATGTTTGTTTTGTACCGTGGTAA
BIP1_down_R	GTATCGACAAGGTGATTGGCCCTGCTG

References

Abramovitch, R. B., Anderson, J. C. and Martin, G. B. (2006) Bacterial elicitation and evasion of plant innate immunity. *Nature Reviews Molecular Cell Biology,* **7,** 601-611.

Abramson, J., Adler, J., Dunger, J., Evans, R., Green, T., Pritzel, A., *et al.* (2024) Accurate structure prediction of biomolecular interactions with AlphaFold 3. *Nature,* **630,** 493-500.

Ahmed, S., Hulbert, A. K., Xin, X. and Neff, M. M. (2024) The ability of Arabidopsis to recover from Basta and its application in isolating Cas9-free mutants. *Front Plant Sci,* **15,** 1408230.

Ahmed, Y. L., Gerke, J., Park, H.-S., Bayram, Ö., Neumann, P., Ni, M., *et al.* (2013) The velvet family of fungal regulators contains a DNA-binding domain structurally similar to NF-κB. *PLOS Biology,* **11,** e1001750.

Alexa, A. and Rahnenfuhrer, J. (2010) topGO: enrichment analysis for gene ontology. *R package version,* **2,** 2010.

Alfano, J. R., Charkowski, A. O., Deng, W.-L., Badel, J. L., Petnicki-Ocwieja, T., van Dijk, K. and Collmer, A. (2000) The *Pseudomonas syringae* Hrp pathogenicity island has a tripartite mosaic structure composed of a cluster of type III secretion genes bounded by exchangeable effector and conserved effector loci that contribute to parasitic fitness and pathogenicity in plants. *Proceedings of the National Academy of Sciences,* **97,** 4856-4861.

Annis, S. L. and Goodwin, P. H. (1997) Recent advances in the molecular genetics of plant cell wall-degrading enzymes produced by plant pathogenic fungi. *European Journal of Plant Pathology,* **103,** 1-14.

Banuelos, M. G., Moreno, D. E., Olson, D. K., Nguyen, Q., Ricarte, F., Aguilera-Sandoval, C. R. and Gharakhanian, E. (2010) Genomic analysis of severe hypersensitivity to hygromycin B reveals linkage to vacuolar defects and new vacuolar gene functions in Saccharomyces cerevisiae. *Curr Genet,* **56,** 121-137.

Bao, M. Z., Schwartz, M. A., Cantin, G. T., Yates, J. R., III and Madhani, H. D. (2004) Pheromone-Dependent Destruction of the Tec1 Transcription Factor Is Required for MAP Kinase Signaling Specificity in Yeast. *Cell,* **119,** 991-1000.

Bayram, Ö., Krappmann, S., Ni, M., Bok, J. W., Helmstaedt, K., Valerius, O., *et al.* (2008) VelB/VeA/LaeA Complex Coordinates Light Signal with Fungal Development and Secondary Metabolism. *Science,* **320,** 1504-1506.

Bebber, D. P. and Gurr, S. J. (2015) Crop-destroying fungal and oomycete pathogens challenge food security. *Fungal Genet Biol,* **74,** 62-64.

Bennett, R. P., Cox, C. A. and Hoeffler, J. P. (1998) Fusion of green fluorescent protein with the Zeocin-resistance marker allows visual screening and drug selection of transfected eukaryotic cells. *Biotechniques,* **24,** 478-482.

Birch, P. R. J., Rehmany, A. P., Pritchard, L., Kamoun, S. and Beynon, J. L. (2006) Trafficking arms: oomycete effectors enter host plant cells. *Trends in Microbiology,* **14,** 8-11.

Bird, A. F. (1983) Changes in the dimensions of the oesophageal glands in root-knot nematodes during the onset of parasitism. *International Journal for Parasitology,* **13,** 343-348.

Bird, D. and Bradshaw, R. (1997) Gene targeting is locus dependent in the filamentous fungus *Aspergillus nidulans*. *Molecular and General Genetics MGG,* **255,** 219-225.

Boch, J., Scholze, H., Schornack, S., Landgraf, A., Hahn, S., Kay, S.*, et al*. (2009) Breaking the Code of DNA Binding Specificity of TAL-Type III Effectors. *Science,* **326,** 1509-1512.

Bolger, A. M., Lohse, M. and Usadel, B. (2014) Trimmomatic: a flexible trimmer for Illumina sequence data. *Bioinformatics,* **30,** 2114-2120.

Bölker, M. (1998) Sex and Crime: Heterotrimeric G Proteins in Fungal Mating and Pathogenesis. *Fungal Genetics and Biology,* **25,** 143-156.

Bolton, M. D. and Thomma, B. P. (2008) The complexity of nitrogen metabolism and nitrogen-regulated gene expression in plant pathogenic fungi. *Physiological and Molecular Plant Pathology,* **72,** 104-110.

Bos, J. I., Armstrong, M. R., Gilroy, E. M., Boevink, P. C., Hein, I., Taylor, R. M.*, et al*. (2010) *Phytophthora infestans* effector AVR3a is essential for virulence and manipulates plant immunity by stabilizing host E3 ligase CMPG1. *Proceedings of the National Academy of Sciences,* **107,** 9909-9914.

Bourett, T. M. and Howard, R. J. (1990) In vitro development of penetration structures in the rice blast fungus *Magnaporthe grisea*. *Canadian Journal of Botany,* **68,** 329-342.

Bourett, T. M. and Howard, R. J. (1992) Actin in penetration pegs of the fungal rice blast pathogen, *Magnaporthe grisea*. *Protoplasma,* **168,** 20-26.

Bozkurt, T. O. and Kamoun, S. (2020) The plant-pathogen haustorial interface at a glance. *J Cell Sci,* **133**.

Bozkurt, T. O., Schornack, S., Win, J., Shindo, T., Ilyas, M., Oliva, R.*, et al*. (2011) *Phytophthora infestans* effector AVRblb2 prevents secretion of a plant immune protease at the haustorial interface. *Proceedings of the National Academy of Sciences,* **108,** 20832-20837.

Bray, N. L., Pimentel, H., Melsted, P. and Pachter, L. (2016) Near-optimal probabilistic RNA-seq quantification. *Nature Biotechnology,* **34,** 525-527.

Brenchley, R., Spannagl, M., Pfeifer, M., Barker, G. L. A., D'Amore, R., Allen, A. M.*, et al*. (2012) Analysis of the bread wheat genome using whole-genome shotgun sequencing. *Nature,* **491,** 705-710.

Brown, D. W., Busman, M. and Proctor, R. H. (2014) *Fusarium verticillioides* SGE1 Is Required for Full Virulence and Regulates Expression of Protein Effector and Secondary Metabolite Biosynthetic Genes. *Molecular Plant-Microbe Interactions®,* **27,** 809-823.

Buscaill, P. and van der Hoorn, R. A. L. (2021) Defeated by the nines: nine extracellular strategies to avoid microbe-associated molecular patterns recognition in plants. *The Plant Cell,* **33,** 2116-2130.

Cain, C. W., Lohse, M. B., Homann, O. R., Sil, A. and Johnson, A. D. (2012) A conserved transcriptional regulator governs fungal morphology in widely diverged species. *Genetics,* **190,** 511-521.

Camacho, C., Coulouris, G., Avagyan, V., Ma, N., Papadopoulos, J., Bealer, K. and Madden, T. L. (2009) BLAST+: architecture and applications. *BMC Bioinformatics,* **10,** 421.

Cao, H., Huang, P., Zhang, L., Shi, Y., Sun, D., Yan, Y., *et al*. (2016) Characterization of 47 Cys2 -His2 zinc finger proteins required for the development and pathogenicity of the rice blast fungus *Magnaporthe oryzae*. *New Phytol,* **211,** 1035-1051.

Cao, Y., Chen, J., Xie, X., Liu, S., Jiang, Y., Pei, M., *et al*. (2022) Characterization of two infection-induced transcription factors of *Magnaporthe oryzae* reveals their roles in regulating early infection and effector expression. *Mol Plant Pathol,* **23,** 1200-1213.

Carolus, H., Pierson, S., Muñoz, J. F., Subotić, A., Cruz, R. B., Cuomo, C. A. and Dijck, P. V. (2021) Genome-Wide Analysis of Experimentally Evolved Candida auris Reveals Multiple Novel Mechanisms of Multidrug Resistance. *mBio,* **12,** 10.1128/mbio.03333-03320.

Cesari, S., Thilliez, G., Ribot, C., Chalvon, V., Michel, C., Jauneau, A., *et al*. (2013) The Rice Resistance Protein Pair RGA4/RGA5 Recognizes the *Magnaporthe oryzae* Effectors AVR-Pia and AVR1-CO39 by Direct Binding. *The Plant Cell,* **25,** 1463-1481.

Chakrabarty, P., Duan, Y. and Gabriel, D. (1997) Cloning and characterization of a member of the *Xanthomonas* avr/pth gene family that evades all commercially utilized cotton R genes in the United States. *Phytopathology,* **87,** 1160-1167.

Chang, J. H., Urbach, J. M., Law, T. F., Arnold, L. W., Hu, A., Gombar, S., *et al*. (2005) A high-throughput, near-saturating screen for type III effector genes from *Pseudomonas syringae*. *Proceedings of the National Academy of Sciences,* **102,** 2549-2554.

Chaparro-Garcia, A., Schwizer, S., Sklenar, J., Yoshida, K., Petre, B., Bos, J. I., *et al*. (2015) *Phytophthora infestans* RXLR-WY effector AVR3a associates with dynamin-related protein 2 required for endocytosis of the plant pattern recognition receptor FLS2. *PLOS ONE,* **10,** e0137071.

Chasse Scott, A., Flanary, P., Parnell Stephen, C., Hao, N., Cha Jiyoung, Y., Siderovski David, P. and Dohlman Henrik, G. (2006) Genome-Scale Analysis Reveals Sst2 as the Principal Regulator of Mating Pheromone Signaling in the Yeast Saccharomyces cerevisiae. *Eukaryotic Cell,* **5,** 330-346.

Chen, L.-Q., Hou, B.-H., Lalonde, S., Takanaga, H., Hartung, M. L., Qu, X.-Q., *et al*. (2010) Sugar transporters for intercellular exchange and nutrition of pathogens. *Nature,* **468,** 527-532.

Chen, Y., Bates, D. L., Dey, R., Chen, P.-H., Machado, A. C. D., Laird-Offringa, I. A., *et al*. (2012) DNA binding by GATA transcription factor suggests mechanisms of DNA looping and long-range gene regulation. *Cell reports,* **2,** 1197-1206.

Chen, Y., Zhai, S., Zhang, H., Zuo, R., Wang, J., Guo, M., *et al*. (2014) Shared and distinct functions of two Gti1/Pac2 family proteins in growth, morphogenesis and pathogenicity of *Magnaporthe oryzae*. *Environmental Microbiology,* **16,** 788-801.

Cheng, J. H., Bredow, M., Monaghan, J. and DiCenzo, G. C. (2021) Proteobacteria contain diverse flg22 epitopes that elicit varying immune responses in *Arabidopsis thaliana*. *Molecular Plant-Microbe Interactions,* **34,** 504-510.

Chinchilla, D., Zipfel, C., Robatzek, S., Kemmerling, B., Nürnberger, T., Jones, J. D. G., *et al*. (2007) A flagellin-induced complex of the receptor FLS2 and BAK1 initiates plant defence. *Nature,* **448,** 497-500.

Chisholm, S. T., Dahlbeck, D., Krishnamurthy, N., Day, B., Sjolander, K. and Staskawicz, B. J. (2005) Molecular characterization of proteolytic cleavage sites of the *Pseudomonas syringae* effector AvrRpt2. *Proceedings of the National Academy of Sciences,* **102,** 2087-2092.

Cho, Y., Ohm, R. A., Grigoriev, I. V. and Srivastava, A. (2013) Fungal-specific transcription factor bf2 activates pathogenicity in Ilternaria brassicicola. *The Plant Journal,* **75,** 498-514.

Choi, J. and Kim, S.-H. (2017) A genome Tree of Life for the Fungi kingdom. *Proceedings of the National Academy of Sciences,* **114,** 9391-9396.

Choi, W. and Dean, R. A. (1997) The adenylate cyclase gene MAC1 of *Magnaporthe grisea* controls appressorium formation and other aspects of growth and development. *The Plant Cell,* **9,** 1973-1983.

Chowdhary, A., Prakash, A., Sharma, C., Kordalewska, M., Kumar, A., Sarma, S., *et al*. (2018) A multicentre study of antifungal susceptibility patterns among 350 *Candida auris* isolates (2009–17) in India: role of the ERG11 and FKS1 genes in azole and echinocandin resistance. *Journal of Antimicrobial Chemotherapy,* **73,** 891-899.

Christie, P. J., Atmakuri, K., Krishnamoorthy, V., Jakubowski, S. and Cascales, E. (2005) Biogenesis, architecture, and function of bacterial type IV secretion systems. *Annu. Rev. Microbiol.,* **59,** 451-485.

Chung, H., Choi, J., Park, S.-Y., Jeon, J. and Lee, Y.-H. (2013) Two conidiation-related Zn(II)2Cys6 transcription factor genes in the rice blast fungus. *Fungal Genetics and Biology,* **61,** 133-141.

Cingolani, P., Platts, A., Wang le, L., Coon, M., Nguyen, T., Wang, L., *et al*. (2012) A program for annotating and predicting the effects of single nucleotide polymorphisms, SnpEff: SNPs in the genome of Drosophila melanogaster strain w1118; iso-2; iso-3. *Fly (Austin),* **6,** 80-92.

Coaker, G., Falick, A. and Staskawicz, B. (2005) Activation of a Phytopathogenic Bacterial Effector Protein by a Eukaryotic Cyclophilin. *Science,* **308,** 548-550.

Coaker, G., Zhu, G., Ding, Z., Van Doren, S. R. and Staskawicz, B. (2006) Eukaryotic cyclophilin as a molecular switch for effector activation. *Molecular Microbiology,* **61,** 1485-1496.

Cook, J. G., Bardwell, L., Kron, S. J. and Thorner, J. (1996) Two novel targets of the MAP kinase Kss1 are negative regulators of invasive growth in the yeast Saccharomyces cerevisiae. *Genes & development,* **10,** 2831-2848.

Cools, H. J., Hawkins, N. J. and Fraaije, B. A. (2013) Constraints on the evolution of azole resistance in plant pathogenic fungi. *Plant Pathology,* **62,** 36-42.

Costa, T. R. D., Felisberto-Rodrigues, C., Meir, A., Prevost, M. S., Redzej, A., Trokter, M. and Waksman, G. (2015) Secretion systems in Gram-negative bacteria: structural and mechanistic insights. *Nature Reviews Microbiology,* **13,** 343-359.

Couto, D. and Zipfel, C. (2016) Regulation of pattern recognition receptor signalling in plants. *Nat Rev Immunol,* **16,** 537-552.

Crous, P. W., Hawksworth, D. L. and Wingfield, M. J. (2015) Identifying and naming plant-pathogenic fungi: past, present, and future. *Annual Review of Phytopathology,* **53,** 247-267.

Cruz-Mireles, N., Eseola, A. B., Osés-Ruiz, M., Ryder, L. S. and Talbot, N. J. (2021) From appressorium to transpressorium—Defining the morphogenetic basis of host cell invasion by the rice blast fungus. *PLOS Pathogens,* **17,** e1009779.

Cruz-Mireles, N., Osés-Ruiz, M., Derbyshire, P., Jégousse, C., Ryder, L. S., Bautista, M. J. A.*, et al*. (2024) The phosphorylation landscape of infection-related development by the rice blast fungus. *Cell,* **187,** 2557-2573.e2518.

Cui, H., Tsuda, K. and Parker, J. E. (2015) Effector-Triggered Immunity: From Pathogen Perception to Robust Defense. *Annual Review of Plant Biology,* **66,** 487-511.

Dagdas, Y. F., Yoshino, K., Dagdas, G., Ryder, L. S., Bielska, E., Steinberg, G. and Talbot, N. J. (2012) Septin-mediated plant cell invasion by the rice blast fungus, *Magnaporthe oryzae*. *Science,* **336,** 1590-1595.

Dallery, J. F., Adelin, É., Le Goff, G., Pigné, S., Auger, A., Ouazzani, J. and O'Connell, R. J. (2019) H3K4 trimethylation by CclA regulates pathogenicity and the production of three families of terpenoid secondary metabolites in *Colletotrichum higginsianum*. *Molecular Plant Pathology,* **20,** 831-842.

Dangl, J. L. and Jones, J. D. G. (2001) Plant pathogens and integrated defence responses to infection. *Nature,* **411,** 826-833.

Davis, E. L., Hussey, R. S., Mitchum, M. G. and Baum, T. J. (2008) Parasitism proteins in nematode–plant interactions. *Current Opinion in Plant Biology,* **11,** 360-366.

de Guillen, K., Ortiz-Vallejo, D., Gracy, J., Fournier, E., Kroj, T. and Padilla, A. (2015) Structure Analysis Uncovers a Highly Diverse but Structurally Conserved Effector Family in Phytopathogenic Fungi. *PLOS Pathogens,* **11,** e1005228.

de Jong, J. C., McCormack, B. J., Smirnoff, N. and Talbot, N. J. (1997) Glycerol generates turgor in rice blast. *Nature,* **389,** 244-244.

de Jonge, R., Peter van Esse, H., Kombrink, A., Shinya, T., Desaki, Y., Bours, R.*, et al*. (2010) Conserved Fungal LysM Effector Ecp6 Prevents Chitin-Triggered Immunity in Plants. *Science,* **329,** 953-955.

De la Concepcion, J. C., Franceschetti, M., Maqbool, A., Saitoh, H., Terauchi, R., Kamoun, S. and Banfield, M. J. (2018) Polymorphic residues in rice NLRs expand binding and response to effectors of the blast pathogen. *Nat Plants,* **4,** 576-585.

De la Concepcion, J. C., Fujisaki, K., Bentham, A. R., Cruz Mireles, N., Sanchez de Medina Hernandez, V., Shimizu, M.*, et al*. (2022) A blast fungus zinc-finger fold effector binds to a hydrophobic pocket in host Exo70 proteins to modulate immune recognition in rice. *Proc Natl Acad Sci U S A,* **119,** e2210559119.

de Vega-Bartol, J. J., Martín-Dominguez, R., Ramos, B., García-Sánchez, M.-A. and Díaz-Mínguez, J. M. (2011) New Virulence Groups in *Fusarium oxysporum f. sp. phaseoli:* The Expression of the Gene Coding for the Transcription Factor ftf1 Correlates with Virulence. *Phytopathology®,* **101,** 470-479.

De Wit, P. J. G. M., Mehrabi, R., Van den Burg, H. A. and Stergiopoulos, I. (2009) Fungal effector proteins: past, present and future. *Molecular Plant Pathology,* **10,** 735-747.

Dean, R. A., Talbot, N. J., Ebbole, D. J., Farman, M. L., Mitchell, T. K., Orbach, M. J.*, et al*. (2005) The genome sequence of the rice blast fungus *Magnaporthe grisea*. *Nature,* **434,** 980-986.

DeFalco, T. A. and Zipfel, C. (2021) Molecular mechanisms of early plant pattern-triggered immune signaling. *Mol Cell,* **81,** 3449-3467.

Deppmann, C. D., Alvania, R. S. and Taparowsky, E. J. (2006) Cross-species annotation of basic leucine zipper factor interactions: Insight into the evolution of closed interaction networks. *Molecular Biology and Evolution,* **23,** 1480-1492.

Derbyshire, M. C. and Raffaele, S. (2023) Till death do us pair: Co-evolution of plant–necrotroph interactions. *Current Opinion in Plant Biology,* **76,** 102457.

Derevnina, L., Contreras, M. P., Adachi, H., Upson, J., Cruces, A. V., Xie, R.*, et al*. (2021) Plant pathogens convergently evolved to counteract redundant nodes of an NLR immune receptor network. *PLOS Biology,* **19,** e3001136.

DeZwaan, T. M., Carroll, A. M., Valent, B. and Sweigard, J. A. (1999) Magnaporthe grisea Pth11p Is a Novel Plasma Membrane Protein That Mediates Appressorium Differentiation in Response to Inductive Substrate Cues. *The Plant Cell,* **11,** 2013-2030.

Dillon, M. M., Almeida, R. N., Laflamme, B., Martel, A., Weir, B. S., Desveaux, D. and Guttman, D. S. (2019) Molecular evolution of Pseudomonas syringae type III secreted effector proteins. *Frontiers in Plant Science,* **10,** 418.

Dodds, P. N. and Rathjen, J. P. (2010) Plant immunity: towards an integrated view of plant–pathogen interactions. *Nature Reviews Genetics,* **11,** 539-548.

Doehlemann, G., Ökmen, B., Zhu, W. and Sharon, A. (2017) Plant Pathogenic Fungi. *Microbiology Spectrum,* **5,** 10.1128/microbiolspec.funk-0023-2016.

Dohlman, H. G., Song, J., Ma, D., Courchesne, W. E. and Thorner, J. (1996) Sst2, a negative regulator of pheromone signaling in the yeast *Saccharomyces cerevisiae*: expression, localization, and genetic interaction and physical association with Gpa1 (the G-protein alpha subunit). *Mol Cell Biol,* **16,** 5194-5209.

Dohlman, H. G. and Thorner, J. (2001) Regulation of G Protein–Initiated Signal Transduction in Yeast: Paradigms and Principles. *Annual Review of Biochemistry,* **70,** 703-754.

Dong, Y., Li, Y., Zhao, M., Jing, M., Liu, X., Liu, M.*, et al*. (2015) Global genome and transcriptome analyses of *Magnaporthe oryzae* epidemic isolate 98-06 uncover novel effectors and pathogenicity-related genes, revealing gene gain and lose dynamics in genome evolution. *PLOS Pathogens,* **11,** e1004801.

Eisermann, I., Garduño-Rosales, M. and Talbot, N. J. (2023) The emerging role of septins in fungal pathogenesis. *Cytoskeleton (Hoboken),* **80,** 242-253.

Emms, D. M. and Kelly, S. (2019) OrthoFinder: phylogenetic orthology inference for comparative genomics. *Genome Biology,* **20,** 238.

Eseola, A. B., Ryder, L. S., Osés-Ruiz, M., Findlay, K., Yan, X., Cruz-Mireles, N.*, et al*. (2021) Investigating the cell and developmental biology of plant infection by the rice blast fungus *Magnaporthe oryzae*. *Fungal Genet Biol,* **154,** 103562.

Espada, M., Eves-van den Akker, S., Maier, T., Vijayapalani, P., Baum, T., Mota, M. and Jones, J. T. (2018) STATAWAARS: a promoter motif associated with spatial expression in the major effector-producing tissues of the plant-parasitic nematode *Bursaphelenchus xylophilus*. *BMC Genomics,* **19,** 1-13.

Eves-van den Akker, S. and Birch, Paul R. J. (2016) Opening the Effector Protein Toolbox for Plant–Parasitic Cyst Nematode Interactions. *Molecular plant,* **9,** 1451-1453.

Fang, W. and Latgé, J. P. (2018) Microbe Profile: Aspergillus fumigatus: a saprotrophic and opportunistic fungal pathogen. *Microbiology (Reading, England),* **164,** 1009-1011.

Fedotova, A., Bonchuk, A., Mogila, V. and Georgiev, P. (2017) C2H2 zinc finger proteins: the largest but poorly explored family of higher eukaryotic transcription factors. *Acta Naturae,* **9,** 47-58.

Fei, W. and Liu, Y. (2023) Biotrophic Fungal Pathogens: a Critical Overview. *Appl Biochem Biotechnol,* **195,** 1-16.

Filloux, A., Hachani, A. and Bleves, S. (2008) The bacterial type VI secretion machine: yet another player for protein transport across membranes. *Microbiology,* **154,** 1570-1583.

Fisher, M. C., Henk, D. A., Briggs, C. J., Brownstein, J. S., Madoff, L. C., McCraw, S. L. and Gurr, S. J. (2012) Emerging fungal threats to animal, plant and ecosystem health. *Nature,* **484,** 186-194.

Flor, H. (1971) Current status of the genefor-gene concept. *Annu. Rev. Phytopathol,* **9,** 275-296.

Fouché, S., Plissonneau, C. and Croll, D. (2018) The birth and death of effectors in rapidly evolving filamentous pathogen genomes. *Current Opinion in Microbiology,* **46,** 34-42.

Francis, M. S., Wolf-Watz, H. and Forsberg, Å. (2002) Regulation of type III secretion systems. *Current Opinion in Microbiology,* **5,** 166-172.

Frawley, D. and Bayram, Ö. (2020) The pheromone response module, a mitogen-activated protein kinase pathway implicated in the regulation of fungal development, secondary metabolism and pathogenicity. *Fungal Genet Biol,* **144,** 103469.

Friendly, M. (2002) Corrgrams. *The American Statistician,* **56,** 316-324.

Froger, A. and Hall, J. E. (2007) Transformation of plasmid DNA into E. coli using the heat shock method. *Journal of visualized experiments : JoVE*, 253.

Gal-Mor, O. and Finlay, B. B. (2006) Pathogenicity islands: a molecular toolbox for bacterial virulence. *Cellular Microbiology,* **8,** 1707-1719.

Galán, J. E. (2009) Common Themes in the Design and Function of Bacterial Effectors. *Cell host & microbe,* **5,** 571-579.

Galán, J. E. and Wolf-Watz, H. (2006) Protein delivery into eukaryotic cells by type III secretion machines. *Nature,* **444,** 567-573.

Gao, R. and Stock, A. M. (2009) Biological insights from structures of two-component proteins. *Annual Review of Microbiology,* **63,** 133-154.

Garcia, N., Farmer, A. N., Baptiste, R. and Fernandez, J. (2023) Gene Replacement by a Selectable Marker in the Filamentous FungusMagnaporthe oryzae. *Bio Protoc,* **13,** e4809.

Gibcus, J. H. and Dekker, J. (2012) The context of gene expression regulation. *F1000 Biol Rep,* **4,** 8.

Gilman, A. G. (1987) G proteins: transducers of receptor-generated signals. *Annu Rev Biochem,* **56,** 615-649.

Gimenez-Ibanez, S., Boter, M., Fernández-Barbero, G., Chini, A., Rathjen, J. P. and Solano, R. (2014) The bacterial effector HopX1 targets JAZ transcriptional repressors to activate jasmonate signaling and promote infection in Arabidopsis. *PLOS Biology,* **12,** e1001792.

Gimenez-Ibanez, S., Hann, D. R., Ntoukakis, V., Petutschnig, E., Lipka, V. and Rathjen, J. P. (2009) AvrPtoB Targets the LysM Receptor Kinase CERK1 to Promote Bacterial Virulence on Plants. *Current Biology,* **19,** 423-429.

Giordano, T. J. and McAllister, W. T. (1990) Optimization of the hygromycin B resistance-conferring gene as a dominant selectable marker in mammalian cells. *Gene,* **88,** 285-288.

Giraldo, M. C., Dagdas, Y. F., Gupta, Y. K., Mentlak, T. A., Yi, M., Martinez-Rocha, A. L.*, et al*. (2013) Two distinct secretion systems facilitate tissue invasion by the rice blast fungus *Magnaporthe oryzae*. *Nat Commun,* **4,** 1996.

Giraldo, M. C. and Valent, B. (2013) Filamentous plant pathogen effectors in action. *Nature Reviews Microbiology,* **11,** 800-814.

Gladieux, P., Condon, B., Ravel, S., Soanes, D., Maciel, J. L. N., Nhani, A., Jr.*, et al*. (2018) Gene Flow between Divergent Cereal- and Grass-Specific Lineages of the Rice Blast Fungus *Magnaporthe oryzae*. *mBio,* **9**.

Göhre, V., Spallek, T., Häweker, H., Mersmann, S., Mentzel, T., Boller, T.*, et al*. (2008) Plant pattern-recognition receptor FLS2 is directed for degradation by the bacterial ubiquitin ligase AvrPtoB. *Current Biology,* **18,** 1824-1832.

Goossens, A., de la Fuente, N., Forment, J., Serrano, R. and Portillo, F. (2000) Regulation of Yeast H+-ATPase by Protein Kinases Belonging to a Family Dedicated to Activation of Plasma Membrane Transporters. *Molecular and Cellular Biology,* **20,** 7654-7661.

Goto, Y., Yamagishi, Y., Shintomi-Kawamura, M., Abe, M., Tanno, Y. and Watanabe, Y. (2017) Pds5 Regulates Sister-Chromatid Cohesion and Chromosome Bi-orientation through a Conserved Protein Interaction Module. *Current Biology,* **27,** 1005-1012.

Grant, C. E., Bailey, T. L. and Noble, W. S. (2011) FIMO: scanning for occurrences of a given motif. *Bioinformatics,* **27,** 1017-1018.

Grant, S. R., Fisher, E. J., Chang, J. H., Mole, B. M. and Dangl, J. L. (2006) Subterfuge and Manipulation: Type III Effector Proteins of Phytopathogenic Bacteria. *Annual Review of Microbiology,* **60,** 425-449.

Grosshans, B. L., Ortiz, D. and Novick, P. (2006) Rabs and their effectors: Achieving specificity in membrane traffic. *Proceedings of the National Academy of Sciences,* **103,** 11821-11827.

Gu, Y., Zavaliev, R. and Dong, X. (2017) Membrane Trafficking in Plant Immunity. *Molecular plant,* **10,** 1026-1034.

Guo, L., Cesari, S., de Guillen, K., Chalvon, V., Mammri, L., Ma, M.*, et al*. (2018) Specific recognition of two MAX effectors by integrated HMA domains in plant immune receptors involves distinct binding surfaces. *Proceedings of the National Academy of Sciences,* **115,** 11637-11642.

Guo, M., Chen, Y., Du, Y., Dong, Y., Guo, W., Zhai, S., *et al*. (2011) The bZIP Transcription Factor MoAP1 Mediates the Oxidative Stress Response and Is Critical for Pathogenicity of the Rice Blast Fungus *Magnaporthe oryzae*. *PLOS Pathogens,* **7,** e1001302.

Guo, M., Tian, F., Wamboldt, Y. and Alfano, J. R. (2009) The majority of the type III effector inventory of *Pseudomonas syringae pv. tomato* DC3000 can suppress plant immunity. *Mol Plant Microbe Interact,* **22,** 1069-1080.

Gupta, Y. K., Dagdas, Y. F., Martinez-Rocha, A. L., Kershaw, M. J., Littlejohn, G. R., Ryder, L. S., *et al*. (2015) Septin-Dependent Assembly of the Exocyst Is Essential for Plant Infection by *Magnaporthe oryzae*. *Plant Cell,* **27,** 3277-3289.

Guttman, D. S., Vinatzer, B. A., Sarkar, S. F., Ranall, M. V., Kettler, G. and Greenberg, J. T. (2002) A functional screen for the type III (Hrp) secretome of the plant pathogen *Pseudomonas syringae*. *Science,* **295,** 1722-1726.

Habich, A., Chaves Vargas, V., Robinson, L. A., Allsopp, L. P. and Unterweger, D. (2025) Distribution of the four type VI secretion systems in *Pseudomonas aeruginosa* and classification of their core and accessory effectors. *Nature Communications,* **16,** 888.

Habig, M., Bahena-Garrido, S. M., Barkmann, F., Haueisen, J. and Stukenbrock, E. H. (2020) The transcription factor Zt107320 affects the dimorphic switch, growth and virulence of the fungal wheat pathogen *Zymoseptoria tritici*. *Molecular Plant Pathology,* **21,** 124-138.

Hahn, M. and Mendgen, K. (2001) Signal and nutrient exchange at biotrophic plant-fungus interfaces. *Curr Opin Plant Biol,* **4,** 322-327.

Hahsler, M., Hornik, K. and Buchta, C. (2008) Getting Things in Order: An Introduction to the R Package seriation. *Journal of Statistical Software,* **25,** 1 - 34.

Hamer, J. E. and and Timberlake, W. E. (1987) Functional Organization of The *Aspergillus Nidulans* Trpc Promoter. *Molecular and Cellular Biology,* **7,** 2352-2359.

Hamer, J. E., Howard, R. J., Chumley, F. G. and Valent, B. (1988) A mechanism for surface attachment in spores of a plant pathogenic fungus. *Science,* **239,** 288-290.

Han, J., Wang, X., Wang, F., Zhao, Z., Li, G., Zhu, X., *et al*. (2021a) The Fungal Effector Avr-Pita Suppresses Innate Immunity by Increasing COX Activity in Rice Mitochondria. *Rice,* **14,** 12.

Han, Z., Yu, R., Xiong, D. and Tian, C. (2021b) A Sge1 homolog in *Cytospora chrysosperma* governs conidiation, virulence and the expression of putative effectors. *Gene,* **778,** 145474.

Harmel, N., Létocart, E., Cherqui, A., Giordanengo, P., Mazzucchelli, G., Guillonneau, F., *et al*. (2008) Identification of aphid salivary proteins: a proteomic investigation of Myzus persicae. *Insect Mol Biol,* **17,** 165-174.

Hemetsberger, C., Herrberger, C., Zechmann, B., Hillmer, M. and Doehlemann, G. (2012) The *Ustilago maydis* Effector Pep1 Suppresses Plant Immunity by Inhibition of Host Peroxidase Activity. *PLOS Pathogens,* **8,** e1002684.

Hernday, A. D., Lohse, M. B., Fordyce, P. M., Nobile, C. J., DeRisi, J. L. and Johnson, A. D. (2013) Structure of the transcriptional network controlling white-opaque switching in *Candida albicans*. *Mol Microbiol,* **90,** 22-35.

Hibbett, D. S., Blackwell, M., James, T. Y., Spatafora, J. W., Taylor, J. W. and Vilgalys, R. (2018) Phylogenetic taxon definitions for Fungi, Dikarya, Ascomycota and Basidiomycota. *IMA Fungus,* **9,** 291-298.

Hoffman, G. A., Garrison, T. R. and Dohlman, H. G. (2000) Endoproteolytic Processing of Sst2, a Multidomain Regulator of G Protein Signaling in Yeast. *Journal of Biological Chemistry,* **275,** 37533-37541.

Hogenhout, S. A. and Bos, J. I. B. (2011) Effector proteins that modulate plant–insect interactions. *Current Opinion in Plant Biology,* **14,** 422-428.

Hogenhout, S. A., Van der Hoorn, R. A. L., Terauchi, R. and Kamoun, S. (2009) Emerging Concepts in Effector Biology of Plant-Associated Organisms. *Molecular Plant-Microbe Interactions®,* **22,** 115-122.

Hoi, J. W. S., Herbert, C., Bacha, N., O'Connell, R., Lafitte, C., Borderies, G.*, et al*. (2007) Regulation and role of a STE12-like transcription factor from the plant pathogen *Colletotrichum lindemuthianum*. *Molecular Microbiology,* **64,** 68-82.

Huang, G., Wang, H., Chou, S., Nie, X., Chen, J. and Liu, H. (2006) Bistable expression of WOR1, a master regulator of white opaque switching in *Candida albicans*. *Proceedings of the National Academy of Sciences,* **103,** 12813-12818.

Huang, J., Si, W., Deng, Q., Li, P. and Yang, S. (2014) Rapid evolution of avirulence genes in rice blast fungus *Magnaporthe oryzae*. *BMC Genetics,* **15,** 45.

Huang, T.-Y., Lee, Y.-Y., Vidal-Diez de Ulzurrun, G. and Hsueh, Y.-P. (2020) Forward genetic screens identified mutants with defects in trap morphogenesis in the nematode-trapping fungus *Arthrobotrys oligospora*. *G3 Genes|Genomes|Genetics,* **11**.

Hulin, M. T., Hill, L., Jones, J. D. G. and Ma, W. (2023) Pangenomic analysis reveals plant NAD+ manipulation as an important virulence activity of bacterial pathogen effectors. *Proceedings of the National Academy of Sciences,* **120,** e2217114120.

Hussey, R. and Mims, C. (1990) Ultrastructure of esophageal glands and their secretory granules in the root-knot nematode Meloidogyne incognita. *Protoplasma,* **156,** 9-18.

Hutcheson, S. W., Bretz, J., Sussan, T., Jin, S. and Pak, K. (2001) Enhancer-binding proteins HrpR and HrpS interact to regulate hrp-encoded type III protein secretion in Pseudomonas syringae strains. *Journal of Bacteriology,* **183,** 5589-5598.

Imran, Q. M., Falak, N., Hussain, A., Mun, B.-G., Sharma, A., Lee, S.-U.*, et al*. (2016) Nitric oxide responsive heavy metal-associated gene AtHMAD1 contributes to development and disease resistance in *Arabidopsis thaliana*. *Frontiers in Plant Science,* **7,** 1712.

Ingolia, N. T., Ghaemmaghami, S., Newman, J. R. S. and Weissman, J. S. (2009) Genome-Wide Analysis in Vivo of Translation with Nucleotide Resolution Using Ribosome Profiling. *Science,* **324,** 218-223.

Jaenisch, R. and Bird, A. (2003) Epigenetic regulation of gene expression: how the genome integrates intrinsic and environmental signals. *Nature Genetics,* **33,** 245-254.

Jeleńska, J., Lee, J., Manning, A. J., Wolfgeher, D. J., Ahn, Y., Walters-Marrah, G.*, et al.* (2021) *Pseudomonas syringae* effector HopZ3 suppresses the bacterial AvrPto1–tomato PTO immune complex via acetylation. *PLOS Pathogens,* **17,** e1010017.

Jeon, J., Park, S.-Y., Chi, M.-H., Choi, J., Park, J., Rho, H.-S.*, et al.* (2007) Genome-wide functional analysis of pathogenicity genes in the rice blast fungus. *Nature Genetics,* **39,** 561-565.

Jia, Y., McAdams, S. A., Bryan, G. T., Hershey, H. P. and Valent, B. (2000) Direct interaction of resistance gene and avirulence gene products confers rice blast resistance. *Embo j,* **19,** 4004-4014.

Jiang, C., Zhang, X., Liu, H. and Xu, J.-R. (2018) Mitogen-activated protein kinase signaling in plant pathogenic fungi. *PLOS Pathogens,* **14,** e1006875.

Jiang, R. H. Y., Tripathy, S., Govers, F. and Tyler, B. M. (2008) RXLR effector reservoir in two *Phytophthora* species is dominated by a single rapidly evolving superfamily with more than 700 members. *Proceedings of the National Academy of Sciences,* **105,** 4874-4879.

Jiang, S., Yao, J., Ma, K.-W., Zhou, H., Song, J., He, S. Y. and Ma, W. (2013) Bacterial effector activates jasmonate signaling by directly targeting JAZ transcriptional repressors. *PLOS Pathogens,* **9,** e1003715.

Johansson, J. and Freitag Nancy, E. (2019) Regulation of *Listeria monocytogenes* Virulence. *Microbiology Spectrum,* **7,** 10.1128/microbiolspec.gpp1123-0064-2019.

John, E., Singh, K. B., Oliver, R. P. and Tan, K.-C. (2021) Transcription factor control of virulence in phytopathogenic fungi. *Molecular Plant Pathology,* **22,** 858-881.

Johnson, K. L., Jones, B. J., Bacic, A. and Schultz, C. J. (2003) The fasciclin-like arabinogalactan proteins of Arabidopsis. A multigene family of putative cell adhesion molecules. *Plant Physiology,* **133,** 1911-1925.

Jones, D. A. B., John, E., Rybak, K., Phan, H. T. T., Singh, K. B., Lin, S.-Y.*, et al.* (2019) A specific fungal transcription factor controls effector gene expression and orchestrates the establishment of the necrotrophic pathogen lifestyle on wheat. *Scientific Reports,* **9,** 15884.

Jones, J. D. G. and Dangl, J. L. (2006) The plant immune system. *Nature,* **444,** 323-329.

Jumper, J., Evans, R., Pritzel, A., Green, T., Figurnov, M., Ronneberger, O.*, et al.* (2021) Highly accurate protein structure prediction with AlphaFold. *Nature,* **596,** 583-589.

Kamoun, S. (2006) A Catalogue of the Effector Secretome of Plant Pathogenic Oomycetes. *Annual Review of Phytopathology,* **44,** 41-60.

Kankanala, P., Czymmek, K. and Valent, B. (2007) Roles for Rice Membrane Dynamics and Plasmodesmata during Biotrophic Invasion by the Blast Fungus. *The Plant Cell,* **19,** 706-724.

Kanzaki, H., Yoshida, K., Saitoh, H., Fujisaki, K., Hirabuchi, A., Alaux, L., *et al*. (2012) Arms race co-evolution of *Magnaporthe oryzae* AVR-Pik and rice Pik genes driven by their physical interactions. *The Plant Journal,* **72,** 894-907.

Karin, M. (1991) Signal transduction and gene control. *Current Opinion in Cell Biology,* **3,** 467-473.

Kaster, K. R., Burgett, S. G. and Ingolia, T. D. (1984) Hygromycin B resistance as dominant selectable marker in yeast. *Curr Genet,* **8,** 353-358.

Kazan, K. and Lyons, R. (2014) Intervention of Phytohormone Pathways by Pathogen Effectors. *Plant Cell,* **26,** 2285-2309.

Kershaw, M. J. and Talbot, N. J. (2009) Genome-wide functional analysis reveals that infection-associated fungal autophagy is necessary for rice blast disease. *Proceedings of the National Academy of Sciences,* **106,** 15967-15972.

Kim, J., Kaleku, J., Kim, H., Kang, M., Kang, H. J., Woo, J., *et al*. (2024) An RXLR effector disrupts vesicle trafficking at ER-Golgi interface for *Phytophthora capsici* pathogenicity. *Molecules and Cells,* **47,** 100158.

Kim, S., Ahn, I. P., Rho, H. S. and Lee, Y. H. (2005) MHP1, a *Magnaporthe grisea* hydrophobin gene, is required for fungal development and plant colonization. *Mol Microbiol,* **57,** 1224-1237.

Kim, S., Kim, C.-Y., Park, S.-Y., Kim, K.-T., Jeon, J., Chung, H., *et al*. (2020) Two nuclear effectors of the rice blast fungus modulate host immunity via transcriptional reprogramming. *Nature Communications,* **11,** 5845.

Kim, S., Park, S.-Y., Kim, K. S., Rho, H.-S., Chi, M.-H., Choi, J., *et al*. (2009) Homeobox Transcription Factors Are Required for Conidiation and Appressorium Development in the Rice Blast Fungus *Magnaporthe oryzae*. *PLOS Genetics,* **5,** e1000757.

Kleemann, J., Rincon-Rivera, L. J., Takahara, H., Neumann, U., Ver Loren van Themaat, E., van der Does, H. C., *et al*. (2012) Sequential delivery of host-induced virulence effectors by appressoria and intracellular hyphae of the phytopathogen *Colletotrichum higginsianum*. *PLoS Pathog,* **8,** e1002643.

Koeck, M., Hardham, A. R. and Dodds, P. N. (2011) The role of effectors of biotrophic and hemibiotrophic fungi in infection. *Cell Microbiol,* **13,** 1849-1857.

Kokla, A. and Melnyk, C. W. (2018) Developing a thief: Haustoria formation in parasitic plants. *Developmental Biology,* **442,** 53-59.

Kong, S., Park, S.-Y. and Lee, Y.-H. (2015) Systematic characterization of the bZIP transcription factor gene family in the rice blast fungus, *Magnaporthe oryzae*. *Environmental Microbiology,* **17,** 1425-1443.

Konishi, Y., Karnan, S., Takahashi, M., Ota, A., Damdindorj, L., Hosokawa, Y. and Konishi, H. (2012) A system for the measurement of gene targeting efficiency in human cell lines using an antibiotic resistance-GFP fusion gene. *Biotechniques,* **53,** 141-152.

Kõressaar, T., Lepamets, M., Kaplinski, L., Raime, K., Andreson, R. and Remm, M. (2018) Primer3_masker: integrating masking of template sequence with primer design software. *Bioinformatics,* **34,** 1937-1938.

Kourelis, J. and van der Hoorn, R. A. L. (2018) Defended to the Nines: 25 Years of Resistance Gene Cloning Identifies Nine Mechanisms for R Protein Function. *Plant Cell,* **30,** 285-299.

Kuo, H.-C., Hui, S., Choi, J., Asiegbu, F. O., Valkonen, J. P. T. and Lee, Y.-H. (2014) Secret lifestyles of Neurospora crassa. *Scientific Reports,* **4,** 5135.

Kuspa, A. (2006) Restriction enzyme-mediated integration (REMI) mutagenesis. *Methods Mol Biol,* **346,** 201-209.

Lahfa, M., Barthe, P., de Guillen, K., Cesari, S., Raji, M., Kroj, T.*, et al.* (2024) The structural landscape and diversity of *Pyricularia oryzae* MAX effectors revisited. *PLOS Pathogens,* **20,** e1012176.

Lam, H. N., Chakravarthy, S., Wei, H.-L., BuiNguyen, H., Stodghill, P. V., Collmer, A.*, et al.* (2014) Global Analysis of the HrpL Regulon in the Plant *Pathogen Pseudomonas syringae pv. tomato* DC3000 Reveals New Regulon Members with Diverse Functions. *PLOS ONE,* **9,** e106115.

Lambou, K., Tag, A., Lassagne, A., Collemare, J., Clergeot, P.-H., Barbisan, C.*, et al.* (2024) The bZIP transcription factor BIP1 of the rice blast fungus is essential for infection and regulates a specific set of appressorium genes. *PLOS Pathogens,* **20,** e1011945.

Langner, T., Białas, A. and Kamoun, S. (2018) The Blast Fungus Decoded: Genomes in Flux. *mBio,* **9**.

Le Naour--Vernet, M., Lahfa, M., Maidment, J. H. R., Padilla, A., Roumestand, C., de Guillen, K.*, et al.* (2025) Structure-guided insights into the biology of fungal effectors. *New Phytologist,* **n/a**.

Leach, J. E. and White, F. F. (1996) Bacterial avirulence genes. *Annual Review of Phytopathology,* **34,** 153-179.

Lee, A. H.-Y., Hurley, B., Felsensteiner, C., Yea, C., Ckurshumova, W., Bartetzko, V.*, et al.* (2012) A bacterial acetyltransferase destroys plant microtubule networks and blocks secretion. *PLOS Pathogens,* **8,** e1002523.

Lee, Y., Robbins, N. and Cowen, L. E. (2023) Molecular mechanisms governing antifungal drug resistance. *Antimicrobials and Resistance,* **1,** 5.

Lehner, B. (2011) Molecular mechanisms of epistasis within and between genes. *Trends Genet,* **27,** 323-331.

Letunic, I. and Bork, P. (2006) Interactive Tree Of Life (iTOL): an online tool for phylogenetic tree display and annotation. *Bioinformatics,* **23,** 127-128.

Lewis, R. E., Liao, G., Hou, J., Prince, R. A. and Kontoyiannis, D. P. (2011) Comparative in vivo dose-dependent activity of caspofungin and anidulafungin against echinocandin-susceptible and-resistant *Aspergillus fumigatus*. *Journal of Antimicrobial Chemotherapy,* **66,** 1324-1331.

Li, G., Zhou, X., Kong, L., Wang, Y., Zhang, H., Zhu, H.*, et al.* (2011) MoSfl1 Is Important for Virulence and Heat Tolerance in *Magnaporthe oryzae*. *PLOS ONE,* **6,** e19951.

Li, G., Zhou, X. and Xu, J.-R. (2012) Genetic control of infection-related development in *Magnaporthe oryzae*. *Current Opinion in Microbiology,* **15,** 678-684.

Li, H. (2023) Protein-to-genome alignment with miniprot. *Bioinformatics,* **39**.

Li, H., Handsaker, B., Wysoker, A., Fennell, T., Ruan, J., Homer, N.*, et al.* (2009) The Sequence Alignment/Map format and SAMtools. *Bioinformatics,* **25,** 2078-2079.

Li, L., Xue, C., Bruno, K., Nishimura, M. and Xu, J.-R. (2004) Two PAK Kinase Genes, CHM1 and MST20, Have Distinct Functions in *Magnaporthe grisea*. *Molecular Plant-Microbe Interactions®,* **17,** 547-556.

Li, M., Chang, P., Pan, X., Imanaka, T., Igarashi, Y. and Luo, F. (2020) Efficient expressions of reporter genes in the industrial filamentous fungus *Sclerotium rolfsii* mediated by *Agrobacterium tumefaciens*. *Fungal Biology,* **124,** 932-939.

Li, Y., Wang, G., Xu, J.-R. and Jiang, C. (2016) Penetration Peg Formation and Invasive Hyphae Development Require Stage-Specific Activation of MoGTI1 in *Magnaporthe oryzae*. *Molecular Plant-Microbe Interactions®,* **29,** 36-45.

Liao, C.-J., Hailemariam, S., Sharon, A. and Mengiste, T. (2022) Pathogenic strategies and immune mechanisms to necrotrophs: Differences and similarities to biotrophs and hemibiotrophs. *Current Opinion in Plant Biology,* **69,** 102291.

Lin, S. Y., Chooi, Y. H. and Solomon, P. S. (2018) The global regulator of pathogenesis PnCon7 positively regulates Tox3 effector gene expression through direct interaction in the wheat pathogen *Parastagonospora nodorum*. *Molecular Microbiology,* **109,** 78-90.

Lindgren, P. B., Peet, R. C. and Panopoulos, N. J. (1986) Gene cluster of *Pseudomonas syringae pv. phaseolicola* controls pathogenicity of bean plants and hypersensitivity of nonhost plants. *Journal of Bacteriology,* **168,** 512-522.

Liu, C., Shen, N., Zhang, Q., Qin, M., Cao, T., Zhu, S.*, et al*. (2022a) *Magnaporthe oryzae* Transcription Factor MoBZIP3 Regulates Appressorium Turgor Pressure Formation during Pathogenesis. *International Journal of Molecular Sciences,* **23,** 881.

Liu, H., Lu, X., Li, M., Lun, Z., Yan, X., Yin, C.*, et al*. (2023) Plant immunity suppression by an exo-β-1,3-glucanase and an elongation factor 1α of the rice blast fungus. *Nature Communications,* **14,** 5491.

Liu, H., Suresh, A., Willard, F. S., Siderovski, D. P., Lu, S. and Naqvi, N. I. (2007) Rgs1 regulates multiple Gα subunits in *Magnaporthe* pathogenesis, asexual growth and thigmotropism. *The EMBO Journal,* **26,** 690-700.

Liu, S. and Dean, R. A. (1997) G protein alpha subunit genes control growth, development, and pathogenicity of *Magnaporthe grisea*. *Mol Plant Microbe Interact,* **10,** 1075-1086.

Liu, T., Song, T., Zhang, X., Yuan, H., Su, L., Li, W.*, et al*. (2014) Unconventionally secreted effectors of two filamentous pathogens target plant salicylate biosynthesis. *Nature Communications,* **5,** 4686.

Liu, W., Liu, J., Ning, Y., Ding, B., Wang, X., Wang, Z. and Wang, G.-L. (2013) Recent progress in understanding PAMP-and effector-triggered immunity against the rice blast fungus *Magnaporthe oryzae*. *Molecular plant,* **6,** 605-620.

Liu, W., Zhou, X., Li, G., Li, L., Kong, L., Wang, C.*, et al*. (2011) Multiple plant surface signals are sensed by different mechanisms in the rice blast fungus for appressorium formation. *PLoS Pathog,* **7,** e1001261.

Liu, X., Gao, Y., Guo, Z., Wang, N., Wegner, A., Wang, J.*, et al*. (2022b) MoIug4 is a novel secreted effector promoting rice blast by counteracting host OsAHL1-regulated ethylene gene transcription. *New Phytologist,* **235,** 1163-1178.

Lopez, V. A., Park, B. C., Nowak, D., Sreelatha, A., Zembek, P., Fernandez, J.*, et al*. (2019) A Bacterial Effector Mimics a Host HSP90 Client to Undermine Immunity. *Cell,* **179,** 205-218.e221.

Lovelace, A. H., Dorhmi, S., Hulin, M. T., Li, Y., Mansfield, J. W. and Ma, W. (2023) Effector Identification in Plant Pathogens. *Phytopathology®,* **113,** 637-650.

Lu, J., Cao, H., Zhang, L., Huang, P. and Lin, F. (2014) Systematic analysis of Zn2Cys6 transcription factors required for development and pathogenicity by high-throughput gene knockout in the rice blast fungus. *PLoS Pathog,* **10,** e1004432.

Lynch, M. and Conery, J. S. (2003) The Origins of Genome Complexity. *Science,* **302,** 1401-1404.

Ma, L.-J., van der Does, H. C., Borkovich, K. A., Coleman, J. J., Daboussi, M.-J., Di Pietro, A.*, et al*. (2010) Comparative genomics reveals mobile pathogenicity chromosomes in *Fusarium*. *Nature,* **464,** 367-373.

Maidment, J. H. R., Franceschetti, M., Maqbool, A., Saitoh, H., Jantasuriyarat, C., Kamoun, S.*, et al*. (2021) Multiple variants of the fungal effector AVR-Pik bind the HMA domain of the rice protein OsHIPP19, providing a foundation to engineer plant defense. *Journal of Biological Chemistry,* **296,** 100371.

Manni, M., Berkeley, M. R., Seppey, M., Simão, F. A. and Zdobnov, E. M. (2021) BUSCO Update: Novel and Streamlined Workflows along with Broader and Deeper Phylogenetic Coverage for Scoring of Eukaryotic, Prokaryotic, and Viral Genomes. *Molecular Biology and Evolution,* **38,** 4647-4654.

Marichal, P., Koymans, L., Willemsens, S., Bellens, D., Verhasselt, P., Luyten, W.*, et al*. (1999) Contribution of mutations in the cytochrome P450 14α-demethylase (Erg11p, Cyp51p) to azole resistance in *Candida albicans*. *Microbiology,* **145,** 2701-2713.

Martínez-Cruz, J., Romero, D., Hierrezuelo, J., Thon, M., de Vicente, A. and Pérez-García, A. (2021) Effectors with chitinase activity (EWCAs), a family of conserved, secreted fungal chitinases that suppress chitin-triggered immunity. *The Plant Cell,* **33,** 1319-1340.

Mathieu, S., Cusant, L., Roux, C. and Corradi, N. (2018) Arbuscular mycorrhizal fungi: intraspecific diversity and pangenomes. *New Phytologist,* **220,** 1129-1134.

McCombe, C. L., Wegner, A., Wirtz, L., Zamora, C. S., Casanova, F., Aditya, S.*, et al*. (2025) Plant pathogenic fungi hijack phosphate signaling with conserved enzymatic effectors. *Science,* **387,** 955-962.

McLachlan, A. and Stewart, M. (1975) Tropomyosin coiled-coil interactions: evidence for an unstaggered structure. *Journal of Molecular Biology,* **98,** 293-304.

Mehrabi, R., Ding, S. and Xu, J.-R. (2008) MADS-Box Transcription Factor Mig1 Is Required for Infectious Growth in *Magnaporthe grisea*. *Eukaryotic Cell,* **7,** 791-799.

Meng, S., Zhiquan, L., Huanbin, S., Zhongling, W., Jiehua, Q., Hui, W.*, et al*. (2021) UvKmt6-mediated H3K27 trimethylation is required for development, pathogenicity, and stress response in *Ustilaginoidea virens*. *Virulence,* **12,** 2972-2988.

Mentlak, T., Talbot, N. and Kroj, T. (2011) Effector Translocation and Delivery by the Rice Blast Fungus *Magnaporthe oryzae*. pp. 219-241.

Mentlak, T. A., Kombrink, A., Shinya, T., Ryder, L. S., Otomo, I., Saitoh, H., *et al*. (2012) Effector-Mediated Suppression of Chitin-Triggered Immunity by *Magnaporthe oryzae* Is Necessary for Rice Blast Disease. *The Plant Cell,* **24,** 322-335.

Micallef, L. and Rodgers, P. (2014) eulerAPE: Drawing Area-Proportional 3-Venn Diagrams Using Ellipses. *PLOS ONE,* **9,** e101717.

Michielse, C., Pfannmüller, A., Macios, M., Rengers, P., Dzikowska, A. and Tudzynski, B. (2014) The interplay between the GATA transcription factors AreA, the global nitrogen regulator and AreB in *Fusarium fujikuroi*. *Molecular Microbiology,* **91,** 472-493.

Michielse, C. B., van Wijk, R., Reijnen, L., Manders, E. M. M., Boas, S., Olivain, C., *et al*. (2009) The Nuclear Protein Sge1 of *Fusarium oxysporum* Is Required for Parasitic Growth. *PLOS Pathogens,* **5,** e1000637.

Miller, J. H. (1985) Mutagenic specificity of ultraviolet light. *Journal of Molecular Biology,* **182,** 45-65.

Misas-Villamil, J. C. and van der Hoorn, R. A. L. (2008) Enzyme–inhibitor interactions at the plant–pathogen interface. *Current Opinion in Plant Biology,* **11,** 380-388.

Molinari, C. and Talbot, N. J. (2022) A Basic Guide to the Growth and Manipulation of the Blast Fungus, *Magnaporthe oryzae*. *Current Protocols,* **2,** e523.

Molloy, B., Shin, D. S., Long, J., Pellegrin, C., Senatori, B., Vieira, P., *et al*. (2024) The origin, deployment, and evolution of a plant-parasitic nematode effectorome. *PLOS Pathogens,* **20,** e1012395.

Moore, L. D., Le, T. and Fan, G. (2013) DNA Methylation and Its Basic Function. *Neuropsychopharmacology,* **38,** 23-38.

Mosquera, G., Giraldo, M. C., Khang, C. H., Coughlan, S. and Valent, B. (2009) Interaction Transcriptome Analysis Identifies *Magnaporthe oryzae* BAS1-4 as Biotrophy-Associated Secreted Proteins in Rice Blast Disease. *The Plant Cell,* **21,** 1273-1290.

Mueller, C. G. and Nordheim, A. (1991) A protein domain conserved between yeast MCM1 and human SRF directs ternary complex formation. *The EMBO Journal,* **10,** 4219-4229.

Mukerjee, M., Kim, J.-E., Park, Y.-S., Kolomiets, M. V. and Shim, W.-B. (2011) Regulators of G-protein signalling in *Fusarium verticillioides* mediate differential host–pathogen responses on nonviable versus viable maize kernels. *Molecular Plant Pathology,* **12,** 479-491.

Münch, S., Lingner, U., Floss, D. S., Ludwig, N., Sauer, N. and Deising, H. B. (2008) The hemibiotrophic lifestyle of Colletotrichum species. *J Plant Physiol,* **165,** 41-51.

Musser, R. O., Hum-Musser, S. M., Eichenseer, H., Peiffer, M., Ervin, G., Murphy, J. B. and Felton, G. W. (2002) Caterpillar saliva beats plant defences. *Nature,* **416,** 599-600.

Naalden, D., van Kleeff, P. J. M., Dangol, S., Mastop, M., Corkill, R., Hogenhout, S. A., *et al*. (2021) Spotlight on the Roles of Whitefly Effectors in Insect–Plant Interactions. *Frontiers in Plant Science,* **12**.

Natale, P., Brüser, T. and Driessen, A. J. M. (2008) Sec- and Tat-mediated protein secretion across the bacterial cytoplasmic membrane—Distinct

translocases and mechanisms. *Biochimica et Biophysica Acta (BBA) - Biomembranes,* **1778,** 1735-1756.

Ngou, B. P. M., Ahn, H.-K., Ding, P. and Jones, J. D. G. (2021) Mutual potentiation of plant immunity by cell-surface and intracellular receptors. *Nature,* **592,** 110-115.

Nicaise, V., Joe, A., Jeong, B. r., Korneli, C., Boutrot, F., Westedt, I.*, et al*. (2013) *Pseudomonas* HopU1 modulates plant immune receptor levels by blocking the interaction of their mRNAs with GRP7. *The EMBO Journal,* **32,** 701-712.

Ning, N., Xie, X., Yu, H., Mei, J., Li, Q., Zuo, S.*, et al*. (2022) Plant peroxisome-targeting effector MoPtep1 is required for the virulence of *Magnaporthe oryzae*. *International Journal of Molecular Sciences,* **23,** 2515.

Nishimura, M., Park, G. and Xu, J.-R. (2003) The G-beta subunit MGB1 is involved in regulating multiple steps of infection-related morphogenesis in *Magnaporthe grisea*. *Molecular Microbiology,* **50,** 231-243.

Noble, L. M. and Andrianopoulos, A. (2013) Fungal Genes in Context: Genome Architecture Reflects Regulatory Complexity and Function. *Genome Biology and Evolution,* **5,** 1336-1352.

Nobori, T., Wang, Y., Wu, J., Stolze, S. C., Tsuda, Y., Finkemeier, I.*, et al*. (2020) Multidimensional gene regulatory landscape of a bacterial pathogen in plants. *Nature Plants,* **6,** 883-896.

Nomura, K., DebRoy, S., Lee, Y. H., Pumplin, N., Jones, J. and He, S. Y. (2006) A bacterial virulence protein suppresses host innate immunity to cause plant disease. *Science,* **313,** 220-223.

Nomura, K., Imboden, L. A., Tanaka, H. and He, S. Y. (2023) Multiple host targets of *Pseudomonas* effector protein HopM1 form a protein complex regulating apoplastic immunity and water homeostasis. *bioRxiv*.

O'Malley, M. R. and Anderson, J. C. (2021) Regulation of the *Pseudomonas syringae* Type III Secretion System by Host Environment Signals. *Microorganisms,* **9,** 1227.

O'Meara, T. R. (2024) Going fishing: how to get what you want from a fungal genetic screen. *mSphere,* **9,** e00638-00623.

Odenbach, D., Breth, B., Thines, E., Weber, R. W. S., Anke, H. and Foster, A. J. (2007) The transcription factor Con7p is a central regulator of infection-related morphogenesis in the rice blast fungus *Magnaporthe grisea*. *Molecular Microbiology,* **64,** 293-307.

Oh, M., Son, H., Choi, G. J., Lee, C., Kim, J. C., Kim, H. and Lee, Y. W. (2016) Transcription factor ART 1 mediates starch hydrolysis and mycotoxin production in *Fusarium graminearum* and *F. verticillioides*. *Molecular Plant Pathology,* **17,** 755-768.

Oikawa, K., Fujisaki, K., Shimizu, M., Takeda, T., Nemoto, K., Saitoh, H.*, et al*. (2024) The blast pathogen effector AVR-Pik binds and stabilizes rice heavy metal-associated (HMA) proteins to co-opt their function in immunity. *PLOS Pathogens,* **20,** e1012647.

Oliveira-Garcia, E., Tamang, T. M., Park, J., Dalby, M., Martin-Urdiroz, M., Rodriguez Herrero, C.*, et al*. (2023) Clathrin-mediated endocytosis facilitates the internalization of *Magnaporthe oryzae* effectors into rice cells. *The Plant Cell*, koad094.

Oliveira-Garcia, E. and Valent, B. (2021) Characterizing the Secretion Systems of *Magnaporthe oryzae*. *Methods Mol Biol,* **2356,** 69-77.

Oliveira-Garcia, E., Yan, X., Oses-Ruiz, M., de Paula, S. and Talbot, N. J. (2024) Effector-triggered susceptibility by the rice blast fungus *Magnaporthe oryzae*. *New Phytologist,* **241,** 1007-1020.

Ong, J. Y., Swidah, R., Monti, M., Schindler, D., Dai, J. and Cai, Y. (2021) SCRaMbLE: A Study of Its Robustness and Challenges through Enhancement of Hygromycin B Resistance in a Semi-Synthetic Yeast. *Bioengineering (Basel),* **8**.

Ontiveros-Cisneros, A., Moss, O., Van Moerkercke, A. and Van Aken, O. (2022) Evaluation of Antibiotic-Based Selection Methods for *Camelina sativa* Stable Transformants. *Cells,* **11**.

Orbach, M. J., Farrall, L., Sweigard, J. A., Chumley, F. G. and Valent, B. (2000) A telomeric avirulence gene determines efficacy for the rice blast resistance gene Pi-ta. *The Plant Cell,* **12,** 2019-2032.

Osés-Ruiz, M., Cruz-Mireles, N., Martin-Urdiroz, M., Soanes, D. M., Eseola, A. B., Tang, B.*, et al*. (2021) Appressorium-mediated plant infection by *Magnaporthe oryzae* is regulated by a Pmk1-dependent hierarchical transcriptional network. *Nat Microbiol,* **6,** 1383-1397.

Oses-Ruiz, M., Sakulkoo, W., Littlejohn, G., Martín-Urdiroz, M. and Talbot, N. (2016) Two independent S-phase checkpoints regulate appressorium-mediated plant infection by the rice blast fungus *Magnaporthe oryzae*. *Proceedings of the National Academy of Sciences,* **114,** 201611307.

Pandey, P., Leary, A. Y., Tumtas, Y., Savage, Z., Dagvadorj, B., Duggan, C.*, et al*. (2021) An oomycete effector subverts host vesicle trafficking to channel starvation-induced autophagy to the pathogen interface. *eLife,* **10,** e65285.

Panstruga, R. (2003) Establishing compatibility between plants and obligate biotrophic pathogens. *Curr Opin Plant Biol,* **6,** 320-326.

Park, A. R., Cho, A.-R., Seo, J.-A., Min, K., Son, H., Lee, J.*, et al*. (2012a) Functional analyses of regulators of G protein signaling in *Gibberella zeae*. *Fungal Genetics and Biology,* **49,** 511-520.

Park, C.-H., Chen, S., Shirsekar, G., Zhou, B., Khang, C. H., Songkumarn, P.*, et al*. (2012b) The *Magnaporthe oryzae* Effector AvrPiz-t Targets the RING E3 Ubiquitin Ligase APIP6 to Suppress Pathogen-Associated Molecular Pattern–Triggered Immunity in Rice. *The Plant Cell,* **24,** 4748-4762.

Park, G., Xue, C., Zhao, X., Kim, Y., Orbach, M. and Xu, J. R. (2006) Multiple upstream signals converge on the adaptor protein Mst50 in *Magnaporthe grisea*. *Plant Cell,* **18,** 2822-2835.

Park, G., Xue, C., Zheng, L., Lam, S. and Xu, J.-R. (2002) MST12 Regulates Infectious Growth But Not Appressorium Formation in the Rice Blast Fungus *Magnaporthe grisea*. *Molecular plant-microbe interactions : MPMI,* **15,** 183-192.

Park, J., Throop, A. L. and LaBaer, J. (2015) Site-specific recombinational cloning using gateway and in-fusion cloning schemes. *Curr Protoc Mol Biol,* **110,** 3.20.21-23.20.23.

Pel, M. J., van Dijken, A. J., Bardoel, B. W., Seidl, M. F., van der Ent, S., van Strijp, J. A. and Pieterse, C. M. (2014) *Pseudomonas syringae* evades host immunity by

degrading flagellin monomers with alkaline protease AprA. *Molecular Plant-Microbe Interactions,* **27,** 603-610.

Pellegrin, C., Damm, A., Sperling, A. L., Molloy, B., Shin, D. S., Long, J.*, et al*. (2025) The SUbventral-Gland Regulator (SUGR-1) of nematode virulence. *Proceedings of the National Academy of Sciences,* **122,** e2415861122.

Petnicki-Ocwieja, T., Schneider, D. J., Tam, V. C., Chancey, S. T., Shan, L., Jamir, Y.*, et al*. (2002) Genomewide identification of proteins secreted by the Hrp type III protein secretion system of *Pseudomonas syringae pv. tomato* DC3000. *Proceedings of the National Academy of Sciences,* **99,** 7652-7657.

Petre, B., Contreras, M. P., Bozkurt, T. O., Schattat, M. H., Sklenar, J., Schornack, S.*, et al*. (2021) Host-interactor screens of *Phytophthora infestans* RXLR proteins reveal vesicle trafficking as a major effector-targeted process. *The Plant Cell,* **33,** 1447-1471.

Petre, B. and Kamoun, S. (2014) How Do Filamentous Pathogens Deliver Effector Proteins into Plant Cells? *PLOS Biology,* **12,** e1001801.

Pettersen, E. F., Goddard, T. D., Huang, C. C., Meng, E. C., Couch, G. S., Croll, T. I.*, et al*. (2021) UCSF ChimeraX: Structure visualization for researchers, educators, and developers. *Protein Science,* **30,** 70-82.

Pfannenstiel, B. T., Zhao, X., Wortman, J., Wiemann, P., Throckmorton, K., Spraker, J. E.*, et al*. (2017) Revitalization of a Forward Genetic Screen Identifies Three New Regulators of Fungal Secondary Metabolism in the Genus *Aspergillus*. *mBio,* **8,** 10.1128/mbio.01246-01217.

Pimentel, H., Bray, N. L., Puente, S., Melsted, P. and Pachter, L. (2017) Differential analysis of RNA-seq incorporating quantification uncertainty. *Nature methods,* **14,** 687-690.

Qian, H., Lin, L., Zhang, Z., Gu, X., Shen, D., Yin, Z.*, et al*. (2024) A MYB-related transcription factor regulates effector gene expression in an oomycete pathogen. *Molecular Plant Pathology,* **25,** e13468.

Qiao, Y., Liu, L., Xiong, Q., Flores, C., Wong, J., Shi, J.*, et al*. (2013) Oomycete pathogens encode RNA silencing suppressors. *Nature Genetics,* **45,** 330-333.

Qin, L., Li, A., Tan, K., Guo, S., Chen, Y., Wang, F. and Wong, K. H. (2019) Universal plasmids to facilitate gene deletion and gene tagging in filamentous fungi. *Fungal Genetics and Biology,* **125,** 28-35.

Quime, B. G., Ryder, L. S. and Talbot, N. J. (2025) Live cell imaging of plant infection provides new insight into the biology of pathogenesis by the rice blast fungus *Magnaporthe oryzae*. *Journal of Microscopy,* **297,** 274-288.

Qutob, D., Kamoun, S. and Gijzen, M. (2002) Expression of a *Phytophthora sojae* necrosis-inducing protein occurs during transition from biotrophy to necrotrophy. *The Plant Journal,* **32,** 361-373.

Radakovic, Z. S., Anjam, M. S., Escobar, E., Chopra, D., Cabrera, J., Silva, A. C.*, et al*. (2018) Arabidopsis HIPP27 is a host susceptibility gene for the beet cyst nematode *Heterodera schachtii*. *Molecular Plant Pathology,* **19,** 1917-1928.

Radhamony, R., Prasad, A. and Srinivasan, R. (2005) T-DNA insertional mutagenesis in *Arabidopsis*: A tool for functional genomics. *Electronic Journal of Biotechnology (ISSN: 0717-3458) Vol 8 Num 1,* **8**.

Raffaele, S. and Kamoun, S. (2012) Genome evolution in filamentous plant pathogens: why bigger can be better. *Nat Rev Microbiol,* **10,** 417-430.

Rao, R. N., Allen, N. E., Hobbs, J. N., Alborn, W. E., Kirst, H. A. and Paschal, J. W. (1983) Genetic and enzymatic basis of hygromycin B resistance in *Escherichia coli*. *Antimicrobial agents and chemotherapy,* **24,** 689-695.

Reilly, M. C., Kim, J., Lynn, J., Simmons, B. A., Gladden, J. M., Magnuson, J. K. and Baker, S. E. (2018) Forward genetics screen coupled with whole-genome resequencing identifies novel gene targets for improving heterologous enzyme production in *Aspergillus niger*. *Applied Microbiology and Biotechnology,* **102,** 1797-1807.

Ren, J., Li, C., Gao, C., Xu, J.-R., Jiang, C. and Wang, G. (2019) Deletion of FgHOG1 Is Suppressive to the mgv1 Mutant by Stimulating Gpmk1 Activation and Avoiding Intracellular Turgor Elevation in *Fusarium graminearum*. *Frontiers in Microbiology,* **10**.

Revell, L. J. (2024) phytools 2.0: an updated R ecosystem for phylogenetic comparative methods (and other things). *PeerJ,* **12,** e16505.

Rispail, N. and Di Pietro, A. (2010) The homeodomain transcription factor Ste12: Connecting fungal MAPK signaling to plant pathogenicity. *Communicative & Integrative Biology,* **3,** 327-332.

Ritchie, M. E., Phipson, B., Wu, D., Hu, Y., Law, C. W., Shi, W. and Smyth, G. K. (2015) limma powers differential expression analyses for RNA-sequencing and microarray studies. *Nucleic Acids Research,* **43,** e47-e47.

Robinson, J. T., Thorvaldsdóttir, H., Winckler, W., Guttman, M., Lander, E. S., Getz, G. and Mesirov, J. P. (2011) Integrative genomics viewer. *Nature Biotechnology,* **29,** 24-26.

Robinson, M. D., McCarthy, D. J. and Smyth, G. K. (2009) edgeR: a Bioconductor package for differential expression analysis of digital gene expression data. *Bioinformatics,* **26,** 139-140.

Roine, E., Wei, W., Yuan, J., Nurmiaho-Lassila, E.-L., Kalkkinen, N., Romantschuk, M. and He, S. Y. (1997) Hrp pilus: an hrp-dependent bacterial surface appendage produced by *Pseudomonas syringae pv. tomato* DC3000. *Proceedings of the National Academy of Sciences,* **94,** 3459-3464.

Rooney, H. C., Van't Klooster, J. W., van der Hoorn, R. A., Joosten, M. H., Jones, J. D. and de Wit, P. J. (2005) *Cladosporium* Avr2 inhibits tomato Rcr3 protease required for Cf-2-dependent disease resistance. *Science,* **308,** 1783-1786.

Rose, J. K., Ham, K. S., Darvill, A. G. and Albersheim, P. (2002) Molecular cloning and characterization of glucanase inhibitor proteins: coevolution of a counterdefense mechanism by plant pathogens. *Plant Cell,* **14,** 1329-1345.

Rouxel, T. and Balesdent, M.-H. (2017) Life, death and rebirth of avirulence effectors in a fungal pathogen of *Brassica* crops, *Leptosphaeria maculans*. *New Phytologist,* **214,** 526-532.

Rueden, C. T., Schindelin, J., Hiner, M. C., DeZonia, B. E., Walter, A. E., Arena, E. T. and Eliceiri, K. W. (2017) ImageJ2: ImageJ for the next generation of scientific image data. *BMC Bioinformatics,* **18,** 529.

Ruiz-Bedoya, T., Wang, P. W., Desveaux, D. and Guttman, D. S. (2023) Cooperative virulence via the collective action of secreted pathogen effectors. *Nature Microbiology,* **8,** 640-650.

Rybak, K., See, P. T., Phan, H. T., Syme, R. A., Moffat, C. S., Oliver, R. P. and Tan, K. C. (2017) A functionally conserved Zn(2) Cys(6) binuclear cluster transcription factor class regulates necrotrophic effector gene expression and host-specific virulence of two major Pleosporales fungal pathogens of wheat. *Mol Plant Pathol,* **18,** 420-434.

Ryder, L. S., Cruz-Mireles, N., Molinari, C., Eisermann, I., Eseola, A. B. and Talbot, N. J. (2022) The appressorium at a glance. *Journal of Cell Science,* **135**.

Ryder, L. S., Dagdas, Y. F., Kershaw, M. J., Venkataraman, C., Madzvamuse, A., Yan, X.*, et al*. (2019) A sensor kinase controls turgor-driven plant infection by the rice blast fungus. *Nature,* **574,** 423-427.

Ryder, L. S., Lopez, S. G., Michels, L., Eseola, A. B., Sprakel, J., Ma, W. and Talbot, N. J. (2023) A molecular mechanosensor for real-time visualization of appressorium membrane tension in *Magnaporthe oryzae*. *Nature Microbiology,* **8,** 1508-1519.

Ryder, L. S. and Talbot, N. J. (2015) Regulation of appressorium development in pathogenic fungi. *Current Opinion in Plant Biology,* **26,** 8-13.

Sakamoto, M. (1949) On the new method of sheath-inoculation of rice plants with blast fungus, *Pyricularia oryzae* for the study of the disease-resistant nature of the plant. *Bull. Inst. Agr. Res. Tohoku Univ. Jpn,* **1,** 120-129.

Sakulkoo, W., Osés-Ruiz, M., Oliveira Garcia, E., Soanes, D. M., Littlejohn, G. R., Hacker, C.*, et al*. (2018) A single fungal MAP kinase controls plant cell-to-cell invasion by the rice blast fungus. *Science,* **359,** 1399-1403.

Sanguankiattichai, N., Buscaill, P. and Preston, G. M. (2022) How bacteria overcome flagellin pattern recognition in plants. *Current Opinion in Plant Biology,* **67,** 102224.

Saunders, D. G. O., Aves, S. J. and Talbot, N. J. (2010) Cell Cycle–Mediated Regulation of Plant Infection by the Rice Blast Fungus. *The Plant Cell,* **22,** 497-507.

Saunders, D. G. O., Breen, S., Win, J., Schornack, S., Hein, I., Bozkurt, T. O.*, et al*. (2012) Host Protein BSL1 Associates with *Phytophthora infestans* RXLR Effector AVR2 and the *Solanum demissum* Immune Receptor R2 to Mediate Disease Resistance *The Plant Cell,* **24,** 3420-3434.

Schamber, A., Leroch, M., Diwo, J., Mendgen, K. and Hahn, M. (2010) The role of mitogen-activated protein (MAP) kinase signalling components and the Ste12 transcription factor in germination and pathogenicity of Botrytis cinerea. *Molecular Plant Pathology,* **11,** 105-119.

Schindelin, J., Arganda-Carreras, I., Frise, E., Kaynig, V., Longair, M., Pietzsch, T.*, et al*. (2012) Fiji: an open-source platform for biological-image analysis. *Nat Methods,* **9,** 676-682.

Schornack, S., Huitema, E., Cano, L. M., Bozkurt, T. O., Oliva, R., Van Damme, M.*, et al*. (2009) Ten things to know about oomycete effectors. *Mol Plant Pathol,* **10,** 795-803.

Scortti, M., Monzó, H. J., Lacharme-Lora, L., Lewis, D. A. and Vázquez-Boland, J. A. (2007) The PrfA virulence regulon. *Microbes and Infection,* **9,** 1196-1207.

Seifert, G. J. (2018) Fascinating Fasciclins: A Surprisingly Widespread Family of Proteins that Mediate Interactions between the Cell Exterior and the Cell Surface. *International Journal of Molecular Sciences,* **19,** 1628.

Seong, K. and Krasileva, K. V. (2021) Computational Structural Genomics Unravels Common Folds and Novel Families in the Secretome of Fungal Phytopathogen *Magnaporthe oryzae*. *Molecular Plant-Microbe Interactions®,* **34,** 1267-1280.

Seong, K. and Krasileva, K. V. (2023) Prediction of effector protein structures from fungal phytopathogens enables evolutionary analyses. *Nature Microbiology,* **8,** 174-187.

Shabab, M., Shindo, T., Gu, C., Kaschani, F., Pansuriya, T., Chintha, R.*, et al*. (2008) Fungal Effector Protein AVR2 Targets Diversifying Defense-Related Cys Proteases of Tomato. *The Plant Cell,* **20,** 1169-1183.

Shan, L., He, P., Li, J., Heese, A., Peck, S. C., Nürnberger, T.*, et al*. (2008) Bacterial effectors target the common signaling partner BAK1 to disrupt multiple MAMP receptor-signaling complexes and impede plant immunity. *Cell host & microbe,* **4,** 17-27.

Shao, F., Golstein, C., Ade, J., Stoutemyer, M., Dixon, J. E. and Innes, R. W. (2003) Cleavage of *Arabidopsis* PBS1 by a bacterial type III effector. *Science,* **301,** 1230-1233.

Shelest, E. (2017) Transcription Factors in Fungi: TFome Dynamics, Three Major Families, and Dual-Specificity TFs. *Frontiers in Genetics,* **8**.

Shi, X., Long, Y., He, F., Zhang, C., Wang, R., Zhang, T.*, et al*. (2018) The fungal pathogen *Magnaporthe oryzae* suppresses innate immunity by modulating a host potassium channel. *PLOS Pathogens,* **14,** e1006878.

Shigenaga, A. M. and Argueso, C. T. (2016) No hormone to rule them all: Interactions of plant hormones during the responses of plants to pathogens. *Seminars in Cell & Developmental Biology,* **56,** 174-189.

Siddique, S., Radakovic, Z. S., Hiltl, C., Pellegrin, C., Baum, T. J., Beasley, H.*, et al*. (2022) The genome and lifestage-specific transcriptomes of a plant-parasitic nematode and its host reveal susceptibility genes involved in trans-kingdom synthesis of vitamin B5. *Nature Communications,* **13,** 6190.

Siderovski, D. P. and Willard, F. S. (2005) The GAPs, GEFs, and GDIs of heterotrimeric G-protein alpha subunits. *Int J Biol Sci,* **1,** 51-66.

Sirajuddin, M., Farkasovsky, M., Hauer, F., Kühlmann, D., Macara, I. G., Weyand, M.*, et al*. (2007) Structural insight into filament formation by mammalian septins. *Nature,* **449,** 311-315.

Skamnioti, P. and Gurr, S. J. (2009) Against the grain: safeguarding rice from rice blast disease. *Trends in Biotechnology,* **27,** 141-150.

Smirnoff, N. and Arnaud, D. (2019) Hydrogen peroxide metabolism and functions in plants. *New Phytol,* **221,** 1197-1214.

Snelders, N. C., Kettles, G. J., Rudd, J. J. and Thomma, B. (2018) Plant pathogen effector proteins as manipulators of host microbiomes? *Mol Plant Pathol,* **19,** 257-259.

Snelders, N. C., Rovenich, H., Petti, G. C., Rocafort, M., van den Berg, G. C. M., Vorholt, J. A.*, et al*. (2020) Microbiome manipulation by a soil-borne fungal plant pathogen using effector proteins. *Nature Plants,* **6,** 1365-1374.

Son, H., Seo, Y.-S., Min, K., Park, A. R., Lee, J., Jin, J.-M.*, et al*. (2011) A Phenome-Based Functional Analysis of Transcription Factors in the Cereal Head Blight Fungus, *Fusarium graminearum*. *PLOS Pathogens,* **7,** e1002310.

Song, D., Dolan, J. W., Yuan, Y. and Fields, S. (1991) Pheromone-dependent phosphorylation of the yeast STE12 protein correlates with transcriptional activation. *Genes & development,* **5,** 741-750.

Soyer, J. L., El Ghalid, M., Glaser, N., Ollivier, B., Linglin, J., Grandaubert, J.*, et al.* (2014) Epigenetic Control of Effector Gene Expression in the Plant Pathogenic Fungus *Leptosphaeria maculans*. *PLOS Genetics,* **10,** e1004227.

Soyer, J. L., Hamiot, A., Ollivier, B., Balesdent, M.-H., Rouxel, T. and Fudal, I. (2015) The APSES transcription factor LmStuA is required for sporulation, pathogenic development and effector gene expression in *Leptosphaeria maculans*. *Molecular Plant Pathology,* **16,** 1000-1005.

Sperschneider, J., Gardiner, D. M., Dodds, P. N., Tini, F., Covarelli, L., Singh, K. B.*, et al.* (2016) EffectorP: predicting fungal effector proteins from secretomes using machine learning. *New Phytologist,* **210,** 743-761.

Staskawicz, B. J., Dahlbeck, D. and Keen, N. T. (1984) Cloned avirulence gene of *Pseudomonas syringae pv. glycinea* determines race-specific incompatibility on *Glycine max (L.) Merr*. *Proceedings of the National Academy of Sciences,* **81,** 6024-6028.

Staskawicz, B. J., Mudgett, M. B., Dangl, J. L. and Galan, J. E. (2001) Common and Contrasting Themes of Plant and Animal Diseases. *Science,* **292,** 2285-2289.

Stock, A. M., Robinson, V. L. and Goudreau, P. N. (2000) Two-component signal transduction. *Annual Review of Biochemistry,* **69,** 183-215.

Streubel, J., Pesce, C., Hutin, M., Koebnik, R., Boch, J. and Szurek, B. (2013) Five phylogenetically close rice genes confer TAL effector-mediated susceptibility to *Xanthomonas oryzae pv. oryzae*. *New Phytologist,* **200,** 808-819.

Swett, C. L., Kirkpatrick, S. C. and Gordon, T. R. (2016) Evidence for a Hemibiotrophic Association of the Pitch Canker Pathogen Fusarium circinatum with Pinus radiata. *Plant Disease,* **100,** 79-84.

Talbot, N. J. (2003) On the trail of a cereal killer: Exploring the biology of *Magnaporthe grisea*. *Annu Rev Microbiol,* **57,** 177-202.

Talbot, N. J., Ebbole, D. J. and Hamer, J. E. (1993) Identification and characterization of MPG1, a gene involved in pathogenicity from the rice blast fungus *Magnaporthe grisea*. *The Plant Cell,* **5,** 1575-1590.

Talbot, N. J., Kershaw, M. J., Wakley, G. E., De Vries, O., Wessels, J. and Hamer, J. E. (1996) MPG1 Encodes a Fungal Hydrophobin Involved in Surface Interactions during Infection-Related Development of *Magnaporthe grisea*. *The Plant Cell,* **8,** 985-999.

Tan, K.-C. and Oliver, R. P. (2017) Regulation of proteinaceous effector expression in phytopathogenic fungi. *PLOS Pathogens,* **13,** e1006241.

Tang, B., Yan, X., Ryder, L. S., Bautista, M. J. A., Cruz-Mireles, N., Soanes, D. M.*, et al.* (2023) Rgs1 is a regulator of effector gene expression during plant infection by the rice blast fungus *Magnaporthe oryzae*. *Proceedings of the National Academy of Sciences,* **120,** e2301358120.

Tang, G., Yuan, J., Wang, J., Zhang, Y.-Z., Xie, S.-S., Wang, H.*, et al.* (2021) *Fusarium* BP1 is a reader of H3K27 methylation. *Nucleic Acids Research,* **49,** 10448-10464.

Tang, W., Ru, Y., Hong, L., Zhu, Q., Zuo, R., Guo, X.*, et al.* (2015) System-wide characterization of bZIP transcription factor proteins involved in infection-

related morphogenesis of *Magnaporthe oryzae*. *Environmental Microbiology,* **17,** 1377-1396.
Taylor, J. W. and Berbee, M. L. (2006) Dating divergences in the Fungal Tree of Life: review and new analyses. *Mycologia,* **98,** 838-849.
Tedford, K., Kim, S., Sa, D., Stevens, K. and Tyers, M. (1997) Regulation of the mating pheromone and invasive growth responses in yeast by two MAP kinase substrates. *Current Biology,* **7,** 228-238.
Teufel, F., Almagro Armenteros, J. J., Johansen, A. R., Gíslason, M. H., Pihl, S. I., Tsirigos, K. D.*, et al*. (2022) SignalP 6.0 predicts all five types of signal peptides using protein language models. *Nature Biotechnology,* **40,** 1023-1025.
Thomma, B. P. H. J., Nürnberger, T. and Joosten, M. H. A. J. (2011) Of PAMPs and Effectors: The Blurred PTI-ETI Dichotomy. *The Plant Cell,* **23,** 4-15.
Thompson, C. J., Movva, N. R., Tizard, R., Crameri, R., Davies, J. E., Lauwereys, M. and Botterman, J. (1987) Characterization of the herbicide-resistance gene bar from *Streptomyces hygroscopicus*. *Embo j,* **6,** 2519-2523.
Tian, C., Li, J. and Glass, N. L. (2011) Exploring the bZIP transcription factor regulatory network in Neurospora crassa. *Microbiology,* **157,** 747-759.
Tian, H., MacKenzie, C. I., Rodriguez-Moreno, L., van den Berg, G. C. M., Chen, H., Rudd, J. J.*, et al*. (2021) Three LysM effectors of *Zymoseptoria tritici* collectively disarm chitin-triggered plant immunity. *Mol Plant Pathol,* **22,** 683-693.
Tian, M., Benedetti, B. and Kamoun, S. (2005) A Second Kazal-like protease inhibitor from *Phytophthora infestans* inhibits and interacts with the apoplastic pathogenesis-related protease P69B of tomato. *Plant Physiol,* **138,** 1785-1793.
Tian, M., Huitema, E., Da Cunha, L., Torto-Alalibo, T. and Kamoun, S. (2004) A Kazal-like extracellular serine protease inhibitor from *Phytophthora infestans* targets the tomato pathogenesis-related protease P69B. *J Biol Chem,* **279,** 26370-26377.
Tollot, M., Assmann, D., Becker, C., Altmüller, J., Dutheil, J. Y., Wegner, C.-E. and Kahmann, R. (2016) The WOPR Protein Ros1 Is a Master Regulator of Sporogenesis and Late Effector Gene Expression in the Maize Pathogen *Ustilago maydis*. *PLOS Pathogens,* **12,** e1005697.
Toruño, T. Y., Stergiopoulos, I. and Coaker, G. (2016) Plant-Pathogen Effectors: Cellular Probes Interfering with Plant Defenses in Spatial and Temporal Manners. *Annual Review of Phytopathology,* **54,** 419-441.
Tsuge, S., Furutani, A. and Ikawa, Y. (2014) Regulatory network of hrp gene expression in *Xanthomonas oryzae pv. oryzae*. *Journal of General Plant Pathology,* **80,** 303-313.
Turrà, D., Segorbe, D. and Di Pietro, A. (2014) Protein kinases in plant-pathogenic fungi: conserved regulators of infection. *Annu Rev Phytopathol,* **52,** 267-288.
Valent, B. and Chumley, F. G. (1991) Molecular genetic analysis of the rice blast fungus, *Magnaporthe grisea*. *Annu Rev Phytopathol,* **29,** 443-467.
Valent, B., Farrall, L. and Chumley, F. (1991) *Magnaporthe grisea* genes for pathogenicity and virulence identified through a series of backcrosses. *Genetics,* **127**.

Valent, B. and Khang, C. H. (2010) Recent advances in rice blast effector research. *Current Opinion in Plant Biology,* **13,** 434-441.

Van Esse, H. P., Bolton, M. D., Stergiopoulos, I., de Wit, P. J. and Thomma, B. P. (2007) The chitin-binding *Cladosporium fulvum* effector protein Avr4 is a virulence factor. *Molecular Plant-Microbe Interactions,* **20,** 1092-1101.

Veneault-Fourrey, C., Barooah, M., Egan, M., Wakley, G. and Talbot, N. J. (2006) Autophagic Fungal Cell Death Is Necessary for Infection by the Rice Blast Fungus. *Science,* **312,** 580-583.

Verma, A., Lee, C., Morriss, S., Odu, F., Kenning, C., Rizzo, N.*, et al.* (2018) The novel cyst nematode effector protein 30D08 targets host nuclear functions to alter gene expression in feeding sites. *New Phytologist,* **219,** 697-713.

Vinson, C., Acharya, A. and Taparowsky, E. J. (2006) Deciphering B-ZIP transcription factor interactions in vitro and in vivo. *Biochimica et Biophysica Acta (BBA) - Gene Structure and Expression,* **1759,** 4-12.

Walker, G. M. and White, A. (2017) Fungal Physiology. *Fungi: Biology and Applications*, 1.

Wallden, K., Rivera-Calzada, A. and Waksman, G. (2010) Type IV secretion systems: versatility and diversity in function. *Cell Microbiol,* **12,** 1203-1212.

Wang, B.-h., Ebbole, D. J. and Wang, Z.-h. (2017) The arms race between *Magnaporthe oryzae* and rice: Diversity and interaction of Avr and R genes. *Journal of Integrative Agriculture,* **16,** 2746-2760.

Wang, H., Wang, S., Wang, W., Xu, L., Welsh, L. R. J., Gierlinski, M.*, et al.* (2023a) Uptake of oomycete RXLR effectors into host cells by clathrin-mediated endocytosis. *The Plant Cell,* **35,** 2504-2526.

Wang, K., Yu, W., Yu, G., Zhang, L., Xian, L., Wei, Y.*, et al.* (2023b) A bacterial type III effector targets plant vesicle-associated membrane proteins. *Mol Plant Pathol,* **24,** 1154-1167.

Wang, L., Chen, H., Li, J., Shu, H., Zhang, X., Wang, Y.*, et al.* (2019) Effector gene silencing mediated by histone methylation underpins host adaptation in an oomycete plant pathogen. *Nucleic Acids Research,* **48,** 1790-1799.

Wang, Q., Huang, Z., Khan, I. A., Li, Y., Wang, J., Wang, J.*, et al.* (2024) Key transcription factors required for outburst of rice blast disease in *Magnaporthe oryzae*. *Phytopathology Research,* **6,** 5.

Wang, R., Ning, Y., Shi, X., He, F., Zhang, C., Fan, J.*, et al.* (2016) Immunity to Rice Blast Disease by Suppression of Effector-Triggered Necrosis. *Current Biology,* **26,** 2399-2411.

Wang, X., Xue, B., Dai, J., Qin, X., Liu, L., Chi, Y.*, et al.* (2018) A novel *Meloidogyne incognita* chorismate mutase effector suppresses plant immunity by manipulating the salicylic acid pathway and functions mainly during the early stages of nematode parasitism. *Plant Pathology,* **67,** 1436-1448.

Watson, N., Linder, M. E., Druey, K. M., Kehrl, J. H. and Blumer, K. J. (1996) RGS family members: GTPase-activating proteins for heterotrimeric G-protein alpha-subunits. *Nature,* **383,** 172-175.

Weld, R. J., Plummer, K. M., Carpenter, M. A. and Ridgway, H. J. (2006) Approaches to functional genomics in filamentous fungi. *Cell Research,* **16,** 31-44.

Wendland, J. (2001) Comparison of Morphogenetic Networks of Filamentous Fungi and Yeast. *Fungal Genetics and Biology,* **34,** 63-82.

Wengler, M. R. and Talbot, N. J. (2025) Mechanisms of regulated cell death during plant infection by the rice blast fungus *Magnaporthe oryzae*. *Cell Death & Differentiation*.

Were, V., Yan, X., Foster, A. J., Sklenar, J., Langner, T., Bentham, A., *et al.* (2024) The blast effector Pwl2 is a virulence factor that modifies the cellular localisation of host protein HIPP43 to suppress immunity. *bioRxiv*, 2024.2001.2020.576406.

Whiteford, J. R. and Spanu, P. D. (2002) Hydrophobins and the interactions between fungi and plants. *Mol Plant Pathol,* **3,** 391-400.

Wilkinson, L. (2011) ggplot2: Elegant Graphics for Data Analysis by WICKHAM, H. *Biometrics,* **67,** 678-679.

Wilkinson, L. (2012) Exact and Approximate Area-Proportional Circular Venn and Euler Diagrams. *IEEE Transactions on Visualization and Computer Graphics,* **18,** 321-331.

Wilson, R. A. and Talbot, N. J. (2009) Under pressure: investigating the biology of plant infection by *Magnaporthe oryzae*. *Nat Rev Microbiol,* **7,** 185-195.

Win, J., Chaparro-Garcia, A., Belhaj, K., Saunders, D. G., Yoshida, K., Dong, S., *et al.* (2012) Effector biology of plant-associated organisms: concepts and perspectives. *Cold Spring Harb Symp Quant Biol,* **77,** 235-247.

Win, J. and Latorre, S. M. (In prep) Pangenome of *Magnaporthe oryzae*.

Winston, F. (2008) EMS and UV mutagenesis in yeast. *Curr Protoc Mol Biol,* **Chapter 13,** Unit 13.13B.

Wong Sak Hoi, J. and Dumas, B. (2010) Ste12 and Ste12-like proteins, fungal transcription factors regulating development and pathogenicity. *Eukaryot Cell,* **9,** 480-485.

Wong, Y. C., Lin, L. C., Melo-Silva, C. R., Smith, S. A. and Tscharke, D. C. (2011) Engineering recombinant poxviruses using a compact GFP-blasticidin resistance fusion gene for selection. *J Virol Methods,* **171,** 295-298.

Wu, C. H. and Derevnina, L. (2023) The battle within: How pathogen effectors suppress NLR-mediated immunity. *Curr Opin Plant Biol,* **74,** 102396.

Wu, Z., Qiu, J., Shi, H., Lin, C., Yue, J., Liu, Z., *et al.* (2021) Polycomb repressive complex 2 coordinates with Sin3 histone deacetylase complex to epigenetically reprogram genome-wide expression of effectors and regulate pathogenicity in *Magnaporthe oryzae*. *bioRxiv*, 2021.2003.2021.436344.

Xiang, T., Zong, N., Zou, Y., Wu, Y., Zhang, J., Xing, W., *et al.* (2008) *Pseudomonas syringae* effector AvrPto blocks innate immunity by targeting receptor kinases. *Current Biology,* **18,** 74-80.

Xiao, Y. and Hutcheson, S. W. (1994) A single promoter sequence recognized by a newly identified alternate sigma factor directs expression of pathogenicity and host range determinants in *Pseudomonas syringae*. *Journal of Bacteriology,* **176,** 3089-3091.

Xiao, Y., Lu, Y., Heu, S. and Hutcheson, S. W. (1992) Organization and environmental regulation of the *Pseudomonas syringae pv. syringae* 61 hrp cluster. *Journal of Bacteriology,* **174,** 1734-1741.

Xing, W., Zou, Y., Liu, Q., Liu, J., Luo, X., Huang, Q., *et al.* (2007) The structural basis for activation of plant immunity by bacterial effector protein AvrPto. *Nature,* **449,** 243-247.

Xu, J.-R., Staiger, C. J. and Hamer, J. E. (1998) Inactivation of the mitogen-activated protein kinase Mps1 from the rice blast fungus prevents penetration of host cells but allows activation of plant defense responses. *Proceedings of the National Academy of Sciences,* **95,** 12713-12718.

Xu, J. R. and Hamer, J. E. (1996) MAP kinase and cAMP signaling regulate infection structure formation and pathogenic growth in the rice blast fungus *Magnaporthe grisea*. *Genes Dev,* **10,** 2696-2706.

Yan, X., Tang, B., Ryder, L. S., MacLean, D., Were, V. M., Eseola, A. B.*, et al.* (2023) The transcriptional landscape of plant infection by the rice blast fungus *Magnaporthe oryzae* reveals distinct families of temporally co-regulated and structurally conserved effectors. *The Plant Cell,* **35,** 1360-1385.

Yano, K., Yamamoto, E., Aya, K., Takeuchi, H., Lo, P.-c., Hu, L.*, et al.* (2016) Genome-wide association study using whole-genome sequencing rapidly identifies new genes influencing agronomic traits in rice. *Nature Genetics,* **48,** 927-934.

Yu, G., Smith, D. K., Zhu, H., Guan, Y. and Lam, T. T.-Y. (2017) ggtree: an r package for visualization and annotation of phylogenetic trees with their covariates and other associated data. *Methods in Ecology and Evolution,* **8,** 28-36.

Yuan, M., Ngou, B. P. M., Ding, P. and Xin, X. F. (2021) PTI-ETI crosstalk: an integrative view of plant immunity. *Curr Opin Plant Biol,* **62,** 102030.

Yuan, Y., Zhang, M., Li, J., Yang, C., Abubakar, Y. S., Chen, X.*, et al.* (2022) The Small GTPase FgRab1 Plays Indispensable Roles in the Vegetative Growth, Vesicle Fusion, Autophagy and Pathogenicity of *Fusarium graminearum*. *Int J Mol Sci,* **23**.

Yue, X.-F., Que, Y.-W., Xu, L., Deng, S.-Z., Peng, Y., Talbot, N. and Wang, Z.-Y. (2015) ZNF1 Encodes a Putative C2H2 Zinc-Finger Protein Essential for Appressorium Differentiation by the Rice Blast Fungus *Magnaporthe oryzae*. *Molecular plant-microbe interactions : MPMI,* **29**.

Yuen, E. L. H., Tumtas, Y., King, F., Ibrahim, T., Chan, L. I., Evangelisti, E.*, et al.* (2024) A pathogen effector co-opts a host RabGAP protein to remodel pathogen interface and subvert defense-related secretion. *Science Advances,* **10,** eado9516.

Zhang, H., Tang, W., Liu, K., Huang, Q., Zhang, X., Yan, X.*, et al.* (2011a) Eight RGS and RGS-like Proteins Orchestrate Growth, Differentiation, and Pathogenicity of *Magnaporthe oryzae*. *PLOS Pathogens,* **7,** e1002450.

Zhang, H., Xue, C., Kong, L., Li, G. and Xu, J. R. (2011b) A Pmk1-interacting gene is involved in appressorium differentiation and plant infection in *Magnaporthe oryzae*. *Eukaryot Cell,* **10,** 1062-1070.

Zhang, J., Shao, F., Li, Y., Cui, H., Chen, L., Li, H.*, et al.* (2007) A *Pseudomonas syringae* effector inactivates MAPKs to suppress PAMP-induced immunity in plants. *Cell host & microbe,* **1,** 175-185.

Zhang, N., Luo, J., Rossman, A. Y., Aoki, T., Chuma, I., Crous, P. W.*, et al.* (2016) Generic names in Magnaporthales. *IMA Fungus,* **7,** 155-159.

Zhang, W., Huang, J. and Cook, D. E. (2021) Histone modification dynamics at H3K27 are associated with altered transcription of in planta induced genes in *Magnaporthe oryzae*. *PLOS Genetics,* **17,** e1009376.

Zhao, C.-R., You, Z.-L., Chen, D.-D., Hang, J., Wang, Z.-B., Ji, M., *et al*. (2023) Structure of a fungal 1,3-β-glucan synthase. *Science Advances,* **9,** eadh7820.

Zhao, X., Kim, Y., Park, G. and Xu, J.-R. (2005) A Mitogen-Activated Protein Kinase Cascade Regulating Infection-Related Morphogenesis in *Magnaporthe grisea*. *The Plant Cell,* **17,** 1317-1329.

Zhao, X. and Xu, J.-R. (2007) A highly conserved MAPK-docking site in Mst7 is essential for Pmk1 activation in *Magnaporthe grisea*. *Molecular Microbiology,* **63,** 881-894.

Zhou, J., Wu, S., Chen, X., Liu, C., Sheen, J., Shan, L. and He, P. (2014) The seudomonas syringae effector HopF2 suppresses *Arabidopsis* immunity by targeting BAK1. *The Plant Journal,* **77,** 235-245.

Zhou, X., Liu, W., Wang, C., Xu, Q., Wang, Y., Ding, S. and Xu, J.-R. (2011) A MADS-box transcription factor MoMcm1 is required for male fertility, microconidium production and virulence in *Magnaporthe oryzae*. *Molecular Microbiology,* **80,** 33-53.

Zipfel, C., Kunze, G., Chinchilla, D., Caniard, A., Jones, J. D., Boller, T. and Felix, G. (2006) Perception of the bacterial PAMP EF-Tu by the receptor EFR restricts *Agrobacterium*-mediated transformation. *Cell,* **125,** 749-760.

Zordan, R. E., Galgoczy, D. J. and Johnson, A. D. (2006) Epigenetic properties of white-opaque switching in *Candida albicans* are based on a self-sustaining transcriptional feedback loop. *Proc Natl Acad Sci U S A,* **103,** 12807-12812.